

R73-53

TC171
M41
H99

0.172

**MATHEMATICAL MODELS OF
THE MASSACHUSETTS BAY**

Part I

**Finite Element Modeling of Two-
Dimensional Hydrodynamic Circulation**

by

JEROME J. CONNOR

and **JOHN D. WANG**

Part II

**Analytical Models For One- and Two-
Layer Systems in Rectangular Basins**

by

DOUGLAS A. BRIGGS

and **OLE S. MADSEN**

MIT
=

RALPH M. PARSONS LABORATORY

for

WATER RESOURCES AND HYDRODYNAMICS

Report No. 172

Prepared with the Support of
Sea Grant Office

National Oceanographic and
Atmospheric Administration

Department of Commerce Washington, D.C.

October 1973

ENG

MIT



**DEPARTMENT
OF
CIVIL
ENGINEERING**



**SCHOOL OF ENGINEERING
MASSACHUSETTS INSTITUTE OF TECHNOLOGY
Cambridge, Massachusetts 02139**

MATHEMATICAL MODELS OF THE MASSACHUSETTS BAY

PART I. FINITE ELEMENT MODELING OF TWO-
DIMENSIONAL HYDRODYNAMIC CIRCULATION

BY

JEROME J. CONNOR

AND

JOHN D. WANG

PART II. ANALYTICAL MODELS FOR ONE- AND TWO-
LAYER SYSTEMS IN RECTANGULAR BASINS

BY

DOUGLAS A. BRIGGS

AND

OLE S. MADSEN

RALPH M. PARSONS LABORATORY
FOR WATER RESOURCES AND HYDRODYNAMICS

Department of Civil Engineering
Massachusetts Institute of Technology

Report No. 172

Prepared with the Support of

Sea Grant Office
National Oceanographic and Atmospheric Administration
Department of Commerce
Washington, D.C.

October 1973

MATHEMATICAL MODELS OF THE MASSACHUSETTS BAY

PART I

FINITE ELEMENT MODELING OF TWO-DIMENSIONAL
HYDRODYNAMIC CIRCULATION IN SHALLOW WATER MASSES

BY

JEROME J. CONNOR

and

JOHN D. WANG

RALPH M. PARSONS LABORATORY
FOR WATER RESOURCES AND HYDRODYNAMICS
Department of Civil Engineering
Massachusetts Institute of Technology

Report No. 172

Prepared with the Support of

Sea Grant Office
National Oceanographic and Atmospheric Administration
Department of Commerce
Washington, D.C.

October 1973

71-190

MATHEMATICAL MODELS OF THE MASSACHUSETTS BAY

ABSTRACT - PART I

FINITE ELEMENT MODELING OF TWO-DIMENSIONAL
HYDRODYNAMIC CIRCULATION IN SHALLOW WATER MASSES

BY

JEROME J. CONNOR

and

JOHN D. WANG

The vertically integrated conservation of mass and momentum equations for shallow water bodies are reviewed. The equations used in this study are based on only two assumptions: hydrostatic pressure and squares of surface elevation gradients negligible with respect to unity. The finite element method is applied to reduce the governing equations to a system of ordinary non-linear differential equations in time for which two different numerical integration schemes are described. Model results are compared with analytical solutions. Also, numerical predictions of the tidal response for Massachusetts Bay are presented.

PART I

ACKNOWLEDGEMENTS

This study constitutes a part of a series of investigations in a major environmental research program on the "Sea Environment in Massachusetts Bay and Adjacent Waters". This program consists of theoretical and field investigations and is under the administrative and technical direction of Dr. Arthur T. Ippen, Institute Professor, Department of Civil Engineering and of Dr. Erik L. Mollo-Christensen, Professor, Department of Meteorology as co-principal investigators. Support of the program is provided in part by the Sea Grant Office of NOAA, Department of Commerce, Washington, D.C. through Grant No. NG-43-72, in part by the Henry L. and Grace Doherty Charitable Foundation, Inc., and in part by the Department of Natural Resources, Commonwealth of Massachusetts through Project No. DMR-73-1. The project which is the subject of this report was conducted by staff members of the Ralph M. Parsons Laboratory for Water Resources and Hydrodynamics and was administered under Project No. DSR 80344 and DSR 81100 at M.I.T.

This report was prepared by Mr. John D. Wang, Research Assistant, and Dr. Jerome J. Connor, Professor of Civil Engineering. The advice and guidance of Dr. Arthur T. Ippen is hereby gratefully acknowledged.

Appreciation is expressed here to Ms. Stephanie M. Demeris for her excellent typing of this manuscript.

TABLE OF CONTENTS

	<u>Page</u>
ABSTRACT	1
TABLE OF CONTENTS	2
LIST OF FIGURES	3
LIST OF SYMBOLS	5
CHAPTER 1 INTRODUCTION	9
CHAPTER 2 BASIC HYDRODYNAMIC EQUATIONS	11
CHAPTER 3 VARIATIONAL STATEMENT	20
CHAPTER 4 FINITE ELEMENT MODEL	22
CHAPTER 5 NUMERICAL INTEGRATION SCHEMES	27
CHAPTER 6 MODEL COMPARISONS AND RESULTS	31
REFERENCES	56

LIST OF FIGURES

<u>Figure</u>		<u>Page</u>
1	Geometrical and Surface Force Notation	12
2	Boundary Notation	17
3	Finite Element Geometric Discretization	23
4	Sketch of Rectangular Channel	32
5	Comparison of Numerical and Analytical Solutions	34
6	Rectangular Model of Massachusetts Bay Analytical Solutions	36
7	Rectangular Model of Massachusetts Bay Dimensions and Element Layout	37
8	Rectangular Model of Massachusetts Bay Finite Element Solution. Surface Elevations	38
9	Rectangular Model of Massachusetts Bay Finite Element Solution. Currents	39
10	Massachusetts Bay. Geographical Boundaries and Finite Element Grid	41
11	Massachusetts Bay Surface Contour Lines at High Tide	42
12	Massachusetts Bay Surface Contour Lines at Low Tide	43
13	Massachusetts Bay Currents at Ebbing Tide	44
14	Massachusetts Bay Currents at Flooding Tide	45
15	Time History of Computed Elevations at Boston and in Cape Cod Bay	46
16	Time History of Computed Currents a. Center of Cape Cod Bay b. 15 km East of Boston	47

<u>Figure</u>		<u>Page</u>
17	Computed Current Field due to Wind Forcing from the North. No Tidal Motion. Steady-state Reached	50
18	Computed Current Field due to Wind Forcing from the South-West. No Tidal Motion. Steady-state Reached	51
19	Superposition of Computed Flood Tide Currents and Wind Driven Currents	52
20	Superposition of Computed Ebb Tide Currents and Wind Driven Currents	53
21	Flood Tide and Wind Driven Current Field	54
22	Ebb Tide and Wind Driven Current Field	55

LIST OF SYMBOLS

A	area
a	tidal amplitude
B_x^*	sum of surface and bottom stress terms in x-direction
B_y^*	sum of surface and bottom stress terms in y-direction
B_x	sum of surface, bottom, coriolis and nonlinear force measures in x-direction
B_y	sum of surface, bottom, coriolis and nonlinear force measures in y-direction
b	superscript signifying bottom
C_f	bottom friction factor
c	wave velocity = \sqrt{gh}
E	truncation error
e	mass source per unit volume
e	superscript signifying eddy viscosity term
(e)	superscript signifying element
f	coriolis parameter = $2\Omega \sin \phi$
f	function
F_p	pressure force resultant
F_{nn}	} internal stress resultants
F_{ns}	
F_{xx}	
F_{yy}	
$F_{xy} = F_{yx}$	

g	gravitational acceleration
g	function
H	total depth = $h+\eta$
h	mean low water (chart) depth
i	subscript signifying node i
k_1, k_2 k_3, k_4	integration variables
L	channel length
M	"mass" matrix
n_1, n_2, n_3	modes of element n
n	normal (outward) coordinate
P	force matrix
p	pressure
Q	velocity component matrix
q_x	mass flux in x-direction
q_y	mass flux in y-direction
q_I	distributed mass inflow per unit area
R	residual
S	boundary
S_f	flux boundary
S_o	ocean boundary
s	tangential coordinate
s	supercript signifying surface
T	tidal period

T	supercript signifying transpose of matrix
t	time
u	x-velocity
v	y-velocity
w	z-velocity
x,y,z	orthogonal coordinates forming a right-handed system. z vertical upwards, x towards east
α	direction cosine
Δt	time increment
$\Delta H, \Delta q_x,$ $\Delta q_y, \Delta Q$	weighting functions
δ	grid dimension measure
δ_ρ	incremental density
$\epsilon_{xx}, \epsilon_{yy},$ ϵ_{xy}	eddy viscosities
ϵ_h	convergence tolerance for heights
ϵ_Q	convergence tolerance for velocities
ζ	function
η	surface elevation above MLW
θ_h	relaxation factor for heights
θ_Q	relaxation factor for velocities
ρ	density
ρ_o	average density
τ	stress
Φ	expansion function
ϕ	latitude

- Ω phase velocity of earth's rotation
- ω phase velocity of tidal excitation
- , (comma) subscript signifying partial differentiation
- . (punctuation) superscript signifying time derivative

CHAPTER 1

INTRODUCTION

Mathematical modelling of circulation and dispersion in water bodies has developed rapidly during the past decade. The major impetus has been the concern for the environment which has necessitated more detailed studies of water quality and especially the development of transient predictive models.

This study is restricted to the development and evaluation of finite element models for predicting the transient response of water bodies due to tidal and wind excitation. Three dimensional solutions are most desirable but the uncertainty of boundary conditions and in the magnitudes of the eddy viscosities and turbulent diffusion coefficients does not justify the effort at this time. Therefore, this study is further restricted to vertically well-mixed two dimensional flow. Irregularity of the boundary geometry and depth are allowed for but the velocities are assumed to be approximately uniform over the depth.

There are a number of recent reports [1-7] describing finite difference models for circulation and dispersion in well-mixed estuaries and coastal waters. The proposed models by Leendertse et al. [3] and Abbot et al [7] appear to be well documented and have extensive supporting software for data generation and plotting.

Finite difference models employ rectangular grids and one has to resort to approximating an irregular boundary with orthogonal segments. This requires a small mesh spacing throughout the domain. Approximate techniques for expanding the mesh in the interior have

been employed but they can introduce additional numerical difficulties.

The finite element method was first applied to fluid flow by Martin [8] who treated two-dimensional steady potential flow. It has since been extended to Navier-Stokes flow [9], lake circulation [10,11], and long wave propagation (12). The method has proven to be particularly convenient for problems involving irregular boundaries since the mesh can be chosen to "fit" the boundary. However, relatively little experience with finite element transient solutions of hyperbolic equations has been accumulated in contrast to finite difference models where stability has been studied extensively [15,16].

In what follows, a consistent derivation of the vertically averaged equations for long wave propagation is presented. The formulation is sufficiently different from existing formulations (Pritchard, Ref. 2) to warrant its inclusion here. Next, the method of weighted residuals [14] is applied to generate a "quasi" variational statement which is the basis for the finite element discretization. Three numerical integration schemes are evaluated for one and two-dimensional test problems discretized with first order triangular elements. The scheme is also applied to Massachusetts Bay, a fairly complex coastal area, and a solution strategy for "adjusting" the bottom friction is discussed.

CHAPTER 2

BASIC HYDRODYNAMIC EQUATIONS

The 3-dimensional forms of the ensemble averaged continuity and momentum equations constitute the basis for the present formulation.

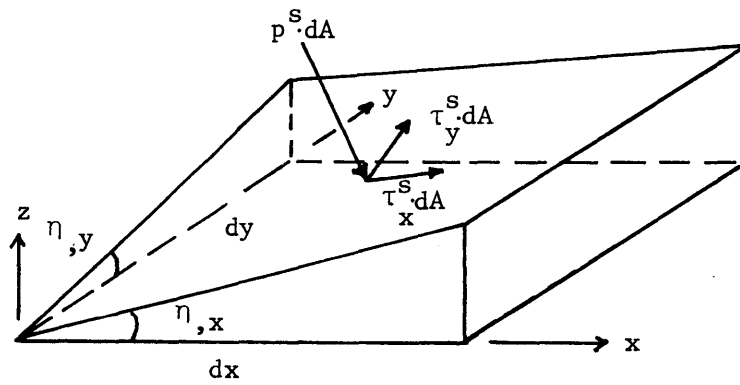
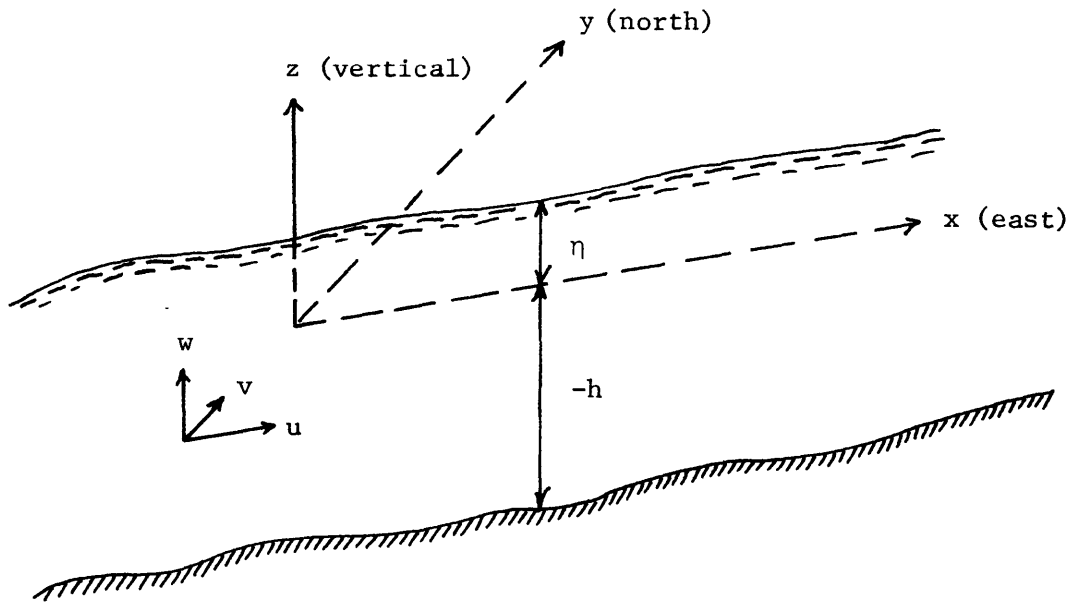
They are

$$\begin{aligned} \frac{\partial \rho}{\partial t} + (\rho u)_{,x} + (\rho v)_{,y} + (\rho w)_{,z} &= e \\ (\rho u)_{,t} + (\rho u^2)_{,x} + (\rho uv)_{,y} + (\rho uw)_{,z} \\ &= \rho f v - p_{,x} + \tau_{xx,x} + \tau_{yx,y} + \tau_{zx,z} \end{aligned} \quad (1)$$

$$\begin{aligned} (\rho v)_{,t} + (\rho uv)_{,x} + (\rho v^2)_{,y} + (\rho vw)_{,z} \\ &= -\rho f u - p_{,y} + \tau_{xy,x} + \tau_{yy,y} + \tau_{zy,z} \end{aligned}$$

where u, v, w are the averaged velocities, e is a source of mass inflow per unit volume, τ are the sums of viscous and Reynolds stresses, ρ is mass density and f is the Coriolis parameter. By definition, the stress components are symmetrical with respect to the subscripts, i.e., $\tau_{xy} = \tau_{yx}$, etc.

A set of 2-dimensional equations is obtained by integrating (1) over the total depth and applying Leibnitz's rule. The notation and the applied surface forces are shown in Figure 1. We assume the surface slope is small and neglect $(\eta_{,x})^2, (\eta_{,y})^2$ with respect to unity. With this approximation, the surface force-interior stress relations for the upper surface reduce to



$$[\eta_{,x}]^2 \ll 1$$

$$[\eta_{,y}]^2 \ll 1$$

$$dA \approx dx dy$$

Figure 1. Geometrical and surface force notation.

$$\begin{aligned}
 \tau_x^s + \eta_{,x} p^s &= \left| -\eta_{,x} (-p + \tau_{xx}) - \eta_{,y} \tau_{yx} + \tau_{zx} \right|_{z=\eta} \\
 \tau_y^s + \eta_{,y} p^s &= \left| -\eta_{,x} \tau_{xy} - \eta_{,y} (-p + \tau_{yy}) + \tau_{zy} \right|_{z=\eta} \\
 -p^s + \eta_{,x} \tau_x^s + \eta_{,y} \tau_y^s &= \left| -p + \tau_{zz} - \eta_{,x} \tau_{xz} - \eta_{,y} \tau_{yz} \right|_{z=\eta}
 \end{aligned} \tag{2}$$

where τ^s are the applied tangential wind stresses and p^s is the external pressure. A similar set applies for the bottom surface.

Leibnitz's rule defines partial differentiation of an integral having variable limits. Its form for x differentiation is

$$\frac{\partial}{\partial x} \int_{g_1}^{g_2} f dz = \int_{g_1}^{g_2} \frac{\partial f}{\partial x} dz + f \Big|_{g_2} \frac{\partial g_2}{\partial x} - f \Big|_{g_1} \frac{\partial g_1}{\partial x} \tag{3}$$

Using the general form of (3) and applying the kinematic relation

$$w \Big|_{z=\zeta} = \frac{D\zeta}{Dt} = \frac{\partial \zeta}{\partial t} + u \frac{\partial \zeta}{\partial x} + v \frac{\partial \zeta}{\partial y} \tag{4}$$

at $\zeta = \eta$ and $\zeta = -h$, assuming the density is constant over depth results in the following "integrated" equations:

$$\begin{aligned}
 \frac{\partial}{\partial t}(\rho H) + \frac{\partial}{\partial x} q_x + \frac{\partial}{\partial y} q_y &= q_I \\
 \frac{\partial}{\partial t} q_x + \frac{\partial}{\partial x} \left(\rho \int_{-h}^{\eta} u^2 dz \right) + \frac{\partial}{\partial y} \left(\rho \int_{-h}^{\eta} uv dz \right) \\
 &= f q_y + \tau_x^s + \tau_x^b + p^s \frac{\partial \eta}{\partial x} + p^b \frac{\partial h}{\partial x} \\
 &+ \frac{\partial}{\partial x} \int_{-h}^{\eta} (-p + \tau_{xx}) dz + \frac{\partial}{\partial y} \int_{-h}^{\eta} \tau_{yx} dz
 \end{aligned} \tag{5}$$

$$\begin{aligned} \frac{\partial}{\partial t} q_y + \frac{\partial}{\partial x} \left(\rho \int_{-h}^{\eta} uvdz \right) + \frac{\partial}{\partial y} \left(\rho \int_{-h}^{\eta} v^2 dz \right) \\ = -fq_x + \tau_y^s + \tau_y^b + p^s \frac{\partial \eta}{\partial y} + p^b \frac{\partial h}{\partial y} \\ + \frac{\partial}{\partial x} \int_{-h}^{\eta} \tau_{xy} dz + \frac{\partial}{\partial y} \int_{-h}^{\eta} (-p + \tau_{yy}) dz \end{aligned}$$

where

$$H = h + \eta$$

$$q_x = \rho \int_{-h}^{\eta} u dz$$

$$q_y = \rho \int_{-h}^{\eta} v dz$$

and q_I is the distributed mass inflow per unit area.

To integrate the nonlinear advective terms we express the velocity components as

$$\begin{aligned} u &= \bar{u}(x,y,t) + u'(x,y,z,t) \\ v &= \bar{v}(x,y,t) + v'(x,y,z,t) \end{aligned} \tag{6}$$

where \bar{u} , \bar{v} denote the vertically averaged velocities and u' , v' represent the vertical deviations. By definition,

$$\begin{aligned} q_x &\equiv \rho H \bar{u} \\ q_y &\equiv \rho H \bar{v} \end{aligned} \tag{7}$$

$$\int_{-h}^{\eta} u' dz = \int_{-h}^{\eta} v' dz = 0$$

Introducing (6) in (5) and grouping terms in a form similar to the 3-dimensional momentum equations, we write the "integrated" momentum equations as

$$\begin{aligned} \frac{\partial}{\partial t}(\rho H) + \frac{\partial}{\partial x} q_x + \frac{\partial}{\partial y} q_y &= q_I \\ \frac{\partial}{\partial t} q_x + \frac{\partial}{\partial x}(\bar{u}q_x) + \frac{\partial}{\partial y}(\bar{v}q_y) &= fq_y + B_x^* + \frac{\partial}{\partial x}(F_{xx} - F_p) + \frac{\partial}{\partial y} F_{yx} \\ \frac{\partial}{\partial t} q_y + \frac{\partial}{\partial x}(\bar{v}q_x) + \frac{\partial}{\partial y}(\bar{v}q_y) &= -fq_x + B_y^* + \frac{\partial}{\partial x} F_{xy} + \frac{\partial}{\partial y}(F_{yy} - F_p) \end{aligned} \quad (8)$$

where B_x^* , B_y^* contain the surface and bottom stress terms, F_p is the pressure force resultant and F_{xx} , F_{xy} , F_{yy} are "equivalent" internal stress resultants due to turbulent and dispersive momentum flux.

$$\begin{aligned} F_p &= \int_{-h}^{\eta} p dz \\ F_{xx} &= \int_{-h}^{\eta} (\tau_{xx} - \rho(u')^2) dz \\ F_{yy} &= \int_{-h}^{\eta} (\tau_{yy} - \rho(v')^2) dz \\ F_{xy} &= F_{yx} = \int_{-h}^{\eta} (\tau_{xy} - \rho u'v') dz \end{aligned} \quad (9)$$

We approximate the flux terms with

$$\begin{aligned} F_{xx} &= \epsilon_{xx} \frac{\partial}{\partial x} q_x \\ F_{yy} &= \epsilon_{yy} \frac{\partial}{\partial y} q_y \\ F_{yx} &= F_{xy} = \epsilon_{xy} \left(\frac{\partial}{\partial y} q_x + \frac{\partial}{\partial x} q_y \right) \end{aligned} \quad (10)$$

One can interpret the ϵ 's as either equivalent Fickian diffusion coefficients or generalized eddy viscosities. In (10) we have allowed for orthotropic behavior. For isotropic flow, (10) applies for arbitrary orientation of x , y , and therefore one has

$$\begin{aligned}\epsilon_{xx} &= \epsilon_{yy} = 2\epsilon \\ \epsilon_{xy} &= \epsilon\end{aligned}\tag{11}$$

Next, we assume the pressure variation with z is hydrostatic,

$$p = \rho g(\eta - z) + p^s\tag{12}$$

and the bottom shear is predicted by a quadratic relation,

$$\begin{aligned}\tau_x^b &= -\frac{C_f}{\rho H^2} q_x (q_x^2 + q_y^2)^{1/2} \\ \tau_y^b &= -\frac{C_f}{\rho H^2} q_y (q_x^2 + q_y^2)^{1/2}\end{aligned}\tag{13}$$

where C_f is a friction factor.

The corresponding forces are

$$\begin{aligned}F_p &= \int_{-h}^{\eta} p dz = p^s H + \frac{\rho g}{2} H^2 \\ B_x^* &= \tau_x^s + \tau_x^b + p^s \frac{\partial H}{\partial x} + \rho g H \frac{\partial h}{\partial x} \\ B_y^* &= \tau_y^s + \tau_y^b + p^s \frac{\partial H}{\partial y} + \rho g H \frac{\partial h}{\partial y}\end{aligned}\tag{14}$$

Lastly, we express the mass density as

$$\rho = \rho_0 + \delta\rho\tag{15}$$

where ρ_0 is constant. The incremental density $\delta\rho$ is small in comparison to ρ_0 for circulation in coastal waters and estuaries. Therefore, we set $\rho = \rho_0$ except for the pressure force terms. This is the Boussinesq approximation.

To complete the formulation, we need to establish the boundary conditions. The total boundary, S , consists of flux segments, S_f , and ocean segments, S_o , as shown in Figure 2. We refer the flux and

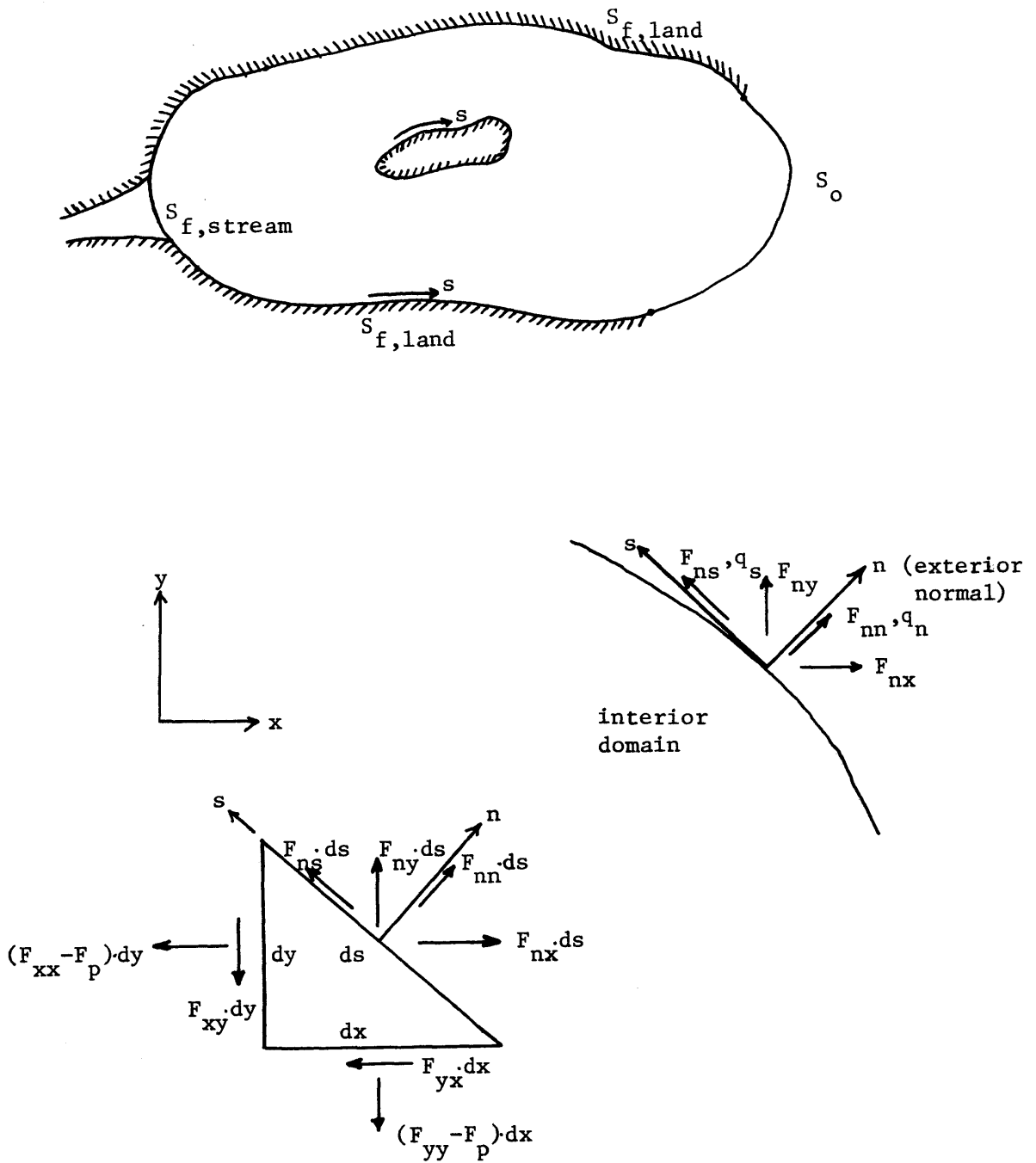


Figure 2. Boundary notation.

boundary force measures to the local reference frame defined by the exterior normal, n , and the tangential direction, s , where $n \rightarrow s$ has the same sense as $x \rightarrow y$.

Mass flux is a vector quantity and its components transform according to

$$q_n = \int_{-h}^{\eta} \rho u_n dz = \alpha_{nx} q_x + \alpha_{ny} q_y$$

$$q_s = \int_{-h}^{\eta} \rho u_s dz = -\alpha_{ny} q_x + \alpha_{nx} q_y \quad (16)$$

$$\alpha_{nx} = \cos(n,x) \quad \alpha_{ny} = \cos(n,y)$$

Consistent with interpreting the momentum flux due to nonuniform velocity distribution through the depth as equivalent internal force resultants, we write

$$F_{nx} = \alpha_{nx} (F_{xx} - F_p) + \alpha_{ny} F_{yx}$$

$$F_{ny} = \alpha_{nx} F_{xy} + \alpha_{ny} (F_{yy} - F_p) \quad (17)$$

and then transform according to (16), obtaining

$$F_{nn} = -F_p + F_{nn}^e$$

$$F_{ns} = F_{ns}^e \quad (18)$$

$$F_{nn}^e = \alpha_{nx}^2 F_{xx} + \alpha_{ny}^2 F_{yy} + 2\alpha_{nx} \alpha_{ny} F_{xy}$$

$$F_{ns}^e = (\alpha_{nx}^2 - \alpha_{ny}^2) F_{xy} + \alpha_{nx} \alpha_{ny} (F_{yy} - F_{xx})$$

On a land boundary (assuming no tidal flats), the flux components are prescribed.

$$q_n = q_s = 0 \quad \text{on } S_{f,land} \quad (19)$$

On an ocean boundary, the normal and tangential boundary forces are prescribed.

$$\begin{aligned} F_{nn} &= \bar{F}_{nn} \\ F_{ns} &= \bar{F}_{ns} \end{aligned} \quad \text{on } S_o \quad (20)$$

On flux boundaries other than land such as at river entrances the normal flux is specified equal to the river mass flow.

$$\begin{aligned} q_n &= \bar{q}_{river} \\ q_s &= 0 \end{aligned} \quad \text{on } S_{river} \quad (21)$$

When the eddy viscosities are neglected, $F^e = 0$, and we cannot prescribe the tangential flux or tangential boundary force. The boundary conditions reduce to

$$q_n = \bar{q}_n \quad \text{on } S_f \quad (22)$$

and

$$F_{nn} = \bar{F} \quad \text{on } S_o \quad (23)$$

In the present model application, equation (23) with $\bar{F}_{nn} = -F_p$ is used although eddy viscosities are assumed non zero in the interior.

CHAPTER 3

VARIATIONAL STATEMENT

The governing equations are (8) and the appropriate boundary conditions. In what follows, we apply Galerkin's method [14] to establish the variational statements which are the basis for the finite element method.

Let ΔH , Δq_x , Δq_y represent weighting functions. We weight the continuity equation with respect to ΔH , the momentum equations with respect to Δq , integrate over the domain, and require the residuals to vanish. We also weight the force boundary conditions on S_0 . The resulting expressions are

$$\iint_A \{ (\rho_0 H)_{,t} + q_{x,x} + q_{y,y} - q_I \} \Delta H dA = 0 \quad (24)$$

and

$$\iint_A \{ q_{x,t} - \frac{\partial}{\partial x} (F_{xx} - F_p) - \frac{\partial}{\partial y} F_{yx} - B_x \} \Delta q_x dA = 0$$

$$\iint_A \{ q_{y,t} - \frac{\partial}{\partial x} F_{xy} - \frac{\partial}{\partial y} (F_{yy} - F_p) - B_y \} \Delta q_y dA = 0 \quad (25)$$

$$\int_{S_0} \{ -\bar{F}_{nx} + \alpha_{nx} (F_{xx} - F_p) + \alpha_{ny} F_{yx} \} \Delta q_x dS = 0$$

$$\int_{S_0} \{ -\bar{F}_{ny} + \alpha_{nx} F_{xy} + \alpha_{ny} (F_{yy} - F_p) \} \Delta q_y dS = 0$$

Here we have included the Coriolis and nonlinear terms in B.

$$B_x = B_x^* + f_{q_y} - \frac{\partial}{\partial x}(\bar{u}q_x) - \frac{\partial}{\partial y}(\bar{u}q_y) \quad (26)$$

$$B_y = B_y^* - f_{q_x} - \frac{\partial}{\partial x}(\bar{v}q_x) - \frac{\partial}{\partial y}(\bar{v}q_y)$$

Applying Gauss's theorem to eliminate the derivatives of the force terms in the momentum equations and combining with the boundary equations leads to the desired form:

$$\begin{aligned} & \iint_A \{ (q_{x,t} - B_x) \Delta q_x + (F_{xx} - F_p)(\Delta q_x)_{,x} + F_{yx}(\Delta q_x)_{,y} \} dA \\ & - \int_{S_o} \bar{F}_{nx} \Delta q_x dS = 0 \\ & \iint_A \{ (q_{y,t} - B_y) \Delta q_y + F_{xy}(\Delta q_y)_{,x} + (F_{yy} - F_p)(\Delta q_y)_{,y} \} dA \\ & - \int_{S_o} \bar{F}_{ny} \Delta q_y dS = 0 \end{aligned} \quad (27)$$

We have required the flux weighting functions to vanish on S_f ,

$$\Delta q_x = \Delta q_y = 0 \quad \text{on } S_f \quad (28)$$

and consequently the boundary integrals on S_f drop out of (27).

CHAPTER 4

FINITE ELEMENT MODEL

The continuity equation (24) and modified momentum equations (27,28) are the starting point for the finite element method. We visualize the domain to consist of subdomains (elements) and take as variables the values of q_x , q_y , H at the points (nodes) defining the discretization. This is illustrated in Figure 3. The distribution of a dependent variable over an elemental domain is expressed in terms of the values of the variable at nodes contained in the element domain and interpolation functions. In this way, the equations are transformed to a set of algebraic equations relating the discrete variables. In the present formulation the simplest elements, viz. triangular with linear interpolation functions, were chosen. However, more complex elements and expansion functions will be implemented in future modeling.

We define the following notation:

$$q_{xi}, q_{yi}, H_i = \text{values at node } i$$

$$\tilde{q}_x^{(e)}, \tilde{q}_y^{(e)}, \tilde{H}^{(e)} \text{ are matrices containing the nodal variables}$$

for an element

(29)

$$N = \text{number of nodes}$$

$$\tilde{Q} = \{q_{x1}, q_{y1}, q_{x2}, \dots, q_{yN}\} = \text{system flux matrix (2N nodal values)}$$

$$\tilde{H} = \{H_1, H_2, \dots, H_N\} = \text{system elevation matrix (N nodal values)}$$

For example, $\tilde{H}^{(e)} = \{H_{n1}, H_{n2}, H_{n3}\}$ for the triangular element shown in Figure 3. The expansions are written as

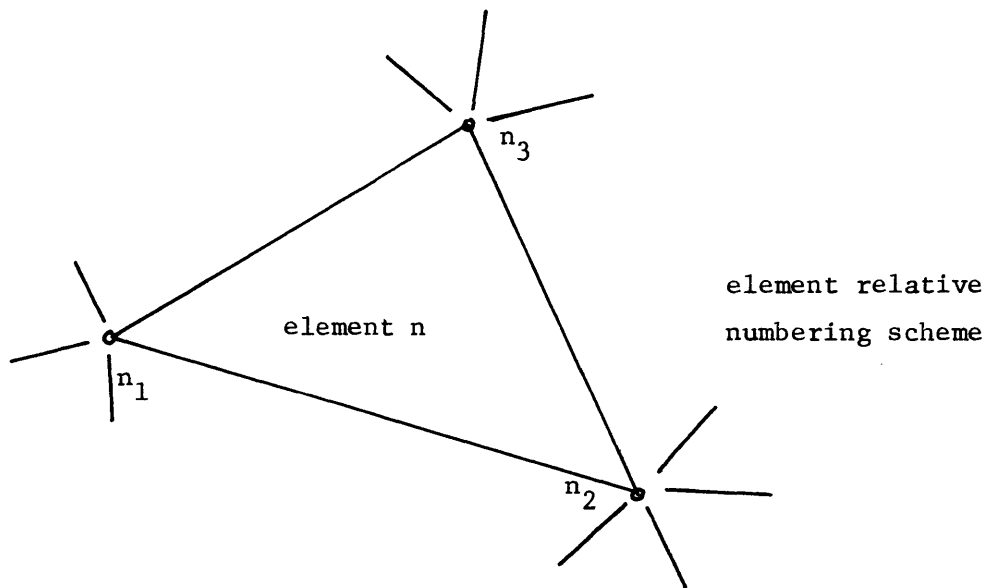
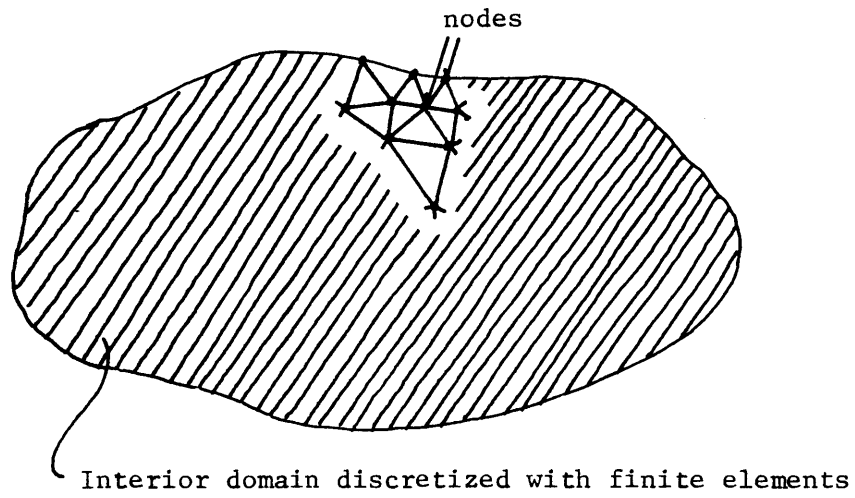


Figure 3. Finite element geometric discretization.
 n_1 , n_2 , n_3 are the actual node numbers
for the nodes in the domain of element n .

$$\begin{aligned}
 q_x &= \tilde{\Phi} q_x^{(e)} \\
 q_y &= \tilde{\Phi} q_y^{(e)} \\
 H &= \tilde{\Phi} H^{(e)}
 \end{aligned}
 \tag{30}$$

where $\tilde{\Phi}$ is a row matrix. We are considering 3 variables per node. One can generalize the approach and allow for a variable number of unknowns per node, i.e., different expansions for flux and elevation, but we prefer to work with the simplest scheme.

In the Galerkin method, one takes the weighting functions identical to the coordinate functions. Since the finite element method employs local functions, the weighting function for a particular nodal variable is finite (non-zero) only for those elements incident on the node. Rather than treat individual nodes, it is more convenient to evaluate element residuals and then superimpose the element contributions at the nodes.

Taking the complete set of weighting functions for an element as

$$\begin{aligned}
 \Delta q_x &= \tilde{\Phi} \Delta q_x^{(e)} \\
 \Delta q_y &= \tilde{\Phi} \Delta q_y^{(e)} \\
 \Delta H &= \tilde{\Phi} \Delta H^{(e)}
 \end{aligned}
 \tag{31}$$

and substituting in (24), (27) results in the following element residuals:

$$\begin{aligned}
 R|_{e1} &= (\Delta q_x^{(e)})^T (M_x^e \frac{\partial q_x^{(e)}}{\partial t} + P_x^e) \\
 &+ (\Delta q_y^{(e)})^T (M_y^{(e)} \frac{\partial q_y^{(e)}}{\partial t} + P_y^{(e)}) \\
 &+ (\Delta H^{(e)})^T (M_h^{(e)} \frac{\partial H^{(e)}}{\partial t} + P_h^{(e)})
 \end{aligned} \tag{32}$$

where

$$\begin{aligned}
 M_x^{(e)} &= \iint_A \phi^T \mathbf{T} \phi \, dA \\
 P_x^{(e)} &= \iint_A [-\phi^T B_x + \phi_{,x}^T (F_{xx} - F_p) + \phi_{,y}^T F_{xy}] \, dA \\
 &\quad - \int_{S_o} \phi^T \bar{F}_{nx} \, dS \\
 P_y^{(e)} &= \iint_A [-\phi^T B_y + \phi_{,x}^T F_{xy} + \phi_{,y}^T (F_{yy} - F_p)] \, dA \\
 &\quad - \int_{S_o} \phi^T \bar{F}_{ny} \, dS \\
 P_h^{(e)} &= \frac{1}{\rho_o} \iint_A \phi^T (q_{x,x} + q_{y,y} - q_I) \, dA
 \end{aligned} \tag{33}$$

The forces and flux derivatives in (33) are evaluated using (30) and the force expressions (10), (14), (26).

The total residual must vanish for arbitrary Δq_{xi} , Δq_{yi} , ΔH_i ($i = 1, 2, \dots, N$). Then,

$$R|_{\text{total}} = \sum_{\text{elements}} R|_{e1} = 0 \quad (34)$$

for arbitrary ΔQ , ΔH .

We write the expanded form of (34) as

$$R|_{\text{total}} = (\Delta Q)^T \left(\underline{M} \frac{\partial}{\partial t} \underline{Q} + \underline{P} \right) + (\Delta H)^T \left(\underline{M}_h \frac{\partial}{\partial t} \underline{H} + \underline{P}_h \right) \quad (35)$$

and it follows that

$$\underline{M} \dot{\underline{Q}} + \underline{P} = \underline{0} \quad (36)$$

$$\underline{M}_h \dot{\underline{H}} + \underline{P}_h = \underline{0}$$

Finally, we introduce the boundary conditions by modifying the rows and columns of \underline{M} corresponding to the prescribed variables and incorporating the prescribed terms in \underline{P} . To minimize notation proliferation, we assume (36) represent the final constrained equations.

CHAPTER 5

NUMERICAL INTEGRATION SCHEMES

Efficient stable numerical integration schemes are essential since a typical problem will involve several hundred node points and integrations over at least one tidal cycle. Complex multi-step methods, although more accurate, require considerably more computation time and storage. Therefore, we have concentrated in this study on investigating the stability and accuracy of relatively simple implicit schemes.

Explicit stability criteria for finite element formulations such as (36) have not yet been developed. The difficulty is due to the arbitrariness of the coefficient matrices (i.e., the elements are confined to a zone adjacent to the diagonal but their magnitudes may be irregular) and also the skew symmetry of the Coriolis and surface elevation terms. One generally has to resort to approximate stability measures based on norms. We make no attempt here to resolve this problem since our primary objective is to evaluate the performance of various schemes.

The simplest scheme is the trapezoidal rule. Its one dimensional form is

$$\begin{aligned} \frac{dy}{dt} &= f(y,t) \\ y_{n+1} - y_n &= \frac{\Delta t}{2} (f_{n+1} + f_n) + E\Delta t \\ E &= \frac{1}{12}(\Delta t)^2 \left| \frac{d^2 f}{dt^2} \right|_{\xi} \quad t_n < \xi < t_{n+1} \end{aligned} \tag{37}$$

Iteration is required since the forcing terms in (36) are non-linear. We include a relaxation factor to accelerate convergence and evaluate the terms in the following order:

$$M_{\tilde{h}}(H^* - H_{\tilde{n}}) = \frac{\Delta t}{2} (P_{\tilde{h},n+1}^{j-1} + P_{\tilde{h},n})$$

$$H_{\tilde{n}+1}^j = \Theta_h H^* + (1 - \Theta_h) H_{\tilde{n}+1}^{j-1}$$

and

$$P_{\tilde{n}+1}^{j-1} = P(H_{\tilde{n}+1}^j, Q_{\tilde{n}+1}^{j-1}, t_{n+1}) \quad (38)$$

$$M(Q^* - Q_{\tilde{n}}) = \frac{\Delta t}{2} (P_{\tilde{n}+1}^{j-1} + P_{\tilde{n}})$$

$$Q_{\tilde{n}+1}^j = \Theta_Q Q^* + (1 - \Theta_Q) Q_{\tilde{n}+1}^{j-1}$$

The mass matrices are factored initially and the iteration and time stepping consists of successive forward and backward substitutions. Convergence is defined by the percentage change in the Euclidian norms for the surface elevation and mass flux vectors.

$$\left(\frac{\sum_{i=1}^N (H_{n+1}^{j+1} - H_{n+1}^j)_i^2}{\sum_{i=1}^N (H_{n+1}^{j+1})_i^2} \right)^{1/2} \leq \epsilon_h$$

(39)

$$\left(\frac{\sum_{i=1}^{2N} (Q_{n+1}^{j+1} - Q_{n+1}^j)_i^2}{\sum_{i=1}^{2N} (Q_{n+1}^{j+1})_i^2} \right)^{1/2} \leq \epsilon_Q$$

where N is the total number of nodes, and ϵ_h, ϵ_Q are the specified tolerances.

The second method examined is the third order predictor-corrector iterative scheme,

$$\frac{dy}{dt} = f(y,t)$$

Predictor:

$$f_{n+1}^1 = 3f_n - 3f_{n-1} + f_{n-2}$$

Corrector:

$$y^* - y_n = \frac{\Delta t}{12}(5f_{n+1}^{j-1} + 8f_n - f_{n-1}) + E \Delta t$$

$$y_{n+1}^j = \Theta y^* + (1 - \Theta) y_{n+1}^{j-1}$$

$$E = \frac{1}{12}(\Delta t)^3 \left| \frac{d^3 f}{dt^3} \right|_{\xi} \quad t_n < \xi < t_{n+1}$$

(40)

This scheme is not self-starting and requires more storage than the trapezoidal rule. However, it is more accurate and usually converges faster. Equations (39) are again taken as the convergence criteria.

The predictor-corrector scheme (40) is coupled with the following version of the fourth order Runge-Kutta method,

$$\frac{dy}{dt} = f(y,t)$$

$$k_1 = \Delta t \cdot f(y_n, t_n)$$

$$k_2 = \Delta t \cdot f(y_n + 0.4k_1, t_n + 0.4\Delta t)$$

$$k_3 = \Delta t \cdot f(y_n + 0.296978k_1 + 0.158760k_2, t_n + 0.455737\Delta t) \quad (41)$$

$$k_4 = \Delta t \cdot f(y_n + 0.218100k_1 - 3.050965k_2 + 3.832864k_3, t_n + \Delta t)$$

$$y_{n+1} = y_n + 0.174760k_1 - 0.551481k_2 + 1.205535k_3 + 0.171185k_4$$

$$E = O(\Delta t^4)$$

This scheme has the lowest bound on the error for this family of Runge-Kutta methods [15].

The solution of a given problem begins with an optional number of integration steps using the Runge-Kutta method, (minimum three time steps) and then shifts to the predictor-corrector method. At any time step it is possible to change back to the Runge-Kutta method to take advantage of its better accuracy. This flexible formulation also makes it very easy to increase or decrease the time increment, Δt , if so desired.

CHAPTER 6

MODEL COMPARISONS AND RESULTS

The objective of this study is to develop a general numerical model for the prediction of 2-dimensional hydrodynamic circulation in waterbodies which are well-mixed through the water column.

Several example problems for which analytical solutions are readily obtainable were solved with the finite element numerical model. These examples demonstrate how the model performs in situations of varying geometry and also show the effect of eddy diffusivity on damping short "noise" waves generated by the numerical scheme due to truncation and round-off errors. A circulation analysis for Massachusetts Bay was carried out.

The initial numerical solutions with the trapezoidal rule required an average of 7 iterations per time step to obtain comparable results. Since the higher accuracy Runge-Kutta method only requires 4 evaluations of the integrand per time step, this was found unsatisfactory. Convergence with the trapezoidal rule can be accelerated by extrapolating the integrand at the start of each new time step. However, this necessitates more storage and the computational effort is now of the same order as the predictor-corrector method. Therefore, subsequent efforts were concentrated on the fourth order Runge-Kutta and third order predictor-corrector methods.

In the first example, the forced standing wave in a rectangular channel without friction or coriolis effect was modeled as shown in Figure 4. The analytical solution is

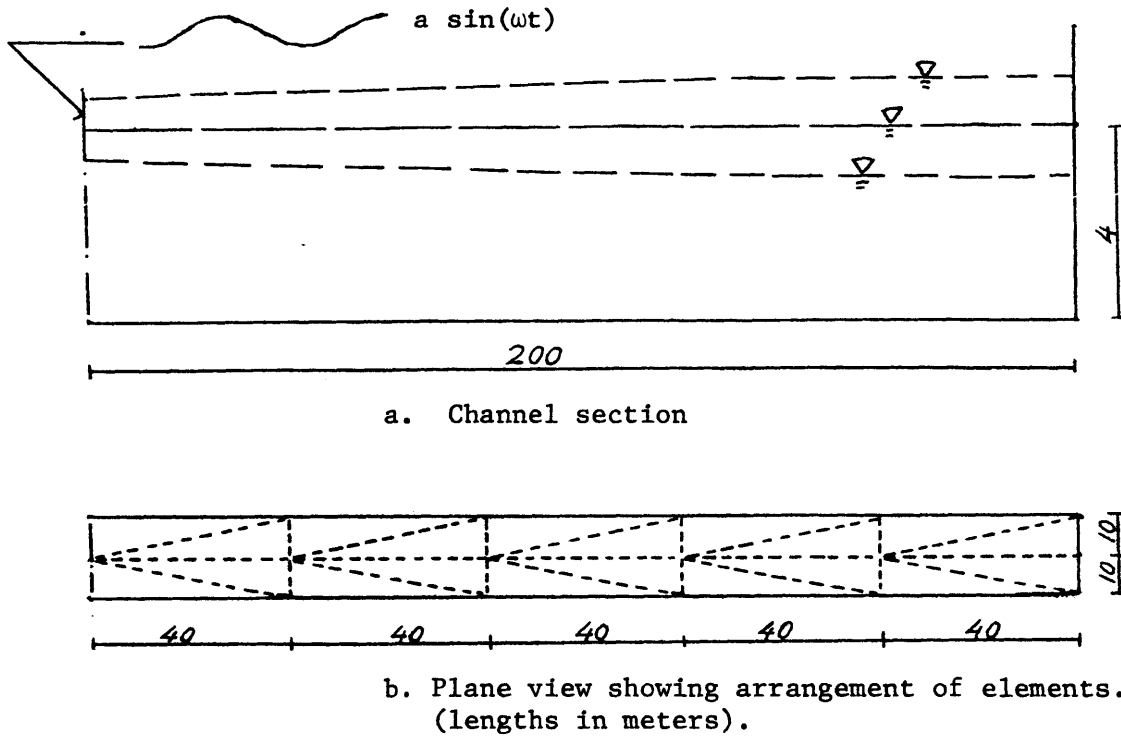


Figure 4. Sketch of rectangular channel.

TABLE 1

Comparison of analytical and numerical solution.

Rectangular channel. Initial velocities given by analytical solution. Runge-Kutta method. $\Delta t=2.5$ sec.

SURFACE HEIGHTS			time	VELOCITIES		
numerical	analytical	difference		numerical	analytical	difference
-1.0000	-1.0000	-	$3T/4$	0.0003	0	0.0003
-1.0217	-1.0210	0.0017		0.0002	0	0.0002
-1.0378	-1.0374	0.0004		0.0003	0	0.0003
-1.0491	-1.0492	0.0001		0.0003	0	0.0003
-1.0565	-1.0563	0.0002		0.0004	0	0.0004
-1.5900	-1.0586	0.0004		0.0001	0	0.0001
0.0000	0	-	T	0.5443	0.5440	0.0003
0.0000	0	0.0000		0.4382	0.4382	0.0000
0.0001	0	0.0001		0.3305	0.3303	0.0002
0.0001	0	0.0001		0.2213	0.2211	0.0002
0.0001	0	0.0001		0.1108	0.1108	0.0000
0.0001	0	0.0001		0.0000	0	0.0000

$$\eta = \frac{a}{\cos \omega \frac{L}{\sqrt{gh}}} \cos\left\{\omega \frac{L}{\sqrt{gh}} \left(\frac{x}{L} - 1\right)\right\} \sin \omega t \quad (42)$$

$$u = - \frac{a \sqrt{gh}}{h \cos \omega \frac{L}{\sqrt{gh}}} \sin\left\{\omega \frac{L}{\sqrt{gh}} \left(\frac{x}{L} - 1\right)\right\} \cos \omega t$$

where the forcing function at the open end, $x = 0$, is

$$\eta_{x=0} = a \sin \omega t$$

and L , h are the channel length and depth. The numerical model was started with the velocity distribution defined by (42) for $t = 0$. For $t > 0$, $\eta = a \sin \omega t$ was prescribed at the 3 open end nodes and the y velocities were set to zero along the boundaries. A comparison of the numerical and analytical results is listed in Table 1. The agreement is very good as expected.

In a "real" situation, one usually does not know the initial velocity field. One possible approach is to start the model with all surface elevations and velocities set to zero (or some other estimated values). The second example demonstrates this type of start up for the rectangular channel. The exact solution was obtained with the method of characteristics. The results with the Runge-Kutta scheme for this problem follow the exact solution closely. However, the predictor-corrector results exhibit an instability characterized by the growth of short waves as demonstrated in Figure 5. This phenomenon was attributed to less accuracy of the scheme. The problem was resolved by introducing some eddy viscosity ($\epsilon_x = \epsilon_y = 2\epsilon_{xy} = 10 \text{ m}^2/\text{sec}$) and again good agreement between analytical and numerical solutions

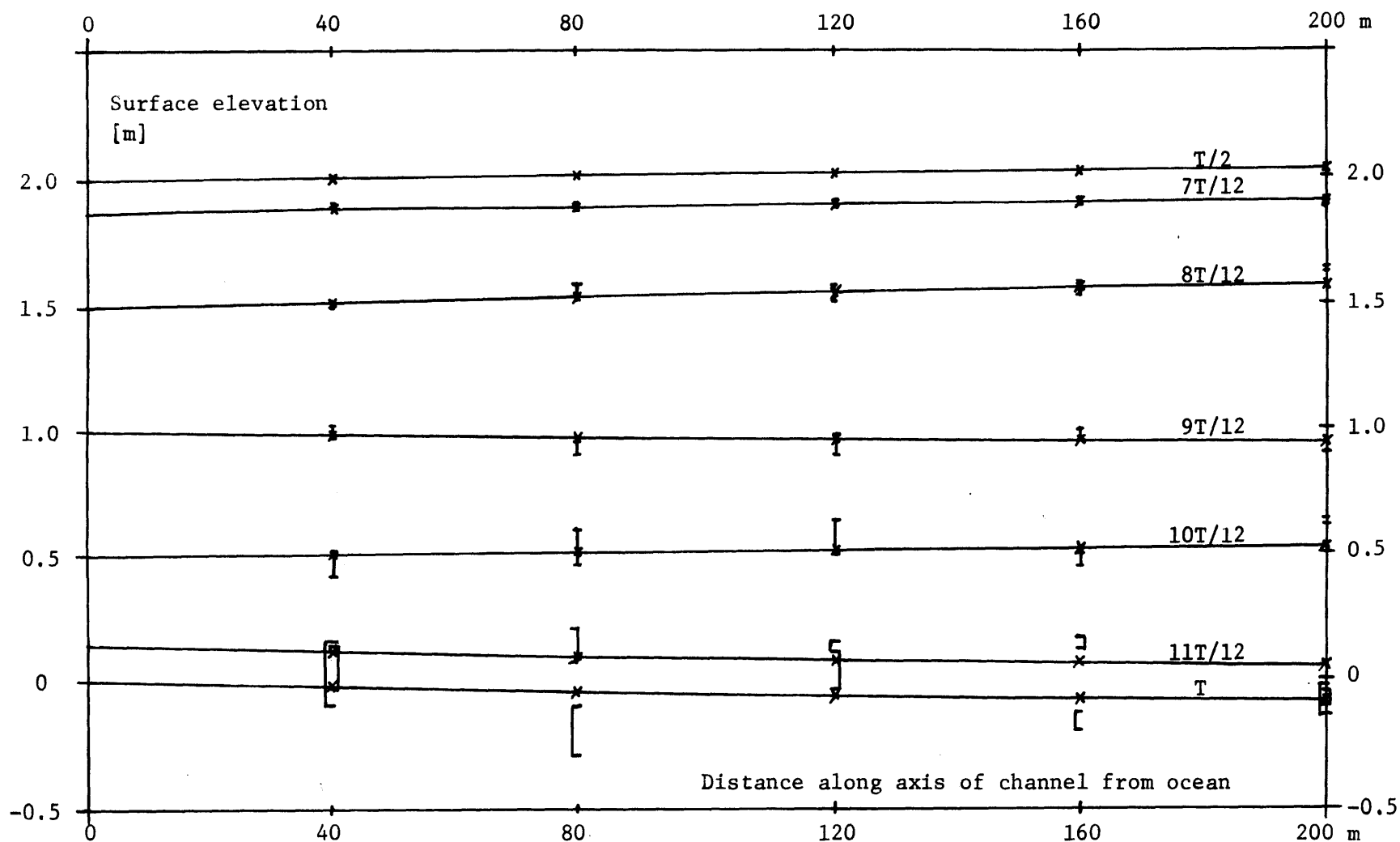


Figure 5. Tidal excitation of one dimensional rectangular channel starting from rest. Comparison of analytical and numerical solutions with and without eddy diffusivity. Integration by predictor-corrector method. $\Delta t=2.5$ sec. Period $T=600$ sec.

— exact solution.

I numerical solution without eddy diffusivity, (value range of 3 cross sectional nodes).

x numerical solution with eddy diffusivity, $\epsilon_x = \epsilon_y = 2\epsilon_{xy} = 10 \text{ m}^2/\text{sec}$.

was obtained. For the same time increments, the predictor-corrector method requires approximately 25% less time than the Runge Kutta scheme.

The 2-dimensional Courant-Friedricks-Lewy stability criterion for explicit differencing of the wave equation is

$$\Delta t \leq \frac{\delta}{\sqrt{2} c} \quad (43)$$

where δ is the grid size and c is the wave velocity. For the rectangular channel we have

$$c = \sqrt{gh} = \sqrt{9.81 \cdot 4} = 626 \text{ m/sec.}$$

so that $10 \text{ m} \leq \delta \leq 40 \text{ m} \rightarrow 1.13 \text{ sec} \leq \Delta t_c \leq 4.5 \text{ sec.}$

The results plotted in Figure 5 were obtained with $\Delta t = 2.5 \text{ sec.}$ When Δt was increased to 5 sec., gradual instability was observed.

An analytical solution in infinite series for the harmonic forcing of a rectangular basin with a slot has recently been derived by Briggs and Madsen [17]. Figure 6 shows their results for a constant depth (36.6 m) model representative of Massachusetts Bay. The model geometry and corresponding finite element layout is shown in Figure 7. The numerically computed surface elevations and current velocities, Figures 8 and 9, compare favorably with the analytical. One explanation for the small discrepancies may be found in the treatment of the ocean boundary condition. In the numerical model the height is prescribed exactly equal to $1.31 \text{ m} \cdot (1 - \cos \omega t)$ across the slot, whereas the analytical solution only satisfies this at four discrete points. The numerical results were obtained with the Runge-Kutta method without bottom friction, eddy viscosity or Coriolis effect. The C-F-L criterion

----- contour lines , (high tide).
velocity, (high water slack).

velocity scale
0 0.5 m/sec

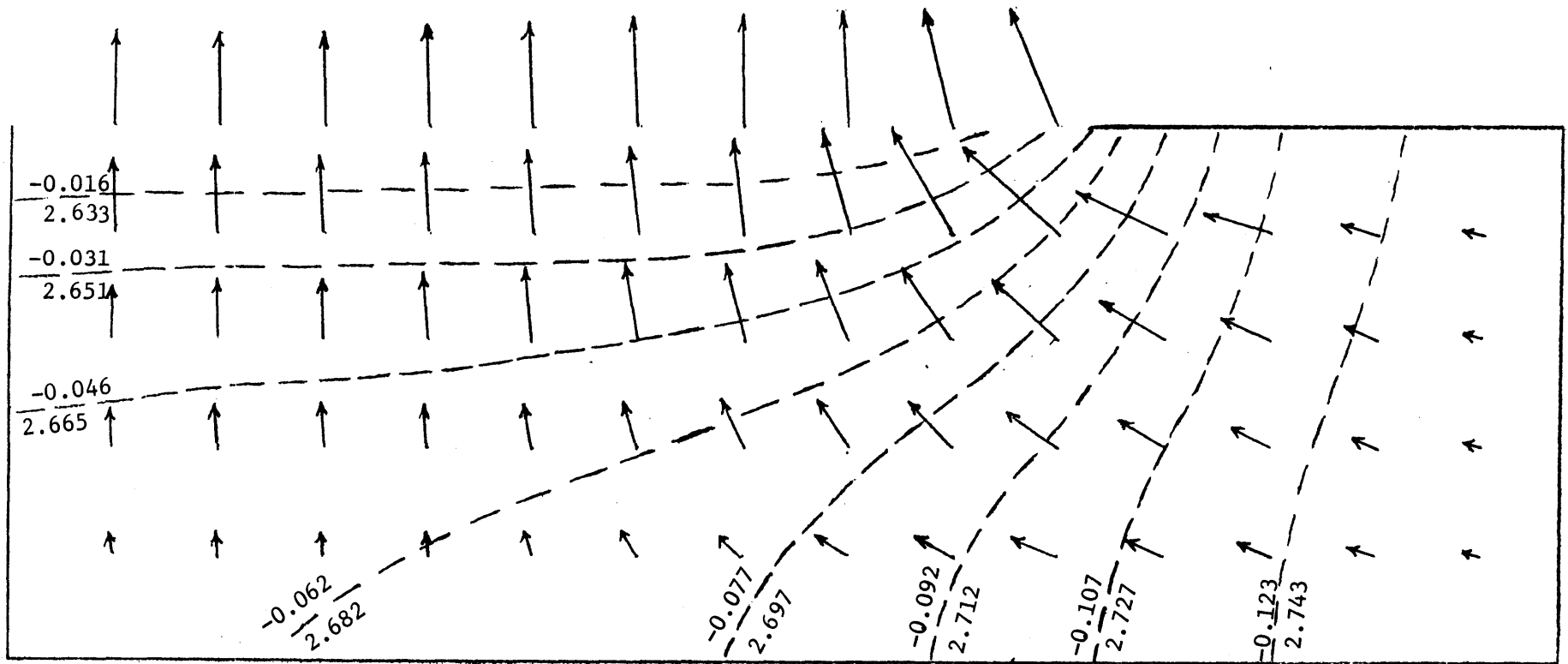
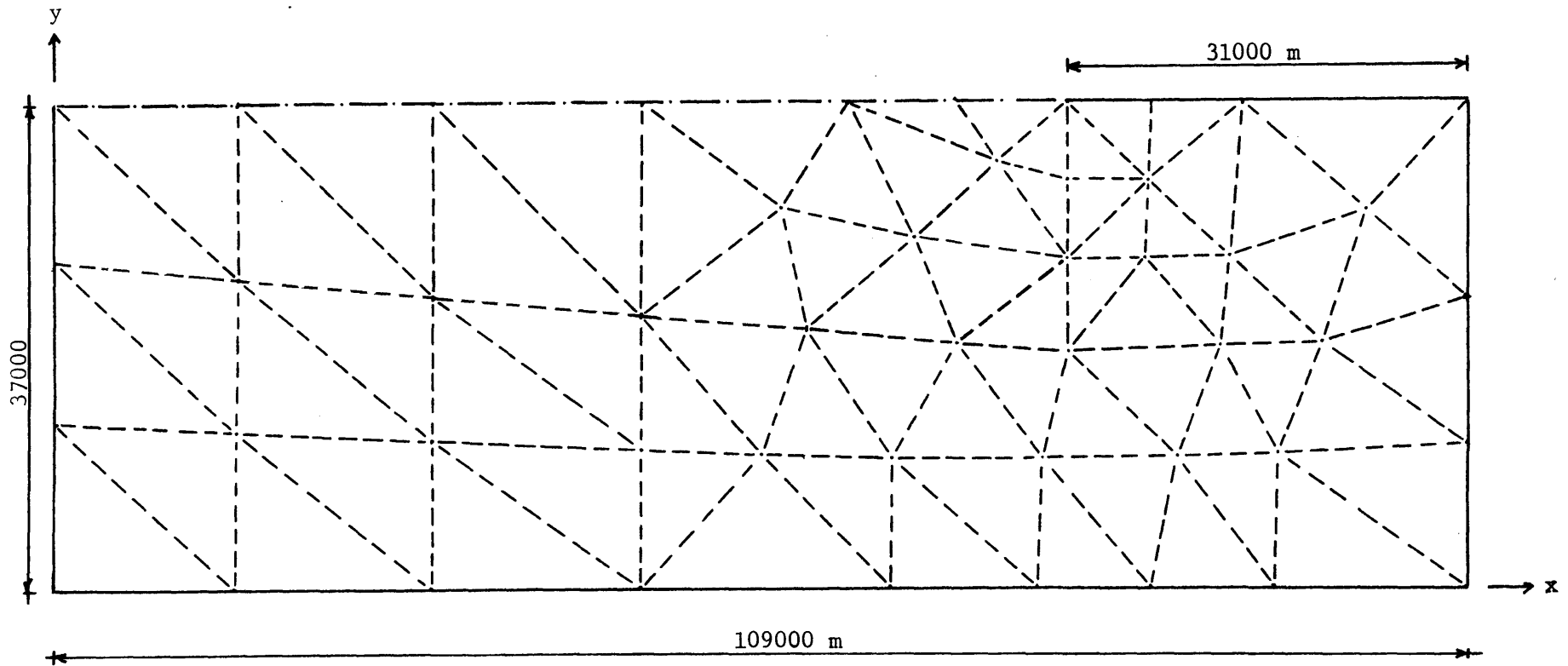


Fig. 6 Rectangular model of Massachusetts Bay.
Analytical solution for surface elevations and currents.
On each contour line the tidal range in meters is indicated.



scale 0 10000 m

Fig. 7. Rectangular model of Massachusetts Bay.
 Dimensions and element layout. Constant depth = 36.6 m.
 71 elements and 48 nodes.

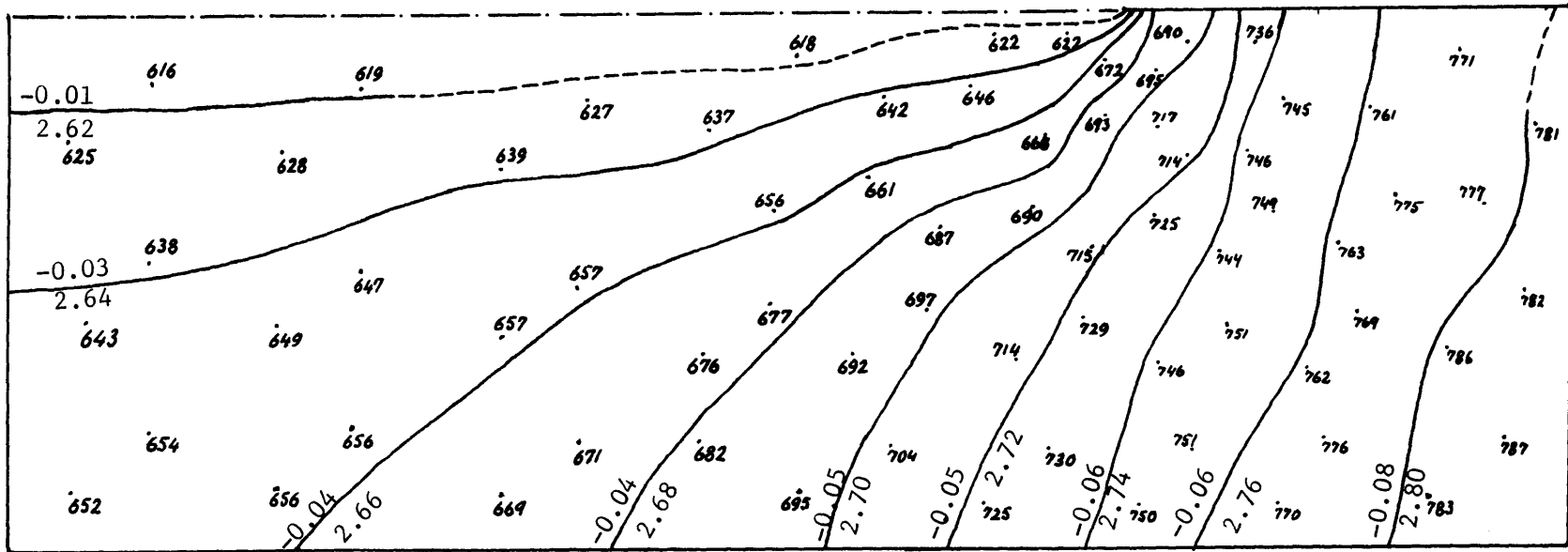
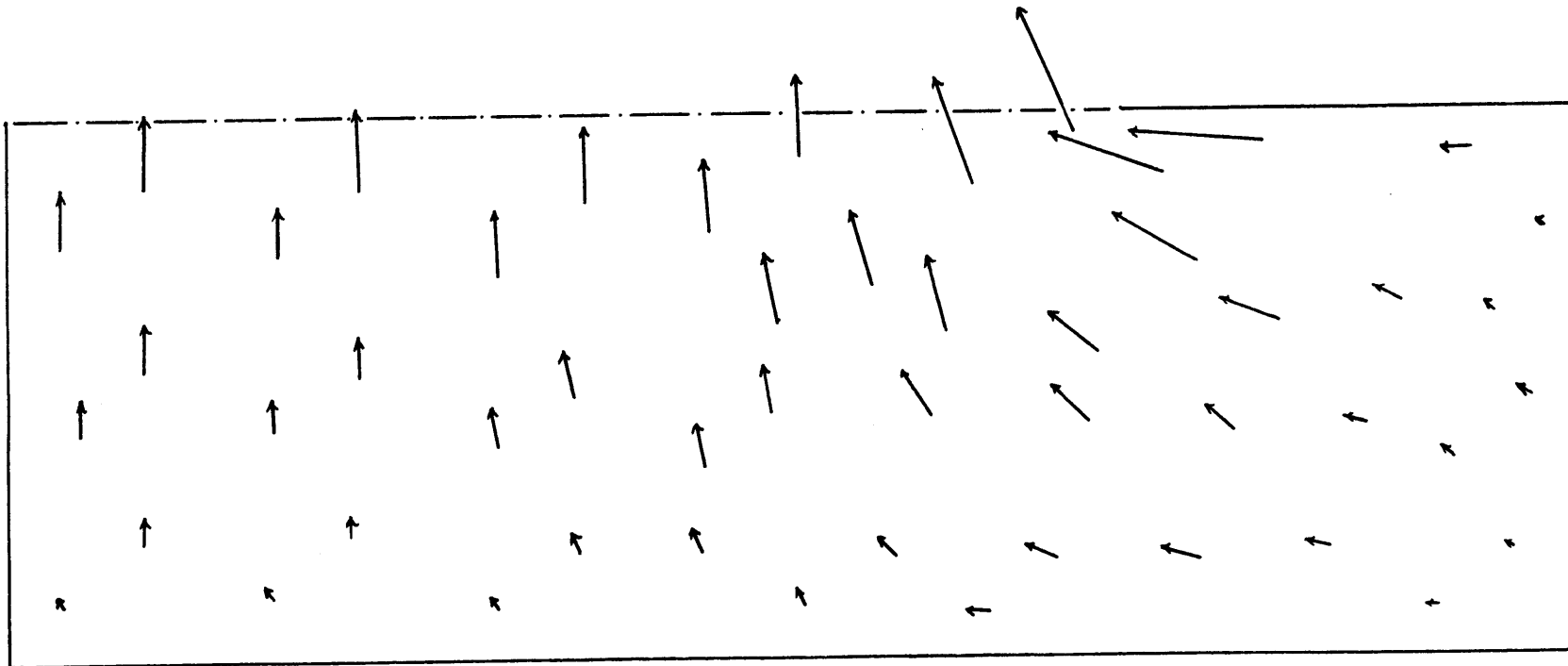


Fig 8. Rectangular model of Massachusetts Bay. Finite element solution. Runge-Kutta method, $\Delta t=200$ sec. Surface elevations at element centroids and surface contour lines after 68000 sec, 1.5 tidal period. The computed approximate tidal range in meters is given for each contour line.

Note: only the decimals are given for centroidal values.




velocity scale 
0.2 m/sec

Fig 9. Rectangular model of Massachusetts Bay.
Finite element solution. Runge-Kutta method, $\Delta t = 200$ sec.
Tidal current velocities after 80000 sec., 1.75 tidal period.

is

$$c = \sqrt{9.81 \cdot 36.6} = 18.9 \text{ m/sec}$$

$$t_c = \frac{\delta}{\sqrt{2c}} = \frac{5700}{1.41 \cdot 18.9} = 214 \text{ sec}$$

and a $t = 200$ sec was selected.

Lastly the tidal and winddriven circulation in Massachusetts Bay was computed. The geographic boundaries and the finite element grid are shown in figure 10. Since very little actual data is available, a model yielding only the gross circulation is appropriate at this time. A fairly coarse grid of 74 elements and 53 nodes was laid out reflecting somewhat the varying bottom topography. The tidal ranges for the two shore nodes at the extremities of the ocean boundary were obtained from tide tables [18] and the tide level was assumed to vary smoothly in between. The Coriolis parameter was determined for a latitude of 42°N , $f = 0.973 \cdot 10^{-4} \text{ sec}^{-1}$. No attempts were made to model lateral inflows at this stage.

An initial solution for pure tidal motion with a small constant value of C_f was carefully examined in order to estimate new improved C_f 's for each element, so that the tidal ranges and lag times at the shore points more closely match available tide table data. In estimating C_f , a strong correlation with local depth was assumed. The final solution for which surface contour lines at high and low tide are shown on Figures 11-12 had C_f varying between $0.0025 \rightarrow 0.0011$. However, to really tune the model, current records at several points are desirable.

The calculated tidal water velocities are shown in Figures 13-14 and typical time histories of surface elevations and velocities are plotted in Figures 15-16.

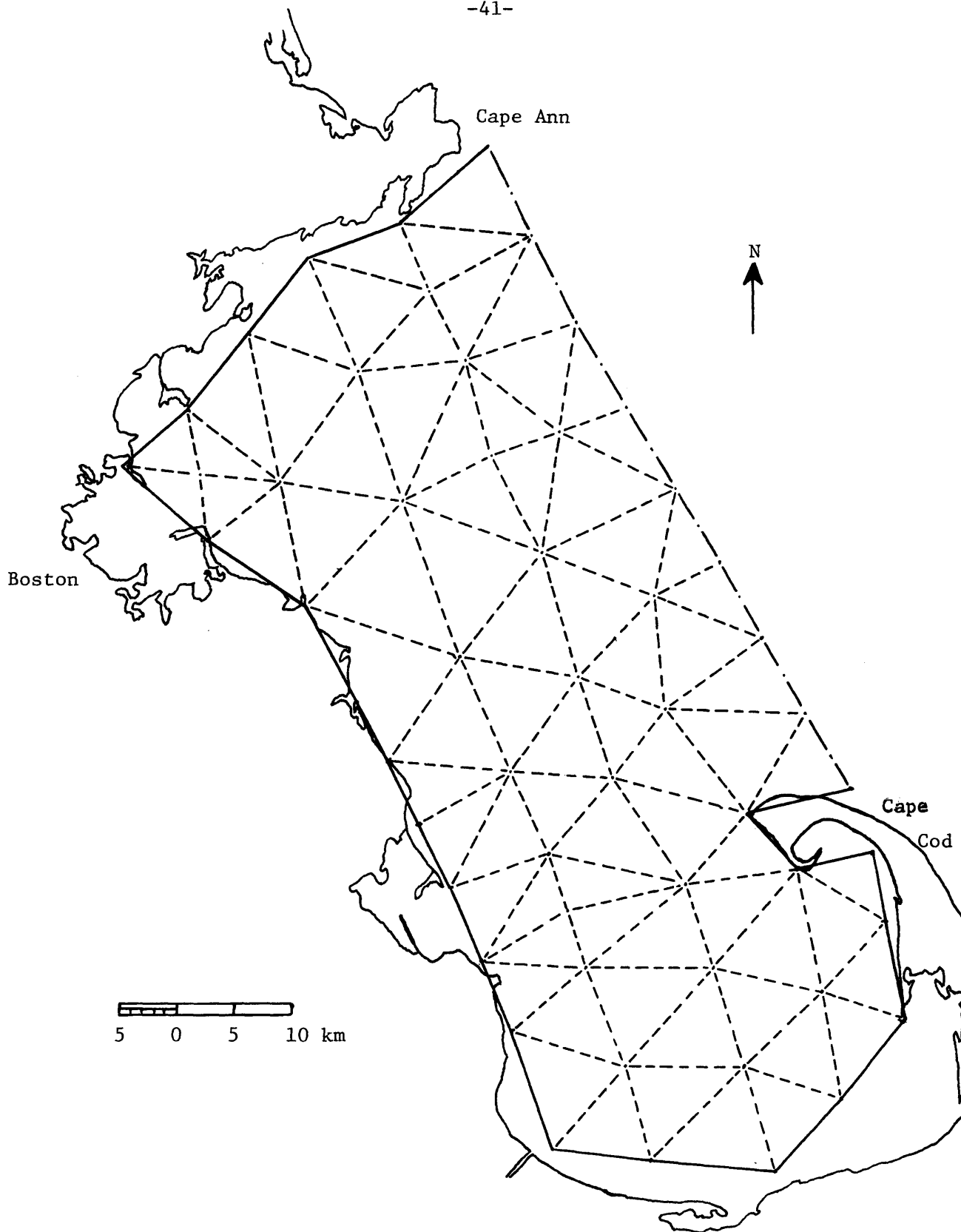


Fig. 10. Massachusetts Bay. Geographical boundaries and finite element grid.

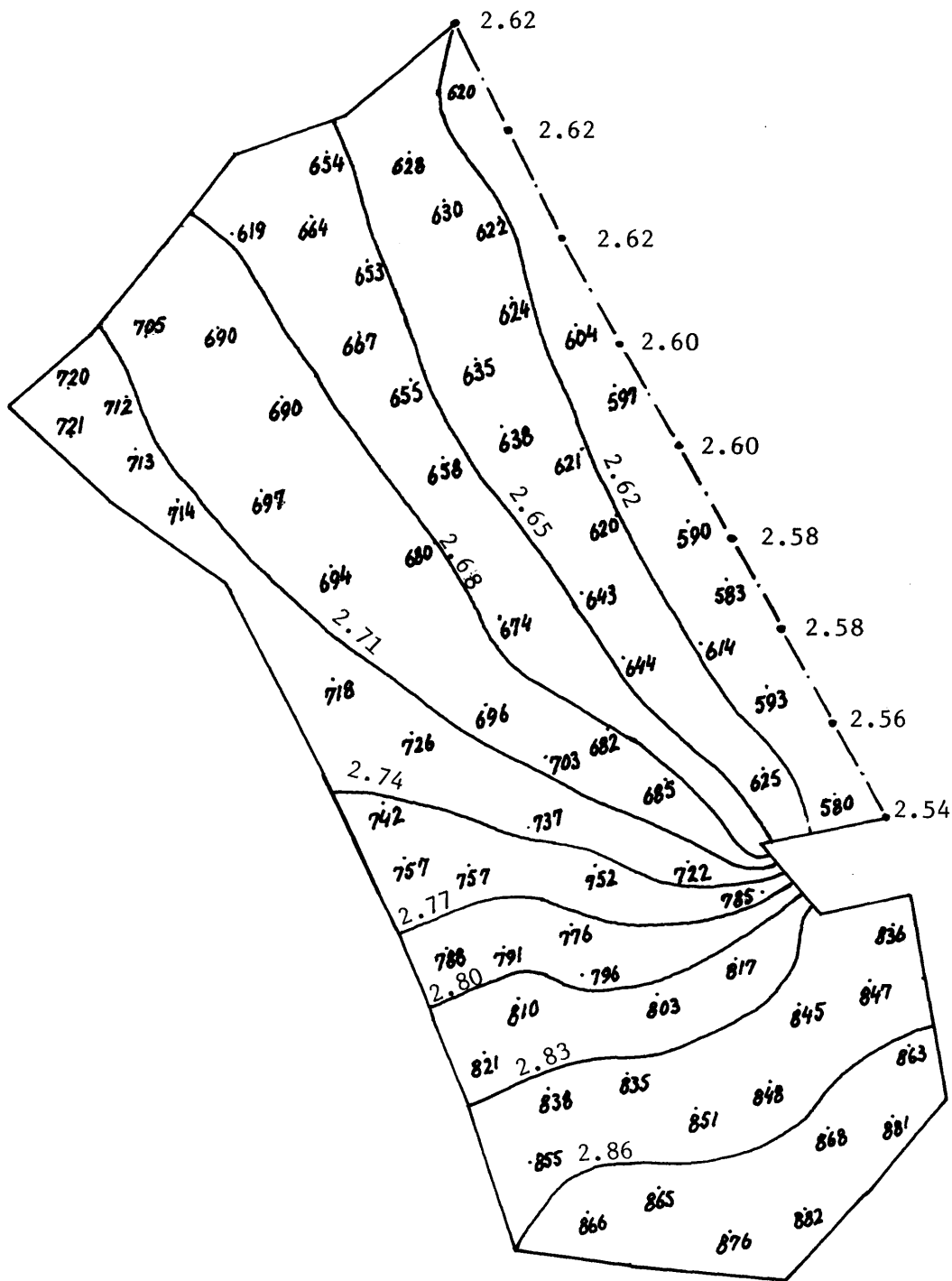


Fig. 11. Surface contour lines after 68000 sec. (1.5 tidal cycle).
The elevations are given in meters above MLW. Note that only decimals are shown for centroidal elevations.

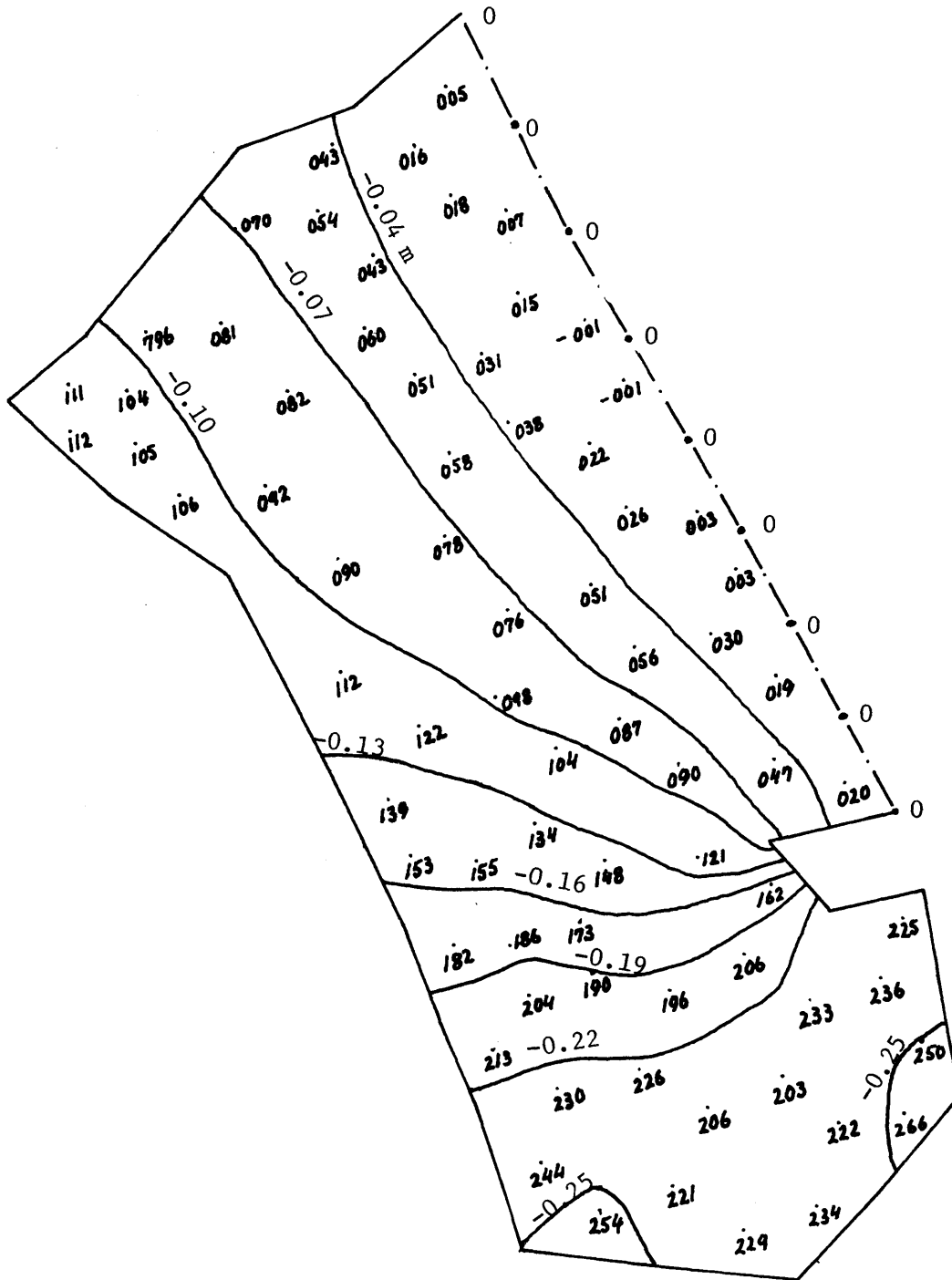


Fig. 12. Surface contour lines after 90000 sec (2 tidal cycles).
Centroidal elevations are given in mm below MLW.

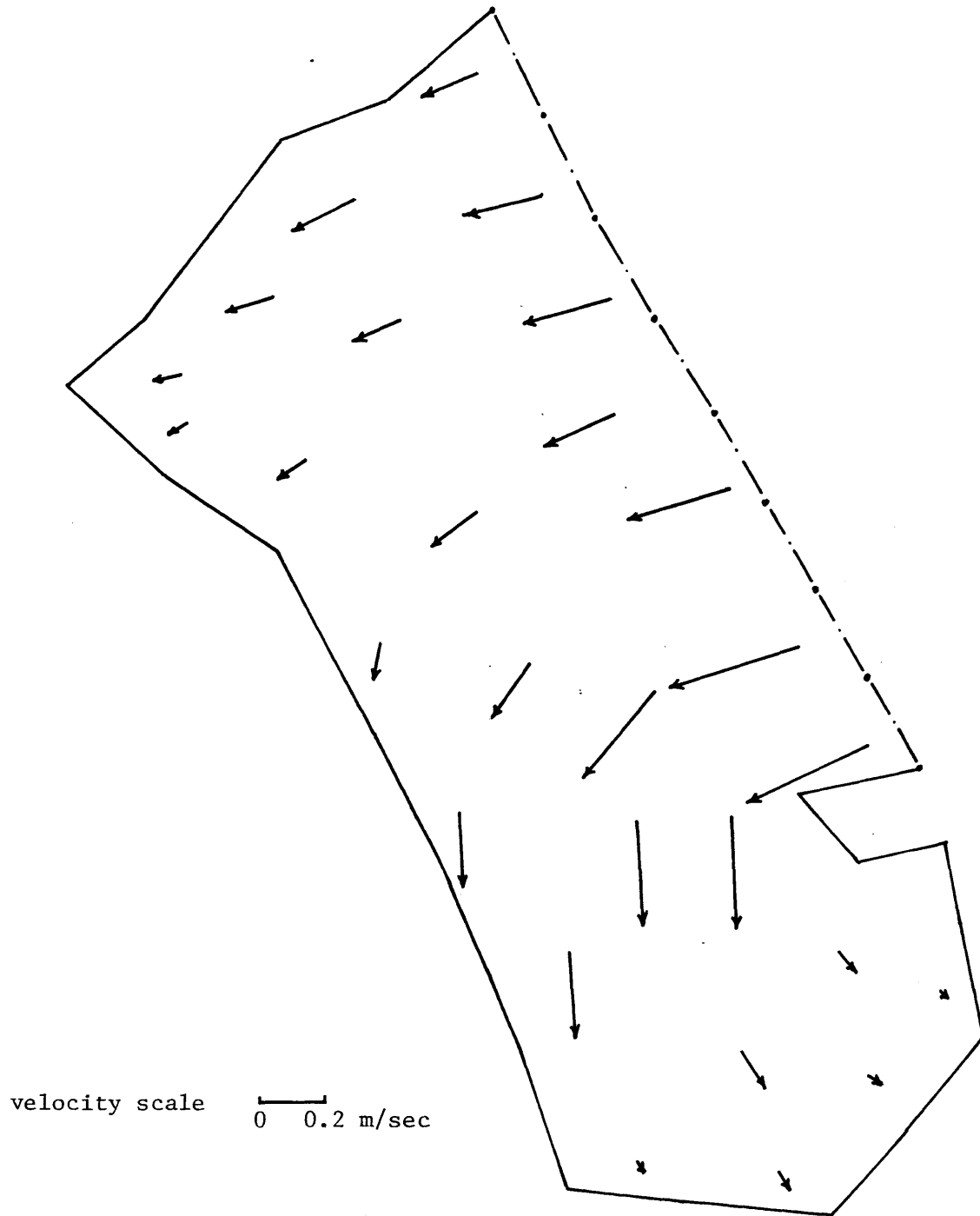


Fig. 13. Computed currents after 56000 sec. (1.25 tidal cycle).
Flooding Tide.

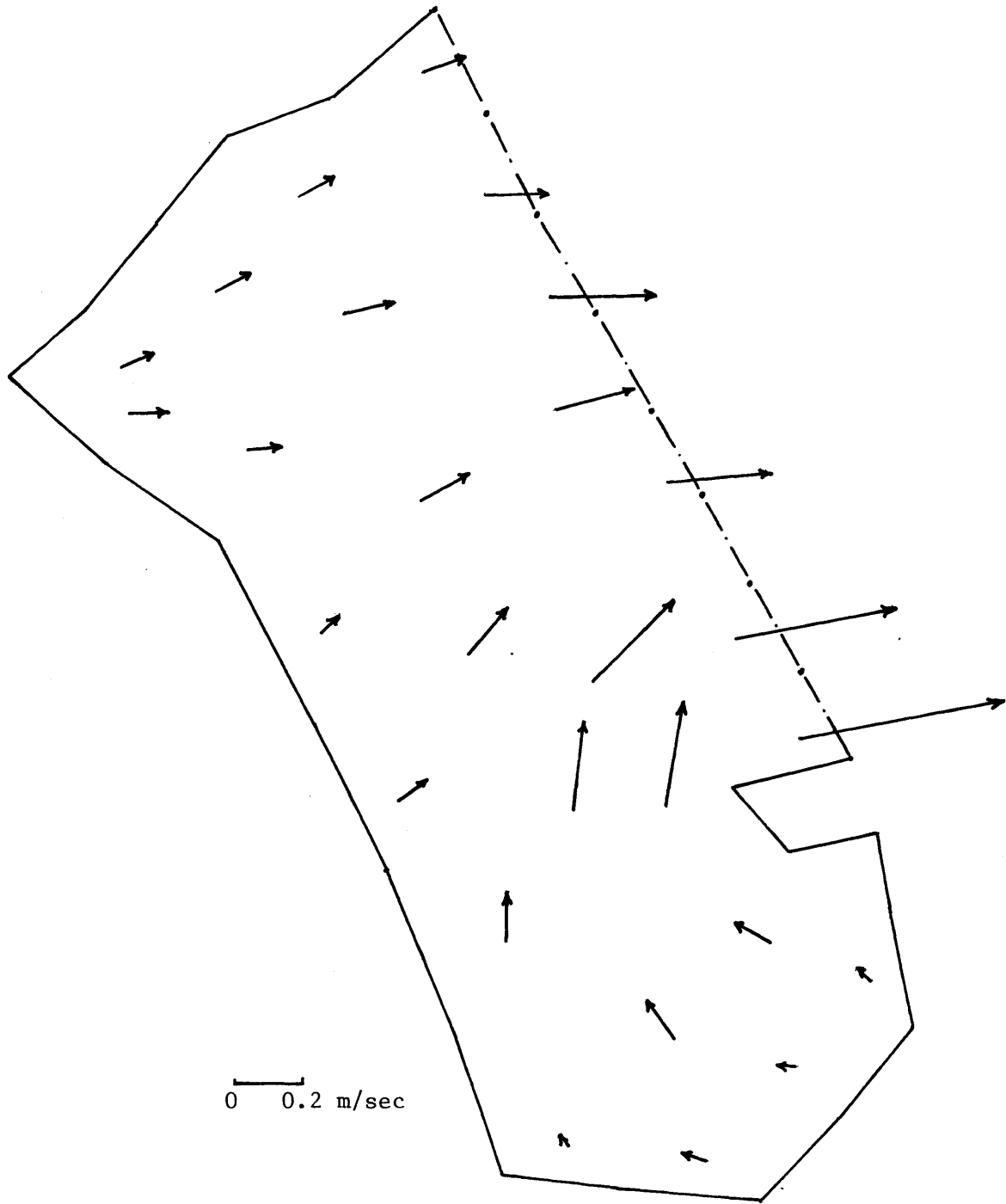
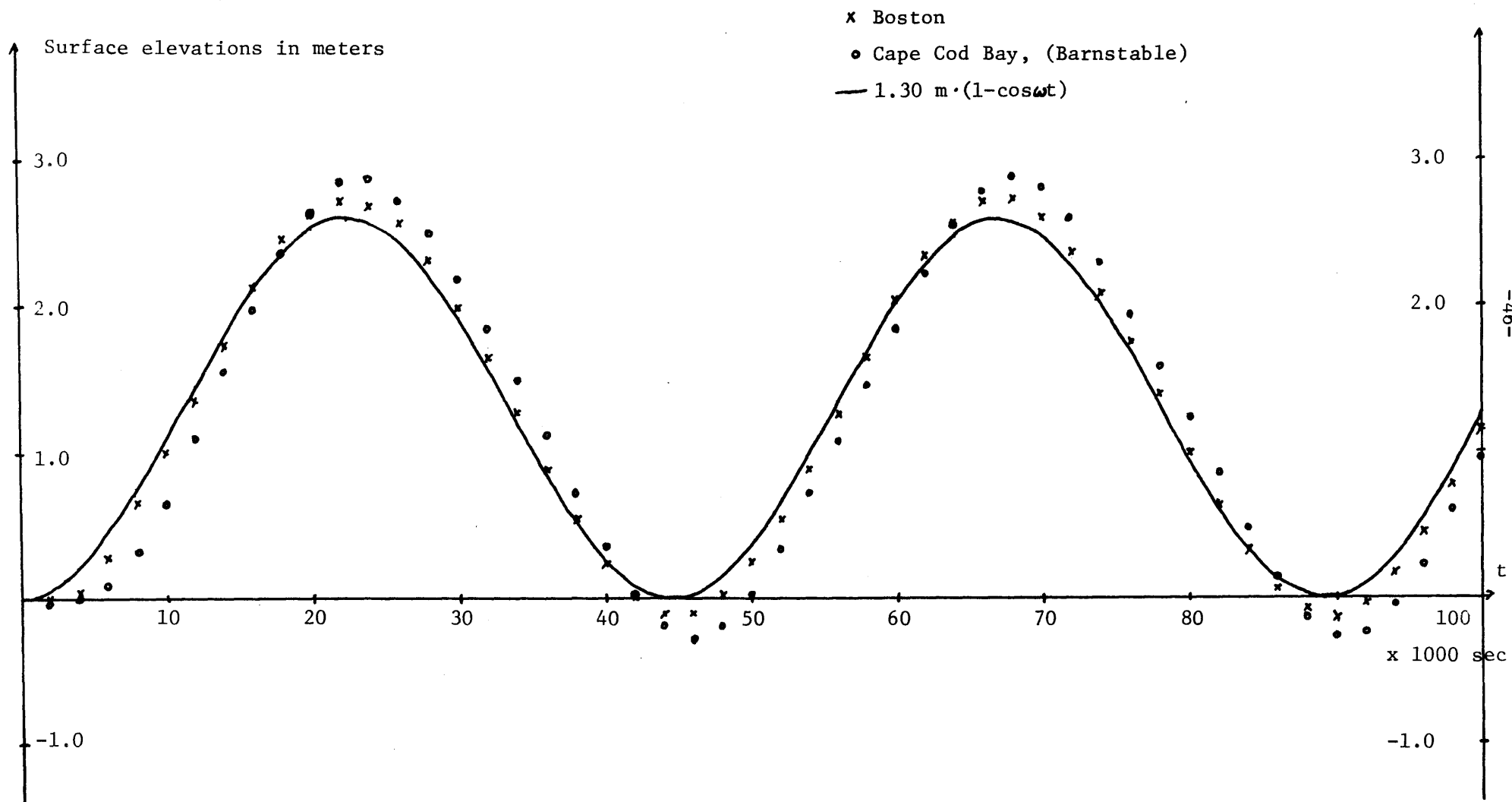


Fig. 14. Computed currents after 78000 sec. (1.75 tidal cycle).
Ebbing tide.

Fig. 15. Time history of computed elevations at Boston and in Cape Cod Bay.



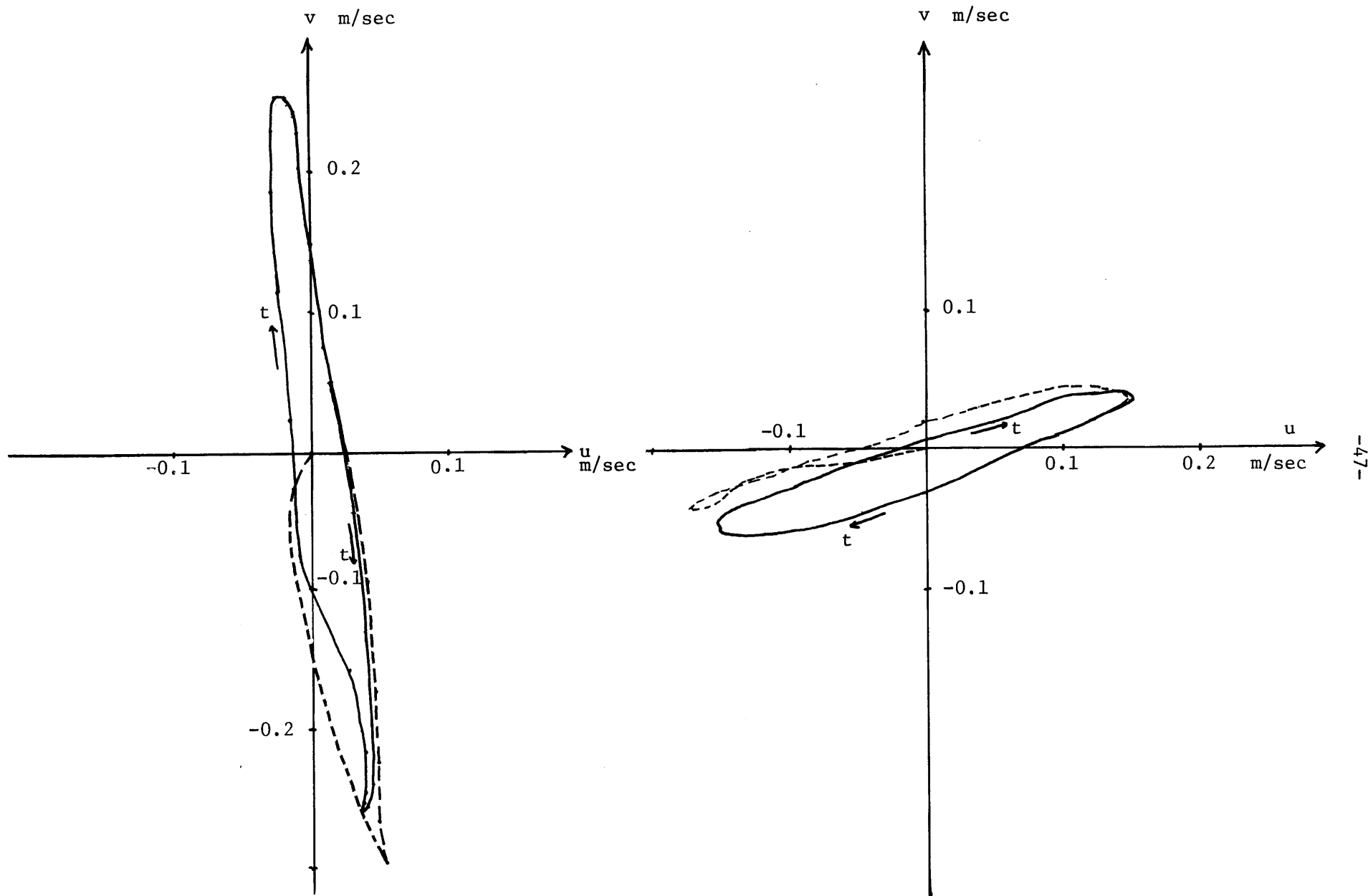


Fig. 16. Time history of computed currents. a) Center of Cape Cod Bay. b) 15 km East of Boston.

The results were obtained using the Runge-Kutta integration scheme neglecting convective terms and eddy diffusion in the momentum equations. The CFL criterion is

$$\Delta t_c \leq \frac{\delta}{\sqrt{2} c} \approx \frac{6000}{\sqrt{2} 19} = 223 \text{ sec.}$$

and a $\Delta t = 200$ sec was selected. The predictor-corrector scheme was applied to the same problem but exhibited gradual instability after one tidal cycle (44600 sec). When Δt was reduced to 150 sec, comparable results were obtained for more than 2 tidal cycles. However, 5% more computing time was required.

Several cases of wind forcing were also investigated. Massachusetts Bay is characterized by a low Rossby number (about 0.1), small surface elevation change compared to the mean depth, and minor effect of bottom friction. Therefore, it is reasonable to assume the response of the system is linear. This is very important since it allows one to use superposition which reduces the computational effort considerably.

To verify the "permissability" of superposition, two wind situations without tidal motion were executed until steady state was essentially achieved. The 10m wind velocity, U_{10} , was 10 m/sec which produces a surface shear stress of approximately 1 dyn/cm^2 according to the relationship given by Wu [19]:

$$\tau^s = \frac{1}{2} \rho_{\text{air}} C \cdot U_{10}^2$$
$$C = 0.5 \cdot 10^{-3} \cdot U_{10}^{1/2} \quad 1 < U_{10} < 15 \text{ m/sec.}$$

This is a frequently measured surface stress in the area.

The steady-state current field for wind from North and South-West are shown in Figures 17, 18. As a preliminary test of linear behavior, a situation with wind from South was also computed yielding numerical values of velocities and surface elevations within 1% of the North wind case.

Figures 19, 20 show Calcomp plots of a superposition of velocities produced by wind from SW alone and pure tidal motion, whereas Figures 21, 22 show the same velocity fields but computed simultaneously. The validity of a linear system assumption as a first approximation is clearly demonstrated.

The limited experience acquired so far has demonstrated that the finite element discretization approach is a reliable and efficient method for fluid flow problems with complex boundaries. Of the two integration schemes tested, the Runge-Kutta method seems to be universally applicable whereas the predictor-corrector scheme is prone to exhibit instability. If the forcing terms are sufficiently complicated to estimate, the savings in iterations may give the latter scheme a computational advantage, even if a smaller time step must be used. This might, for instance, be the case when the convective terms must be retained. Also the improved stability through the smoothing effect of adding diffusive terms needs further examination.

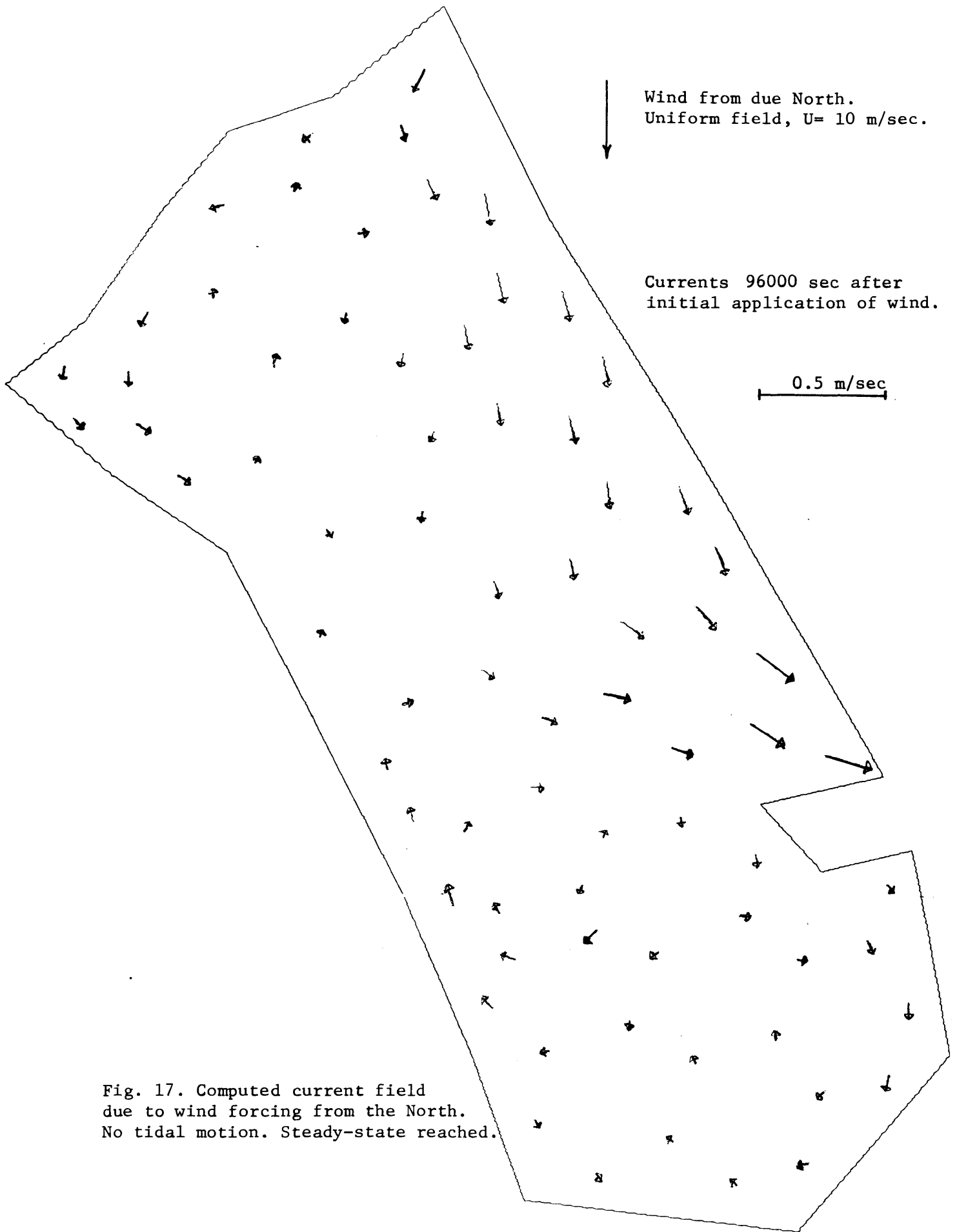


Fig. 17. Computed current field due to wind forcing from the North. No tidal motion. Steady-state reached.

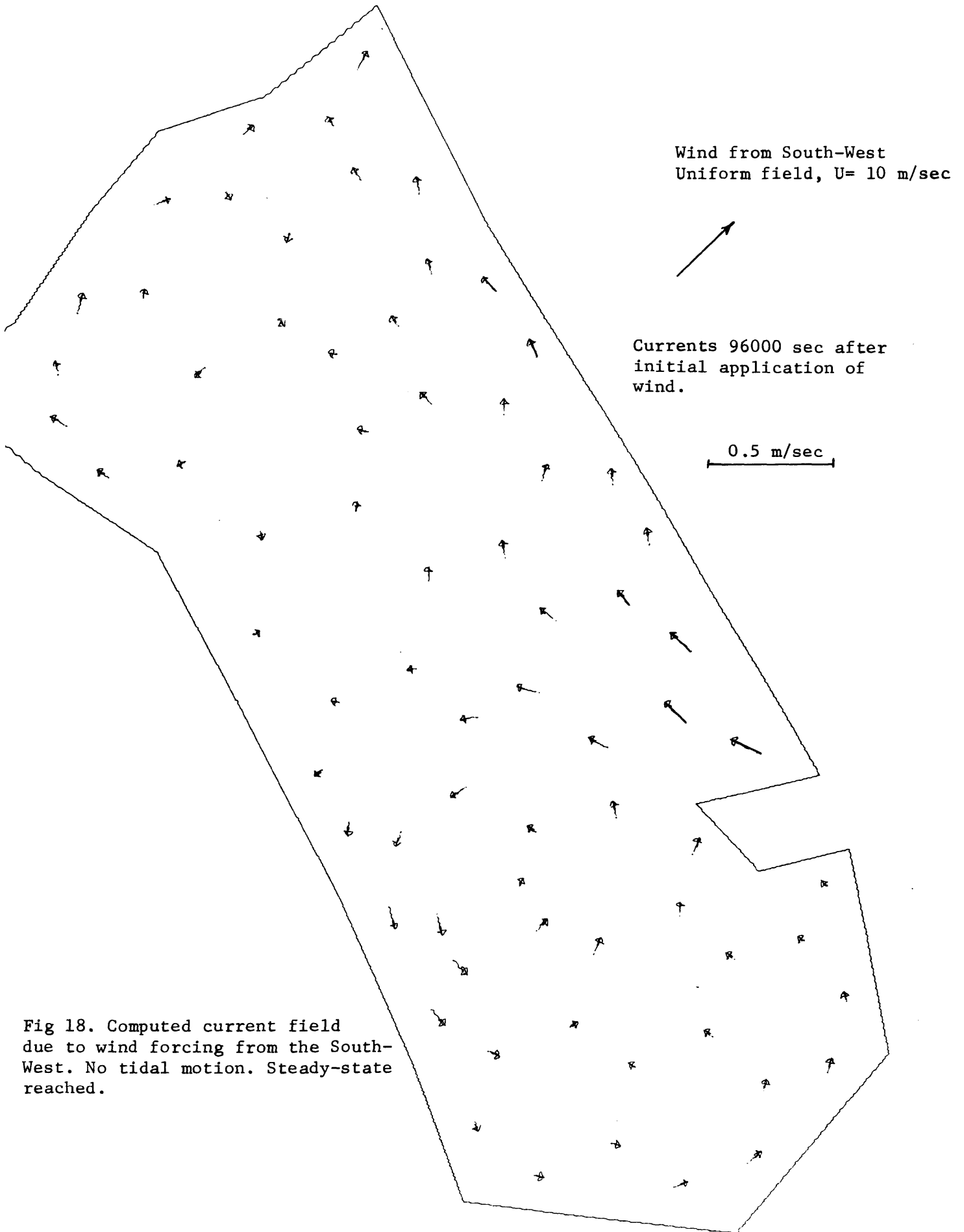


Fig 18. Computed current field due to wind forcing from the South-West. No tidal motion. Steady-state reached.

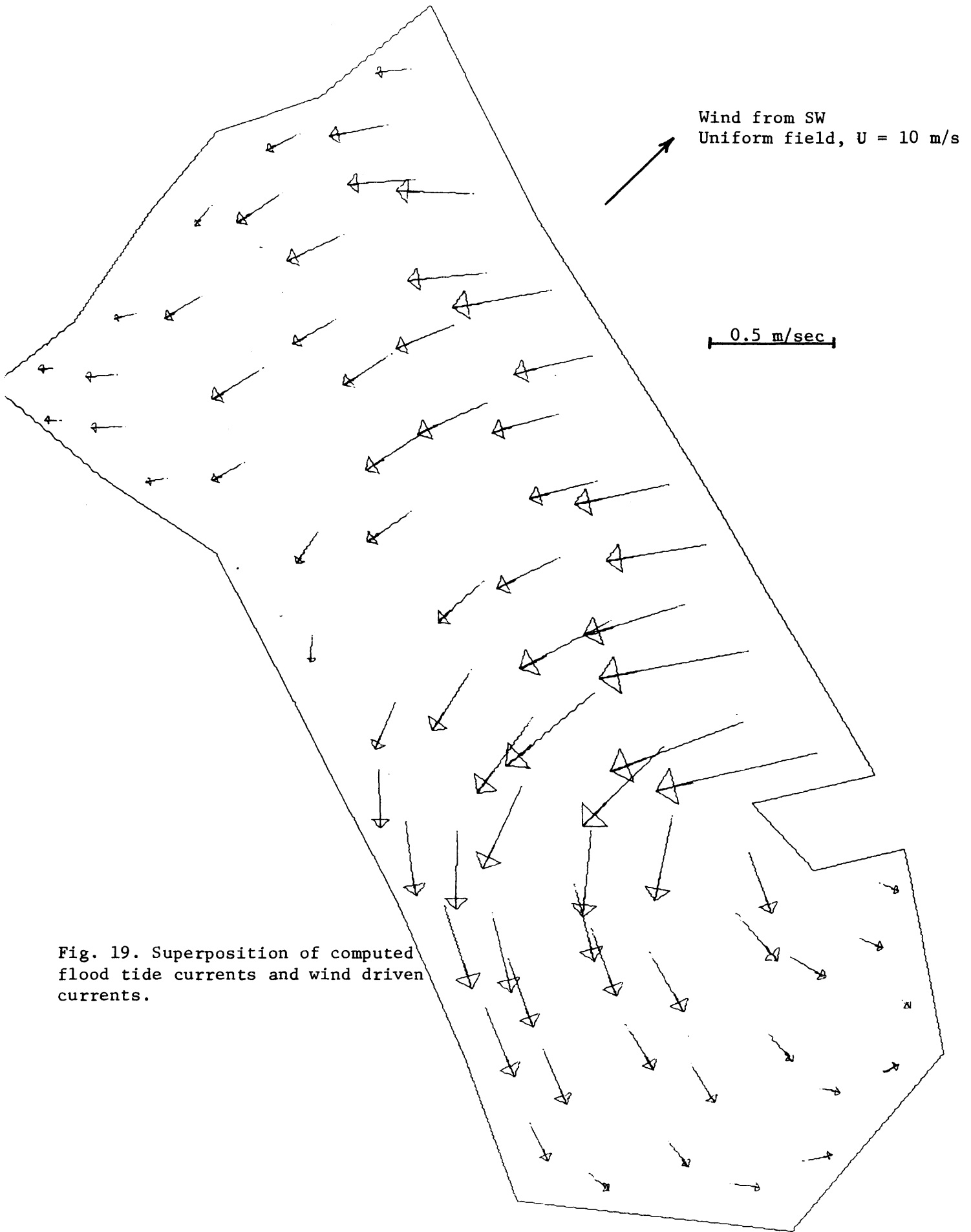


Fig. 19. Superposition of computed flood tide currents and wind driven currents.

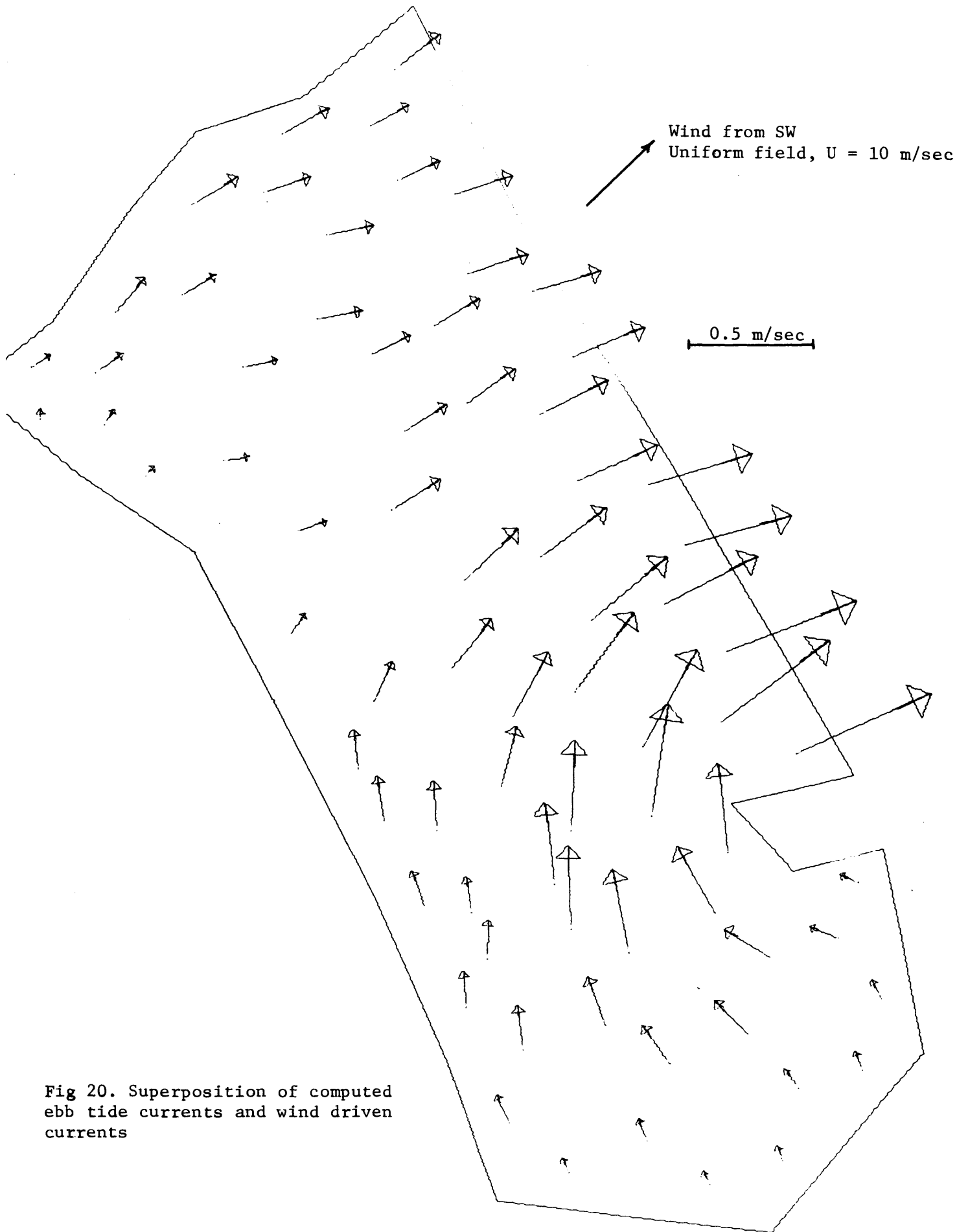


Fig 20. Superposition of computed ebb tide currents and wind driven currents

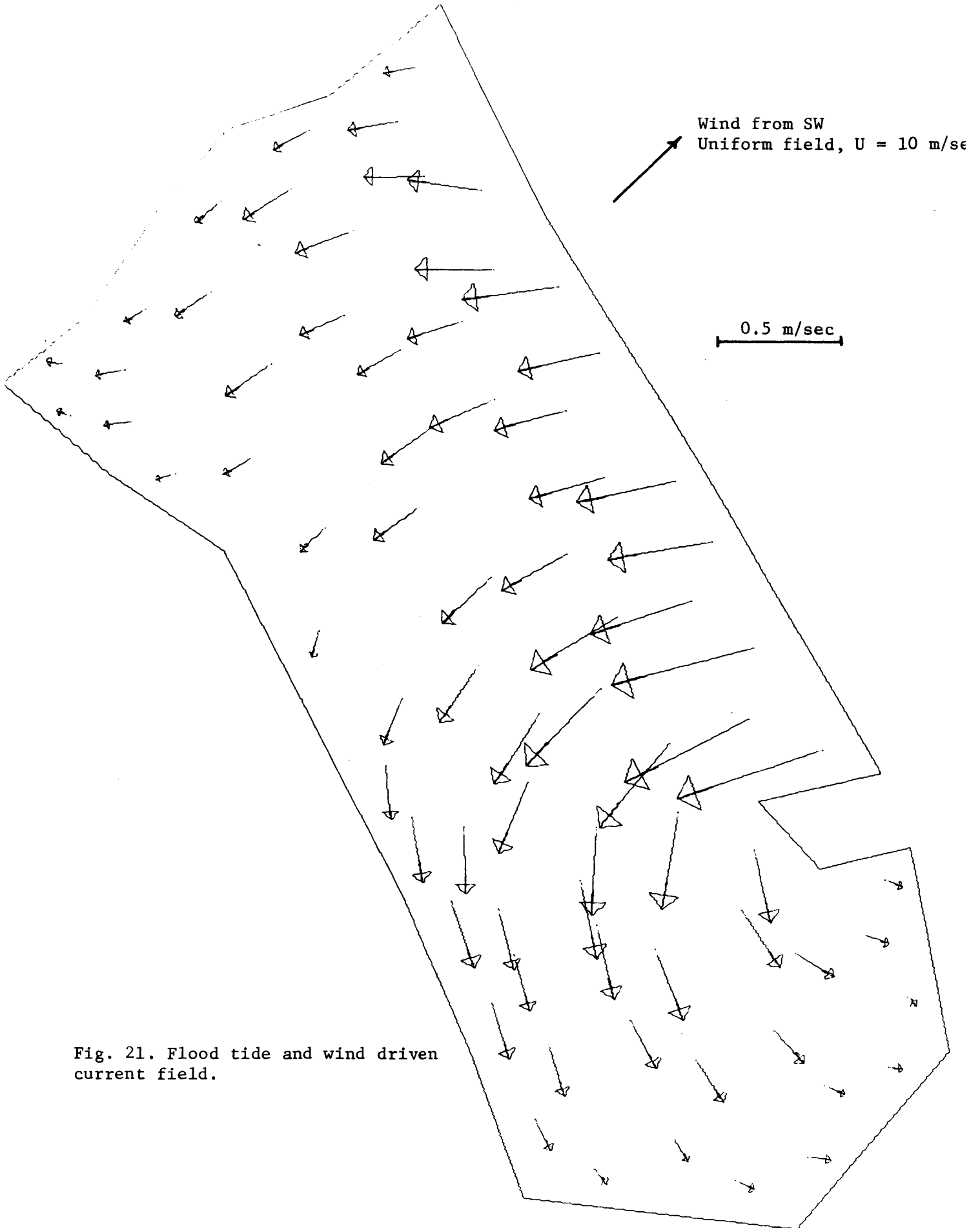


Fig. 21. Flood tide and wind driven current field.

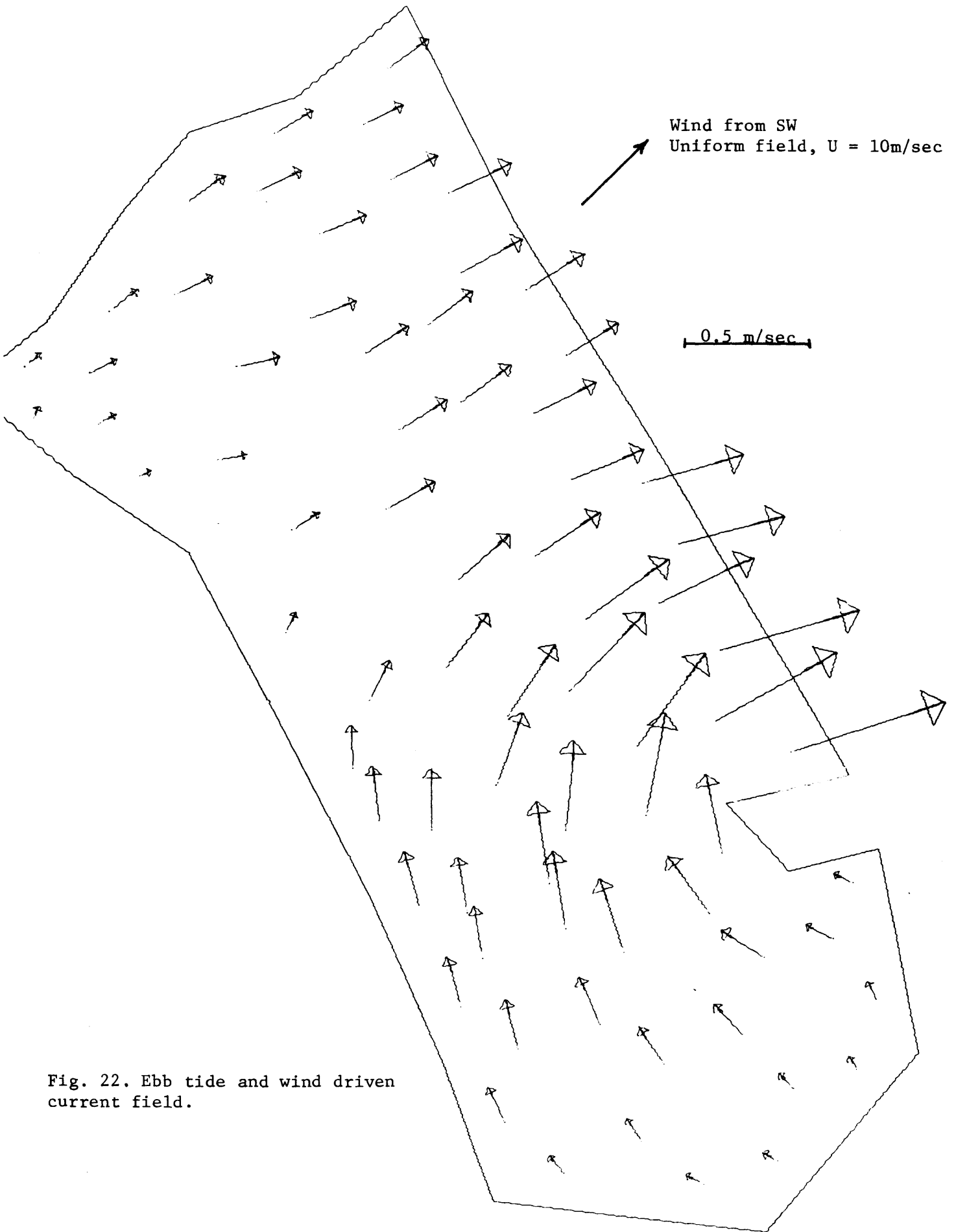


Fig. 22. Ebb tide and wind driven current field.

REFERENCES

1. Reid, R.O. and B.R. Bodine: "Numerical Model for Storm Surges in Galveston Bay", Journal of the Waterways and Harbors Division, ASCE, Vol. 94, No. WW1, 1968
2. "Estuarine Modeling: An Assessment", Water Pollution Control Research Series, Water Quality Office, Environmental Protection Agency, Feb., 1971
3. Leendertse, J.J.: "A Water Quality Model for Well-Mixed Estuaries and Coastal Seas, Vol. I, Principles of Computation", Memorandum RM-6230-RC, The Rand Corporation, Santa Monica, California, Feb., 1970
4. Masch, F.D. and N.J. Shankar: "Mathematical Simulation of Two-Dimensional Horizontal Convective-Dispersion in Well-Mixed Estuaries", Int. Assoc. for Hydraulic Research, 1971
5. Brady, D.K. and J.C. Geyer: "Development of a General Computer Model for Simulating Thermal Discharges in Three Dimensions", Edison Electric Institute Publication No. 72-902, Feb., 1972
6. Pearce, B.R.: "Numerical Calculation of the Response of Coastal Waters to Storm Systems", TR 12, Coastal and Oceanographic Engineering Lab., University of Florida, August, 1972
7. Abbott, M.B., Damsgaard, A. and G. S. Rodenhuis: "System 21, Jupiter", Journal of Hydraulic Research, Vol. 11, No. 1, 1973
8. Martin, H.C.: "Finite Element Analysis of Fluid Flows", Proc. 2nd Conf. Matrix Meth. Str. Mech., AFFDL TR68-50, Wright-Patterson AFB, Ohio, 1969
9. Tong, P.,: "The Finite Element Method for Fluid Flow", Recent Advances in Matrix Methods of Structural Analysis and Design", R. Gallagher et al (Editors) U. of Alabama Press, 1971
10. Proceedings, 14th Conf. on Great Lakes Research, Int. Assoc. for Great Lake Research, 1971
11. Loziuk, L., Anderson, J. and T. Belytschko: "Hydrothermal Analysis by Finite Element Method", J. Hyd. Div., ASCE, Vol. 98, No. HY11, November, 1972
12. Davis, J.M., Ph.D. Thesis, University College of Swansea, Sept., 1972
13. Guymon, G.: "Finite Element Solution for General Fluid Motion", J. Hyd. Div., ASCE, Vol. 99, No. HY 6, June, 1973

14. Finlayson, B.A. and L. E. Scriven: "The Method of Weighted Residuals and its Relation to Certain Variational Principles for the Analysis of Transport Processes," Chemical Engineering Science, Vol. 20, 1965
15. Ralston, A.: "A First Course in Numerical Analysis", McGraw Hill, 1965
16. Richtmyer, R.D. and K.W. Morton: "Difference Methods for Initial-Value Problems", Interscience (Wiley), Second Edition, 1967
17. Briggs, D. and O. Madsen, Department of Civil Engineering, M.I.T., Private communication
18. U.S. Department of Commerce, NOAA, Tide Tables, East Coast of North and South America, 1973
19. Wu, J.: "Wind Stress and Surface Roughness at Air-Sea Interface", J. Geoph. Res., V. 74, No. 2, Jan., 1969

MATHEMATICAL MODELS OF THE MASSACHUSETTS BAY

PART II

ANALYTICAL MODELS FOR ONE- AND TWO-
LAYER SYSTEMS IN RECTANGULAR BASINS

BY

DOUGLAS A. BRIGGS

AND

OLE S. MADSEN

RALPH M. PARSONS LABORATORY

FOR WATER RESOURCES AND HYDRODYNAMICS

Department of Civil Engineering

Massachusetts Institute of Technology

Report No. 172

Prepared with the Support of

Sea Grant Office
National Oceanographic and Atmospheric Administration
Department of Commerce
Washington, D.C.

October 1973

MATHEMATICAL MODELS OF THE MASSACHUSETTS BAY

ABSTRACT - PART II

ANALYTICAL MODELS FOR ONE- AND TWO-
LAYER SYSTEMS IN RECTANGULAR BASINS

BY

DOUGLAS A. BRIGGS

AND

OLE S. MADSEN

A need for qualitative information concerning the hydrodynamics of Massachusetts Bay has been seen from recent oceanographic measurements and current studies in the Bay area. In response to this, two analytical models have been derived for a simple rectangular configuration which can be applied to the geometry of Massachusetts Bay. A one layer model has been developed to simulate the conditions found during the winter season when the water column is well mixed. A two layer model represents the stratified case generally observed, with the presence of a strong thermocline, during the summer.

Both models are derived from the linearized long wave equations in two dimensions and analytical solutions are obtained by neglecting Coriolis force, bottom friction, and wind stress. The models are depth averaged and the geometry of the Bay is represented by a rectangle. The boundary conditions are specified as zero normal velocity along the walls and a constant surface slope across the opening connecting Massachusetts Bay to the ocean.

The results of the two models indicate that the surface elevations at high tide are fairly insensitive of the assumed conditions (one or two layer model). However, for the two layer model, relatively large interfacial waves are predicted as well as velocities which at some locations in the upper layer, are directed shoreward on the ebbing tide, rather than seaward. Comparison of available field observations with these results verify, qualitatively, that these conditions do exist and shows that if a model capable of predicting velocities in the Bay is desired, it must incorporate the conditions corresponding to a two layer flow.

PART II

ACKNOWLEDGEMENTS

This study constitutes a part of a series of investigations in a major environmental research program on the "Sea Environment in Massachusetts Bay and Adjacent Waters". This program consists of theoretical and field investigations and is under the administrative and technical direction of Dr. Arthur T. Ippen, Institute Professor, Department of Civil Engineering and of Dr. Erik L. Mollo-Christensen, Professor, Department of Meteorology as co-principal investigators. Support of the program is provided in part by the Sea Grant Office of NOAA, Department of Commerce, Washington, D.C. through Grant No. NG-43-72, in part by the Henry L. and Grace Doherty Charitable Foundation, Inc., and in part by the Department of Natural Resources, Commonwealth of Massachusetts through Project No. DMR-73-1. The project which is the subject of this report was conducted by staff members of the Ralph M. Parsons Laboratory for Water Resources and Hydrodynamics and was administered under Project No. DSR 80344 and DSR 81100 at M.I.T.

This report was prepared by Mr. Douglas A. Briggs, Research Assistant, and Dr. Ole S. Madsen, Assistant Professor of Civil Engineering and formed the subject of a thesis for the M.S. degree, which Dr. Madsen supervised. His advice and guidance is hereby gratefully acknowledged.

Many staff members at the Laboratory were involved in the field observations utilized for comparison with the results of the two models developed in this report. The assistance of the following is sincerely acknowledged in this connection: Dr. Bryan R. Pearce, Research Associate, George C. Christodoulou, Ms. Sheila Frankel, Mr. William F. Leimkuhler, Mr. Edward F. McCaffrey, Mr. Robert F. Paquette, and Mr. John D. Wang. Appreciation is expressed here, also, to Ms. Stephanie M. Demeris for her excellent typing of this manuscript.

TABLE OF CONTENTS

	<u>Page</u>
TITLE PAGE	1
ABSTRACT	2
ACKNOWLEDGEMENTS	3
TABLE OF CONTENTS	4
LIST OF FIGURES	6
LIST OF TABLES	8
LIST OF SYMBOLS	9
CHAPTER I INTRODUCTION	11
CHAPTER II THEORY AND DERIVATION OF THE ONE AND TWO LAYER MODELS	14
2.1 Linear Long Waves	14
2.2 One Layer Model	15
2.3 Two Layer Model	23
CHAPTER III RESULTS OF THE ONE LAYER MODEL	36
3.1 Computational Aspects	36
3.1.1 Mathematical Simulation of the Ocean Boundary	36
3.1.2 Number of Terms Required in the Determination of η	49
3.2 Data Available for Comparison	49
3.3 Discussion of the Model Results	50
CHAPTER IV RESULTS OF THE TWO LAYER MODEL	54
4.1 Computational Considerations	54
4.1.1 Results of the Two Layer Model	54
4.1.2 Model Sensitivity	63

	<u>Page</u>
4.2 Available Data for Comparison	69
4.3 Discussion of the Model Results	77
CHAPTER V CONCLUDING REMARKS	84
BIBLIOGRAPHY	87
APPENDIX A LISTING OF THE PROGRAM USED FOR COMPUTATIONS PRESENTED IN CHAPTER IV	88

LIST OF FIGURES

<u>Figure</u>	<u>Title</u>	<u>Page</u>
1-A	Massachusetts Bay, Depth Contours in Feet	12
2-A	One Layer Model, Coordinate System and Nomenclature	16
2-B	Geometry of Massachusetts Bay for the One and Two Layered Models	19
2-C	Two Layer Model, Coordinate System and Nomenclature	24
3-A	Massachusetts Bay, Observed Differences in Tidal Amplitude at High Tide	38
3-B	One Layer Model of Massachusetts Bay, One Increment Channel	41
3-C	One Layer Model of Massachusetts Bay, with Stellwagen Bank Closed	44
3-D	One Layer Model of Massachusetts Bay, Four Increment Channel	46
3-E	Numerical Model of Massachusetts Bay	48
4-A	Two Layer Model of Massachusetts Bay at High Tide. $h_1 = 100.0$ Ft., $h_2 = 20.0$ Ft.	58
4-B	Two Layer Model of Massachusetts Bay. Velocities at Maximum Ebb. $h_1 = 100.0$ Ft., $h_2 = 20.0$ Ft.	60
4-C	Two Layer Model of Massachusetts Bay at High Tide. $h_1 = 80.0$ Ft., $h_2 = 40.0$ Ft.	62
4-D	Two Layer Model of Massachusetts Bay. Velocities at Maximum Ebb. $h_1 = 80.0$ Ft., $h_2 = 40.0$ Ft.	64
4-E	Velocity Variations as a Function of h_1 and h_2	68

<u>Figure</u>	<u>Title</u>	<u>Page</u>
4-F	C.T.D. Cast Taken in Massachusetts Bay	71
4-G	Current Drogue Study in Massachusetts Bay. July 27, 1972	76
4-H	Current Drogue Study in Massachusetts Bay. July 31, 1972	78
4-I	Two Layer Model of Massachusetts Bay. Velocities at Maximum Ebb. $h_1 = 100.0$ Ft., $h_2 = 20.0$ Ft.	82

LIST OF TABLES

<u>Table</u>	<u>Title</u>	<u>Page</u>
4-1	Sensitivity of B_0 to the Choice of Interfacial Amplitude	65
4-2	Observed Spatial Variation in Depth of Interface below the Surface	73

LIST OF SYMBOLS

A_0	Constant governing the surface profile
B_0	Constant governing the interfacial profile
A_n	Constants evaluated at integer values of n
B_n	Constants evaluated at integer values of n
C_f	Bottom shear stress coefficient
f	Coriolis acceleration
g	Acceleration of gravity
h	Average depth of the Bay
h_1	Depth of layer one (lower layer)
h_2	Depth of layer two (upper layer)
H	Surface wave height
H_1	Interfacial wave height
k	Wave number
L	Surface wave length
L_1	Interfacial wave length
m	Wave number
N	Value where m_{n_2} becomes imaginary
t	Time
T	Tidal period of 12.4 hours
u	Depth averaged velocity in the x-direction
u_1	Depth averaged velocity in layer one, x-direction
u_2	Depth averaged velocity in layer two, x-direction
U	Depth averaged velocity

U_1	Depth averaged velocity in layer one
U_2	Depth averaged velocity in layer two
v	Depth averaged velocity in the y-direction
v_1	Depth averaged velocity in layer one, y-direction
v_2	Depth averaged velocity in layer two, y-direction
V	Total volume of fluid above mean sea level
V_1	Volume of fluid in layer one above the mean interfacial level
V_2	Volume of fluid in layer two above mean sea level
x_0	Length of the Bay geometry, x-direction
x_1	Boundary of the channel opening
x_2	Boundary of the channel opening
y_0	Width of the Bay geometry, y-direction
η	Surface amplitude
η_1	Interfacial amplitude (layer one)
η_2	Surface amplitude (layer two)
λ	Linearized bottom friction term
ρ_1	Density, layer one
ρ_2	Density, layer two
τ_b	Bottom shear stress
τ_i	Interfacial shear stress
τ_s	Surface or wind stress
ϕ	Latitude
ω	$\frac{2\pi}{T}$
ω_e	Angular velocity of the earth

CHAPTER I

INTRODUCTION

Massachusetts Bay, as seen in Figure 1-A, lies at the eastern edge of Massachusetts and is surrounded by land on three sides. The average depth of the Bay is approximately 120 feet with the ocean boundary between the tip of Cape Ann and the tip of Cape Cod, a distance of the order 41.0 nautical miles. Located on the northwest is Boston Harbor through which three rivers, the Charles, the Chelsea, and the Mystic, flow into the Bay. In addition, the Cape Cod Canal exerts an effect on the Bay circulation by allowing an exchange with Buzzards Bay to the southwest.

The results of current observations and other oceanographic measurements recently taken in Massachusetts Bay have shown the occurrence of some interesting and unusual conditions. Field data concerning the vertical structure of temperature, salinity, and density suggests that a rather pronounced stratification exists during the summer months. Drogue studies during periods of pronounced stratification exhibited some rather peculiar phenomena. Thus, it was found that shallow drogues during ebbing tide proceeded towards the shore rather than seaward, as expected. Although the well mixed situation, encountered during the winter season, is of interest and will be considered, it is the stratified case that is of primary concern since it is this situation that exhibits the most unusual condition.

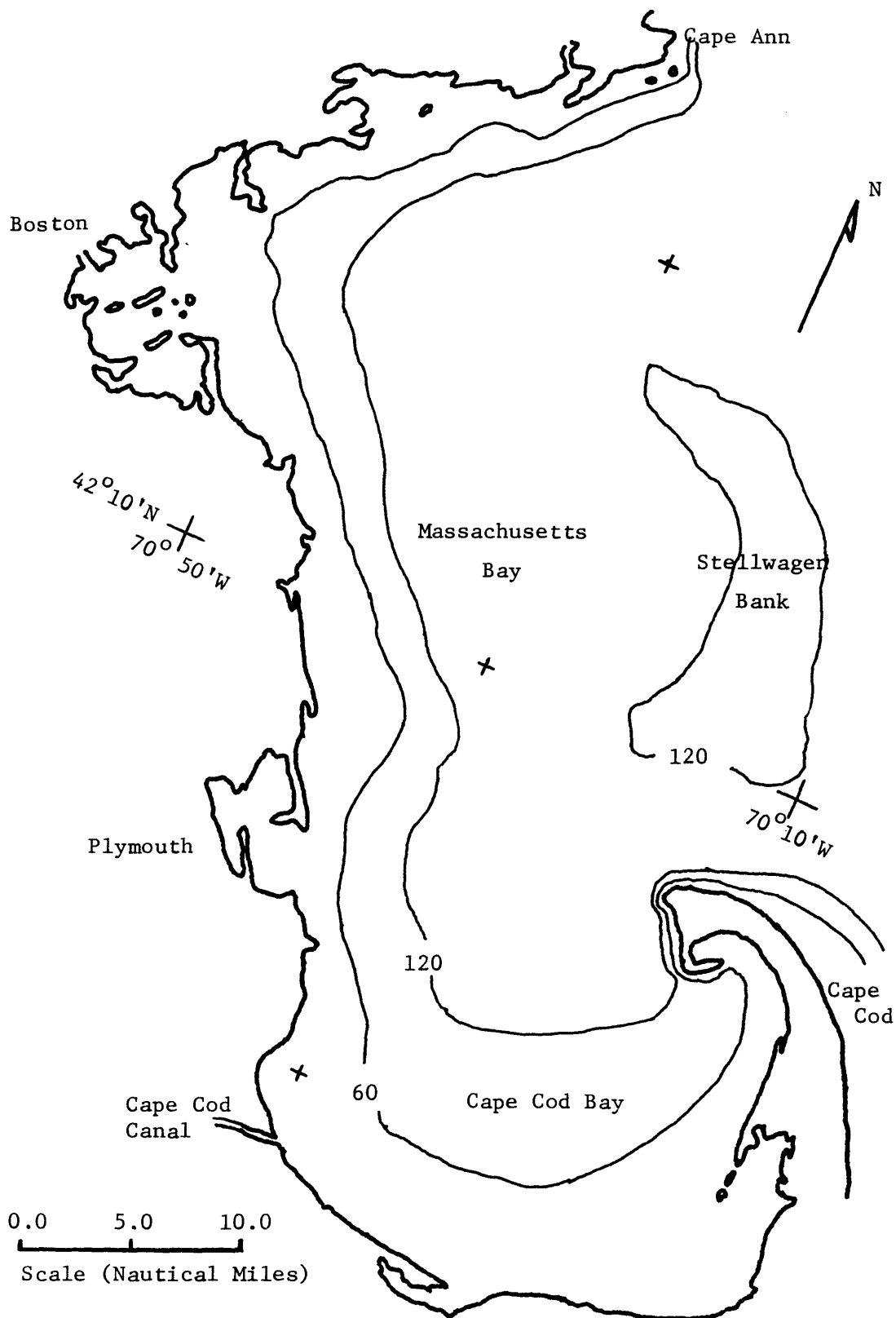


Figure 1-A: Massachusetts Bay, Depth Contours in Feet

Thus it was felt that a simple model predicting the hydrodynamics of Massachusetts Bay, shown in Figure 1-A, could lead to source insight into the Bay circulation and possibly explain some of the unusual field observations. Consequently, the theoretical development of two analytical models, a one layer model representing the well mixed case and a two layer model representing the stratified case, was undertaken in an attempt to explain some of these conditions. The primary quality of the desired model was that it be simple, such that an analytical solution could be obtained and readily evaluated. This was attained by the simplifying assumption of a depth averaged rectangular configuration for the Bay area. Further, by linearizing the governing equations neglecting Coriolis force, bottom friction, and wind stress, a simple analytical solution was obtained, which qualitatively explains some of the observed phenomena.

The models predict currents and amplitudes for the entire area of Massachusetts Bay. Results of the model show a difference in the predicted current pattern, suggesting the necessity of including, in a more sophisticated model, the effects of stratification if an accurate prediction of the current field is desired. By comparing the results of the two layer model with field observations, it is demonstrated that such occurrences as relatively large interfacial waves and currents flowing toward the boundaries in the upper layer during an ebbing tide are qualitatively explained by the simple two layer model presented here.

CHAPTER II

THEORY AND DERIVATION OF THE ONE AND TWO LAYERED MODELS

2.1 Linear Long Waves

Two dimensional long wave propagation has, in the past decade, received considerable attention from both analytical and numerical modelers as the system of equations describes a physical situation of considerable interest to the coastal engineer. Able to predict the hydrodynamics associated with storm surge and tidal-wave propagation, models utilizing long wave theory have provided engineers and related practitioners with the ability to predict tidal currents and elevations in estuaries and coastal areas.

The long wave equations describe flow in the nearly horizontal direction, with the implication that the pressure distribution is hydrostatic and that the vertical accelerations are negligible. Due to the fact that even numerical solutions of the non-linear equations are rather difficult to obtain, the present models will be restricted to the linearized equations of motion in two dimensions. The equations, which are vertically averaged, neglect convective accelerations and allow a simplistic approach in their application to Massachusetts Bay.

Derivation of the one and two layered models are quite similar in nature and both include, in the governing equations, Coriolis force and frictional forces.

However, in order to preserve simplicity, we neglect the influence of the Coriolis force as well as bottom and interfacial

friction in the application of the two models.

2.2 One Layered Model

The dynamic equations for the one layered model can be derived through the application of the Navier-Stokes equations for incompressible fluids. The equations of continuity can be derived by summing the mass flux through a control volume. Representation of the coordinate system and nomenclature for the one layered model is found in Figure 2-A. In linearized form, assuming constant depth and vertically averaged velocities, the governing momentum equations for tidal wave propagation, including bottom friction and Coriolis force, become in the x and y directions respectively:

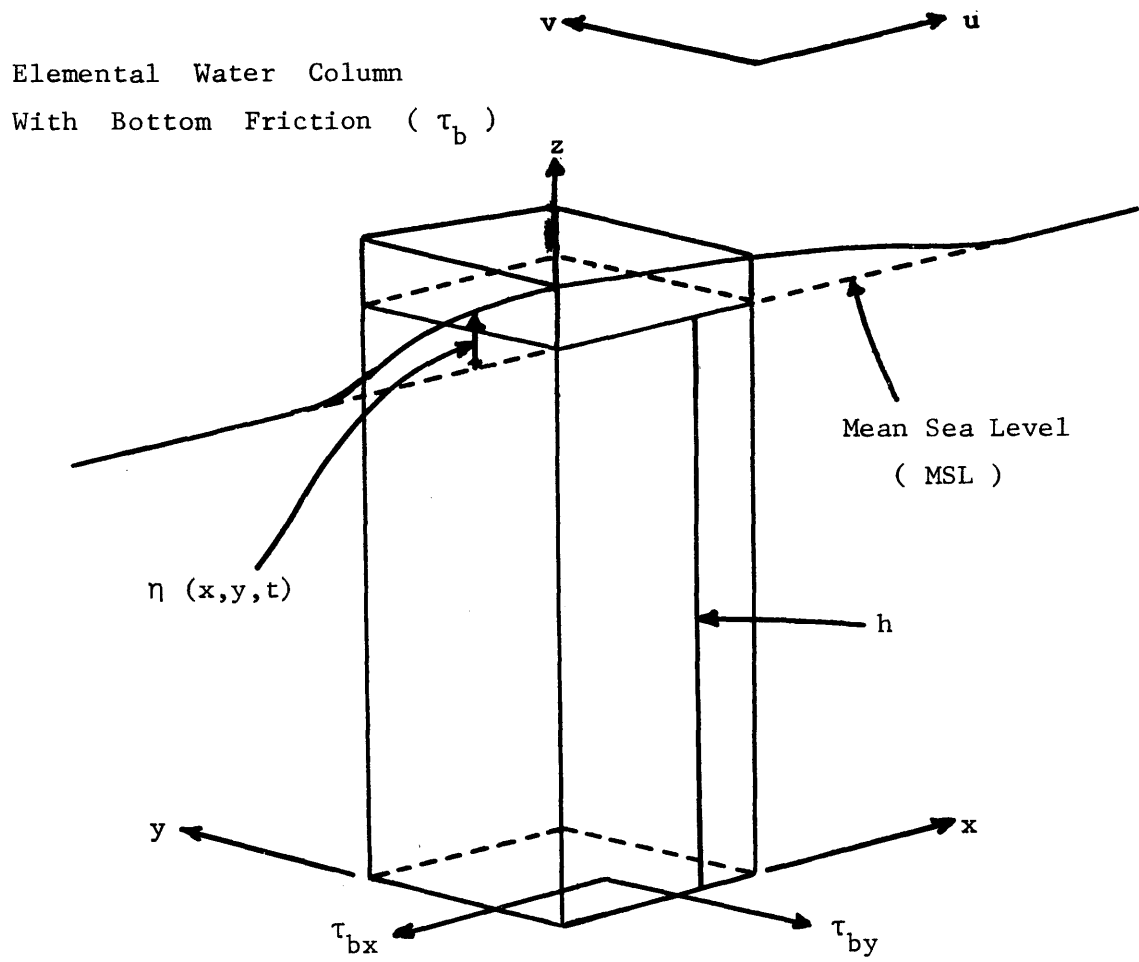
$$g \frac{\partial \eta}{\partial x} + \frac{\partial u}{\partial t} - \frac{1}{2} C_f U \frac{1}{h} u - 2\omega_e (\sin\phi)v = 0 \quad (2.1A)$$

$$g \frac{\partial \eta}{\partial y} + \frac{\partial v}{\partial t} - \frac{1}{2} C_f U \frac{1}{h} v + 2\omega_e (\sin\phi)u = 0 \quad (2.1B)$$

where u and v are respectively components of the water velocity in the x and y directions, t is time, g is acceleration due to gravity, η is the surface elevation relative to mean sea level, C_f is the local shear-stress coefficient, $U = \sqrt{u^2 + v^2}$, h is the depth, ω_e is the angular velocity of the earth, and ϕ is the latitude. The linearized form of the continuity equation is:

$$\frac{\partial \eta}{\partial t} + \frac{\partial(hu)}{\partial x} + \frac{\partial(hv)}{\partial y} = 0 \quad (2.2)$$

Assuming periodic motion, where $\omega = \frac{2\pi}{T}$ and T equals the tidal period of 12.4 hours;



One Layer Model

Coordinate System and Nomenclature

Figure 2-A

$$(u, v) = \text{Real} \{(u, v)e^{i\omega t}\} \quad (2.3A)$$

$$\eta = \text{Real} \{\eta e^{i\omega t}\} \quad (2.3B)$$

it can be shown after linearization of the friction term by letting

$\lambda = \frac{1}{2} C_f U \frac{1}{h}$ and by setting $f = 2 \omega_e (\sin\phi)$ that:

$$g \frac{\partial \eta}{\partial x} + i\omega u - \lambda u - fv = 0 \quad (2.4A)$$

$$g \frac{\partial \eta}{\partial y} + i\omega v - \lambda v + fu = 0 \quad (2.4B)$$

Equation (2.4B) can be solved for v which is then introduced into Equation (2.4A) giving u in the form:

$$u = - \frac{g}{i\omega - \lambda + \frac{f^2}{i\omega - \lambda}} \frac{\partial \eta}{\partial x} - \frac{fg}{(i\omega - \lambda)^2 + f^2} \frac{\partial \eta}{\partial y} \quad (2.5A)$$

By the same manner solving for u in Equation (2.4A) v can be obtained as:

$$v = - \frac{g}{i\omega - \lambda + \frac{f^2}{i\omega - \lambda}} \frac{\partial \eta}{\partial y} + \frac{fg}{(i\omega - \lambda)^2 + f^2} \frac{\partial \eta}{\partial x} \quad (2.5B)$$

Differentiating equation Equation (2.5A) with respect to x and Equation (2.5B) with respect to y and multiplying both by h allows substitution of the $\frac{\partial(hu)}{\partial x}$ and $\frac{\partial(hv)}{\partial y}$ terms in Equation (2.2). The continuity equation now becomes:

$$\frac{\partial \eta}{\partial t} - \frac{gh}{i\omega - \lambda + \frac{f^2}{i\omega - \lambda}} \left(\frac{\partial^2 \eta}{\partial x^2} + \frac{\partial^2 \eta}{\partial y^2} \right) = 0 \quad (2.6)$$

By letting $\frac{\partial \eta}{\partial t} = i\omega\eta$ the governing equation for η in the one layer model becomes in final form:

$$\frac{\partial^2 \eta}{\partial x^2} + \frac{\partial^2 \eta}{\partial y^2} + \frac{\omega^2}{gh} \left(1 + i \frac{\lambda}{\omega} - \frac{(f/\omega)^2}{1 + i \frac{\lambda}{\omega}} \right) \eta = 0 \quad (2.7)$$

The special case of no bottom friction, $\lambda = 0$, and no Coriolis force, $f = 0$, leads to:

$$\frac{\partial^2 \eta}{\partial x^2} + \frac{\partial^2 \eta}{\partial y^2} + \frac{\omega^2}{gh} \eta = 0 \quad (2.8)$$

It is clear from (2.5A), (2.5B) and (2.7) that a non-zero bottom shear stress will introduce a phase difference between u , v and $\frac{\partial \eta}{\partial x}$ and $\frac{\partial \eta}{\partial y}$. The magnitude of the term $\frac{\lambda}{\omega}$ may be estimated, from an assumption of $C_f \approx 0.005$, $h = 120$ ft, and $U \approx 1$ ft/sec, to be $\frac{1}{8}$ which indicates that it is reasonable to neglect this term.

It is worth noting in the governing equation, the importance of Coriolis effect on Massachusetts Bay where the mid-latitude is approximately 42°N . The Coriolis term in Equation (2.7) is of the order 0.45 since $(\frac{f}{\omega})^2 \approx \sin^2 42^\circ$, and obviously neglecting f is a relatively poor assumption. However, by retaining Coriolis, the boundary conditions become complicated and difficult to solve and since the purpose of the study is to develop a simple qualitative model, f is set equal to zero.

Now that the simplified governing equation has been developed for the one layered model, the various conditions must be imposed on the boundaries to specify the particular problem. As shown in

Figure 2-B, a simple geometry has been assumed with effectively impermeable walls on all sides except at $y = y_0$ between x_1 and x_2 where there is an opening representing the ocean boundary between Massachusetts Bay and the Gulf of Maine.

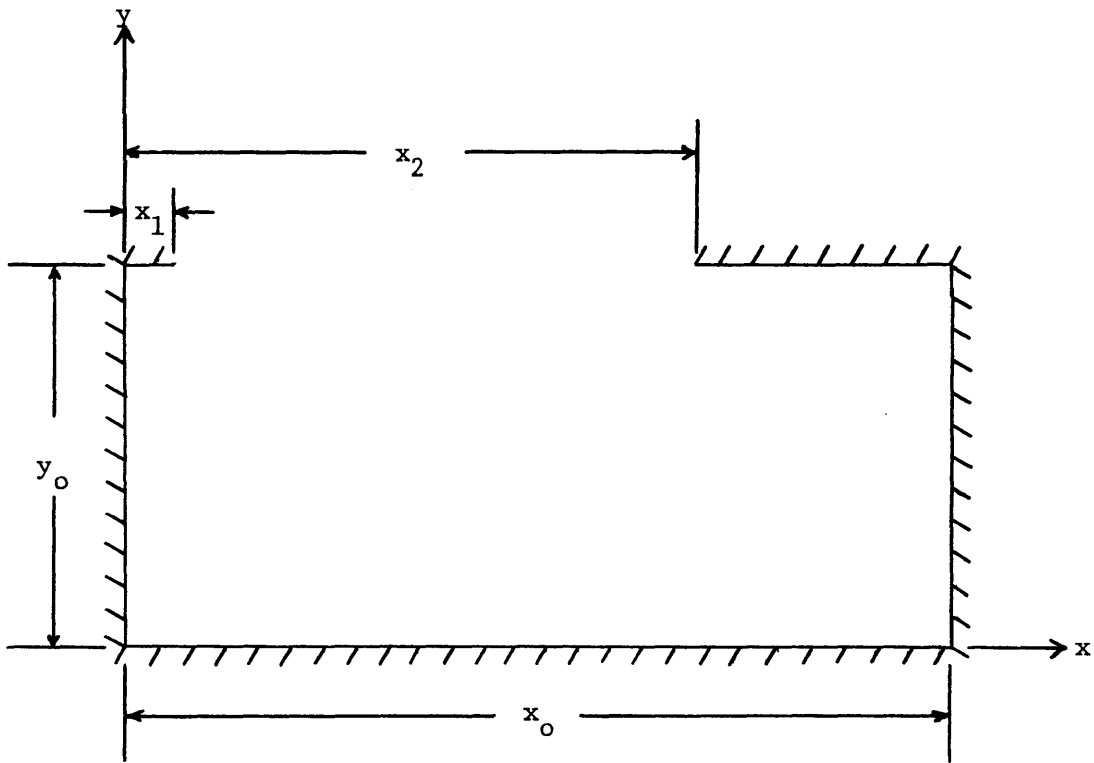


Figure 2-B: Geometry of Massachusetts Bay For The One and Two Layered Models.

Consequently the velocities can be specified along the walls such that $u = 0$ at $x = 0$ and x_0 for all y and that $v = 0$ at $y = 0$ for all x and at $y = y_0$ for $0 < x < x_1$, $x_2 < x < x_0$. Neglecting Coriolis effects it is seen that $u = 0$ corresponds to $\frac{\partial \eta}{\partial x} = 0$ from Equation (2.5A) and that $v = 0$ corresponds to $\frac{\partial \eta}{\partial y} = 0$ from Equation (2.5B). Consequently the boundary conditions may be summarized as:

$$\text{At } x = 0 \quad \frac{\partial \eta}{\partial x} = 0 \quad (2.9A)$$

$$\text{At } x = x_0 \quad \frac{\partial \eta}{\partial x} = 0 \quad (2.9B)$$

$$\text{At } y = 0 \quad \frac{\partial \eta}{\partial y} = 0 \quad (2.9C)$$

$$\text{At } y = y_0 \quad \frac{\partial \eta}{\partial y} = 0 \quad \begin{array}{l} 0 \leq x \leq x_1 \\ x_2 \leq x \leq x_0 \end{array} \quad (2.9D)$$

If the width of the opening between x_2 and x_1 is small it may be assumed that $\frac{\partial \eta}{\partial y}$ or v is constant over the entire opening. A gross conservation of mass consideration then gives, with Ψ being the volume of fluid in the bay above mean sea level:

$$\Psi = \int dx \int \eta dy$$

$\frac{\partial \Psi}{\partial t}$ = rate of change of volume within the bay must be equal to the inflow through the opening. This can be written as:

$$\frac{\partial \Psi}{\partial t} = -v(x_2 - x_1)h \quad \text{at } y = y_0 \quad (2.10)$$

From Equation (2.5B), assuming no friction and no Coriolis effect, it can be shown that:

$$\frac{\partial \eta}{\partial y} = \frac{i\omega}{g} \frac{1}{(x_2 - x_1)h} \frac{\partial \Psi}{\partial t} \quad (2.11)$$

Assuming that the tidal motion within the bay is periodic where $\Psi = \Psi e^{i\omega t}$ or $\frac{\partial \Psi}{\partial t} = i\omega \Psi$ the last boundary condition can be determined:

$$\text{At } y = y_0 \quad \frac{\partial \eta}{\partial y} = -\frac{\omega^2}{gh} \frac{1}{x_2 - x_1} \Psi \quad x_1 \leq x \leq x_2 \quad (2.12)$$

The solution can be expected to be determined except for a constant since only derivatives are prescribed as boundary conditions. This constant is determined from considerations of the amplitude of the tidal motion at some point in the bay.

The boundary conditions specified in (2.9A) and (2.9B) suggest an x-dependence in the solution of η such that $\eta = \cos k_n x$. It is apparent that $\frac{\partial \eta}{\partial x} = 0$ at $x = 0$ and also at $x = x_0$ if $k_n x_0 = n\pi$ for $n = 0, 1, 2, \dots$. Thus k_n will take the form:

$$k_n = \frac{n\pi}{x_0} \quad (2.13)$$

The boundary condition in (2.9C) suggests a dependency in y such that $\eta = \cos m_n y$. As a result $\frac{\partial \eta}{\partial y} = 0$ at $y = 0$ and consequently a solution of the following form will be sought:

$$\eta = e^{i\omega t} \sum_0^{\infty} A_n \cos k_n x \cos m_n y \quad (2.14)$$

The solution must satisfy the governing equation (2.8), and by substituting the general solution (2.14) into (2.8) m_n can be solved in terms of k_n :

$$m_n = \sqrt{\frac{\omega^2}{gh} - k_n^2} \quad n = 0, 1, 2, \dots \quad (2.15)$$

For the particular case of Massachusetts Bay $h \approx 120$ feet and $x_0 = 59$. NM (nautical miles) and it can be shown that m_n is imaginary for $n > 0$. Since we are seeking only that portion of the solution which is real and by the fact that $\cos i \alpha = \cosh \alpha$ the general solution may be written as:

$$\eta = e^{i\omega t} \left\{ A_0 \cos m_0 y + \sum_{n=1}^{\infty} A_n \cos k_n x \cosh m_n y \right\} \quad (2.16)$$

where m_0 is evaluated for $n = 0$ in Equation (2.15). The constants A_n must be determined from the remaining boundary conditions specified at $y = y_0$.

Evaluating the volume of water in the bay, Ψ , it can be shown that only the term corresponding to $n = 0$ contributes to the volume since integration of the terms for $n > 0$ from $x = 0$ to x_0 give zero by virtue of the boundary conditions. Hence:

$$\Psi = \frac{1}{m_0} A_0 x_0 \sin m_0 y_0 \quad (2.17)$$

which determines the boundary condition, stated in (2.12), to be satisfied at $y = y_0$.

The y derivative of the solution given by Equation (2.16) can now be matched at $y = y_0$ with the boundary conditions given in (2.9D) and (2.12) with Ψ from (2.17). Through a Fourier expansion the coefficients A_n can be determined leading to the final form of the general solution:

$$\eta = A_o e^{i\omega t} \left\{ \cos m_o y - \sum_{n=1}^{\infty} \frac{2m_o \sin m_o y_o (\sin k_n x_2 - \sin k_n x_1)}{m_n k_n (x_2 - x_1)} \frac{\cosh m_n y}{\sinh m_n y_o} \cos k_n x \right\} \quad (2.18)$$

where A_o can be evaluated once the elevation η at some point in the Bay is known.

2.3 Two Layered Model

Derivation of the two layered analytical model is similar to the one layered one although discrete differences appear with the introduction of the second layer. The dynamic equations are again formulated in two dimensions by the application of the Navier-Stokes equations and the continuity relationships through a mass balance. The model is able to predict water surface and interface profiles and velocities in both layers.

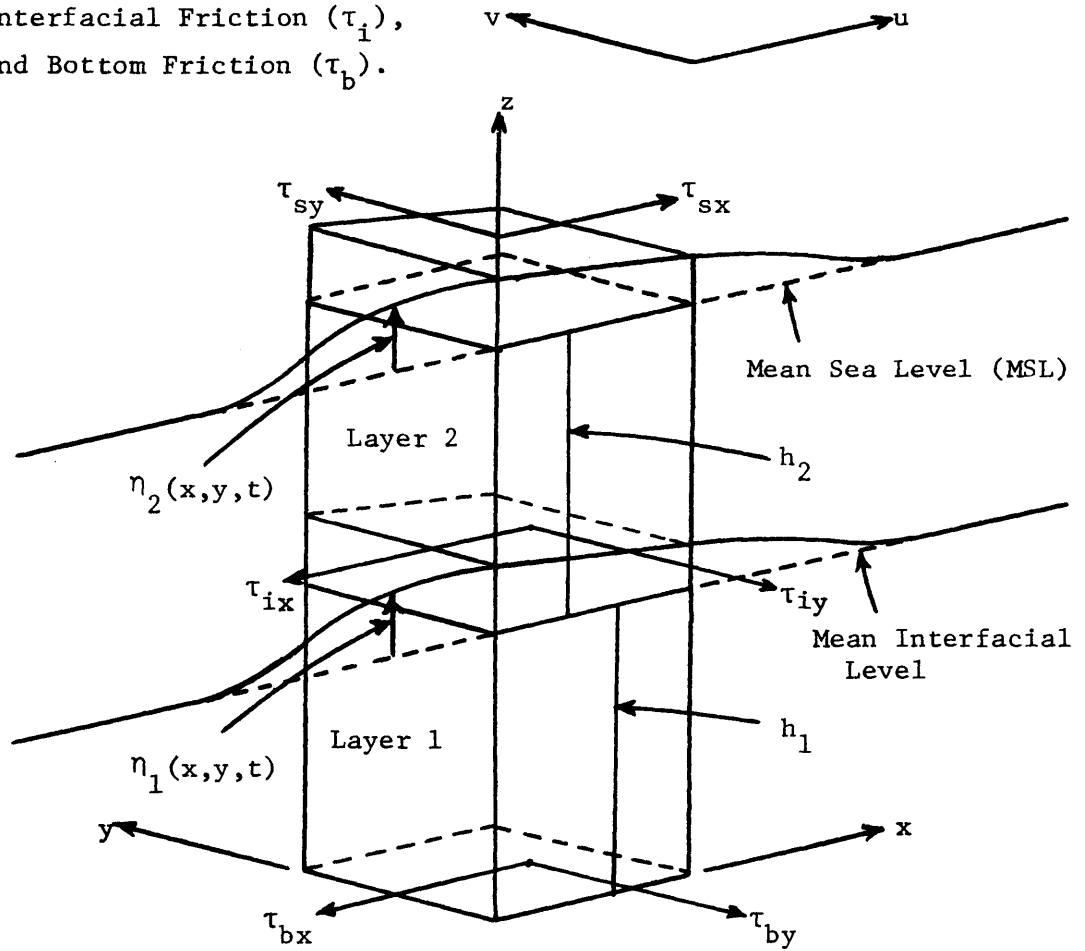
Representation of the coordinate system for the two layered model is shown in Figure 2-C. The lower layer is specified as layer one and the upper layer as layer two with the subscripts 1 and 2, respectively. With this the dynamic equations, in linear form, for the two layered model become:

Layer 1, x-direction

$$\frac{\partial u_1}{\partial t} + \frac{\rho_2}{\rho_1} g \frac{\partial \eta_2}{\partial x} + \frac{\rho_1 - \rho_2}{\rho_1} g \frac{\partial \eta_1}{\partial x} - \frac{1}{2} C_f U_1 \frac{1}{h_1} u_1 + \frac{\tau_{ix}}{\rho_1 h_1} =$$

$$2\omega_e (\sin \phi) v_1 = 0 \quad (2.19A)$$

Elemental Water Column With
 Surface Friction (τ_s),
 Interfacial Friction (τ_i),
 and Bottom Friction (τ_b).



Two Layer Model
 Coordinate System and Nomenclature

Figure 2-C

Layer 1, y-direction

$$\frac{\partial v_1}{\partial t} + \frac{\rho_2}{\rho_1} g \frac{\partial \eta_2}{\partial y} + \frac{\rho_1 - \rho_2}{\rho_1} g \frac{\partial \eta_1}{\partial y} - \frac{1}{2} C_f U_1 \frac{1}{h_1} v_1 + \frac{\tau_{iy}}{\rho_1 h_1} + 2\omega_e (\sin \phi) u_1 = 0 \quad (2.19B)$$

Layer 2, x-direction

$$\frac{\partial u_2}{\partial t} + g \frac{\partial \eta_2}{\partial x} - \frac{\tau_{ix}}{\rho_2 h_2} + \frac{\tau_{sx}}{\rho_2 h_2} - 2\omega_e (\sin \phi) v_2 = 0 \quad (2.19C)$$

Layer 2, y-direction

$$\frac{\partial v_2}{\partial t} + g \frac{\partial \eta_2}{\partial x} - \frac{\tau_{iy}}{\rho_2 h_2} + \frac{\tau_{sy}}{\rho_2 h_2} + 2\omega_e (\sin \phi) u_2 = 0 \quad (2.19D)$$

where ρ is the density, τ_{ix} and τ_{iy} are the interfacial friction terms, and τ_s indicates a surface wind shear stress. The remaining terms were defined in the one layer model and remain the same. The conservation of mass equations are similar to those in the previous model and when linearized take the form:

Layer 1

$$\frac{\partial \eta_1}{\partial t} + \frac{\partial (h_1 u_1)}{\partial x} + \frac{\partial (h_1 v_1)}{\partial y} = 0 \quad (2.20A)$$

Layer 2

$$\frac{\partial \eta_2}{\partial t} + \frac{\partial (h_2 u_2)}{\partial x} + \frac{\partial (h_2 v_2)}{\partial y} - \frac{\partial \eta_1}{\partial t} = 0 \quad (2.20B)$$

The above continuity equations have assumed two immiscible fluids,

i.e., no exchange of mass across the interface. If a mass exchange between the two layers were considered the interfacial friction would be influenced by the associated momentum transfer across the interface. For a discussion of this reference is given in Pedersen (1972). The governing equations are the linearized form of those given by Grubert and Abbott (1972).

It is obvious that retaining the Coriolis and the frictional terms tends to make the governing equations quite lengthy and difficult to solve. Consequently, the bottom and interfacial friction terms, the Coriolis force, and surface shear stress will be set equal to zero in order to retain the simplicity that is desired in the model.

It is important to note the result of the steady state condition, as in the case of wind setup, where $\frac{\partial u}{\partial t}$ and $\frac{\partial v}{\partial t}$ are zero. It can be shown that if $\frac{\partial \eta_2}{\partial x}$ and $\frac{\partial \eta_2}{\partial y}$ do not equal zero then the momentum equations for layer one, given by (2.19A) and (2.19B), reduce to:

x-direction

$$\frac{\partial \eta_1}{\partial x} = - \frac{\rho_2}{\rho_1 - \rho_2} \frac{\partial \eta_2}{\partial x} \quad (2.21A)$$

y-direction

$$\frac{\partial \eta_1}{\partial y} = - \frac{\rho_2}{\rho_1 - \rho_2} \frac{\partial \eta_2}{\partial y} \quad (2.21B)$$

Obviously, if the densities of the two fluids are within a few percent of each other, the slope of the interface is far greater than that of the surface. In addition the slope of one is tilted in an opposite direction from the other.

In Massachusetts Bay the density of one layer is generally within 0.4 percent of the other. Since the two densities are so close together, an approximate form of the momentum equations for layer one could be obtained by replacing $\frac{\rho_2}{\rho_1}$ in η_2 by unity.

Again summing the tidal motion in the bay to be periodic we take:

$$(\eta_1, \eta_2, u_1, u_2, v_1, v_2) = \text{Real} (\eta_1, \eta_2, u_1, u_2, v_1, v_2) e^{i\omega t}$$

$$\left(\frac{\partial u_1}{\partial t}, \frac{\partial u_2}{\partial t}, \frac{\partial v_1}{\partial t}, \frac{\partial v_2}{\partial t} \right) = i\omega (u_1, u_2, v_1, v_2)$$

the governing equations can be derived for velocities and elevations.

Velocities in the upper layer, u_2 and v_2 , can be obtained directly from the momentum Equations (2.19C) and (2.19D)

$$u_2 = - \frac{g}{i\omega} \frac{\partial \eta_2}{\partial x} \quad (2.22A)$$

$$v_2 = - \frac{g}{i\omega} \frac{\partial \eta_2}{\partial y} \quad (2.22B)$$

By taking the derivative of u_2 with respect to x and the derivative of v_2 with respect to y , the $\frac{\partial(h_2 u_2)}{\partial x}$ and $\frac{\partial(h_2 v_2)}{\partial y}$ terms can be obtained and introduced into the continuity equation for layer two, (2.20B). In terms of η_2 the governing equation for the interface profile becomes:

$$\eta_1 = \eta_2 + \frac{gh_2}{\omega^2} \left(\frac{\partial^2 \eta_2}{\partial x^2} + \frac{\partial^2 \eta_2}{\partial y^2} \right) \quad (2.23)$$

The x and y derivatives of η_1 can now be introduced into Equations (2.19A) and (2.19B) respectively. By this the velocities in the lower layer are determined as:

$$u_1 = -\frac{g}{i\omega} \frac{\partial \eta_2}{\partial x} - \frac{g}{i\omega} \frac{\rho_1 - \rho_2}{\rho_1} \frac{gh_2}{\omega^2} \left(\frac{\partial^3 \eta_2}{\partial x^3} + \frac{\partial^3 \eta_2}{\partial x \partial y^2} \right) \quad (2.24A)$$

$$v_1 = -\frac{g}{i\omega} \frac{\partial \eta_2}{\partial y} - \frac{g}{i\omega} \frac{\rho_1 - \rho_2}{\rho_1} \frac{gh_2}{\omega^2} \left(\frac{\partial^3 \eta_2}{\partial x^2 \partial y} + \frac{\partial^3 \eta_2}{\partial y^3} \right) \quad (2.24B)$$

Now that the velocities in layer one have been derived, it only remains to determine the equation governing η_2 . It should be noted that the development of the governing equations has specified all velocities and η_1 in terms of η_2 . The surface profile, η_2 , can be determined in much the same manner in which η_1 was found, i.e., $\frac{\partial(h_1 u_1)}{\partial x}$ and $\frac{\partial(h_1 v_1)}{\partial y}$ can be derived from Equations (2.24A) and (2.24B) respectively and along the Equation (2.23) can be introduced into the Conservation of Mass equation for layer one, (2.20A). Consequently, the governing equation for η_2 takes the form:

$$\eta_2 + \frac{g(h_1 + h_2)}{\omega^2} \left(\frac{\partial^2 \eta_2}{\partial x^2} + \frac{\partial^2 \eta_2}{\partial y^2} \right) + \frac{gh_1}{\omega^2} \frac{gh_2}{\omega^2} \frac{\rho_1 - \rho_2}{\rho_1} \left(\frac{\partial^4 \eta_2}{\partial x^4} + \frac{2\partial^4 \eta_2}{\partial x^2 \partial y^2} + \frac{\partial^4 \eta_2}{\partial y^4} \right) = 0 \quad (2.25)$$

For the case $\rho_1 = \rho_2$ it should be noted that the above equation reduces to the linear long wave equation in two dimensions.

The same geometry used in the one layered model will be applied to the two layered situation. As shown in Figure 2-B, the Bay is assumed rectangular with impermeable boundaries except for the section between Cape Cod and Cape Ann which is open to the Gulf of Maine. The boundary conditions are formulated by specifying the velocities,

in both layers, equal to zero along the walls and can be summarized as:

$$u_1, u_2 = 0 \quad \text{at } x = 0 \text{ and } x_0 \quad (2.26A)$$

$$v_1, v_2 = 0 \quad \text{at } y = 0 \quad (2.26B)$$

This suggests a solution of the following form:

$$\eta_2 = i\omega t \sum_0^{\infty} A_n \cos k_n x \cos m_n y \quad (2.27)$$

where the constants A_n , k_n , and m_n must be determined for each n .

Applying now the boundary conditions in (2.26A) to the assumed solution for u_2 , given by Equations (2.22A) and (2.27), k_n can be derived in the following form:

$$k_n = \frac{n\pi}{x_0} \quad n = 0, 1, 2, \dots$$

which is the same as derived previously for the one layered case and will satisfy u_1 as given in Equation (2.24A).

The condition that v_2 is equal to zero at $y = 0$ can be applied to the solution for v_2 as given by Equations (2.22B) and (2.27). Combined with the expression for v_1 it is seen that both have a y dependence given by $\sin m_n y$ which vanishes at y equal to zero. Thus the assumed solution, as given by Equation (2.27), meets all the specified boundary conditions and seems promising as the general solution for η_2 .

Since k_n has been determined it now remains to find the

expression for m_n . Introducing the assumed solution for η_2 into the governing equation for the surface profile, Equation (2.25), yields an expression which can be reduced to the form $am_n^4 + bm_n^2 + c = 0$. As it is quadratic, the expression can be solved directly for m_n to the following point.

$$m_n^2 = -k_n^2 + \frac{1}{2} \frac{\omega^2}{gh_2} \frac{h_1+h_2}{h_1} \frac{\rho_1}{\rho_1-\rho_2} \left(1 \pm \sqrt{1 - 4 \frac{\rho_1-\rho_2}{\rho_1} \frac{h_1 h_2}{(h_1+h_2)^2}} \right)$$

The quantity $4 \frac{\rho_1-\rho_2}{\rho_1} \frac{h_1 h_2}{(h_1+h_2)^2} \leq \frac{\rho_1-\rho_2}{\rho_1}$ which will be far smaller than unity. Thus, the approximation can be made that $\sqrt{1-\epsilon}$ equals $1 - \frac{1}{2} \epsilon$. With this the final form of m_n is obtained as:

$$m_{n1} = \sqrt{\frac{\omega^2}{g(h_1+h_2)} - k_n^2} \quad (2.29A)$$

$$m_{n2} = \sqrt{\frac{\omega^2}{gh_2} \frac{\rho_1}{\rho_1-\rho_2} \frac{h_1+h_2}{h_1} - \frac{\omega^2}{g(h_1+h_2)} - k_n^2} \quad (2.29B)$$

where (2.29A) is seen to be identical to the result obtained for the one layer model, (2.15). Thus when the Bay dimensions are small compared to the tidal wave length it can be seen that m_{n1} is imaginary except for $k_n = 0$. However, m_{n2} will start out by being real if $\frac{\rho_1-\rho_2}{\rho_1}$ is sufficiently small, but at some $n = N$, m_{n2} will also become imaginary. Hence, the solution may be written as:

$$\begin{aligned}
\eta_2 = e^{i\omega t} & \left\{ A_0 \cos m_{o1} y + \sum_{n=1}^{\infty} A_n \cos k_n x \cosh m_{n1} y \right. \\
& + B_0 \cos m_{o2} y + \sum_{n=1}^{N-1} B_n \cos k_n x \cos m_{n2} y + \\
& \left. \sum_{n=N}^{\infty} B_n \cos k_n x \cosh m_{n2} y \right\} \quad (2.30)
\end{aligned}$$

The solution for η_1 can now also be written in terms of A_n and B_n by the substitution of Equation (2.30) into Equation (2.23). From (2.30) and the similarity between (2.29A) and (2.15) it is obvious that the terms involving the constants A_n are similar to our one layer model, whereas the terms involving B_n express the influence of the two layered system.

As previously discussed, a gross conservation of mass consideration can be defined as:

$$\Psi = \int dy \int \eta dx$$

Applying this to the total water column and integrating from $x = 0$ to x_0 and $y = 0$ to y_0 yields the equation for the volume of fluid in the bay.

$$\Psi_{\text{total}} = \int dy \int \eta_2 dx = x_0 \left[A_0 \frac{1}{m_{o1}} \sin(m_{o1} y_0) + B_0 \frac{1}{m_{o2}} \sin(m_{o2} y_0) \right] \quad (2.31A)$$

By the same method the volume, Ψ_1 , of the lower layer, can be determined since the solution to η_1 has been determined:

$$\begin{aligned} \Psi_1 = \int dy \int \eta_1 dx = x_o [A_o \frac{1}{m_{o_1}} \sin(m_{o_1} y_o) + B_o \frac{1}{m_{o_2}} \sin(m_{o_2} y_o)] \\ - x_o \frac{gh_2}{\omega^2} [A_o m_{o_1} \sin(m_{o_1} y_o) + B_o m_{o_2} \sin(m_{o_2} y_o)] \end{aligned} \quad (2.31B)$$

The change in volume within each layer, $\frac{\partial \Psi_1}{\partial t}$ and $\frac{\partial \Psi_2}{\partial t}$, is periodic and must be equal to the inflow through the opening. Consequently, as in the one layer model, the following can be written:

$$\frac{\partial \Psi_1}{\partial t} = -v_1(x_2-x_1)h_1 \quad \text{at } y = y_o \quad (2.32A)$$

$$\frac{\partial(\Psi_{\text{total}} - \Psi_1)}{\partial t} = -v_2(x_2-x_1)h_2 \quad \text{at } y = y_o \quad (2.32B)$$

Since v_2 is given by Equation (2.22B) it can be shown that, by substitution of v_2 into Equation (2.32B), $\frac{\partial \eta_2}{\partial y}$ will take the form:

$$\frac{\partial \eta_2}{\partial y} = -\frac{\omega^2}{gh_2(x_2-x_1)} (\Psi_{\text{total}} - \Psi_1) \quad (2.33)$$

By the fact that Ψ_1 and Ψ_{total} are given and since $\frac{\partial \eta_2}{\partial y}$ can be obtained from Equation (2.30) the above equation can be expressed completely in terms of A_n and B_n . Similarly, v_1 can be obtained by substitution of the solution for η_2 into Equation (2.24B) which when introduced into Equation (2.32A) also, by knowing Ψ_1 , gives an expression completely in A_n and B_n . These equations become:

Layer 1 (Bottom Layer)

$$\begin{aligned}
 & A_{o_1} m_{o_1} \sin m_{o_1} y_o - \sum_{n=1}^{\infty} A_{n n_1} m_{n_1} \cos k_n x \sinh m_{n_1} y_o + B_{o_2} m_{o_2} \sin m_{o_2} y_o \\
 & + \sum_{n=1}^{N-1} B_{n n_2} m_{n_2} \cos k_n x \sin m_{n_2} y_o - \sum_{n=N}^{\infty} B_{n n_2} m_{n_2} \cos k_n x \sinh m_{n_2} y_o \\
 & - \frac{\rho_1 - \rho_2}{\rho_1} \frac{gh_2}{\omega^2} \left[\sum_{n=1}^{\infty} - A_{n n_1} k_n^2 m_{n_1} \cos k_n x \sinh m_{n_1} y_o \right. \\
 & + \sum_{n=1}^{\infty} A_{n n_1} m_{n_1}^3 \cos k_n x \sinh m_{n_1} y_o + \sum_{n=1}^{N-1} B_{n n_2} k_n^2 m_{n_2} \cos k_n x \sin m_{n_2} y_o \\
 & - \sum_{n=N}^{\infty} B_{n n_2} k_n^2 m_{n_2} \cos k_n x \sinh m_{n_2} y_o + \sum_{n=1}^{N-1} B_{n n_2} m_{n_2}^3 \cos k_n x \sin m_{n_2} y_o \\
 & \left. + \sum_{n=N}^{\infty} B_{n n_2} m_{n_2}^3 \cos k_n x \sinh m_{n_2} y_o \right] =
 \end{aligned}$$

$$\left. \begin{aligned}
 & + \frac{\omega^2}{gh_1(x_2 - x_1)} v_1 & x_1 < x < x_2 \\
 & 0 & \text{elsewhere}
 \end{aligned} \right\}$$

(2.34A)

Layer 2 (Top Layer)

$$A_0 m_{o_1} \sin m_{o_1} y_0 - \sum_{n=1}^{\infty} \frac{m_{n_1}}{2} A_n \sinh m_{n_1} y_0 + B_0 m_{o_2} \sin m_{o_2} y_0$$

$$+ \sum_{n=1}^{N-1} \frac{m_{n_2}}{2} B_n \sin m_{n_2} y_0 - \sum_{n=N}^{\infty} \frac{m_{n_2}}{2} B_n \sinh m_{n_2} y_0 =$$

$$\left\{ \begin{array}{ll} \frac{\omega^2}{gh_2(x_2-x_1)} (\Psi_{\text{total}} - \Psi_1) & x_1 < x < x_2 \\ 0 & \text{elsewhere} \end{array} \right.$$

(2.34B)

Since the functions $\cos k_n x$ with $k_n = n\pi/x_0$ are orthogonal on the interval $x = 0, x_0$; each equation can be multiplied through by $\cos k_m x$ and integrated from 0 to x_0 . By this method two equations, each with two unknowns, A_n and B_n , are obtained for each n .

Representatively, these take the form:

$$a_n A_n + b_n B_n = c_n A_0 + d_n B_0 \quad (2.35A)$$

$$a'_n A_n + b'_n B_n = c'_n A_0 + d'_n B_0 \quad (2.35B)$$

where the coefficients $a_n, b_n, c_n,$ and d_n in both equations are known functions of n . Thus, in principle (2.35A) and (2.35B) could be solved to give the constants A_n and B_n as functions of n, A_0 and B_0 .

From the discussion following the derivation of (2.30) it is

clear that the constants A_0 and B_0 , although not independent, govern primarily the surface and interface elevations respectively. It should be noted that by letting B_0 equal to zero the solution for η_2 as given by Equation (2.30) approximates the form of the general solution for η in the one layer model.

The constants A_0 and B_0 must be specified by some type of field information, either elevations or velocities, at a known location. Specifying A_0 and B_0 allows the two equations to be solved for A_n and B_n which can then be introduced into the governing equation for η_2 . With this the remaining velocities or profiles can be determined through the appropriate governing equations.

CHAPTER III

RESULTS OF THE ONE LAYER MODEL

The one layer model represents the well mixed situation generally found in Massachusetts Bay during the winter months. Oceanographic data collected by the U. S. Department of the Interior (1959) shows that for the duration of the winter season the water column is fairly uniform in temperature and salinity because of the absence of a thermocline. As a result the Bay can be assumed of constant density with the one layer model being quite representative of the physical situation. The one layer model is consequently able to yield a simple prediction of the surface profile and currents due to the tidal action in the Bay for the winter season.

3.1 Computational Aspects

3.1.1 Mathematical Simulation of the Ocean Boundary

In the development of the general solution for the one layer model, as given by Equation (2.18), it was stated that to predict the surface profile and velocities the constant A_0 must be determined by field data. This field information which is required for the evaluation of A_0 can either be a tidal amplitude or current information specifying speed and direction for some known point in Massachusetts Bay. Since it is generally quite difficult to extract tidal current information from current meter records, a specified surface elevation will be used for the determination of A_0 . Specifically, the tidal range at Boston Light, located just outside Boston Harbor, has been

determined by the National Ocean Survey (1973) to be 9.0 feet with a corresponding tidal amplitude of 4.5 feet. This information was obtained from tide gauge records taken at Boston Light located on Little Brewster Island shown in Figure 3-A. With the geometry and coordinate system specified for the one layer model, Boston Light can be located at $x = 10.0$ NM, $y = 0.0$ NM.

Since the reference datum for the surface elevation in the one layer model is mean sea level (MSL) it will be the tidal amplitude with which we are concerned. Thus, using 4.5 feet for η at the x, y coordinates specified above, A_0 can be determined for a particular geometrical configuration from Equation (2.18). With the determination of this constant, the current field and surface profile for the entire Bay can be computed. It should be cautioned that A_0 is discrete for only one geometrical configuration. Changing the depth of the Bay or the width of the opening demands that A_0 be recalculated regardless of the fact that the same surface elevation is prescribed at the same location.

The constant A_0 actually determines the magnitude of the forcing function to be applied at the open boundary, across which the tidal amplitude is considered constant. In the one layer model the boundary conditions are so chosen that no interaction between the motion in the bay and that in the ocean is considered. This has implications where the exciting frequency is close to a resonant frequency. However, this plays a minor role in the case of tidal excitation of Mass Bay as will be discussed later (Section 3.3).

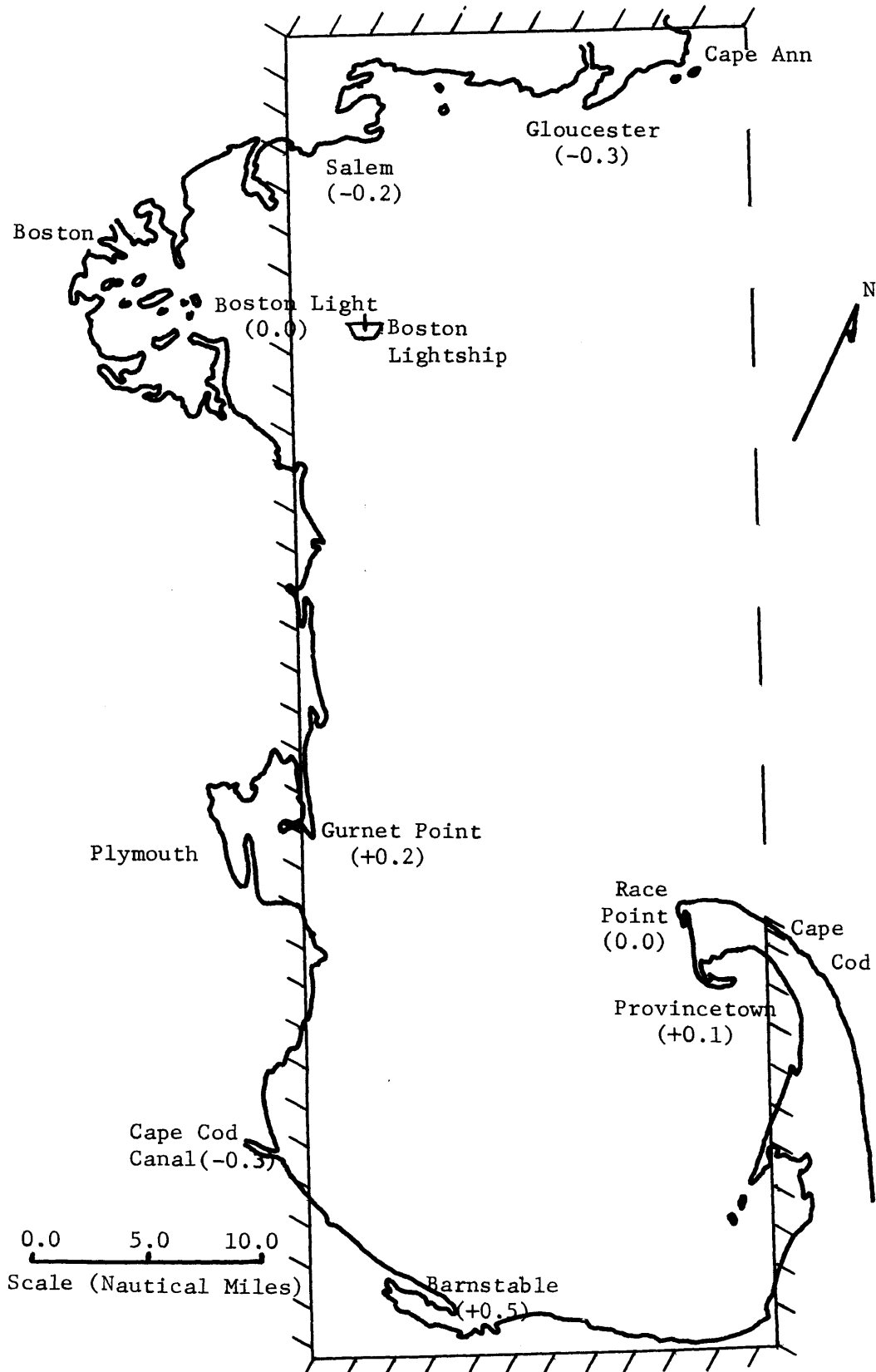


Figure 3-A: Massachusetts Bay; Observed Differences in Tidal Amplitude at High Tide, Measured in Feet. Reference Station-Boston Light.

Consequently, by specifying the tidal amplitude at $y = y_0$, the two dimensional bay appears to be driven by a wave with the magnitude a function of A_0 .

The boundary condition, specified at $y = y_0$ for $x_1 \leq x \leq x_2$, is given by Equation (2.12) and derived by considering the mass flux through the channel opening. An important assumption in determining this boundary condition is the assumption of $\frac{\partial \eta}{\partial y}$ or v being constant over the entire width of the opening. This assumption has previously been made by Ippen and Goda (1963) and would appear reasonable for narrow openings. It should be pointed out that the specified value of $\frac{\partial \eta}{\partial y}$ over the opening, as given by (2.12), is a function of A_0 . Since the value of A_0 is determined by matching the tidal amplitude at one point, it is not possible to satisfy the assumed condition of a constant tidal amplitude across the opening. However, the opening between x_1 and x_2 can be divided into increments and, since the governing equations are linear, the solution for η can be matched at the center of each increment. This method of solution will be discussed in detail later in this chapter.

The one layer analytical model for Massachusetts Bay was computed for a number of variations of the geometrical configuration presented in Figure 2-B. For the purposes of the model the bay is assumed rectangular with a length of 59.0 NM represented as x_0 and a width of 20.0 NM represented by y_0 . The width of the opening, given by $x_2 - x_1$ and representing the ocean boundary, is assumed to be 41.0 NM while the average depth in the Bay is equal to

approximately 120 feet.

Although a number of variations were introduced into the geometry in an attempt to simulate different conditions that could exist, only three variations will be discussed in this report. The first and most basic is the configuration presented in Figure 3-B which represents the geometry specified in the theoretical development of the one layer model. Initially, by setting η equal to 4.5 feet at Boston Light, the constant A_0 can be calculated. The surface profile and current field in Massachusetts Bay can then be computed with the results shown in Figure 3-B. Computed at time $t = 0$ from Equation (2.18), η is plotted in feet above mean sea level and corresponding to the amplitude at high tide. The surface elevation is seen to increase toward the southern or lower portion of the Bay. The speed and direction of the tidal current is given in knots during maximum ebb flow and is the result of plotting U where, as before, $U = \sqrt{u^2 + v^2}$. As can be seen by their governing equations, these velocities are functions of the surface slopes, $\frac{\partial \eta}{\partial x}$ and $\frac{\partial \eta}{\partial y}$, and they are consequently perpendicular to the co-tidal lines. Since the equations are periodic the surface profile attains a maximum slope at $t = \frac{T}{4} + n \frac{T}{2}$ for $n = 0, 1, 2, \dots$ with maximum velocities occurring simultaneously over the entire bay.

The model to this point has matched the surface elevation, η , with the boundary condition given by Equation (2.12) at only one point in the opening, i.e., $\frac{x_2 - x_1}{2}$. It is obvious from the results presented in Figure 3-B that the surface slope between x_1 and x_2

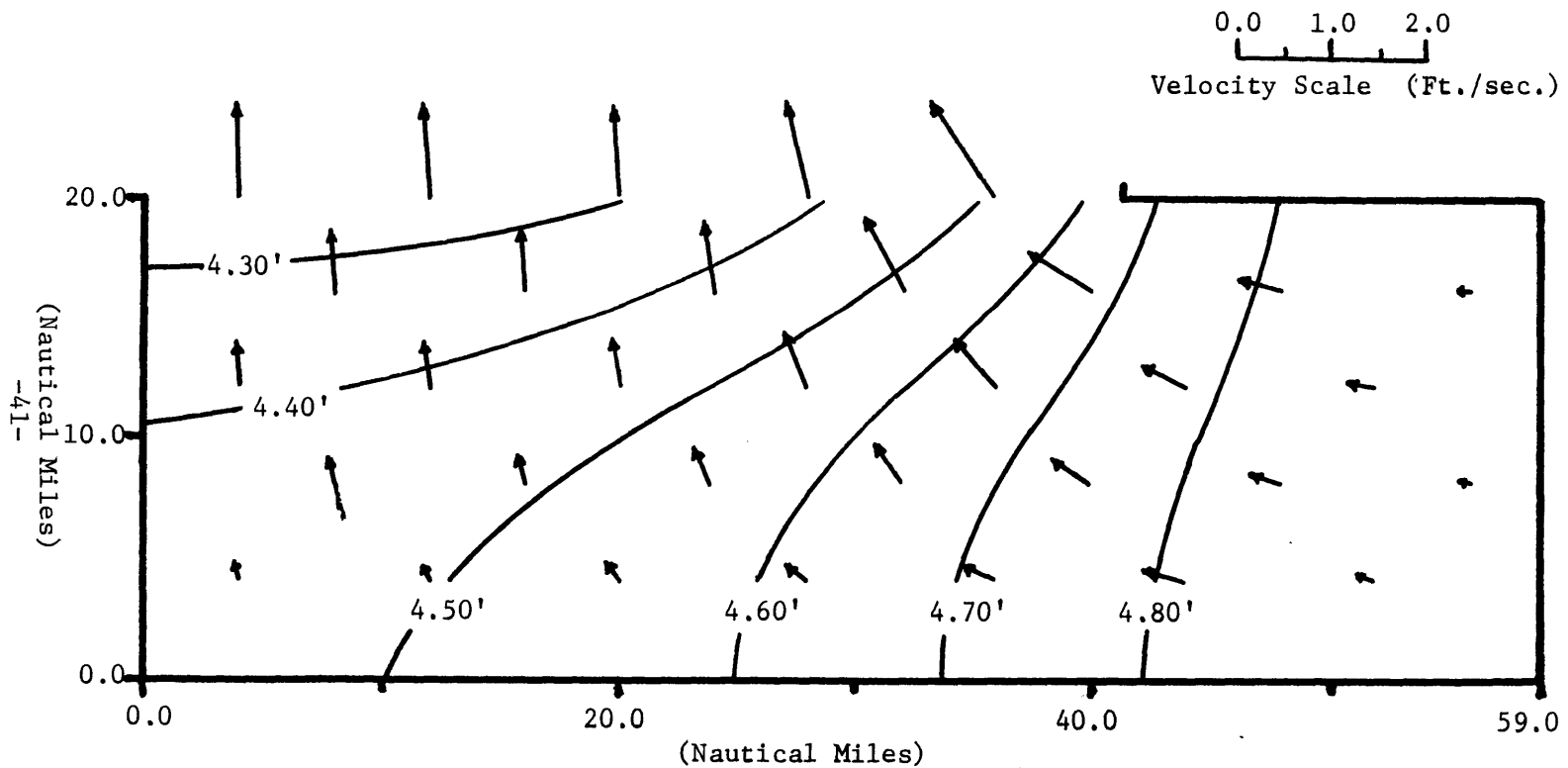


Figure 3-B: One Layer Model of Massachusetts Bay 1 Increment Channel. Surface Profile at High Tide in Feet Above MSL. Velocities at Maximum Ebb in Ft./sec.

does not equal zero and in fact the tidal amplitude varies of the order 0.40 feet across the opening. Although seemingly insignificant, this contradicts the physical assumption that η remains constant across the opening. As mentioned before, a method exists such that η can be matched at more than one point along $y = y_0$ between x_1 and x_2 . This is possible since the solution for η is obtained from a linear governing equation. Consequently, by dividing the opening into a number of sections the effect that one section exerts on the remaining sections can be computed. The surface elevation for the center point of each section can then be determined as the effects from the other sections are additive at that point. Computationally this requires, for n sections, the solution of n equations with n unknowns. This allows the surface elevation to be matched at n points across the opening therefore forcing the surface profile, at $y = y_0$, to better approximate the condition of η constant across the opening.

This method can be applied to the particular situation involving a partial constriction across the channel between x_1 and x_2 . In particular, this is introduced in an attempt to model the effect that Stellwagen Bank exerts on the tidal flow into Massachusetts Bay. From Figure 1-A it can be seen that Stellwagen Bank is a shoal area between Cape Ann and Cape Cod where the average depth of the Bank is approximately 90 feet, although in some areas depths of less than 60 feet occur. Since the possibility exists that the shoal could form a partial blockage to the tidal flux between the Gulf of Maine

and Massachusetts Bay, a method to model such an effect was introduced. This consisted of dividing the channel opening into two smaller channels separated by an impermeable constriction from $x = 16.5$ NM to $x = 29.0$ NM as shown in Figure 3-C. Representatively, the method of solution for this problem containing two channels, designated I and II, becomes:

$$a_I A_I + b_I B_{II} = C \quad (3.1A)$$

$$a_{II} A_I + b_{II} B_{II} = C \quad (3.1B)$$

where A_I and B_{II} are the values of the arbitrary constants for the two solutions obtained where one of the two openings is considered open and the other closed. a_I and b_I can be calculated and reflect the magnitude of the influence of A_I and B_{II} respectively at the center of one opening and a_{II} and b_{II} reflect the same influence for the second channel. C is the magnitude of the tidal amplitude that is to be matched at the center points of both channels. From this, Equations (3.1A) and (3.1B) can be solved for the two unknown constants A_I and B_{II} .

The surface profile for this variation of the one layer model is plotted in Figure 3-C. With an amplitude of 4.5 feet specified at Boston Light, an increase in the surface elevation of almost 0.20 feet occurs behind the assumed impermeable wall separating the two openings. This result casts some doubt on the validity of this particular model, which will be discussed later (Section 3.3), and velocities are therefore not shown.

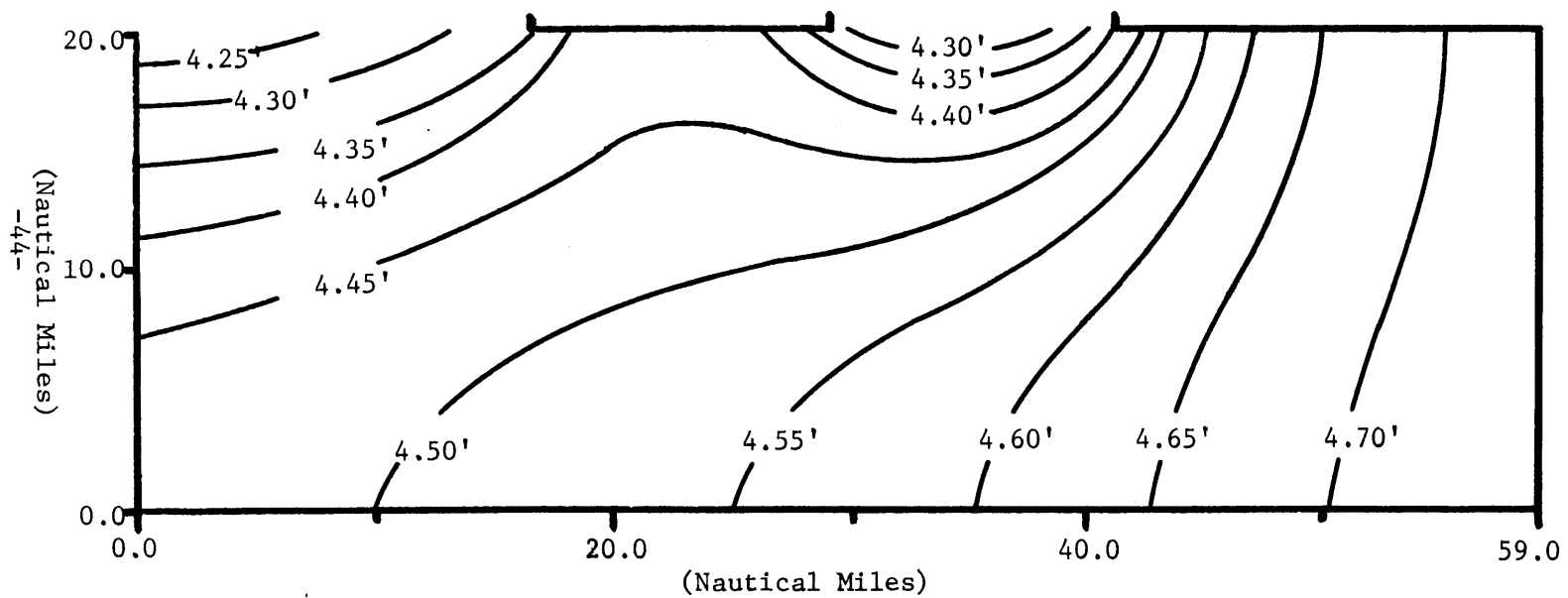


Figure 3-C: One Layer Model of Massachusetts Bay with Stellwagen Bank Closed.
 Surface Profile at High Tide in Feet above MSL.

The third variation of the one layer model is similar to the model previously discussed with a full opening between $x_1 = 0.0$ NM and $x_2 = 41.0$ NM. Although the channel width is again 41.0 NM, the difference occurs in the treatment of the opening and the corresponding matched conditions. Here the channel is divided into four increments which, for reasons previously discussed, allows a better approximation of the boundary condition that η be constant across the opening, since a relatively flat surface profile, at $y = y_0$, is produced for each of the 10.25 NM increments. The method of solution discussed in the Stellwagen Bank model was employed and resulted in four equations and four unknowns with the matching point for η occurring in the center of each increment.

Results of this model are plotted in Figure 3-D and show the surface profile across the opening much more horizontal, and consequently more representative of our assumed boundary condition, than that given by the situation where η is matched at only one point. Obviously, dividing the channel into increments is advantageous since the boundary conditions are better satisfied. However, for a large number of channel increments, the solution becomes tedious to evaluate since the solution will consist of the summation of n infinite series where n is the number of channel subdivisions.

It should be noted that although the value of $\frac{\partial \eta}{\partial y} (v)$ is specified constant across each incremental opening, it was not imposed that $\frac{\partial \eta}{\partial y}$ be the same for all increments. The solution, however, clearly shows that $\frac{\partial \eta}{\partial y} (v)$ is essentially the same for all increments, except

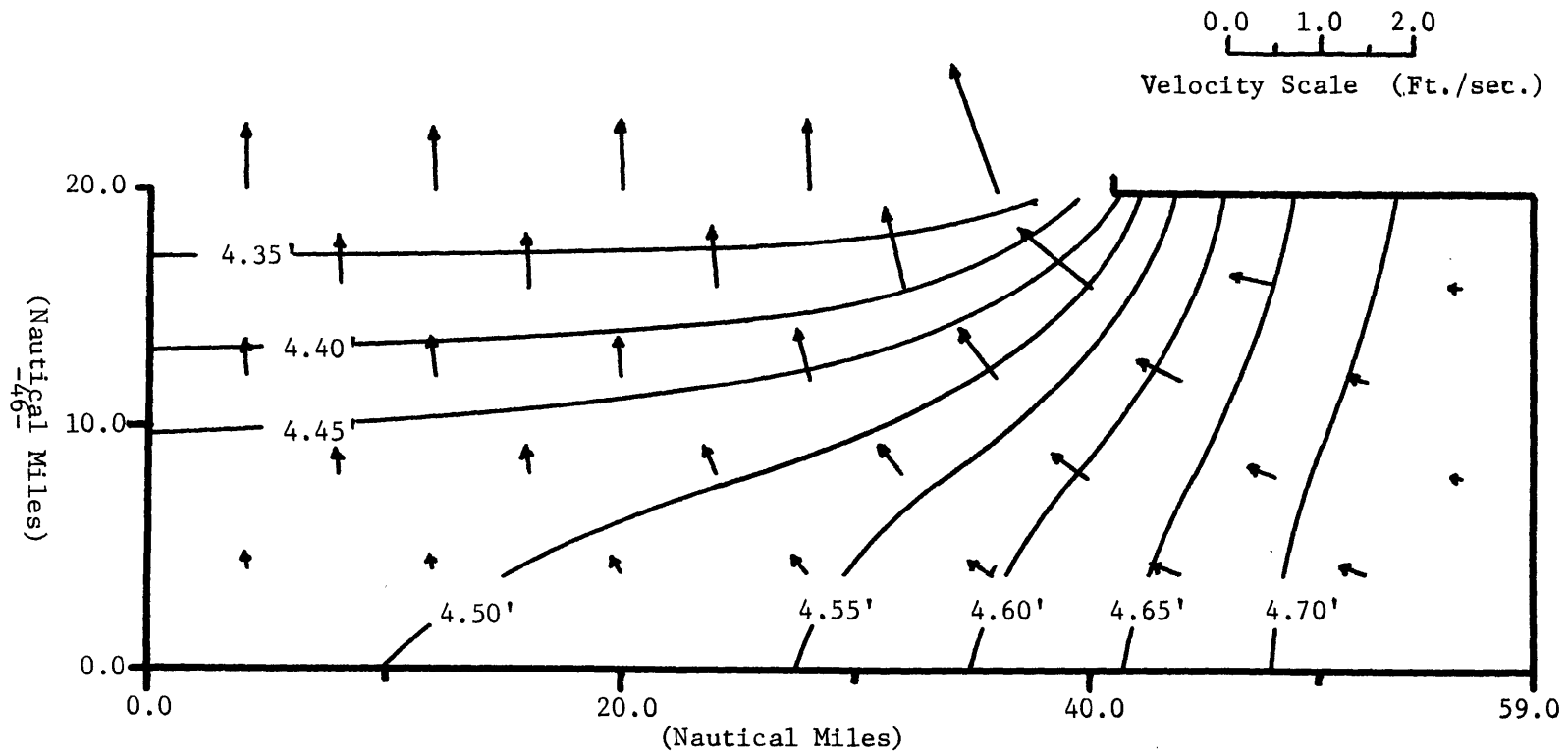


Figure 3-D: One Layer Model of Massachusetts Bay 4 Increment Channel. Surface Profile at High Tide in Feet above MSL. Velocities at Maximum Ebb in Ft./sec.

for a region close to the tip of Cape Cod, where deviations can be expected.

Alternate to an analytical solution, the hydrodynamic equations for the transient response of water bodies to tidal excitation can be solved by numerical methods. In particular, the finite element model has been applied to many problems in coastal and ocean engineering. Conner and Wang (1973) have recently applied such a model to the configuration of Massachusetts Bay. The model is restricted to vertically well mixed two dimensional flow and can incorporate both irregular geometry and variable depth. The numerical model employs triangular elements of varying dimensions and was first applied to a simple geometry identical to that for which results of the analytical model have been presented.

The surface profile and velocities are computed for the finite element model such that the results can be compared directly to the one layer analytical model. The numerical model is shown in Figure 3-E and neglects bottom friction, eddy viscosity, and Coriolis effects. Results for the numerical model compare favorably with those given by the analytical solution shown in Figures 3-B and 3-D. It can be seen that only small differences exist and these are partially explainable since the boundary conditions along the ocean opening are treated differently in the two models. The analytical model satisfies the boundary elevation criteria at discrete points (one for the case presented in Figure 3-B and four for the results given by Figure 3-D) whereas the numerical model satisfies the condition of constant

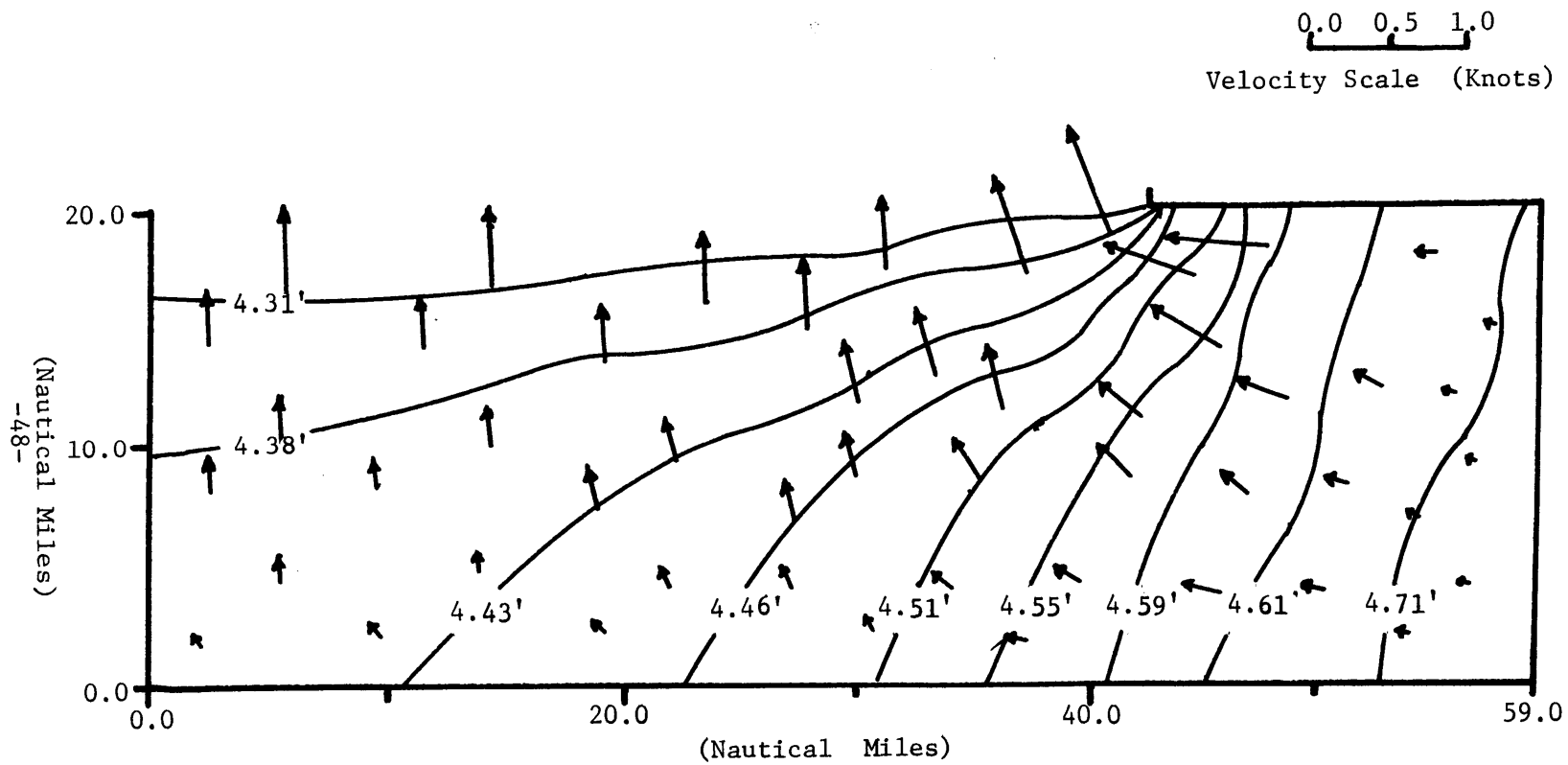


Figure 3-E: Numerical Model of Massachusetts Bay. Surface Profile at High Tide in Feet above MSL. Velocities at Maximum Ebb in Knots.

amplitude across the opening exactly. Comparison of the results of the analytical solution with those from the numerical model serve to demonstrate the close agreement between the two approaches and one of the reasons for developing the analytical one layer model was in fact to furnish Conner and Wang (1973) with a particular solution which could be used to test their numerical schemes.

3.1.2 Number of Terms Required in the Determination of η

The solution for η , given by Equation (2.18) and the solution for u and v , given respectively by Equations (2.5A) and (2.5B), were programmed on the Hewlett-Packard 2114B digital computer, allowing rapid computation of the surface profile and currents for the one layer model. It is important to note that the solution for η contains a summation for $n = 1$ to ∞ . A test for convergence of the summation and the number of terms required was of primary concern. Results clearly indicated that convergence was achieved by $n = 25$ although all computations for the one layer model were carried to $n = 100$.

3.2 Data Available for Comparison

Verification of the results of the one layer model, especially the predicted surface profiles, requires field information on the variation in tidal range over the Bay. Tide data taken by the National Ocean Survey (1973) in Massachusetts Bay has provided this information and has allowed the determination of the differences in tidal amplitude and surface slope. With Boston Light as the reference point, Figure 3-A shows the differences in tidal amplitude for selected locations around the Bay perimeter.

The information can be directly compared with the results of the one layer analytical model. The surface profile shown in Figures 3-B and 3-D, where the channel between x_1 and x_2 is completely open, produces some interesting facts when compared with field observations. Both models appear somewhat conservative in predicting the longitudinal slope from one end of the Bay to the other. Interestingly, the model with a one increment channel, shown in Figure 3-B, best approximates the surface slope computed from the tidal records in Cape Cod Bay. When comparing the surface elevation at specific locations, it can be seen that the four increment channel gives a close comparison at Race Point and Provincetown while the one increment case compares favorably at Gurnet Point and in the Gloucester Area.

Information on tidal currents around the Bay also allows a qualitative comparison of the model results with field data. Current observations taken by Butman (1971) confirm that velocities are of the same order of magnitude as those predicted by the model. However, these predicted results of velocities may be somewhat affected by the neglect of Coriolis force and the comparison can only be considered qualitative.

3.3 Discussion of the Model Results

The results of the one layer model for tidal amplitudes, when compared with available field information, are certainly acceptable for many situations, in spite of the many simplifying assumptions made in the development of the model and its application. Some of these assumptions will be discussed in the following.

One of the terms neglected during the development of the governing equations was the effect of friction on the tidal motion. As mentioned previously, the bottom shear stress, τ_b , creates a tidal phase lag from one part of the Bay to another. However, it can be seen from the National Ocean Survey Tide Tables (1973) that phase differences between the north and south end of Massachusetts Bay are small and, at high tide, average only about 10 minutes. Consequently, the neglect of friction seems appropriate for the physical situation considered.

Another important consideration is the possibility of resonant oscillations occurring as a result of the tidal forces. For an analysis of wave induced oscillations in harbors by Ippen and Goda (1963), the resonant characteristics of simple geometrical configurations has been determined. Applying their work on the frequency response of asymmetric harbors to the configuration assumed for Massachusetts Bay, where the tidal wave length is of the order 456.0 NM, since $L = T\sqrt{gh}$, the following can be concluded: (1) No resonant oscillations occur in Massachusetts Bay as a result of tidal excitation, since even the first resonant mode cannot be excited and (2) A wave length of less than 300 NM would be required to excite the first harmonic.

Figure 1-A shows that in the southern portion of Massachusetts Bay, more properly called Cape Cod Bay, gradual shoaling exists from approximately 13.0 NM offshore to the shoreline along the lower end of the Bay. The possibility exists that an additional increase in tidal range could occur in this area as the situation is quite analogous to a progressive two dimensional reflecting wave from a gently sloping

beach. That the tidal wave in the southern part of the Bay may be regarded approximately as a two dimensional standing wave in the x-direction is evident from the results given in, for example, Figure 3-D. This problem was treated by Doret and Madsen (1972) and using their results an increase in tidal amplitude, due to the shoaling at the lower end of the Bay, may be estimated to be of the order 0.06 ft., which is insignificant although giving a closer agreement between predicted and observed tidal amplitudes in this part of the Bay.

The variation simulating the effect of Stellwagen Bank on the tidal motion of Massachusetts Bay, although producing some interesting results, exhibits an increase in tidal amplitude behind the assumed barrier. Since the average depth of the shoal is only about 30 feet less than the average depth of the Bay, the effect of this increase in surface elevation will result in a considerable amount of volume exchange taking place over the shoal. This is not consistent with our assumption of an impermeable barrier, and consequently this model is discarded.

Certain known phenomena occurring in Massachusetts Bay contribute to some of the differences seen between the analytical results and field data. One of these is the body of water contained within the area surrounding Boston Harbor. This is a relatively shallow basin that most surely influences the hydrodynamics of the Bay, especially since it is the discharge point for three rivers in the Boston area. Additionally, the Cape Cod Canal, which forms an artery between Massachusetts Bay and Buzzards Bay 15 NM to the southwest, has a strong

effect on η as can be seen in Figure 3-A. A 0.5 foot discrepancy exists between the model results and the observed tidal height at the entrance to the Canal. Obviously, the fact that a phase lag of approximately 2.5 hours between the two Bays contributes to this discrepancy. These features should of course be simulated in a more sophisticated model.

In spite of the many assumptions involved, the one layer model seems quite representative of the physical situation observed in Massachusetts Bay as was seen from the results presented in Section 3.1.1. Comparison of the analytical results with tide data especially demonstrates the predictability of the model with a fully open channel between x_1 and x_2 . Although the surface profile given by the four increment channel in Figure 3-D better satisfies the imposed boundary conditions than that given by the one increment situation in Figure 3-B, the goodness of one variation over the other, when compared to field information, is difficult to assess. The tidal velocities given by the model are less reliable than the surface elevations but may produce an overview of the current field that can be expected in the Bay. Thus, keeping the desired simplicity of the model in mind, we conclude that results of the one layer model, with just one opening considered in its entirety, gives a reasonable description of the tidal motion in Massachusetts Bay.

CHAPTER IV

RESULTS OF THE TWO LAYER MODEL

The two layer analytical model, as mentioned previously, was developed in response to the physical characteristics encountered in Massachusetts Bay during the spring, summer, and fall. Oceanographic observations since 1925 at the Boston Lightship, as reported by the U. S. Department of the Interior (1959), show that the thermocline generally forms in May and overturns in September and October. Thus, stratification due to the variation in both temperature and salinity prevails for approximately six months out of the year.

Although the thermocline is quite variable in depth, historical data taken at Boston Lightship locates the average depth of the interface 30 feet below the surface. Water depth at the Lightship, which is approximately six nautical miles east of the entrance to Boston Harbor, is 100 feet at mean low water. (It should be noted that the Lightship, not to be confused with Boston Light, was moved to a new location on July 1, 1973. All references to Boston Lightship in this report are for its previous position of $42^{\circ}20.4' N$, $70^{\circ}45.5' W$).

4.1 Computational Considerations

4.1.1 Results of the Two Layer Model

The stratified case was developed as a simple model with the capability of determining velocities and elevations in both layers. Derivation of the governing equations for the stratified model parallels the theoretical development of the one layer model such

that the solutions for all velocities and the interface elevation η_1 are specified in terms of the surface elevation η_2 .

The general solution for η_2 , given by Equation (2.30), is a function of the constants A_n and B_n and it can be shown that A_0 essentially governs the surface profile while the motion of the interface is governed essentially by B_0 . By setting B_0 equal to zero, in Equation (2.30), η_2 takes the form:

$$\begin{aligned} \eta_2 = & A_0 \cos m_{o_1} y + \sum_{n=1}^{\infty} A_n \cos k_n x \cosh m_{n_1} y \\ & + \sum_{n=1}^{N-1} B_n \cos k_n x \cosh m_{n_2} y + \sum_{n=N}^{\infty} B_n \cos k_n x \cosh m_{n_2} y \end{aligned} \quad (4.1)$$

and it can be shown by calculation that the summation of the terms containing B_n for $n > 0$ is small compared to the summation of the terms containing A_n 's.

The solution for B_0 equal to zero shows that η_2 closely approximates the solution for η in the one layer model. Thus, we identify the constant A_0 as the one essentially governing the surface elevations whereas the value of the constant B_0 is reflected in the interface elevations.

The procedure for solving for the constants A_0 and B_0 contained in the general solution for η_2 , Equation (2.30), is discussed in Chapter II and is similar to the method for determining A_0 in the one layer model. For the stratified case, both a surface amplitude relative to mean sea level (MSL) and an interfacial amplitude

relative to the mean interfacial level must be specified at some point within the Bay. Alternatively, current velocities could be specified in each of the two layers although, as explained in the preceding chapter, this data is often difficult to interpret from current records. With information on the surface and interface the two constants can be determined either through an iterative process or directly by rearrangement of the equations given representatively by (2.35A) and (2.35B).

Oceanographic data in the form of vertical profiles of temperature and salinity in Massachusetts Bay have been taken by various agencies and institutions. Unfortunately it is difficult to determine, with any degree of accuracy, the amplitude of the interface for a given location as the variation of temperature representing the thermocline is not discrete but varies rapidly in the vertical direction over a distance of as much as ten feet. As a result, unlike the information on the surface profile which is fairly well documented, the amplitude of the interface was specified arbitrarily at a certain location to allow for the determination of the two constants in Equation (2.30). Choosing the coordinates of $x = 10.0$ NM, $y = 5.0$ NM, the surface elevation, from the results of the one layer model, has been found to be of the order 4.5 feet. It is reasonable to assume that, for an h_2 of 20 feet, the amplitude of the interface is approximately 5/6 the amplitude of the surface wave. Consequently, η_1 was chosen as 3.5 feet at this location.

With this information, the constants A_0 and B_0 can be computed for the two layer model. Through the solutions for the velocities and elevations given in the theoretical development, the surface and interfacial profiles and currents can be computed for Massachusetts Bay. The geometry of the stratified model is the same as that assumed for the one layer case where $x_1 = 0.0$ NM and $x_2 = 41.0$ NM. Results of the one layer model indicate that the fully open channel with no constrictions gave a fair representation of the physical situation and consequently only this configuration will be considered for the two layer model.

The solutions for the amplitude and velocities, as in the one layer model, contain summations for $n = 1$ to ∞ . Although convergence in this model was obtained by $n = 50$, the large number of computations required that the equations be solved on the IBM 370/155 computer located at M.I.T. A listing of this computer program, written in Fortran, can be found in Appendix A.

Results of the two layer analytical model can now be determined for a particular situation similar to that frequently found in Massachusetts Bay. Taken from actual field observations, the following parameters were first specified as input into the model. $h_1 = 100$ feet, $h_2 = 20$ feet, $\rho_1 = 1.02558$ g/cm³, $\rho_2 = 1.02250$ g/cm³. By additionally setting $\eta_1 = 3.5$ feet and $\eta_2 = 4.5$ feet at $x = 10.0$ NM, $y = 5.0$ NM, the interface and surface amplitudes can be computed by respectively Equations (2.23) and (2.30) with the resulting profiles shown in Figure 4-A. It can be seen that the surface profile is quite

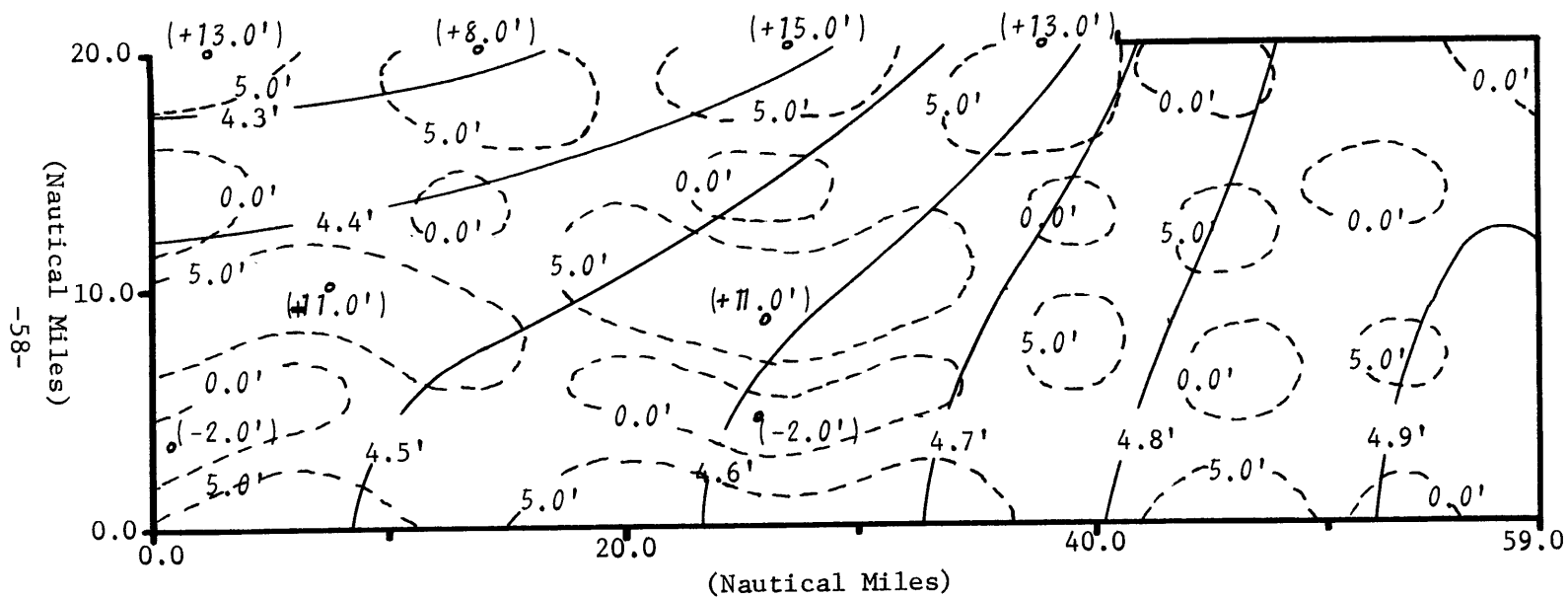


Figure 4-A: Two Layer Model of Massachusetts Bay at High Tide. Amplitudes Measured in Feet.

Surface Profile, η_2 —————

Interfacial Profile, η_1 - - - - -

$h_2 = 20.0 \text{ Ft.}, \rho_2 = 1.02250 \text{ g/cm}^3$

$h_1 = 100.0 \text{ Ft.}, \rho_1 = 1.02558 \text{ g/cm}^3$

similar to that given by the one layer model (Figure 3-B) with the same geometrical configuration. Although the surface amplitude of 4.5 feet is specified at a slightly different location than in the one layer situation, the surface slope compares favorably with the model results and observational data previously presented. The surface profiles were smoothed slightly as small perturbations occurring in the contour lines were neglected.

From Figure 4-A it can be seen that the interfacial profile predicted for the two layer model exhibits some rather interesting and unusual results. Measured relative to the mean interfacial level, h_1 , this particular model shows the interface oscillating vertically from - 2.0 feet to + 15.0 feet with a wave length of the order 11.0 nautical miles. Since the solution for η_1 is periodic, the model resultingly predicts a standing wave which, at high tide, rises to within 10 feet of the free surface.

Velocities for this particular case are shown in Figure 4-B. The velocities are specified in terms of x and y derivatives of η_2 and consequently the surface profile determines the magnitude and direction of both U_1 and U_2 . By the nature of the equations for u_2 and v_2 , given respectively by Equations (2.22A) and (2.22B), the currents predicted in the upper layer are always perpendicular to the lines of constant surface amplitude with the velocity a function of the existing surface slope. The currents in the lower layer are specified as a function of both the first and third derivatives of η_2 . It will be noticed that the magnitude of U_1 is greater than that

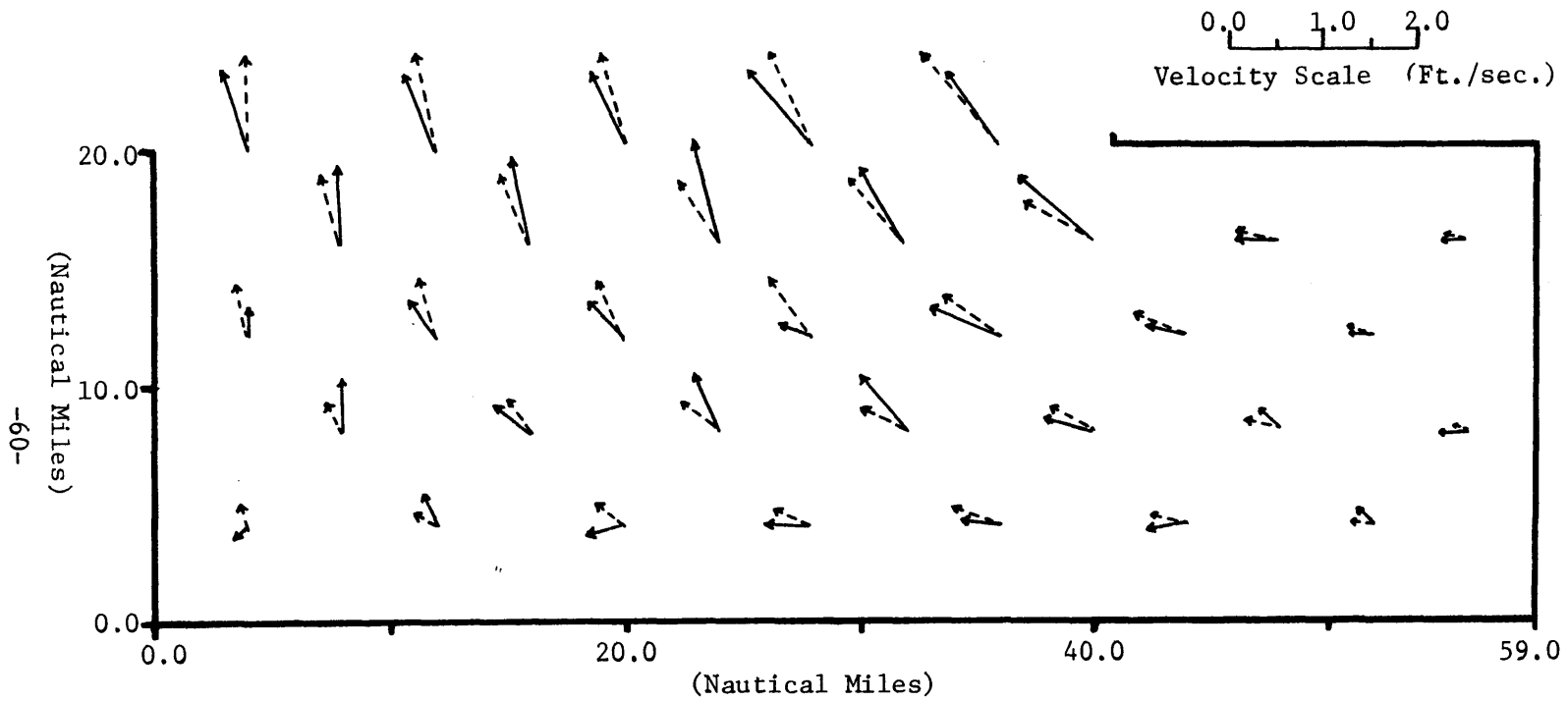


Figure 4-B: Two Layer Model of Massachusetts Bay.
Velocities at Maximum Ebb in Ft./sec.

U_2 (Upper Layer) ———

U_1 (Lower Layer) - - - - -

$h_2 = 20.0$ Ft., $\rho_2 = 1.02250$ g/cm³

$h_1 = 100.0$ Ft., $\rho_1 = 1.02558$ g/cm³

of U_2 at some positions in the model; at other locations the reverse is true. Of greater importance is the prediction that the directions of the currents in the two layers do not coincide.

The two layer analytical model was changed slightly and the amplitudes and velocities were computed for a second set of circumstances. The geometrical configuration remained the same; however, the difference in density between the two layers was increased slightly from the 0.3 per cent, given in the first set of results, to 0.5 per cent. The new densities were specified as $\rho_1 = 1.0050 \text{ g/cm}^3$ and $\rho_2 = 1.000 \text{ g/cm}^3$. In addition, the depth of the interface was increased by 20 feet such that $h_1 = 80.0$ feet and $h_2 = 40.0$ feet. The surface and the interfacial amplitudes were again specified at $x = 10.0$ NM, $y = 5.0$ NM under the same set of assumptions as discussed earlier. Thus, again by setting $\eta_2 = 4.5$ feet it is reasonable to assume the amplitude of the interface as $(\frac{h_1}{h_1+h_2})\eta_2$ or 3.0 feet. For these conditions the stratified model was again solved for the area of Massachusetts Bay.

The surface and interfacial profiles for this model are shown in Figure 4-C. Obviously, much more activity exists here than in the previously discussed case. The surface profile, in this extreme case, reflects the influence of the interfacial waves. Close examination of the results of Figure 4-C as compared with Figure 3-B reveal the fact that the surface is lower, relatively, over an interfacial crest and higher over an interfacial trough. This serves to demonstrate the dependence of η_1 on η_2 as discussed in the theoretical

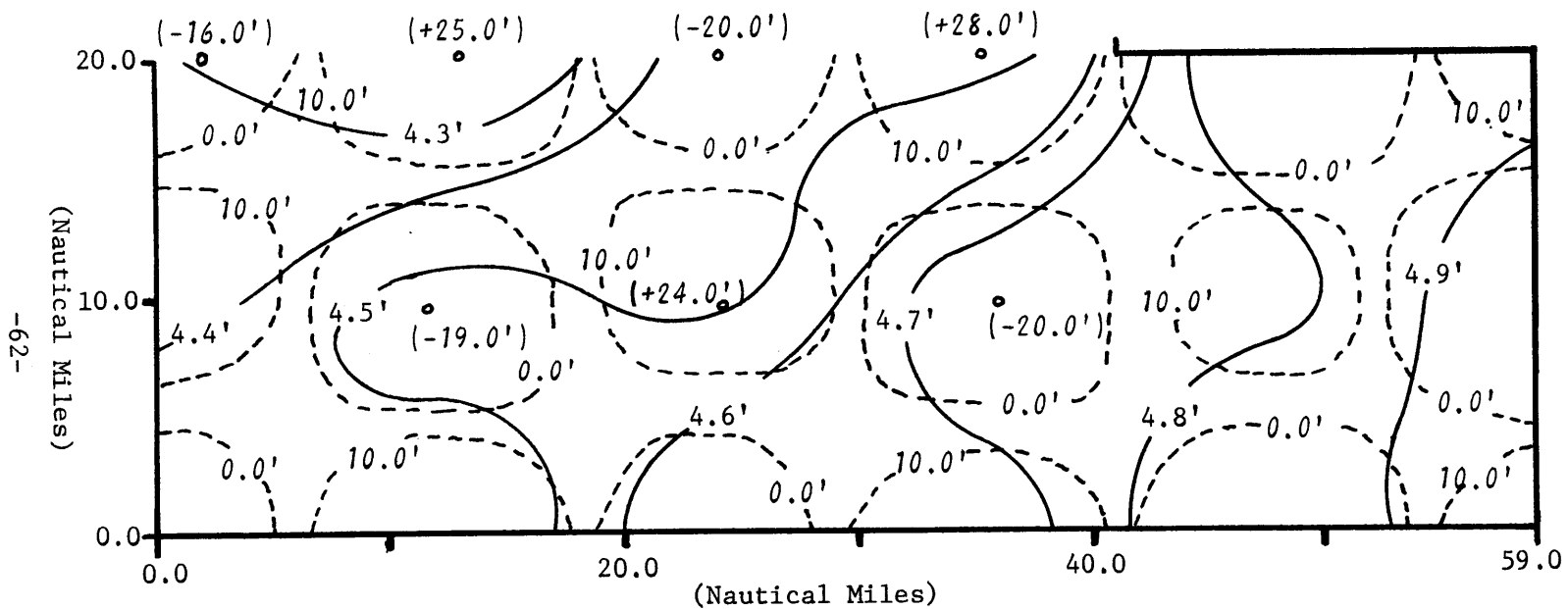


Figure 4-C: Two Layer Model of Massachusetts Bay at High Tide. Amplitudes Measured in Feet.

Surface Profile, η_2 ———

Interfacial Profile, η_1 - - - - -

$$h_2 = 40.0 \text{ Ft.}, \rho_2 = 1.0000 \text{ g/cm}^3$$

$$h_1 = 80.0 \text{ Ft.}, \rho_1 = 1.0050 \text{ g/cm}^3$$

development of the two layer model. The interface exhibits some exceedingly large waves with a height of the order 50 feet and a wave length of approximately 24.0 NM.

The velocities in the upper and lower layer for this particular situation are given in Figure 4-D. Of primary importance in the results is the fact that, with large vertical displacements of the interface, currents in the two layers are quite variable and, at some positions, almost opposing each other. The currents in the vicinity of the boundaries are also unusual by the fact that, at some locations, on the ebbing (outgoing) tide, which is shown, they flow towards the walls and away from the channel opening in the upper layer. Resultingly, the interface and surface profiles and speed and direction of the currents are extremely variable and physically difficult to determine since the various parameters appear to be quite sensitive to position. This is in qualitative agreement with available field observations to be presented later in this chapter, which indicate that, to a degree, this condition persists.

4.1.2 Model Sensitivity

The two layer analytical model was computed for a number of geometrical configurations and physical conditions in an attempt to check the sensitivity of the solution. As seen by the amplitudes and velocities predicted for the two cases just discussed, the model is very sensitive to changes in the interfacial depth and /or changes in density. Consequently, an attempt to quantify the importance of these and other variables has been completed through a sensitivity analysis. The results are presented herein.

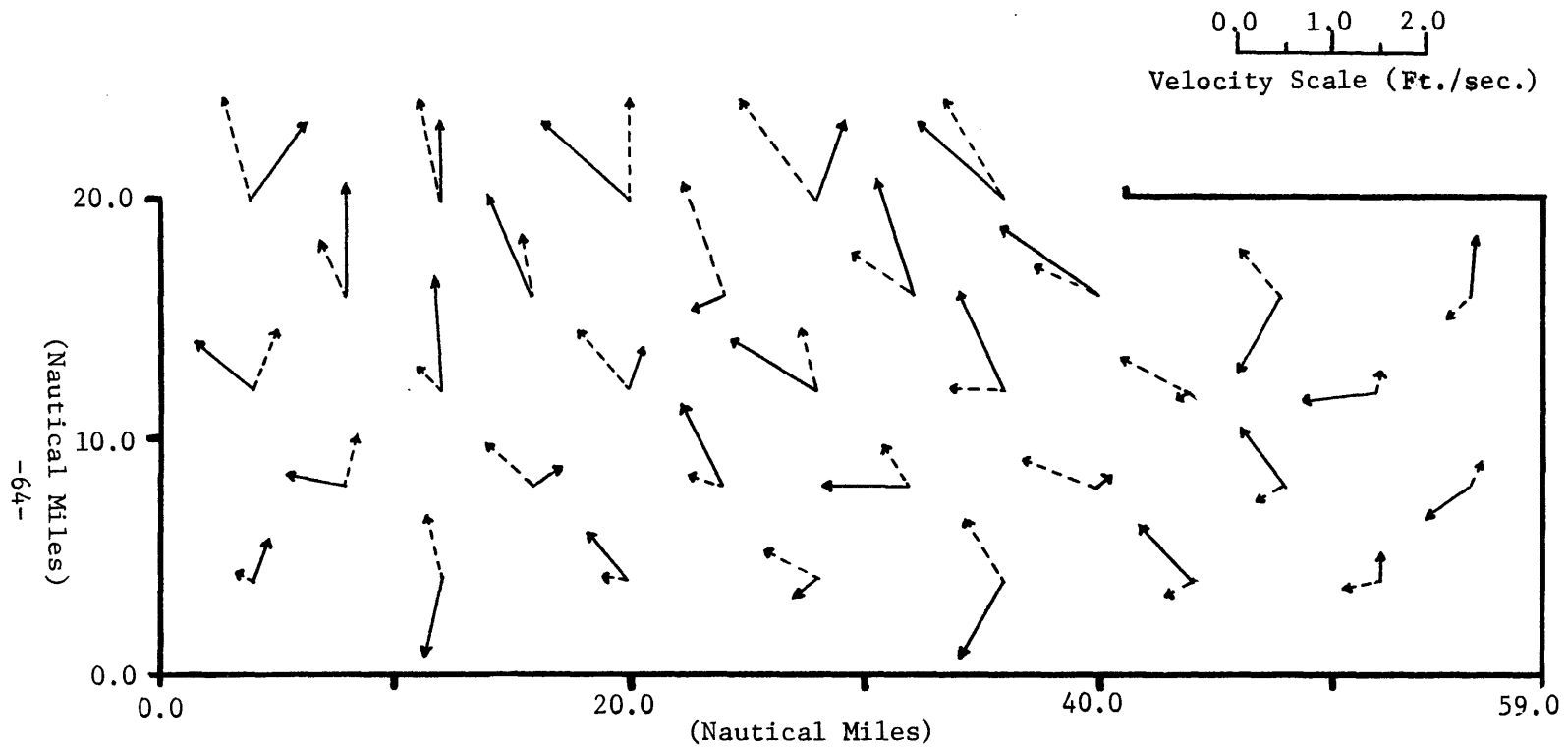


Figure 4-D: Two Layer Model of Massachusetts Bay.
Velocities at Maximum Ebb in Ft./sec.

U_2 (Upper Layer) ———

U_1 (Lower Layer) - - - - -

$h_2 = 40.0$ Ft., $\rho_2 = 1.0000$ g/cm³

$h_1 = 80.0$ Ft., $\rho_1 = 1.0050$ g/cm³

The two constants A_0 and B_0 that were required in the general solution for η_2 shall be first discussed. As pointed out in Section 4.1.1, the constants are generally determined through the application of field data prior to their introduction into Equation (2.30). Also noted was the fact that the value of A_0 primarily governs the surface profile, η_2 , while the value of B_0 is the determining factor in the shape of the interface, η_1 . In checking the sensitivity of the two, it was found that by varying the constant A_0 the surface and interface reacted by the same order of magnitude while a small change in the constant B_0 brought almost no change to the surface profile although creating interfacial disturbances of significantly different magnitudes. Thus, it can be concluded that, in determining the value of B_0 , the initial conditions specified for the interface must be chosen carefully and as precisely as possible. The following clearly demonstrates the situation and the sensitivity of the interface to B_0 :

Constant Conditions:		$h_1 = 80.0 \text{ ft.}$	$\rho_1 = 1.0050 \text{ g/cm}^3$	
		$h_2 = 40.0 \text{ ft.}$	$\rho_2 = 1.0000 \text{ g/cm}^3$	
Specified Elevations @ $x = 10.0 \text{ NM}$, $y = 5.0 \text{ NM}$		Resulting Constants		Maximum Interfacial Wave Height
η_1 (ft.)	η_2 (ft.)	A_0	B_0	H_1 (ft.)
3.0	4.5	4.684	-0.00790	50
3.5	4.5	4.685	-0.00491	28
4.32	4.5	4.670	0.0	7

Table 4-1: Sensitivity of B_0 to the Choice of Interfacial Amplitude

As a consequence of the large interfacial variations shown in the results of the two layer model and in view of the above information concerning the constants A_0 and B_0 , it is apparent that the model is very sensitive to the location at which η_1 is initially specified. In the two cases presented for the two layer model, both the surface and interfacial amplitude were specified at the coordinates $x = 10.0$ NM, $y = 5.0$ NM. From Figure 4-A and Figure 4-C it can be seen that this position is approximately mid-way between the trough and the crest of the interfacial standing wave. Obviously then small changes in the interfacial wave amplitude at this point will force the solution for η_1 to predict relatively large vertical displacements in the areas of the troughs and crests. Clearly, the solution to this problem is to first determine, for a particular set of conditions, the locations of the 'highs' and the 'lows' of the interfacial waves. This information can be used in the choice of location where the value of η_1 and η_2 should be measured in order to give the best possible resolution such that the model will give reasonable results and an interfacial wave the least sensitive to errors in the measurements.

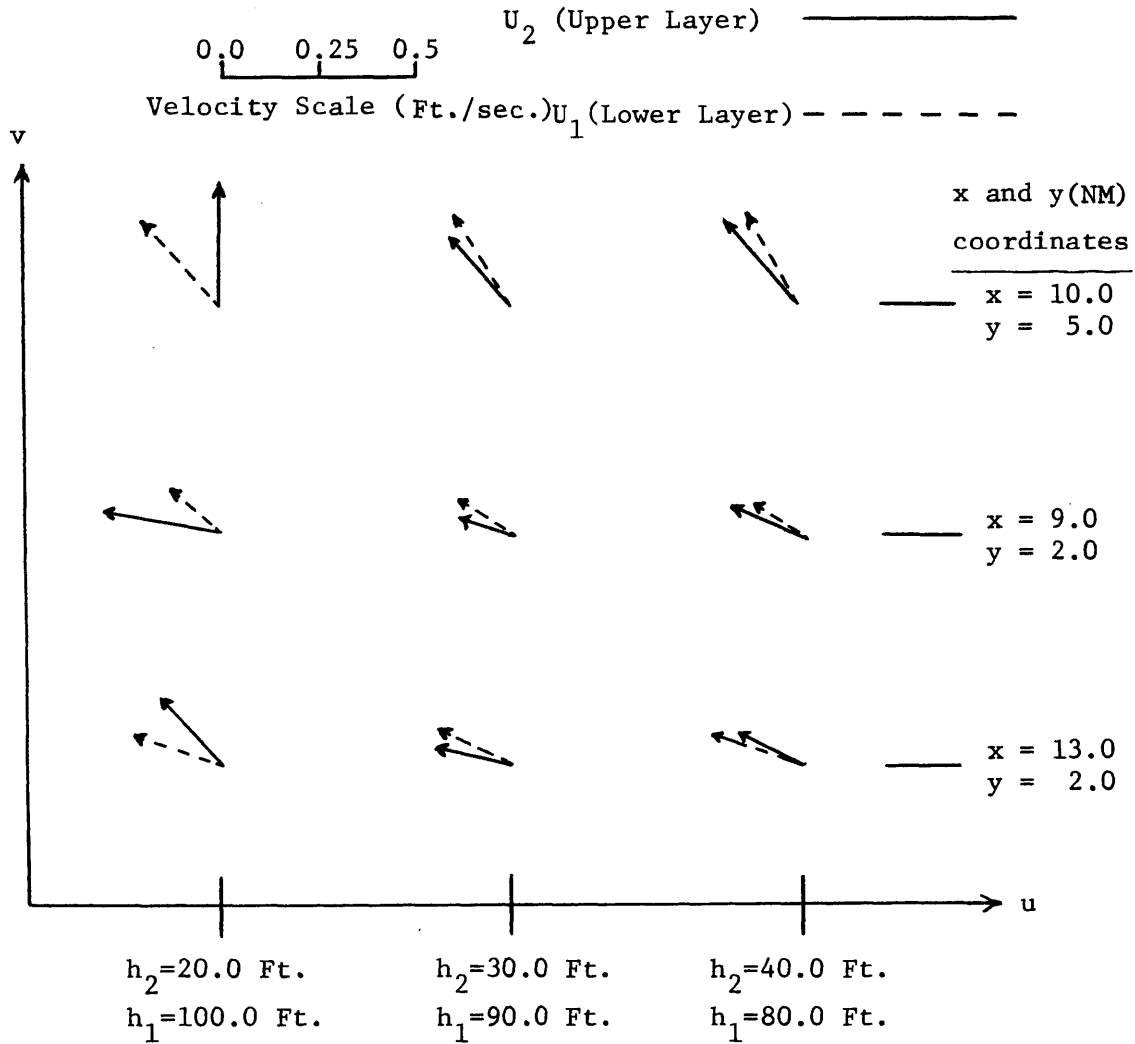
Variation of the geometrical configuration, especially that of the length scale, was an additional criteria which could produce changes in the results. The average length, x_0 , of the Bay was assumed to be of the order 59.0 NM and all the results presented were computed on this basis. To assure that the solution was not sensitive or that no unusual conditions existed in the particular

configuration, the two layer analytical model was run for a number of different lengths. The most important aspect of this analysis was that the results generally indicated that the amplitude and length would be of the same order of magnitude and that, for all practical purposes, a small change in the value of x_0 would produce no unusual results.

Results of density variations have already been indicated by the two cases discussed in Section 4.1.1. The sensitivity of the solution to changes in density are quite pronounced again affecting primarily the profile of the interface. As previously mentioned, the average difference in density found in Massachusetts Bay between the upper and lower layer during stratification is of the order 0.3 per cent. That condition was presented by Figures 4-A and 4-B with the second set of results, Figures 4-C and 4-D, showing $\Delta\rho$ of the extreme value of 0.5 per cent. Differences between the two sets of results cannot be attributed only to the change in $\Delta\rho$ since some influence is possible due to the variation of h_1 and h_2 .

The last set of parameters which merit discussion are the values of h_1 and h_2 . With h_1 representing the thickness of the lower layer and h_2 the thickness of the upper layer, the sum of the two was always equal to 120 feet, the average depth of Massachusetts Bay. Sensitivity of the solution to variations in h_1 and h_2 was checked in a number of cases with the result that by increasing the value of h_1 the interfacial amplitude decreased as did the interfacial wave length.

From (2.20B) it is clear that the influence of changing $\Delta\rho$ and the relative magnitude of h_1 and h_2 are related, in that they combine to give the wave number m_{n_2} . To illustrate the variations with the various parameters, the velocities at selected points are presented in Figure 4-E.



Values of other parameters.

At $x=10.0$, $y=5.0$
 $\eta_1=3.5$ Ft., $\eta_2=4.5$ Ft.

$\rho_1=1.02558$ g/cm³
 $\rho_2=1.02250$ g/cm³

Figure 4-E: Velocity Variations as a Function of h_1 and h_2

Most of the discussion concerning the sensitivity of the model to various parameters has been discussed in terms of the changes occurring in the interface. However, the surface profile and velocities in the two layers also exhibit variation as shown in Figure 4-E, although relatively minor, when changes occur in the geometry or in the specified conditions. By far though the most significant example of sensitivity in the model is exhibited by the interface and its reaction to variation of the input parameters.

4.2 Available Data for Comparison

Results of the two layer analytical model can be compared with available field observations for the Massachusetts Bay area. The field data consists mainly of information on the surface profile, temporal and spatial measurements of the temperature and salinity structure, and current drogue measurements. A large number of oceanographic observations have been collected in the Bay by various agencies and institutions during the summer months and the data presented here gives a good overview of the condition present during stratification.

Data compiled in the National Ocean Survey Tide Tables (1973) is used for a comparison with the surface amplitude predicted by the two layer model. This information is taken from observational records at various locations around the Bay perimeter as shown in Figure 3-A.

The vertical structure of temperature over the water column has been one of the most widely studied oceanographic phenomena for

many decades. Temperature observations at Boston Lightship have been taken on a daily basis since 1925 and have afforded many insights into the thermal conditions in Massachusetts Bay. Thus far, the level of the interface has been generally considered a function of the thermocline although this is not strictly true since the variation of salinity also affects the density of sea water. Consequently, with the advent of the newer oceanographic instrumentation, in particular the CTD (Conductivity, Temperature, and Depth), salinity along with temperature can be determined allowing the calculation of a true density profile for each station recorded. Although the thermocline and density gradient normally coincide, neither is discrete but occur as a gradual variation over relatively large vertical distances. Hence, it is difficult to determine, with any precision, the exact depth of the interface and to detect small perturbations that may occur at this level.

As an example of this problem, a sample C.T.D. cast, taken in the vicinity of Boston Lightship, is shown in Figure 4-F. Fortunately though the model predicts relatively large vertical variations of η_1 and consequently the data presented herein will attempt to verify, qualitatively, some of the conditions that may exist.

Oceanographic observations from a buoy located in Stellwagen Basin, approximately 5.5 NM west of Stellwagen Bank, were taken by Halpern in July and August, 1966. Vertical observations of temperature were collected at the position $42^{\circ}16.5'$ N, $70^{\circ}24.5'$ W for a total of 5 days with the result that the temporal variation of the thermocline

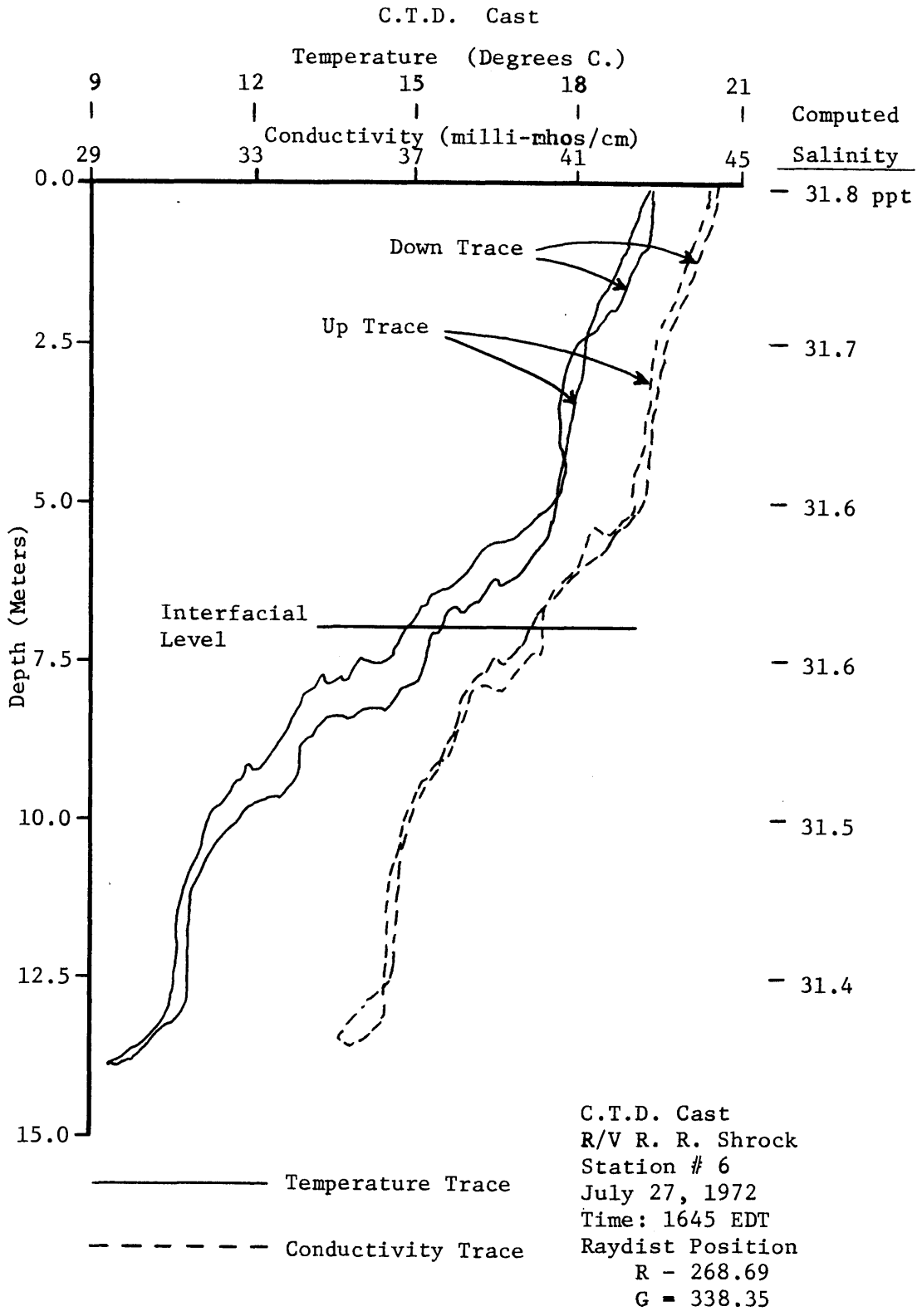


Figure 4-F: C.T.D. Cast Taken in Massachusetts Bay

was well documented at this point of space for a period of time. Halpern reported his observations in a paper on the short-period internal waves in Massachusetts Bay (Halpern, 1971a) and again in a discussion of semidurnal internal tides in Massachusetts Bay (Halpern, 1971b). Concerned primarily with the vertical movement of the thermocline, no information on salinity was obtained and consequently temperature measurements will serve as the primary indicator for the degree and depth of stratification.

Halpern's data locates the average depth of the thermocline approximately 40 feet below the surface with a semidurnal variation of temperature at this depth of approximately 11°F. The most interesting information concerns the vertical displacement of the thermocline, or for our purpose, the interface, with the result that the amplitude of the interfacial wave is of the order 15 feet. Clearly, this is of great interest since the model predicts a periodic motion of a similar magnitude. Although the motion of the interface, from Halpern's observations, is not a purely sinusoidal function, the possibility exists that this is the result of non-linear effects associated with water spilling over Stellwagen Bank on the flooding tide which are also responsible for generation of short period internal waves. However, for our purposes, the information serves to qualitatively confirm some of the predictions given by the two layer model.

A second set of measurements, spatial in nature, are presented to further verify the motion of the interface. In particular,

oceanographic observations, using the C.T.D., have been taken by M.I.T. under the Massachusetts Bay Sea Grant Program. This data has been collected aboard the research vessels R.R. Shrock and Walter E. Phipps allowing a quick on-board determination of the temperature and salinity structure at each station. Almost 20 of these C.T.D. profiles were taken in the Bay on a chemistry cruise conducted on July 25 and 26, 1973. Resultingly, the depth of the interface was determined at a number of locations approximately 5.0 NM apart. The observations used for comparison, although not entirely synoptic, were taken as close to the time predicted for low tide as possible in order to reduce the effects of periodic motion. The 45°F isotherm was used for the depth of the thermocline since it was the temperature at which the largest density gradient occurred. Using this temperature as the indicator for the interface, the results of three of these C.T.D. stations are presented.

C.T.D. Stations - July 26, 1973
Low Tide (NOS Tide Tables) 1432 EDT

Station Number	Time (EDT)	Position Lat. & Long.	x & y (NM) Coordinates	Water Depth (Ft.)	Depth (Ft.) of 45°F Isotherm
14	1300	42°05.8' N 70°31.3' W	x = 32.0 y = 6.0	135	27
15	1340	42°09.8' N 70°31.2' W	x = 28.0 y = 8.0	146	43
16	1430	42°14.0' N 70°37.0' W	x = 22.0 y = 6.0	103	26

Table 4-2: Observed Spatial Variation in Depth of Interface below the Surface

These stations, located along the western side of Massachusetts Bay close to the 120 foot contour, point to the fact that vertical variations of the order 17.0 feet occur in the interface over a horizontal distance of approximately 5.0 NM. Obviously this information supports the fact that relatively large interfacial waves can be found in the Bay as predicted by the two layer model and shown in Figure 4-A and 4-C.

Information on the currents in Massachusetts Bay, occurring during stratification, has also been collected by M.I.T. These studies were generally completed through the use of drogues or drifters that employed a large subsurface vane set at a preselected depth and suspended from a relatively small surface float. During stratification, the depth of the vanes was normally determined as a function of the level of the interface with one set of vanes placed in the upper layer and a second set in the lower layer. By following the path of the surface floats the speed and direction of the currents could be computed for the two depths. With this information some idea of the velocity profile could be determined as well as the variability in speed and direction of the two layers.

One such current study was conducted on July 27, 1972 aboard the M.I.T. research vessel R.R. Shrock. Through the C.T.D. casts taken on this cruise, one of which is shown in Figure 4-F, the depth of the thermocline was estimated at approximately 20.0 feet. Average densities for the two layers were computed from the temperature and salinity information with the result that $\rho_1 \approx 1.02558 \text{ g/cm}^3$ and $\rho_2 \approx 1.02250 \text{ g/cm}^3$. It should be noted that these were the conditions

specified in the two layer model shown by Figures 4-A and 4-B. Results of this current drogue study are given in Figure 4-G and it can be seen that the drogue depths were selected so as to be representative of the conditions existing in the two layers. Shown are the directions and velocities of the currents for a seven hour duration taken during an ebbing tide from high to low water. It can be seen that for approximately half of the duration the drogues in the upper layer proceeded southwesterly while those in layer one moved more in a southerly direction and at a slower velocity. During this time the Bay was considered to be in a steady state condition since a 5 to 10 knot wind had been blowing from the northeast for the past 18 hours. However, at approximately the mid-point of the observations, the wind shifted to the southeast 5 to 10 knots and continued in that direction for the remainder of the day. At this time it can be seen that the drogues changed direction such that the surface layer reacted directly to the wind stress. The lower layer apparently also reacted by moving in a northeasterly direction which is to be expected if the interface was forced down as a result of the thickness of the surface layer increasing due to the wind setup. It is the steady state condition for which model predictions of the currents in the two layers can be made. Consequently it is the first half of the drogue observations that is of interest for comparison with the model results as will be discussed in the next section. However, the results point out the great importance of wind driven currents. The last field data to be considered will be

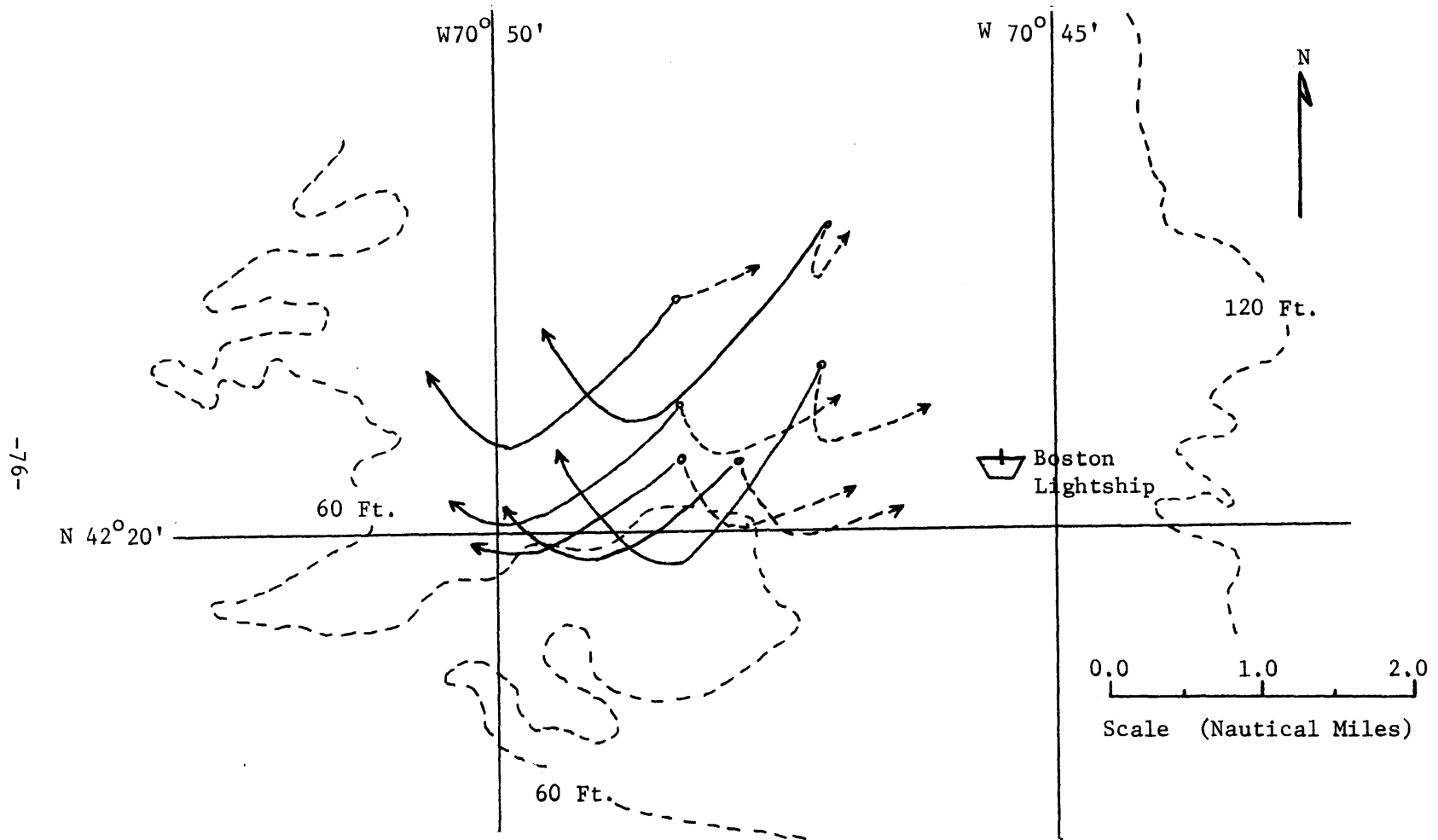


Figure 4-G: Current Drogue Study of Massachusetts Bay, July 27, 1972. Ebbing Tidal Cycle. Average Velocity Upper Layer ≈ 0.35 Knots. Average Velocity Lower Layer ≈ 0.20 Knots.

Drogue Depth, 6.5 Ft. —————

Drogue Depth, 33.0 Ft. - - - - -

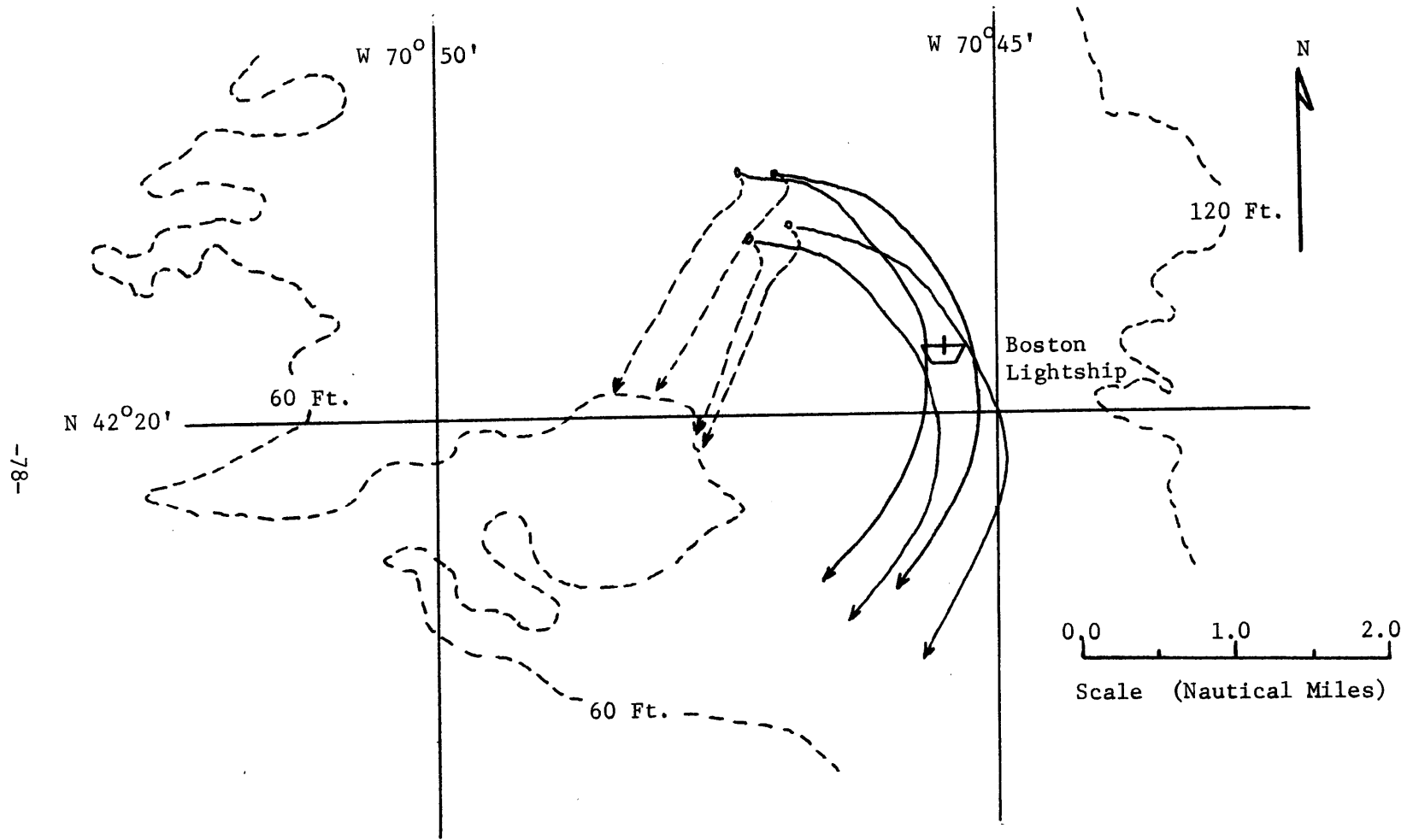
Interface Depth ≈ 20 Ft.

that taken during a second drogoue study conducted for M.I.T. on July 31, 1972. Although the C.T.D. was inoperable this particular day, it can be assumed that approximately the same density conditions and interfacial depth exist as were recorded from the study completed on July 27. Again the Bay can be assumed in steady state since the wind, for the past 18 hours, was generally from the south at 5 to 10 knots. Only a slight wind shift to the southwest was observed during the drogoue observations and this was considered to have a negligible effect on the currents.

Results of this study are shown in Figure 4-H where the observations were taken from low to high tide during the flooding situation. Although the currents in the lower layer maintained a relatively constant speed and direction, the upper layer revealed a slow change in direction swinging from almost east to around to south-southwest. The important consideration in these observations is that, for most of the time, there is an angular difference between the currents in the two layers. In addition, both drogoue studies show that, it is indeed observed that, the currents in the upper layer can proceed in a direction quite different from that normally expected during either a flooding or ebbing tide if only a one layer model is considered.

4.3 Discussion of the Model Results

The need to include the effect of a two layer model has been seen by the conditions existing in Massachusetts Bay during the summer months. The results of this model have been shown and can now



-78-

Figure 4-H: Current Drogue Study of Massachusetts Bay, July 31, 1972. Flooding Tidal Cycle.

Average Velocity Upper Layer \approx .55 Knots
 Average Velocity Lower Layer \approx .25 Knots

Drogue Depth, 6.5 Ft. —————

Drogue Depth, 33.0 Ft. - - - - -

Interfacial Depth \approx 20 Ft.

be compared with field observations of both currents and elevations. However, the comparisons will generally show agreement only in a qualitative sense since the interface separating the two layers in the Bay is rarely well defined and generally can only be determined within certain limits. This uncertainty is reflected in our arbitrary choice of specifying the interfacial amplitude at $x = 10$ NM, $y = 5$ NM. Consequently the comparisons will be qualitative in nature but will serve to demonstrate the ability of the two layer model to explain some of the conditions that have been observed in Massachusetts Bay.

The results of the surface and interfacial profiles will be compared first with the available field data. Similar to the profile for η given in the one layer model for a fully open channel, Figure 3-B, the surface profile shown in Figure 4-A compares quite closely with the observed tidal amplitudes around the Bay. The surface profile given in Figure 4-C does not, in the details, compare as well with the results of the one layer model presented in Figure 3-B. Thus, the large interfacial waves result in a significant variation in the surface contours. This large difference in surface contours is, however, not of great significance when considering the fact that the contours are drawn for intervals of 0.1 feet. Thus, in terms of actual surface elevation, the predictions are not drastically different between the one and two layer models.

The interfacial profile, given by the solution for η_1 exhibits the most dramatic and somewhat unexpected characteristics. The

results shown in Figures 4-A and 4-B are the amplitude and velocities predicted for the same densities and interfacial depth as observed in Massachusetts Bay during the current drogue study of July 27, 1972. Resultingly the predicted interfacial profile is considered to be fairly representative of the physical situation that could exist. However, due to instrument problems, only a limited number of C.T.D. casts were taken during the drogue study. Consequently, the model predictions will be compared with vertical observations taken by Halpern in Stellwagen Basin and by the M.I.T. C.T.D. stations of July, 1973.

The total vertical variation of the thermocline, as observed by Halpern, was of the order of 30 feet giving an interfacial amplitude of approximately 15 feet. Comparing this value with the results in Figure 4-A shows that the order of magnitude is certainly reasonable since the model also predicts an η_1 of 15 feet. In fact, considering the sensitivity of the model to changes in h_2 and without further knowledge of the conditions surrounding Halpern's data, the prediction for η_1 can actually be considered reasonably good.

The information obtained from the C.T.D. casts, taken by M.I.T. in July, 1973, verify the fact that interfacial waves exist in Massachusetts Bay. This data was synoptic in the sense that it was taken as close to low tide as possible when hopefully slack conditions existed. Unfortunately, the actual wave length, L_1 , of the interface could not be computed from the limited field data taken although the model predicts an L_1 of the order 11.0 NM as seen in

Figure 4-A. It should be mentioned that a similar condition has been noted and discussed by other investigators under the subject of internal waves. It is obvious that the interfacial waves, qualitatively, predicted by the two layer model, are evidenced both by Halpern's data and M.I.T.'s C.T.D. casts.

Currents predicted in the two layers can be compared directly with current drogue observations shown in Figures 4-G and 4-H. As previously mentioned, the first set of results presented for the stratified model are determined for the same conditions as observed in the field during the drogue studies. These results are presented in expanded form in Figure 4-I and show the variability that can be expected in the currents along the boundary in Massachusetts Bay. It is important to note that the two drogue studies were also completed close to the Boston Lightship and the western edge of the Bay in a location, as shown by the predicted results in Figure 4-I, where currents vary drastically with location and are predicted to flow shoreward during an ebbing tide and seaward during the flood in the upper layer. Although the model results do not predict the exact direction given by the drogues, due probably to the effects of Boston Harbor and the surrounding geometry in addition to the neglect of Coriolis force, it is obvious that the model shows that a large difference in current directions is possible during stratification in this area. This is in qualitative agreement with observations as shown in Figures 4-G and 4-H.

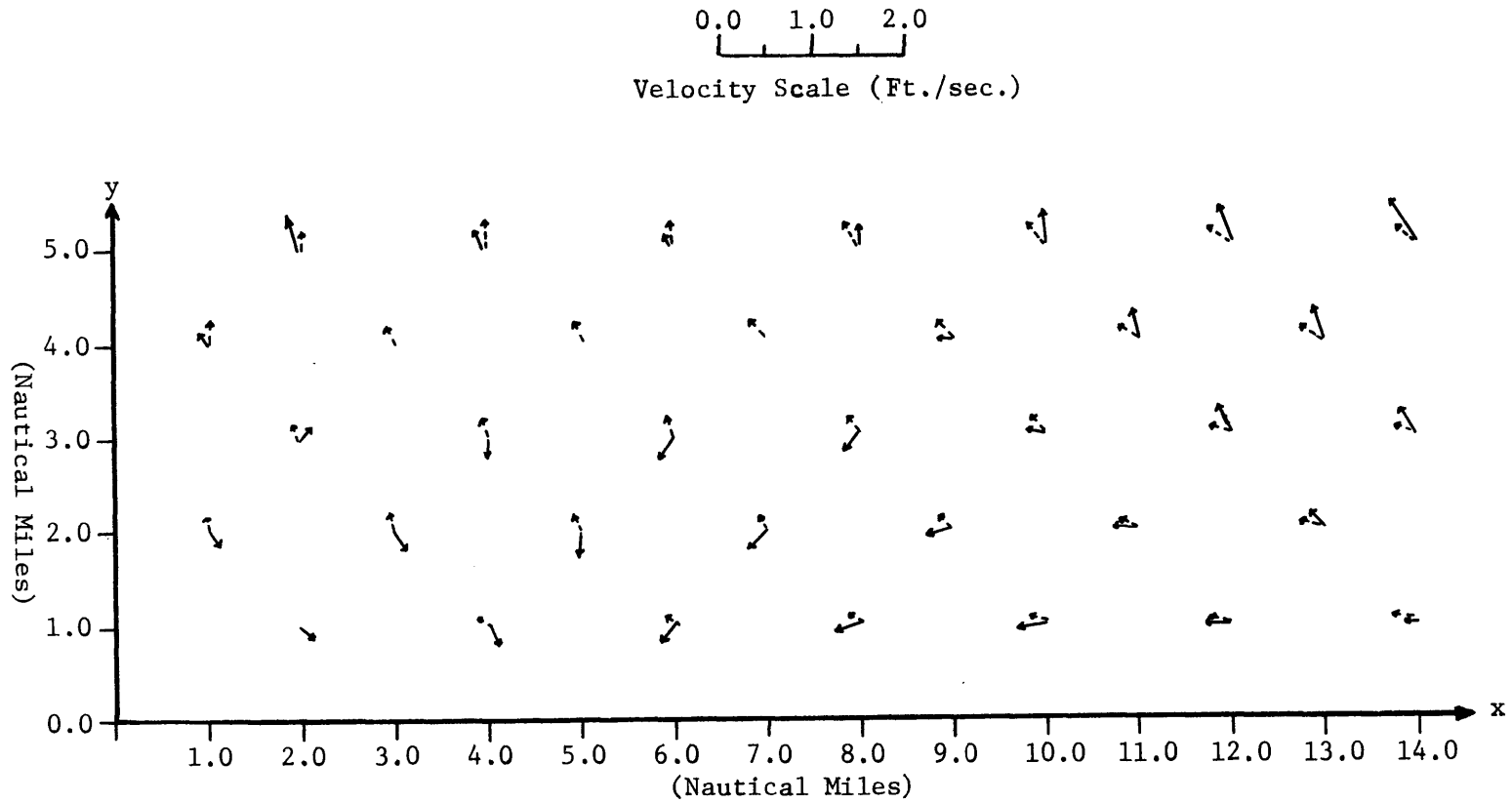


Figure 4-1: Two Layer Model of Massachusetts Bay.
Velocities at Maximum Ebb in Ft./sec.

U_2 (Upper Layer) —————

U_1 (Lower Layer) - - - - -

$h_2 = 20.0 \text{ Ft.}, \rho_2 = 1.02250 \text{ g/cm}^3$

$h_1 = 100.0 \text{ Ft.}, \rho_1 = 1.02558 \text{ g/cm}^3$

In addition to showing an angular difference in the current direction in the two layers, it demonstrates the sensitivity of the observations to location, especially when close to the boundary. From the results of the two layer model shown in Figure 4-I, an angular change of up to 180° in the current direction in the upper layer can be observed over a distance of only a few miles in the Bay

CHAPTER V

CONCLUDING REMARKS

Two analytical models have been derived for a geometrical configuration similar to that of Massachusetts Bay. A simplistic approach was taken in the theoretical development of the models by depth averaging the linear long wave equations in two dimensions. By neglecting Coriolis force, bottom friction, and wind stress the models were able to represent the tidal circulation for both the uniformly well mixed and stratified case and to explain qualitatively some of the conditions encountered during field observations. Results of the two models were presented for a number of geometrical variations and physical conditions and compared with various types of field observations for verification of the model predictions.

The one layer model, representing the situation generally found during the winter, was discussed first and compared with tidal data and current observations. Comparison of the results of the model with tide gauge observations demonstrated the ability of the model to predict, quite closely, the surface profile for Massachusetts Bay. Velocities of the tidal currents also compared favorably with field data in a qualitative sense, and generally were the same order of magnitude. Current direction was the most difficult to verify as current meter records were often quite variable in this respect showing the effects of localized conditions.

Results of the two layer analytical model were considered more revealing in the sense that insight was gained into the conditions present during stratification. These results were compared with various types of field observations in an attempt to verify qualitatively the significance of using a two layer model to predict interface and surface profiles and currents. Reasonably good agreement was found when comparing the predicted surface profile with the observed tidal amplitudes. Differences between the predicted tidal amplitudes of the one layer model are minor and the differences between the two models and the observed tidal amplitudes can be attributed to the effects of Boston Harbor, the Cape Cod Canal, and the sloping bottom of the lower Bay.

Comparisons of the interfacial profile and current velocities predicted by the model with available field data are generally more qualitative since the physical conditions, especially the depth of the interface as well as the amplitude of the interfacial wave, that govern the solution cannot be determined very accurately. However, observations by both Halpern and M.I.T. verify the existence of interfacial waves and show the amplitude of the same order of magnitude as that predicted by the two layer model.

Currents predicted by the model were the most difficult to verify by field measurements since the physical observations clearly exhibit a high degree of variability over the tidal cycle. The drogue studies were apparently subject to variations due to relatively small changes in wind direction and, in the area surveyed, the observations are

probably affected by the flux in and out of Boston Harbor. In view of these existing conditions only a qualitative comparison can be made. This comparison however shows that the velocities predicted by the model are within the order of magnitude of those measured in Massachusetts Bay, also the observed curiosity of having shoreward current in the upper layer during an ebbing tide is made plausible by a similar prediction by the two layer model.

The two layer analytical model has clearly demonstrated its ability to explain qualitatively observed phenomena as well as giving an insight into conditions that are not readily apparent. Although it represents a highly simplified approach to a rather complex physical problem, it produces useful information on Massachusetts Bay and can assist the coastal engineer in solving problems related to the ocean environment.

Obviously, the development of more sophisticated one and two layer models would be advantageous. It was shown in the theoretical development that Coriolis force exerts some influence and from comparing model results with field data it can be seen that including Boston Harbor, the Cape Cod Canal, and introducing a wind stress would more realistically describe the physical conditions. However, the objective was to develop a simple analytical model of Massachusetts Bay and thereby demonstrate that if current predictions are desired one should indeed have a two layer model. This goal has been achieved in the qualitative agreement of predicted and observed phenomena in Massachusetts Bay.

BIBLIOGRAPHY

- Butman, B. (1971) "Some Short Term Current Observations in Massachusetts Bay", M.I.T., Department of Earth and Planetary Sciences, Unpublished Report.
- Christodoulou, G.C. and Leimkuhler, W.F. (1973) "Report of NOMES Current Observations", M.I.T., Department of Civil Engineering, Unpublished Report.
- Conner, J.J. and Wang, J.D. (1973) "Finite Element Modeling of Two Dimensional Hydrodynamic Circulation in Shallow Water Masses", M.I.T., Department of Civil Engineering, Technical Report No. 171.
- Day, C.G. (1959) "Oceanographic Observations, 1957, East Coast of the United States", U. S. Department of the Interior, Special Scientific Report -- Fisheries, No. 282.
- Doret, S. D. and Madsen, O. S. (1972) "Special Studies Dealing with Run-Up on Impermeable Breakwaters", M.I.T., Department of Civil Engineering, Unpublished Report.
- Frankel, S. L. and Pearce, B.R. (1973) "Chemistry Data Report on the Massachusetts Bay Area", M.I.T., Department of Civil Engineering, Unpublished Report.
- Grubert, J.P. and Abbott, M.B. (1972) "Numerical Computation of Stratified Nearly Horizontal Flows", Journal of the Hydraulics Division, A.S.C.E., Vol. 98, No. HY 10.
- Halpern, D. (1971,a) "Observations on Short-period Internal Waves in Massachusetts Bay", Journal of Marine Research, Vol. 29, No. 2.
- Halpern, D. (1971,b) "Semidiurnal Internal Tides in Massachusetts Bay", Journal of Geophysical Research, Vol. 76, No. 27.
- Ippen, A.T. and Goda, Y. (1963) "Wave Induced Oscillations in Harbors: The Solution for a Rectangular Harbor Connected to the Open Sea", M.I.T., Department of Civil Engineering, Technical Report No. 59.
- Pedersen, F.G. (1972) "Gradually Varying Two-Layer Stratified Flow", Journal of the Hydraulics Division, A.S.C.E., Vol. 98, No. HY 1.
- U.S. Department of Commerce, NOAA (1972) "Tide Tables High and Low Water Predictions, 1973", U.S. Government Printing Office, Washington, D.C.

APPENDIX A

LISTING OF THE PROGRAM USED FOR THE
COMPUTATIONS PRESENTED IN CHAPTER IV

The program used for the computation of the solution for the two layer model is presented along with a sample of the output. The "comment cards" should make the program self-explanatory.

```

C TWO LAYER MODEL OF MASSACHUSETTS BAY
C SIMPLE RECTANGULAR GEOMETRY, OPENING ALONG ONE SIDE FROM X1 TO X2
C AVERAGE BAY DEPTH ASSUMED TO BE 120 FEET
C PROGRAM COMPUTES AMPLITUDES AND VELOCITIES FOR TWO LAYER FLOW
REAL K, M1, M2, M01, M02, MN1, MN2
DIMENSION K(100), A(100), B(100)
C SPECIFY BAY CONDITIONS (RH01, RH02, H1, H2) ON NEXT FOUR CARDS
RH01=1.02558
RH02=1.0225
H1=100.0
H2=20.0
C SPECIFY INPUT CONDITIONS AT A GIVEN LOCATION
C I.E. (ETA11 AND ETA22 AT X AND Y COORDINATES)
ETA11=3.5
ETA22=4.5
X=10.0
Y=5.0
C END OF INPUT CONDITIONS
C *****
C SPECIFIED CONSTANTS FOR MASSACHUSETTS BAY
X=X*6076.1
Y=Y*6076.1
RH03=(RH01-RH02)/RH01
G=32.1725
PI=3.1415926535
W=(2.*PI)/(12.4*3600.)
C=(RH03*G*H2)/W**2
XC=59.0*6076.1
X1=0.0
X2=41.0*6076.1
Y0=20.0*6076.1
M1=((W**2*(H1+H2))/(G*H2*RH03*H1))-((W**2)/(G*(H1+H2)))
M2=(W**2)/(G*(H1+H2))
M01=M1**.5
M02=M2**.5
C COMPUTES A0 AND B0 BY ITERATION

```

```

AC=-0.01
BC=4.0
A INC=0.01
E INC=0.1
10 AC=AC+A INC
20 BC=BC+B INC
F5=C.0
F6=C.0
F7=C.0
N=0
50 N=N+1
K(N)=(N*PI)/X0
MN1=M1-K(N)**2.
MN2=M2-K(N)**2.
IF (MN1) 70, 70, 65
65 CCNTINUE
MN1=MN1**.5
MN2=(-MN2)**.5
-06- ANL2=(-.5*MN1*SIN(MN1*YC))
BNL2=(.5*MN2*SINH(MN2*YC))
C1=(-MN1*SIN(MN1*YO))
C2=C*(K(N)**2*MN1*SIN(MN1*YO)+MN1**3*SIN(MN1*YO))
ANL1=C1+C2
D1=MN2*SINH(MN2*YO)
D2=C*(-K(N)**2*MN2*SINH(MN2*YO)+MN2**3*SINH(MN2*YO))
BNL1=D1+D2
F5=COS(MN1*Y)
F6=COSH(MN2*Y)
CC TC 80
70 CCNTINUE
MN1=(-MN1)**.5
MN2=(-MN2)**.5
ANL2=.5*MN1*SINH(MN1*YC)
BNL2=.5*MN2*SINH(MN2*YO)
E1=MN1*SINH(MN1*YO)
E2=C*(-K(N)**2*MN1*SINH(MN1*YO)+MN1**3*SINH(MN1*YO))

```



```

ANL1=E1+E2
F1=MN2*SINH(MN2*Y0)
F2=C*(-K(N)**2*MN2*SINH(MN2*Y0)+MN2**3*SINH(MN2*Y0))
BNL1=F1+F2
F5=COSH(MN1*Y)
F6=COSH(MN2*Y)
80  CCNTINUE
G1=(-2.*W**2*(SIN(K(N)*X2)-SIN(K(N)*X1))/(G*H1*(X2-X1)*K(N))
G2=SIN(M01*Y0)*((1/M01)-(G*H2*M01)/W**2)
G3=SIN(M02*Y0)*((1/M02)-(G*H2*M02)/W**2)
ACL1=G1*G2
ECL1=G1*G3
G4=(SIN(K(N)*X2)-SIN(K(N)*X1))/((X2-X1)*K(N))
ACL2=(-M01*SIN(M01*Y0))*G4
BCL2=(-M02*SIN(M02*Y0))*G4
G5=A0*ACL1+B0*BCL1
G6=A0*ACL2+B0*BCL2
-16- A(N)=(G5/BNL1-G6/BNL2)/(ANL1/BNL1-ANL2/BNL2)
      B(N)=(G5/ANL1-G6/ANL2)/(BNL1/ANL1-BNL2/ANL2)
H5=COS(K(N)*X)*(A(N)*F5+B(N)*F6)+H5
H6=K(N)**2*COS(K(N)*X)*(A(N)*F5+B(N)*F6)+H6
H7=COS(K(N)*X)*(A(N)*MN1**2*F5+B(N)*MN2**2*F6)+H7
IF(50-N) 85, 50, 50
85  CCNTINUE
ETA2=H5+(A0*COS(M01*Y)+E0*COS(M02*Y))
ETA1=ETA2-(G*H2/W**2)*((H6+H7+A0*M1*COS(M01*Y)+B0*M2*COS(M02*Y)))
IF (B0-6.0) 6,33,33
6   CCNTINUE
IF (ETA2-ETA22) 20, 35, 29
29  IF (BINC-C.0001)35, 35, 30
30  BC=B0-BINC
    BINC=BINC/10.0
    IF(BINC-C.0001)35,35,20
33  IF (A0-1.0)7, 7, 45
7   CONTINUE
35  IF (ETA1-ETA11) 10, 45, 40

```

```

40  AC=AO-AINC
    AINC=AINC/10.0
    IF (AINC-0.00001) 45,45,10
45  CONTINUE
    AC=AO+AINC
    BC=BO+BINC
58  FORMAT (1H1,'          AO =',F7.4,20X,'BO =',F8.5, '//)
    WRITE (6,58) BO, AO
59  FORMAT (1H0,'COMPUTES AN AND BN FOR N = 1 TO 50 ',//)
    WRITE (6, 59)
C    COMPUTES AN AND BN FOR N = 1 TO 50
    CC 185 N = 1, 50
    K(N)=(N*PI)/X0
    MN1=M1-K(N)**2.
    MN2=M2-K(N)**2.
    IF (MN1) 170, 170, 160
160  CONTINUE
    MN1=MN1**.5
    MN2=(-MN2)**.5
-92- ANL2=(-.5*MN1*SIN(MN1*YC))
    BNL2=(.5*MN2*SINH(MN2*YC))
    C1=(-MN1*SIN(MN1*YO))
    C2=C*(K(N)**2*MN1*SIN(MN1*YO)+MN1**3*SIN(MN1*YO))
    ANL1=C1+C2
    D1=MN2*SINH(MN2*YO)
    D2=C*(-K(N)**2*MN2*SINH(MN2*YO)+MN2**3*SINH(MN2*YO))
    BNL1=D1+D2
    GC TO 180
170  CONTINUE
    MN1=(-MN1)**.5
    MN2=(-MN2)**.5
    ANL2=.5*MN1*SINH(MN1*YC)
    BNL2=.5*MN2*SINH(MN2*YO)
    E1=MN1*SINH(MN1*YO)
    E2=C*(-K(N)**2*MN1*SINH(MN1*YO)+MN1**3*SINH(MN1*YO))
    ANL1=E1+E2

```

```

F1=MN2*SINH(MN2*Y0)
F2=C*(-K(N)**2*MN2*SINH(MN2*Y0)+MN2**3*SINH(MN2*Y0))
BNL1=F1+F2
180 CCNTINUE
G1=(-2.*W**2*(SIN(K(N)*X2)-SIN(K(N)*X1))/(G*H1*(X2-X1)*K(N)))
G2=SIN(MC1*YC)*((1/MC1)-(G*H2*MC1)/W**2)
G3=SIN(MC2*YC)*((1/MC2)-(G*H2*MC2)/W**2)
ACL1=G1*G2
BCL1=G1*G3
G4=(SIN(K(N)*X2)-SIN(K(N)*X1))/((X2-X1)*K(N))
ACL2=(-MC1*SIN(MC1*YC))*G4
BCL2=(-MC2*SIN(MC2*YC))*G4
G5=A0*ACL1+B0*BCL1
G6=A0*ACL2+B0*BCL2
A(N)=(G5/BNL1-G6/BNL2)/(ANL1/BNL1-ANL2/BNL2)
E(N)=(G5/ANL1-G6/ANL2)/(BNL1/ANL1-BNL2/ANL2)
WRITE (6, 60) N, A(N), E(N)
60  FORMAT (10X, I4, 10X, E12.5, 10X, E12.5)
185 CCNTINUE
C  COMPUTES  ETA 1  AND  ETA 2
C  COMPUTES  VELOCITIES  U1,  V1,  U2,  V2
110  Y=2.C*6076.1
      WRITE (6, 115)
115  FORMAT (1H1, 5X, ' COMPUTES  ETA  AND  VELOCITIES  FOR  TWO  LAYER
1ED  FLOW')
      WRITE (6, 120)
120  FORMAT (1H0,5X,'X (NM)',5X,'Y (NM)',10X,'ETA-1 (FT)',5X,'U1 (FPS)'
1,5X,'V1 (FPS)',10X,'ETA-2 (FT)',5X,'U2 (FPS)',5X,'V2 (FPS)')
      X=-6076.1
140  X=X+6076.1
      P1=0.0
      P2=0.0
      P3=0.0
      P4=0.0
      P5=0.0
      P6=0.0

```

```

F7=C.0
CC 220 N = 1, 50
MN1=M1-K(N)**2
MN2=M2-K(N)**2
IF (M1-K(N)**2) 200, 19C, 190
190 CONTINUE
MN1=MN1**.5
MN2=(-MN2)**.5
P1=(-K(N)*SIN(K(N)*X)*(A(N)*COS(MN1*Y)+B(N)*CCSH(MN2*Y)))+P1
P2=(COS(K(N)*X)*(-A(N)*MN1*SIN(MN1*Y)+B(N)*MN2*SINH(MN2*Y)))+P2
E2XXX=K(N)**3*SIN(K(N)*X)*(A(N)*COS(MN1*Y)+B(N)*COSH(MN2*Y))
E2YYX=+A(N)*MN1**2*COS(MN1*Y)-B(N)*MN2**2*COSH(MN2*Y)
P3=E2XXX+(+K(N)*SIN(K(N)*X))*E2YYX+P3
E2XXY=+A(N)*MN1*SIN(MN1*Y)-B(N)*MN2*SINH(MN2*Y)
E2YYY=A(N)*MN1**3*SIN(MN1*Y)+B(N)*MN2**3*SINH(MN2*Y)
P4=+K(N)**2*COS(K(N)*X)*E2XXY+COS(K(N)*X)*E2YYY+P4
F5=COS(MN1*Y)
F6=COSH(MN2*Y)
CC TO 210
200 CONTINUE
MN1=(-MN1)**.5
MN2=(-MN2)**.5
P1=(-K(N)*SIN(K(N)*X)*(A(N)*COSH(MN1*Y)+B(N)*COSH(MN2*Y)))+P1
P2=(COS(K(N)*X)*(+A(N)*MN1*SINH(MN1*Y)+B(N)*MN2*SINH(MN2*Y)))+P2
E2XXX=K(N)**3*SIN(K(N)*X)*(A(N)*COSH(MN1*Y)+B(N)*COSH(MN2*Y))
E2YYX=-A(N)*MN1**2*COSH(MN1*Y)-B(N)*MN2**2*COSH(MN2*Y)
P3=E2XXX+(+K(N)*SIN(K(N)*X))*E2YYX+P3
E2XXY=-A(N)*MN1*SINH(MN1*Y)-B(N)*MN2*SINH(MN2*Y)
E2YYY=A(N)*MN1**3*SINH(MN1*Y)+B(N)*MN2**3*SINH(MN2*Y)
P4=+K(N)**2*COS(K(N)*X)*E2XXY+COS(K(N)*X)*E2YYY+P4
F5=COSH(MN1*Y)
F6=COSH(MN2*Y)
210 CCNTINUE
H5=COS(K(N)*X)*(A(N)*F5+B(N)*F6)+H5
H6=K(N)**2*COS(K(N)*X)*(A(N)*F5+B(N)*F6)+H6
H7=COS(K(N)*X)*(A(N)*MN1**2*F5+B(N)*MN2**2*F6)+H7

```

```

220 CONTINUE
D=G**2*R+C3*H2/W**3
ETA2=H5+(A0*COS(M01*Y)+E0*COS(M02*Y))
ETA1=ETA2-(G*H2/W**2)*((H6+H7+A0*M1*COS(M01*Y)+B0*M2*COS(M02*Y)))
U2=(-G/h)*P1
V2=(-G/h)*(P2+(-A0*M01*SIN(M01*Y)-B0*M02*SIN(M02*Y)))
U1=U2-D*(P3)
V1=V2-D*((A0*M01**3*SIN(M01*Y)+B0*M02**3*SIN(M02*Y)+P4))
X5=X/6076.1
Y5=Y/6076.1
WRITE (6, 230) X5, Y5, ETA1, U1, V1, ETA2, U2, V2
230 FORMAT (5X,F5.2,6X,F5.2,11X,F8.4,7X,F8.4,5X,F8.4,10X,F8.4,7X,F8.4,
15X,F8.4)
IF (X-(58.*6076.1)) 140, 140, 240
240 CCNTINUE
300 STOP
END

```

SAMPLE OF COMPUTER PROGRAM OUTPUT

$$A_o = -0.058$$

$$B_o = 4.686$$

COMPUTES ETA AND VELOCITIES FOR TWO LAYERED FLOW

<u>X (NM)</u>	<u>Y (NM)</u>	<u>ETA-1 (FT)</u>	<u>U1 (FPS)</u>	<u>V1 (FPS)</u>	<u>ETA-2 (FT)</u>	<u>U2 (EPS)</u>	<u>V2 (FPS)</u>
10.00	10.00	4.1789	- 0.1582	0.1886	4.4359	- 0.1615	0.1886

7266°024

171
141
199

179



MATHEMATICAL MODELS OF THE MASSACHUSETTS BAY

Part III

A Mathematical Model for The Dispersion of Suspended Sediments in Coastal Waters

by

GEORGIOS C. CHRISTODOULOU

WILLIAM F. LEIMKUHNER

and ARTHUR T. IPPEN

MIT RALPH M. PARSONS LABORATORY
for
WATER RESOURCES AND HYDRODYNAMICS

Report No. 179

Prepared with the Support of
Sea Grant Office
National Oceanic and
Atmospheric Administration
Department of Commerce, Washington, D.C.

January 1974

ENG

MIT



DEPARTMENT
OF
CIVIL
ENGINEERING

SCHOOL OF ENGINEERING
MASSACHUSETTS INSTITUTE OF TECHNOLOGY
Cambridge, Massachusetts 02139

MATHEMATICAL MODELS OF THE MASSACHUSETTS BAY

PART III. A MATHEMATICAL MODEL FOR THE DISPERSION
OF SUSPENDED SEDIMENTS IN COASTAL WATERS

BY

GEORGIOS C. CHRISTODOULOU

WILLIAM F. LEIMKUHLER

AND

ARTHUR T. IPPEN

RALPH M. PARSONS LABORATORY
FOR WATER RESOURCES AND HYDRODYNAMICS

Department of Civil Engineering
Massachusetts Institute of Technology

Report No. 179

Prepared with the Support of

Sea Grant Office
National Oceanic and Atmospheric Administration
Department of Commerce, Washington, D.C.

RECEIVED
MAY 14 1974
M. I. T. LIBRARIES

MATHEMATICAL MODELS OF THE MASSACHUSETTS BAY

ABSTRACT - PART III

A MATHEMATICAL MODEL FOR THE DISPERSION OF
SUSPENDED SEDIMENTS IN COASTAL WATERS

by

GEORGIOS C. CHRISTODOULOU

WILLIAM F. LEIMKUHLER

and

ARTHUR T. IPPEN

A three-dimensional analytical model is proposed for the description of the dispersion of fine suspended sediments in coastal waters. The model basically predicts the quasi-steady state sediment concentration as a function of space and tidal time and the deposition pattern in the region surrounding a continuous vertical line source. It requires that the sediment settling velocities and the hydrodynamic features of the area, the net drift and the tidal velocities as well as the dispersion coefficients be known. Effects of wave action and vertical stratification are not explicitly considered. A separation of variables technique permits a rather independent treatment of the vertical and horizontal distributions; they are linked primarily through the decay factor, which represents the loss of material to the bottom.

The model is applied to a hypothetical dredging situation in Massachusetts Bay. Values for the hydrodynamic parameters were obtained from the analysis of field data collected during the past year. Laboratory experiments were carried out for the determination of settling rates of clays in seawater, in view of unknown flocculation factors. Stoke's law was considered adequate for silt and very fine sand.

The model results indicated very long and relatively narrow dispersion patterns, under the assumption of constant drift direction. The net drift and the sediment settling velocity seem to be the most important factors controlling the dispersion of fines in coastal waters.

0720834

PART III

ACKNOWLEDGEMENTS

This study constitutes a part of a series of investigations in a major environmental research program on the "Sea Environment in Massachusetts Bay and Adjacent Waters". This program consists of theoretical and field investigations and is under the administrative and technical direction of Dr. Arthur T. Ippen, Institute Professor, Department of Civil Engineering and of Dr. Erik L. Mollo-Christensen, Professor, Department of Meteorology as co-principal investigators. Support of the program is provided in part by the Sea Grant Office of NOAA, Department of Commerce, Washington, D.C. through Grant No. NG-43-72, in part by the New England Offshore Mining Environmental Study (NOMES) of NOAA, in part by the Henry L. and Grace Doherty Foundation, Inc., and in part by the Department of Natural Resources, Commonwealth of Massachusetts through Project No. DMR-73-1. The project which is the subject of this report was conducted by staff members of the Ralph M. Parsons Laboratory for Water Resources and Hydrodynamics and was administered under Project No. DSR 80344, 80575 and 81100 at M.I.T.

All computer work was carried out at the M.I.T. Information Processing Center. The authors gratefully acknowledge the work of Ms. Sheila L. Frankel, who contributed laboratory results on background measurements of suspended sediment in Massachusetts Bay; she also assisted in the collection of current and suspended sediment field data along with Dr. Bryan R. Pearce, project coordinator, Mr. Edward F. McCaffrey, chief technician, Mr. Douglas A. Briggs, Mr. Cortis Cooper, Mr. Robert F. Paquette and Mr. John D. Wang.

Appreciation is expressed here to Ms. Susan M. Johnson and Ms. Stephanie M. Demeris for their excellent typing of this manuscript.

TABLE OF CONTENTS

	<u>Page</u>
TITLE PAGE	1
ABSTRACT	2
ACKNOWLEDGMENTS	3
TABLE OF CONTENTS	4
LIST OF FIGURES	6
LIST OF TABLES	8
LIST OF SYMBOLS	9
CHAPTER 1 INTRODUCTION	13
CHAPTER 2 REVIEW OF PREVIOUS RESEARCH	17
CHAPTER 3 THE MATHEMATICAL MODEL	27
3.1 Basic assumptions	27
3.2 Structure of the model	29
CHAPTER 4 THE VERTICAL CONCENTRATION DISTRIBUTION	34
4.1 The Normalized Equilibrium Distribution	34
4.2 Boundary Conditions-Determination of the Decay Rate	38
4.3 Sediment Settling Velocities	41
4.4 Flocculation Characteristics and Effects	44
4.5 Settling Tube Experiments on Clay Suspensions	45
4.5.1 Experimental program and procedures	45
4.5.2 Discussion of results	54
CHAPTER 5 THE HORIZONTAL DISTRIBUTION OF AVERAGE CONCENTRATION	57
5.1 Solution of the Differential Equation	57
5.2 Net Drift and Tidal Velocities	61
5.3 Dispersion Coefficients	67

TABLE OF CONTENTS (Ct'd)

	<u>Page</u>	
CHAPTER 6	SYNTHESIS OF THE MODEL COMPONENTS	74
	6.1 Concentration Distribution of a Group of Sediments	74
	6.2 Total Sediment Concentration	76
	6.3 Rate of Deposition	77
CHAPTER 7	APPLICATION TO DREDGING IN MASSACHUSETTS BAY	80
	7.1 General Comments on the Project NOMES	80
	7.2 The Sediment Source	81
	7.3 Composition of the Initial Mixture	83
	7.4 Background Concentrations of Suspended Sediment	87
	7.5 Determination of Parameters From Drogue Data	88
	7.6 Results and Discussion	106
CHAPTER 8	CONCLUSIONS AND RECOMMENDATIONS	121
REFERENCES		124
APPENDIX A	SETTLING TUBE MEASUREMENTS	127
APPENDIX B	COMPUTER PROGRAM FOR ANALYSIS OF DROGUE DATA	131
APPENDIX C	COMPUTER PROGRAM FOR THE HORIZONTAL DISTRI- BUTION OF AVERAGE CONCENTRATION	141

LIST OF FIGURES

<u>Figure</u>		<u>Page</u>
1	Sediment Settling Tube	47
2	Correlation of turbidity and total suspended sediment Concentration from Field Data	48
3	Turbidimeter Calibration Curves for Clay Suspensions	50
4	Technique for Sediment Separation into Groups of Settling Velocities (30)	52
5	Settling Tube Results for the 10 mg/l Initial Concentration Runs	53
6	Settling Tube Results for the 100 mg/l Initial Concentration Runs	53
7	Schematic Representation of the Vertical Velocity Profile and the Weights Associated with the Drogues	65
8	Approximate Geometry of Massachusetts Bay	84
9	Droge Used in Massachusetts Bay Current Studies	84
10	Droge Paths in the Study of February 21-22, 1973	89
11	Droge Paths in the Study of March 28-29, 1973	90
12	Droge Paths in the Study of June 11-12-13, 1973	91
13	Flow Chart of Model Procedures	92
14	Technique for Determining Magnitude and Direction of Tidal Velocities	95
15	Distribution of Average Concentration for Conditions of February 21-22, 1973	103
16	Distribution of Average Concentration for Conditions of March 28-29, 1973	104
17	Distribution of Average Concentration for Conditions of June 11-12, 1973	105
18	Normalized Vertical Profiles Under Average Conditions	113

LIST OF FIGURES (ct'd)

<u>Figure</u>		<u>Page</u>
19a,b	Distribution of Average Concentration, \bar{c} , of Groups 1 and 2 Under Average Conditions, at High Water Slack	114
19c	Distribution of Average Concentration, \bar{c} , of Group 3 Under Average Conditions	115
19d,e	Distribution of Average Concentration, \bar{c} , of Groups 4 and 5 Under Average Conditions, at High Water Slack	116
20	Deposition Rates of Sediment Group 3 Under Average Conditions	119
21	Percentage of Total Discharge of Group 3 Deposited Within Area Shown, Under Average Conditions	119

LIST OF TABLES

<u>Table</u>		<u>Page</u>
1	Separation of Fines into Groups	43
2	Distribution of Clays Tested into Groups	56
3	Composition of Dredging Fines in Terms of Settling Velocity	86
4	Parameters for Conditions of February 21-22, 1973	99
5	Parameters for Conditions of March 28-29, 1973	100
6	Parameters for Conditions of June 11-12, 1973	101
7	Dispersion Coefficients	108
8	Average Conditions	112
9	Length, in Multiples of the Depth, of Area with Concentration \bar{c} Larger Than Indicated (for average conditions)	112

LIST OF SYMBOLS

- a = Reference depth for the vertical sediment distribution
- A = Overall probability that a particle reaching the bottom is deposited there
- A = Cross-sectional area (in one-dimensional models)
- c = Concentration of suspended sediments
- \bar{c} = Average concentration over the depth (or the cross section)
- c_o = Total concentration of sediments in mixture injected
- c_{oi} = Concentration of a particular group in mixture injected
- c_a = Reference concentration at depth a for the vertical distribution
- c'' = Spatial deviation of local concentration from the average value over the depth (or the cross section)
- d = Particle diameter
- D = Rate of deposition
- \bar{D} = Average value of D over the tidal cycle
- E = Dispersion coefficient
- E_x, E_y = Dispersion coefficients in x and y directions, respectively
- E_L = Longitudinal dispersion coefficient (in one-dimensional models)
- E_d = Part of the dispersion coefficient associated with the velocity variations over the depth (or the cross-section)
- f = The Darcy-Weisbach friction factor
- g = Acceleration of gravity
- h = Total water depth
- H = Height of water column in settling tube experiments

- k = Von Karman's constant
 ℓ = Length scale for diffusion
 $2\ell_T$ = Movement due to tide (see Figure 14)
 L = Distance from the source
 m = Mass rate of injection of the sediment-seawater mixture
 m_i = Mass rate of injection of sediment group i
 n = Number of tidal cycles to steady state
 M = Total mass injected
 $P(\zeta)$ = Probability density function of the vertical position of particles, used by Elder (2-7). Analogous to $\phi(\zeta)$
 r_o = Pipe radius in Taylor's formula (Equation 2-5)
 r_i, r_e = Source and sink terms in general dispersion Equation (2-3)
 s = $\bar{\tau} e^{-\alpha(t-\tau)}$, variable used in the transformation of the differential equation for τ (see Section 5.1)
 t = Time
 T = Tidal period
 T_I = Initial time, after which diffusion modelling is valid
 T' = Time scale for mixing, as defined by Fischer
 u, v = Local velocities (at depth z) along x and y directions, respectively
 u'', v'' = Spatial deviations of u, v from their respective depth-averaged values u, v
 u_f = Net drift velocity (at depth z) along x axis
 u_T, v_T = Max tidal velocities (at depth z) along x, y axes, respectively
 u_* = Shear velocity

- U, V = Mean velocities over the depth in x,y directions, respectively
- U_s, V_s = Mean-weighted velocities over the depth, i.e. transport rates along x,y directions, respectively (taking into consideration the nonuniform sediment distribution over the vertical)
- U_f = Depth-averaged drift velocity along x axis
- U_T, V_T = Depth-averaged max tidal velocities along x,y axes
- U_{fs} = Mean transport rate along the net drift
- U_{TS}, V_{TS} = Transport rates associated with the max tidal velocity in x,y directions
- U_m = Representative velocity magnitude for the determination of u_*
- Ψ = Volume rate of injection of the sediment-seawater mixture
- w_s = Sediment settling velocity
- x, y = Horizontal coordinates along net drift and normal to it
- z = Vertical coordinate, increasing upwards
- Z = Exponent in the expression of the vertical sediment distribution = $\frac{w_s}{k\beta u_*}$
- α = Decay rate in the two-dimensional dispersion equation for the depth-averaged concentration
- β = ϵ_z / ϵ_m
- γ_s = Sediment specific weight
- γ_w = Seawater specific weight
- δ = Thickness of layer of sediment deposited

- ϵ = Horizontal turbulent (eddy) diffusion coefficient
 ϵ_x, ϵ_y = Turbulent diffusion coefficients along x,y directions
 $\epsilon_z, \epsilon_\zeta$ = Vertical sediment diffusion coefficient
 $\bar{\epsilon}_z$ = Mean value of ϵ_z over the depth
 ϵ_m = Vertical momentum transfer coefficient
 ζ = z/h , non-dimensional depth
 η, ξ = Transformation of horizontal coordinates y,x (see Section 5.1)
 λ = Constant of proportionality in formulas for the dispersion coefficient
 λ_i = c_{oi}/c_o , proportion of group i in initial sediment mixture
 ν = Kinematic viscosity
 ρ = Density
 ρ_e = Effective density of loosely deposited sediment
 ρ_s = Sediment density
 ρ_w = Seawater density
 σ^2 = Variance of sediment (or tracer) distribution along an axis
 τ = Dummy time variable (see Section 5.1)
 τ_o = Bottom shear stress
 $\phi(\zeta)$ = Normalized vertical sediment distribution
 $\omega = \frac{2\pi}{T}$

Note: A prime is used to denote non-dimensional parameters, except for T' (see Section 5.1)

CHAPTER 1

INTRODUCTION

Suspended sediments of inorganic and organic origin exist in most coastal waters in varying small concentrations. Their presence arises either from natural sources or increasingly from man's activities near and off the shores. Natural erosion processes take place inland and produce suspended sediment which eventually reach the estuaries and the sea. Man has contributed to this natural supply by construction, waste disposal, agricultural and irrigation practices, and in more recent years provides additional amounts of sediments by extension of his activities to the shorelines and coastal waters.

The amount of sediment naturally present in the coastal environment must be considered a part of this environment, and all biological activity has in time come to quasi-equilibrium with this as with all other factors present. A drastic change in sediment concentration could hinder some natural processes possibly causing severe damage to many forms of life.

More specifically, suspended solid particles contribute to the turbidity of the waters and hence affect biological processes through the extinction of light. Thus, increased concentrations could impair the growth of many organisms locally as well as some distance away from the disturbance created by man. In addition, these particles, wherever they are deposited, could directly affect plant and animal life on the sea bed.

A growing concern has therefore arisen with regard to this type of pollution and the prediction of the movement and dispersion of the fine sediments introduced into a coastal area by dredging or dumping has become a most important problem. In order to make such a prediction, it is first necessary that the hydrodynamic characteristics of the area be known. Thus the problem requires information concerning dynamic characteristics such as the magnitudes and directions of tidal and non-tidal currents, the distribution of the velocities in the vertical direction, the vertical and horizontal dispersion rates, the effects of wind and waves, and other parameters. All of these depend upon the geometry and the geographical position of the body of water under consideration, in addition to the meteorological conditions. However, the geometry is usually complex and the meteorological conditions cannot be readily forecast. Theoretical approaches to the determination of the velocity field must therefore be based on simplifying assumptions.

The limited knowledge of sediment transport behavior, coupled with the hydrodynamic complexities, makes the problem one of extreme difficulty. The sediments of interest consist typically of very fine material. For the most part they fall into the silt and clay range. In the presence of sea water, electrochemical forces become important, causing flocculation, that is, the individual grains form larger aggregates which have lower density and mostly increased settling rates.

In spite of these complications, theoretical investigations can still lead to some significant results. Even under gross assumptions,

these results provide at least qualitative information, which can form the basis for more sophisticated approaches toward a good understanding of the process.

Previous investigations of the behavior of solid suspensions have dealt for the most part with single aspects of the problem. These studies are briefly reviewed in a following section.

The present study is an attempt to solve the general problem of sediment dispersion in coastal waters by combining the results of previous analytical investigations, field measurements, and laboratory experiments. Several simplifying assumptions were made to this end and a specific three-dimensional analytical model is proposed for a description of the processes involved. Numerical models may be developed as a further step. Nevertheless, it is believed that an analytical solution, relatively simple and generally applicable, can serve as a first approximation for the prediction of sediment transport and dispersion in coastal waters.

This analytical model starts with the general three-dimensional dispersion equations to which a separation of variables technique is applied so that the vertical concentration distribution can be treated independently. A single layer shear flow is then assumed, and the equilibrium concentration profile is found for the vertical direction, as is done in open channel flow. Stokes' law for settling velocities of sediments other than clays is applied. For clays such velocities were determined in a laboratory settling tube, however, without specific examination of the flocculation process.

A velocity field is assumed consisting of the superposition of a net drift and a sinusoidal tidal velocity at any angle to the net drift. Taking into consideration the nonuniform sediment distribution over the vertical, a technique for the analysis of current data was developed to provide values of the advection and dispersion factors in the two-dimensional dispersion equation which is then solved for the quasi-steady state case. It is further shown that in addition to the concentrations of suspended sediment as a function of time and space, deposition patterns on the sea bottom can also be derived.

This work was initiated as a complementary study to the Sea Grant Project, "The Sea Environment of Massachusetts Bay and Adjacent Waters", and to the New England Offshore Mining Environmental Study (NOMES-NOAA) which involved an experimental dredging operation planned in Massachusetts Bay for the summer of 1974. While the actual dredging operation has been cancelled, base line measurements were made during the past year and provided some input for the parameters needed for the application of the analytical model to a natural coastal environment.

The relative importance of the various parameters for predictive purposes is established. Thus field measurements can be planned with better judgement as to whether certain quantities should be determined accurately or can be estimated approximately without serious effects on the ultimate dispersion patterns.

CHAPTER 2

REVIEW OF PREVIOUS RESEARCH

There have been quite a number of studies related to the subject of the present work. Most of these, however, have dealt with only one aspect of the problem.

The relative vertical distribution of suspended sediment in a turbulent stream can be stated in analytical form when a suitable velocity distribution function is introduced into the differential equation for the equilibrium between turbulent upward transport of sediment and downward settling due to gravity. The latter relation was first established by Schmidt (1925) to describe the distribution of dust particles in the air. In the 1930's, Ippen (16) and Rouse (26) introduced the velocity distribution functions by Krey and Von Karman, respectively, with identical results. A linear shear distribution for a steady, two-dimensional flow was also assumed. The well-known solution is:

$$\frac{c}{c_a} = \left[\frac{h-z}{h-a} \frac{a}{z} \right]^Z \quad (2-1)$$

where

$$Z = \frac{w_s}{k\beta u_*}$$

c_a = the reference concentration at elevation a

h = the total depth

- w_s = the settling velocity of the particles
 k = the Von Karman constant
 $\beta = \epsilon_z / \epsilon_m$, the ratio of the sediment mass exchange coefficient
to the momentum transfer coefficient
 $u_* = \sqrt{\frac{\tau_o}{\rho}}$, the shear velocity
 τ_o = the bottom shear stress
 ρ = fluid density

Dobbins (6) investigated the problem of vertical sediment distribution in the transient state, and by a separation of variables technique he obtained a solution as a series expression. He also conducted experiments to verify his results.

Since that time, the parameters appearing in the exponent, Z , of Equation (2-1) have become the subject of research. The Von Karman constant was found to depend upon the near-bed concentration, while $k = 0.4$ applies strictly only to clear water. Furthermore, the velocity distribution changes due to the presence of suspended sediments, as Ippen pointed out (17). These changes, however, are significant only in the case of high sediment concentrations, and therefore are not considered important to the present work.

Another subject of debate was the coefficient β , which has been found to take on values both higher and lower than unity (18). Nevertheless, for fine sediments most investigators agree on a value of β close to 1.

The greatest difficulties arise in estimates of the proper values for the settling velocities of the suspended particles. Stoke's law is adequate for very fine sands, however it is not readily applied to clay particles because the settling rates of clays are altered by flocculation. In this process large groups of particles with high settling rates are formed from collision of smaller ones. Flocculation takes place to a high degree in the sea environment. Partheniades (24,25) and Krone (7,20) have done extensive work in the field of deposition of fine clays in estuaries and generally in salt water. While the mechanism of collision is well understood, the rates of sedimentation are, in general, far from being quantitatively determined. Because of the need for some form of quantitative prediction of settling rates in the present study, it was decided that some laboratory experiments should be performed. Sections 4-4 and 4-5 deal with this problem of flocculation in more detail.

Recently, Jobson and Sayre, in a series of papers have approached the problem of dispersion in a uniform open channel flow with turbulent shear, through a two-dimensional model, i.e. not considering lateral variations of velocity

$$\frac{\partial c}{\partial t} + u(z) \frac{\partial c}{\partial x} = \frac{\partial}{\partial z} \left(\epsilon_z \frac{\partial c}{\partial z} \right) + w_s \frac{\partial c}{\partial z} + \epsilon_x \frac{\partial^2 c}{\partial x^2} \quad (2-2)$$

where ϵ_z = the turbulent diffusion coefficient in the vertical direction

ϵ_x = the turbulent diffusion coefficient in the longitudinal direction which is considered constant

$u(z)$ = the longitudinal velocity at depth z

w_s = the fall velocity of the particles

Sayre (27) worked on the transient distribution of suspended solids in the silt range. He used the method of moments to formulate a finite difference scheme, which provides values for the moments of the distribution of the suspension. He elaborated on the bottom boundary condition, introducing a bed absorbency factor and an entrainment factor. He also investigated their effect upon the dispersion process. Jobson and Sayre (18,19) incorporated these two factors into one coefficient, called A , which effectively represents the overall probability that a particle settling to the bed is deposited there. Its importance was examined, but its value was not determined for any particular sediment. The two-dimensional equation was simplified for the steady state by omitting the term $\frac{\partial c}{\partial t}$, and assuming $\epsilon_x \frac{\partial^2 c}{\partial x^2}$ as negligible. The resulting numerical solution was compared to experimental results. They stated in their conclusions that the fall velocity is the primary factor for controlling the rate of descent of the sediment matter; the effect of turbulence on the fall velocity was negligible compared to the effects of grouping due to the injection method. The accuracy of the vertical diffusivity (ϵ_z) distribution was found not to be particularly important for the determination of the vertical concentration profiles.

Other researchers, working mainly on the dispersion of pollutants, tried to estimate the longitudinal dispersion coefficient E_L , appearing

in the general one-dimensional dispersion equation as stated by Harleman (12):

$$\frac{1}{A} \frac{\partial(A\bar{c})}{\partial t} + \frac{1}{A} \frac{\partial}{\partial x} (AU\bar{c}) = \frac{1}{A} \frac{\partial}{\partial x} (AE_L \frac{\partial \bar{c}}{\partial x}) + \frac{r_i}{\rho} + \frac{r_e}{\rho} \quad (2-3)$$

where A = the (variable) cross-sectional area of the channel
 U, \bar{c} = the cross-sectional averages of velocity and concentration, respectively

$$\frac{r_i}{\rho}, \frac{r_e}{\rho} = \text{source and sink terms}$$

E_L is the sum of the longitudinal diffusivity and a term accounting for the velocity variations over the cross section:

$$E_L = \epsilon_x + \frac{\frac{1}{A} \int_A u''c'' dA}{-\frac{\partial \bar{c}}{\partial x}} \quad (2-4)$$

where u'', c'' are the spatial deviations of the velocity and concentration from their mean values, U and \bar{c} . The second term is normally much greater than the first.

G.I. Taylor first developed in 1954 a theoretical formula for determining E_L in a circular pipe, assuming a logarithmic velocity distribution. His formula was

$$E_L = 10.1 r_o u_* \quad (2-5)$$

where r_o = the radius of the pipe.

Elder in 1959 (8) carried out a similar computation for steady, uniform, two-dimensional (i.e. infinitely wide) open channel flow with a logarithmic velocity distribution and found

$$E_L = 5.9 hu_* \quad (2-6)$$

where h = the depth of the channel.

Both Taylor and Elder verified their results by tracer experiments. Elder, in addition, pointed out that his formula is valid only for suspensions of uniform vertical distribution and that a similar analysis could be done for particles having a non-uniform distribution, by considering the deviations of the local velocity from the mean-weighted velocity, rather than from the average velocity. The mean-weighted velocity is:

$$U_s = \int_0^1 P(\zeta)u d\zeta \quad (2-7)$$

where $P(\zeta)$ = the probability density function of the position of the particles, analogous to their vertical distribution.

u = the local velocity

ζ = non-dimensional depth z/h

Later on, Fischer (9) suggested that in a natural river lateral variations of velocity are more significant than vertical ones. His formula for finding the longitudinal dispersion based on the lateral depth-averaged velocity distribution gives values of at least an order

of magnitude higher than Taylor's values. Fischer also tried to estimate the "initial time", T_I , after which the dispersion resulting from an instantaneous injection is adequately described by models of the form of Equation (2-3). He defined a time scale for cross-sectional mixing, $T' = \frac{\ell^2}{\epsilon}$, where ℓ is the distance over which diffusion takes place (e.g. the distance from the point of maximum velocity in the cross section to the channel boundary) and ϵ the diffusion coefficient in the corresponding direction. He concluded that for a pollutant initially uniformly distributed over the cross section, $T_I \cong 0.4T'$.

These studies increased the understanding of the dispersion process in natural streams, but the extension of their conclusions to estuaries, where the flow includes a periodic component, and, moreover, to coastal waters is not straightforward.

For estuaries, Harleman (12) proposed that Taylor's basic equation could be used, modified so as to include the hydraulic radius instead of the pipe radius and also have an increased coefficient (by a factor of 2) to account for natural non-uniformities. He suggested using the average value of the absolute magnitude of the velocity over the tidal cycle. More detailed approaches to the problem of sinusoidal tidal velocities were made by Holley and Harleman (15) and Holley, Harleman, and Fischer (14). In the former it was found that the fluctuations of the dispersion coefficient due to the tide become insignificant after 1 to 2 tidal cycles following injection. In the latter it was suggested that two dispersion coefficients could be computed, one from the vertical and one from the lateral velocity variation and the larger

should be used in the dispersion equation. It was found that the "initial time" was approximately $T_I = 0.2T'$, that is, about half its value for steady flow. Finally, it was indicated that an order of magnitude accuracy in the value of the dispersion coefficient was adequate for modelling continuous injections. This conclusion is very important for the present study, in view of the difficulty involved in the determination of this coefficient.

Another approach to the dispersion in periodic flow was made by Okubo (23), who assumed a linear oscillating velocity profile and worked with the method of moments to find the variance σ_x^2 of the longitudinal distribution. From this the dispersion coefficient could be defined as

$$E_x = \frac{\sigma_x^2}{2t} \quad (2-8)$$

In periodic flow the coefficient has only half its value for a steady flow of the same velocity.

Okubo also presented an excellent review of previous work relative to the horizontal diffusion coefficient in the ocean. He collected information from numerous experiments and correlated the diffusion coefficient to a characteristic length scale (22). The purely diffusive process, however, does not contribute significantly to the overall dispersion of sediments and therefore is not of great significance to the present study.

Lately, three-dimensional models for dispersion problems began to appear. Wnek and Fochtman (33) combined some of the previous ideas

to develop a mathematical model for dispersion of pollutants in near-shore waters; assuming constant dispersion coefficients in all three directions they found an analytical solution in terms of error functions for the case of infinitely distant boundaries, which they adjusted for a finite depth by the method of images. However, they considered only neutrally buoyant particles. Also, they did not include tidal currents in the model.

Tetra Tech published a report (31) on the dispersion of radioactive debris due to an underwater explosion; this was a detailed study in which a three-layer model was developed to account for the thermocline and the transfer between layers was considered. The vertical profiles of the ocean currents were examined and a vertical density gradient was taken into account. The solution of the model was performed numerically by the method of moments and numerous computer plots of the concentration and other parameters vs. time and space were presented in the report. In this study, the particles were also assumed to be neutrally buoyant. Furthermore, the effect of the bottom was considered negligible, since the model dealt with deep oceans rather than coastal areas.

In addition to mathematical models, major field studies were also carried out in some areas, specifically for estimating the hydrodynamic characteristics of relevance to dispersion of suspended particles. For example, current meter and dye studies were made in the Gulf of Maine (1). The dispersion coefficient was found to be larger in the direction of the stronger current, as expected, but the natural variations of the parameters were too large to establish a reliable

correlation between dispersion and current magnitudes.

Finally, under the NOMES project itself, a discharge of glass beads simulating the sediment entrainment due to offshore mining was performed in June 1973 (21,13). At that time Hess had developed a preliminary model for predicting the dispersion of suspended matter (21). The model was intended to give only rough estimates and thus some factors such as the tide and the vertical diffusion were not considered. He used the same dispersion coefficient for all directions as obtained from a surface dye study combined with aerial photographs taken in the summer of 1972.

CHAPTER 3

THE MATHEMATICAL MODEL

3.1 Basic Assumptions

The analytical solution required several assumptions concerning the geometry of the water body, the velocity field, and the characteristics of the sediments.

The sediments are assumed to be introduced continuously into the water body along a uniform vertical line source, at a constant rate. The sediment is assumed to consist of a number of grain size groups, each having a certain settling velocity, w_s . These settling velocities are considered to be constant over the depth. Flocculation of particles in the clay range is taken into consideration as discussed in Sections 4.4 and 4.5.

The location of the line source is assumed to be far enough from the shore so that problems due to the land-sea boundaries do not arise. Amongst these, for example, is the action of breaking waves. In deeper water the effect of waves is negligible and need not be considered. Wave action may have some influence on sediment suspension, but it affects it only indirectly by increasing vertical diffusion.

The depth of the body of water is assumed to be constant. If the resulting movement of sediments does not extend to areas with significantly different depth, this assumption is justified in view of the great simplification involved.

In the ideal case of a straight shoreline, the velocity field near the shore would normally consist of a longshore current and some tidal component normal to the coast. However, since the area of interest is a considerable distance offshore, this is not necessarily true. Therefore, for purposes of generality, the tidal and net drift directions are not assumed as normal to each other. These directions are not easily determined in any particular coastal region. The difficulties increase as the geometry of the area becomes more complicated and field measurements are necessary for the determination of the prevailing current directions and magnitudes.

The coordinate system is set up with the origin on the bottom at the position of the vertical line source, the x-axis parallel to the net drift, the y-axis normal to the drift, and the z-axis vertical upwards. The flow field is modeled as a one layer system, that is, no thermocline is considered.

The currents are assumed as functions of depth, z , only, and invariable in the horizontal directions. The tidal velocities are, of course, also functions of time. Thus, the flow field may be represented as follows:

$$\text{x-axis: } u(z,t) = u_T(z) \sin \omega t + u_f(z) \quad (3-1.a)$$

$$\text{y-axis: } v(z,t) = v_T(z) \sin \omega t \quad (3-1.b)$$

$$\text{z-axis } w = 0 \quad (3-1.c)$$

where

u_f = net drift velocity

u_T, v_T = the components of the maximum tidal velocity,
assumed sinusoidal

Since many of the assumptions would not apply near the shore, a detailed shoreline configuration is not essential to the model. For simplicity, it may be represented by a straight line or a set of straight lines.

3.2 Structure of the Model

Under the above assumptions, the mass balance equation for suspended matter is:

$$\frac{\partial c}{\partial t} + u \frac{\partial c}{\partial x} + v \frac{\partial c}{\partial y} - w_s \frac{\partial c}{\partial z} = \frac{\partial}{\partial x} (\epsilon_x \frac{\partial c}{\partial x}) + \frac{\partial}{\partial y} (\epsilon_y \frac{\partial c}{\partial y}) + \frac{\partial}{\partial z} (\epsilon_z \frac{\partial c}{\partial z}) \quad (3-2)$$

where w_s is the particle settling velocity and $\epsilon_x, \epsilon_y, \epsilon_z$ are the turbulent or eddy diffusivities in the three corresponding directions. The two horizontal diffusivities are normally independent of x and y and equal. Therefore, Equation (3-2) can be written as:

$$\frac{\partial c}{\partial t} + u \frac{\partial c}{\partial x} + v \frac{\partial c}{\partial y} - w_s \frac{\partial c}{\partial z} = \epsilon_x \frac{\partial^2 c}{\partial y^2} + \epsilon_y \frac{\partial^2 c}{\partial x^2} + \frac{\partial}{\partial z} (\epsilon_z \frac{\partial c}{\partial z}) \quad (3-3)$$

The depth, h , in coastal areas is, in general, much smaller than the horizontal dimensions. Therefore, vertical equilibrium is achieved after a relatively short time. In general, this time depends on the depth and the vertical diffusivity, ϵ_z , provided that the particles are small. Using the definition of "time scale" for diffusion T' (g,14), it is found to be h^2/ϵ_z . This is believed to be an upper bound for the time to equilibrium, since the settling velocity acts in addition to the vertical diffusivity. It should be noted that the diffusion-type modeling of the process does not hold for short times after the beginning of the injection, as already mentioned in Chapter 2. Also, the model is not expected to be valid in the immediate vicinity of the sediment source, because the time needed for vertical equilibrium implies some excursion of the sediment away from the source, before the model is reliable.

Once vertical equilibrium is established the shape of the vertical profile does not depend upon the magnitude of concentration over some range. This assumption is basic to the solution of the model, for it permits independent treatment of the vertical and horizontal distributions. In fact, the concentration, c , can be represented as the product of a depth-averaged function, \bar{c} , and a normalized function of depth, ϕ :

$$c(x,y,z,t) = \bar{c}(x,y,t)\phi(\zeta), \quad \zeta = z/h \quad (3-4)$$

where

$$\int_0^1 \phi(\zeta) d\zeta = 1 \quad (3-4a)$$

The parameters u , v , c can be written

$$\begin{aligned} u &= U + u'' \\ v &= V + v'' \\ c &= \bar{c} + c'' \end{aligned} \quad (3-5)$$

where U , V , \bar{c} are the depth-averaged values of the velocities and concentration, and u'' , v'' , c'' are the spatial deviations about these average values. Thus, Equation (3.3) becomes

$$\begin{aligned} \frac{\partial c}{\partial t} + (U + u'') \frac{\partial(\bar{c} + c'')}{\partial x} + (V + v'') \frac{\partial(\bar{c} + c'')}{\partial y} - w_s \frac{\partial c}{\partial z} \\ = \epsilon_x \frac{\partial^2 c}{\partial x^2} + \epsilon_y \frac{\partial^2 c}{\partial y^2} + \frac{\partial}{\partial z} (\epsilon_z \frac{\partial c}{\partial z}) \end{aligned} \quad (3-6)$$

Averaging over the depth and taking into account

- i) the Leibnitz Rule for differentiation of integrals
- ii) the fact that $\int_0^h u'' dz = 0$, $\int_0^h v'' dz = 0$, $\int_0^h c'' dz = 0$
- iii) simplifications such as $\frac{\partial}{\partial x} c'' = \frac{\partial}{\partial y} c'' = 0$

the equation takes the form

$$\begin{aligned} \frac{\partial \bar{c}}{\partial t} + U \frac{\partial \bar{c}}{\partial x} + V \frac{\partial \bar{c}}{\partial y} - \frac{w_s \bar{c}}{h} [\phi(1) - \phi(0)] \\ = E_x \frac{\partial^2 \bar{c}}{\partial x^2} + E_y \frac{\partial^2 \bar{c}}{\partial y^2} + \frac{\bar{c}}{h^2} [\epsilon_\zeta \frac{\partial \phi}{\partial \zeta} \Big|_{\zeta=1} - (\epsilon_\zeta \frac{\partial \phi}{\partial \zeta}) \Big|_{\zeta=0}] \end{aligned} \quad (3-7)$$

where

$$E_x = \epsilon_x + \frac{\int_0^h u'' c'' dz}{-h \frac{\partial \bar{c}}{\partial x}}, \quad E_y = \epsilon_y + \frac{\int_0^h u'' c'' dz}{-h \frac{\partial \bar{c}}{\partial y}} \quad (3-7a,b)$$

The coefficients E_x and E_y account for both the turbulent diffusion and the dispersion due to the non-uniform velocity distribution. They are referred to simply as the dispersion coefficients. In the case of heavy particles, which have more variable concentrations over the depth, the mean transport rates should be used (Elder (8)) rather than the mean velocities. That is,

$$U_s = \frac{\int_0^h u c dz}{\int_0^h c dz} = \frac{1}{h} \int_0^h u \frac{c}{\bar{c}} dz = \int_0^1 u \phi d\zeta \quad (3-8a)$$

and similarly $V_s = \int_0^1 v \phi d\zeta \quad (3-8b)$

These weighted velocities, U_s and V_s , describe the advective motion of the centroid of the dispersing suspended matter. They are the product of the corresponding mean water velocities over the depth and the coefficient a , as defined by Ippen (17). It is evident that

the physical meaning of the dispersion coefficients given by Equations (3.7a,b) is modified accordingly. Their second term should account for the velocity deviations about the weighted-mean values, as defined in Equations (3.8a,b).

Equation (3.7) can be further written

$$\frac{\partial \bar{c}}{\partial t} + U_s \frac{\partial \bar{c}}{\partial x} + V_s \frac{\partial \bar{c}}{\partial y} = E_x \frac{\partial^2 \bar{c}}{\partial x^2} + E_y \frac{\partial^2 \bar{c}}{\partial y^2} - \alpha \bar{c} \quad (3-9)$$

where

$$\alpha = \frac{w_s}{h} [\phi(0) - \phi(1)] + \frac{1}{h^2} \left[\left(\epsilon_\zeta \frac{\partial \phi}{\partial \zeta} \right)_{\zeta=0} - \left(\epsilon_\zeta \frac{\partial \phi}{\partial \zeta} \right)_{\zeta=1} \right] \quad (3.10a)$$

or

$$\alpha = \left[\frac{w_s \phi(0)}{h} + \frac{1}{h^2} \left(\epsilon_\zeta \frac{\partial \phi}{\partial \zeta} \right)_{\zeta=0} \right] - \left[\frac{w_s \phi(1)}{h} + \frac{1}{h^2} \left(\epsilon_\zeta \frac{\partial \phi}{\partial \zeta} \right)_{\zeta=1} \right] \quad (3.10b)$$

Equation (3.9) has the familiar form of a two-dimensional dispersion equation, with α representing the decay constant. The meaning of α can also be understood in view of Equation (3.10b). The first term represents the rate of loss of material to the bottom, while the second term expresses the gain of material through the surface. The latter may be assumed zero. These considerations will be discussed in Section 4.2.

The vertical distribution, represented by the normalized function $\phi(\zeta)$, plays a key role in the determination of the horizontal distribution. It not only readily defines the decay rate α (Equation 3.9, 3.10) but also affects the advective terms (3.8a and b) and the dispersion coefficients.

CHAPTER 4

THE VERTICAL CONCENTRATION DISTRIBUTION

4.1 The Normalized Equilibrium Distribution

Because of the assumption that the shape of the vertical profile does not depend upon the horizontal variations, it is possible to solve for the vertical distribution first. In fact, this order is essential, since important parameters for the solution of the horizontal distribution require knowledge of the normalized function $\phi(\zeta)$. In addition, the main objective of this work is to obtain the quasi-steady state solution of the entire problem. The distribution over the vertical dimension will be the first to come to equilibrium because of the relatively small value of h^2/ϵ_z . Thus, total equilibrium is obtained when the horizontal (depth-averaged) concentration distribution reaches steady state, provided that the time needed for this is sufficiently larger than h^2/ϵ_z .

Because of the relatively short duration of the transition period, only the equilibrium state of the vertical distribution will be considered here. The vertical profile of suspended sediments over the depth, under equilibrium conditions, is described by the Schmidt equation:

$$\epsilon_z \frac{\partial c}{\partial z} + w_s c = 0 \quad (4-1)$$

where c = the concentration of suspended matter at depth z
 w_s = the settling velocity of the grain size considered
 ϵ_z = the vertical mass diffusivity for sediment

This equation expresses a balance between the tendency of the particles to settle ($w_s c$) and the upward flux of sediments due to diffusion ($\epsilon_z \frac{\partial c}{\partial z}$). In order to solve for c it is necessary to provide expressions for w_s and ϵ_z . The latter is a function of z , whereas w_s can be considered constant.

The sediment diffusivity ϵ_z is related to the turbulent momentum transfer coefficient ϵ_m by the relation

$$\epsilon_z = \beta \epsilon_m \quad (4-2)$$

where β is close to unity for the very small particles with which the present work is concerned. The value of ϵ_m is obtained from the velocity profile. In the case of a logarithmic velocity distribution and of the related linear shear distribution in a uniform open channel flows, the distribution of ϵ_m over the depth is parabolic. The solution to the Schmidt equation under the above assumptions is

$$c = c_a \left[\frac{h/z-1}{h/a-1} \right]^Z \quad (4-3)$$

$$\text{where } z = \frac{w_s}{\beta k u_*} = 2.5 \frac{w_s}{u_*} \quad (\text{for } \beta = 1, k = 0.4) \quad (4-4)$$

In Equation (4-3) a is a reference depth at which the concentration c_a is supposedly known. The shear velocity, u_* , is related to the mean velocity and the Weisbach-Darcy friction factor, f , by the relation

$$u_* = \sqrt{\frac{f}{8}} U_m \quad (4-5)$$

The value of U_m to be used here should represent a mean current magnitude regardless of direction. For flat bed conditions the friction factor may be given an average value close to $f \approx 0.02$, thus $u_* \approx \frac{1}{20} U_m$.

The one-layer shear flow with a logarithmic velocity profile assumed here may be a poor description of coastal currents, especially during the summer season when a definite thermocline exists. Nevertheless, recalling that wave action and density differences have been neglected in the level of sophistication of this model, the shear effects become primary factors of transport and dispersion of suspended matter. Furthermore, the logarithmic velocity profile was adopted in view of the extensive work done in justifying its application to open-channel flow and the lack of adequate field information to propose a different profile. A different assumption about the vertical velocity profile would lead to a different distribution of ϵ_z . However the vertical concentration distribution is not very sensitive to changes in

ϵ_z , as Jobson has stated (19). The general procedures shown in this model can be easily made to comply with any profile that might be found to prevail in a specific coastal area. Thus, the generality of this study is not restricted by the velocity profile assumption.

It can be seen from Equation (4-3) that the shape of the vertical profile for a particular grain size (i.e. w_g) and certain flow conditions (i.e. u_*) is constant, provided that the concentrations are sufficiently low so that k can be assumed constant (The actual magnitude of the profile depends, of course, on the reference value c_a). Therefore, the assumption made in Chapter 3 regarding the similarity of the vertical profiles is justified.

Recalling that $c = \bar{c}\phi$, Equation (4-3) can be written in terms of $\phi(\zeta)$:

$$\phi(\zeta) = \phi(a/h) \left[\frac{h/z-1}{h/a-1} \right]^z \quad (4-6)$$

Before proceeding to more details, it should be mentioned that the Schmidt equation is not valid very close to the bottom. It is fairly well-established that in the lower 4-5% of the total depth, the concentration is approximately constant, not obeying Equation (4-3) although measurements in that zone are difficult both in the laboratory, because of the size of the instruments, and in the field, because of the interference of the bed-load transport.

In light of this approximation, it is convenient to chose a reference depth $a = 0.05 h$ which yields the following normalized

profile:

$$\phi(\zeta) = \phi(0.05) \left[\frac{1/\zeta - 1}{20 - 1} \right]^Z \quad \text{for } \zeta \geq 0.05 \quad (4-7)$$

$$\phi(\zeta) = \phi(0.05) \quad \text{for } \zeta \leq 0.05$$

In most cases the reference concentration c_a for Equation (4-3) has to be determined experimentally. However, due to the fact that $\phi(\zeta)$ is a normalized function, the determination of $\phi(0.05)$ can be performed analytically, by combining (4-7) with Equation (3-4a), i.e. $\int_0^1 \phi(\zeta) d\zeta = 1$. The resulting value of $\phi(0.05)$ is

$$\phi(0.05) = \frac{1}{\left[0.05 + \int_{0.05}^1 \left[\frac{1/\zeta - 1}{19} \right]^Z d\zeta \right]} \quad (4-8)$$

The integral can be evaluated numerically for several values of Z , corresponding to different settling velocities. This is done through a computer program, which then finds $\phi(0.05)$ and the whole vertical distribution according to Equation (4-7). This program is presented in Appendix B, as part of the larger program developed for the model and discussed in Chapter 7.

4.2 Boundary Conditions - Determination of the Decay Rate

In order to determine the decay factor α of the depth-averaged distribution, it can be seen from Equation (3.10) that the values of the normalized vertical distribution and its derivative must be known

at the bottom ($\zeta = 0$) and the surface ($\zeta = 1$).

From Equation (4-7) it is evident that $\phi(1) = 0$

Also $\epsilon_{\zeta} = 0$ at $\zeta = 1$

$$\text{Thus, } \alpha = \frac{w_s}{h} \phi(0) + \frac{1}{h^2} (\epsilon_{\zeta} \frac{d\phi}{d\zeta})_{\zeta=0} \quad (4-9)$$

In the general case, the bottom boundary condition may be expressed (18,19) as

$$\epsilon_z \frac{dc}{dz} + (1-A)w_s c = 0 \quad \text{at } z = 0 \quad (4-10)$$

This can be written

$$\frac{\epsilon_{\zeta}}{h} \frac{dc}{d\zeta} + (1-A)w_s c = 0 \quad \text{or}$$

$$\frac{\epsilon_{\zeta}}{h} \frac{d\phi}{d\zeta} + (1-A)w_s \phi = 0 \quad \text{at } \zeta = 0 \quad (4-11)$$

The quantity "A" represents the overall probability that a particle reaching the bottom will stay there and will not be resuspended. It refers to a time average of the percentage of particles sticking to the bottom relative to all particles that reach it. In fact, A does not distinguish between those particles that simply "bounce" off the bottom and those that remain at the bottom being replaced by other, newly scoured, particles. It is believed that A is related to the flow conditions, specifically the mean velocity and bottom shear and also to the sediment characteristics, particularly the degree of

cohesion. The lower the flow velocity or bottom shear, the higher A is expected to be, approaching unity.

For fine cohesive sediments, some quantitative relations have been derived. Partheniades (24,25) tried to determine the minimum shear stress under which all suspended matter is deposited, and the equilibrium concentrations of clays in suspension under certain flow conditions. Einstein and Krone (7) conducted experiments with "San Francisco Bay mud" and found a linear relation between the percentage deposited and the bottom shear. These results, however, were derived with specific sediments and experimental techniques and cannot be easily extended.

In general, A is a very uncertain factor to predict and accurate values have to be determined experimentally for every particular problem. For the low velocities prevailing in coastal areas, A is expected to be close to unity. As Jobson and Sayre (19,27) have reported, changes in A seem to affect the vertical profile only very close to the bottom.

Nevertheless, A is very important for the horizontal distribution. It is directly related to the decay constant α . In fact, Equation (4-11) may be written:

$$\frac{1}{h} \left(\epsilon_{\zeta} \frac{d\phi}{d\zeta} \right)_{\zeta=0} + w_s \phi(0) = A w_s \phi(0) \quad (4-11a)$$

By comparison of Equations (4-9) and (4-11a) it is evident that

$$\alpha = \frac{A w_s \phi(0)}{h} \quad (4-12)$$

It must be mentioned that the assumption of constant $\phi(\zeta)$ in the interval $0 \leq \zeta \leq 0.05$ (Section 4.1) implies $\left. \frac{d\phi}{d\zeta} \right|_{\zeta=0} = 0$, which is inconsistent with any value of A other than 1, as it can be readily seen from Equation (4-11). For $A < 1 \Rightarrow \left. \frac{d\phi}{d\zeta} \right|_{\zeta=0} < 0 \Rightarrow \phi(0) > \phi(0.05)$. It would be possible to modify this small lower portion of the vertical profile so that various values of A can be incorporated. The correction, however, would be insignificant in view of the many uncertainties involved in the near-bottom concentrations. Hence, Equations (4-7) are considered herein as giving an adequate description of the vertical profile, regardless of the value of A.

4.3 Sediment Settling Velocities

The settling velocity is the most important sediment characteristic. It affects directly the vertical distribution (Equation 4-4) and indirectly the horizontal distribution, mainly through the decay factor (Equation 4-12).

In the present work only fine particles are of interest. Their fineness is essentially associated with their ability to stay in suspension for a sufficiently long time so that they can travel a reasonable distance away from the source before being deposited. The terms "sufficiently" and "reasonable" are of course vague; it remains for the engineer to estimate appropriate values for every particular problem, based on such factors as depth, magnitude of currents, etc.

In the case of the area of interest in Massachusetts Bay, the depth is approximately 30 meters. If the particles are required to

travel for at least one hour before being deposited, the maximum settling velocity of interest is of the order of 0.8 cm/sec. Particles with such small settling velocities are considered to follow Stoke's law:

$$w_s = \frac{gd^2}{18\nu} (\gamma_s - \gamma_w) \quad (4-13)$$

where d = the diameter of the particle

g = the acceleration of gravity

ν = the kinematic viscosity of the water

γ_s = the specific weight of the sediment considered

γ_w = the specific weight of seawater

Substituting, $g = 981 \text{ cm/sec}^2$

$\gamma_s \approx 2.65$ for natural sand and silt,

$\gamma_w \approx 1.025$ for a mean temperature of 10°C and a salinity of 33 ‰

$\nu \approx 1.31 \times 10^{-2} \text{ cm}^2/\text{sec}$ (at 10°C)

the resulting settling velocity is

$$w_s = 0.68 \times 10^4 d^2 \quad (4-13a)$$

Therefore, $w_s = 0.8 \text{ cm/sec}$ corresponds to a particle size of $d = 0.0108 \text{ cm} = 108 \mu$. In the present work particles smaller than 100μ will be considered.

Stoke's law refers to spherical particles of diameter d . Particles having the same volume and weight but different shapes have significantly different settling velocities. However the settling velocity, not the actual shape and size of a particle, is the sediment characteristic most essential to this study; thus, the particles can be classified in terms of "equivalent Stoke's diameters".

Following the MIT soil classification, the sediments are divided into groups of particle sizes and characterized as "very fine sand", "silt" and "clay" as shown in Table 1. The settling velocities are computed using Equation (4.13a). The mean velocity of the group will be used as the representative value for all sediments belonging to it. The value for the clay group corresponds to $d = 1 \mu$. The distribution of each group can be examined independently if the interaction between various groups is assumed negligible (29). This is true for low concentrations.

Table 1. Separation of Fines into Groups

Group Name	Particle Size range (μ .)	Settling Velocities w_s (cm/sec)		
		lowest	highest	mean
Very fine sand	60-100	0.245	0.680	0.462
Coarse silt	20-60	2.72×10^{-2}	0.245	0.136
Medium silt	6-20	2.45×10^{-3}	2.72×10^{-2}	1.43×10^{-2}
Fine silt	2-6	2.72×10^{-4}	2.45×10^{-3}	1.36×10^{-3}
Clay	< 2		2.72×10^{-4}	0.68×10^{-4}

4.4 Flocculation Characteristics and Effects

While for the sand and silt range the above considerations are adequate for the determination of the settling rates, the phenomenon of flocculation does not allow such a simplified approach for the clay range. Flocculation is the process of formation of large aggregates of particles by the association of many smaller ones. It is due to the collision of individual particles and to the cohesive and electro-chemical nature of clay particles in saline water.

Several investigators have tried in the past to present a comprehensive description of the flocculation process. It is known that collision of particles may be caused by three different mechanisms (20):

i) Brownian motion, in which the rate of collision depends on the temperature

ii) Local shear or velocity gradients, in which the rate of collisions depends on the size of the particles and the magnitude of the gradient

iii) Differences in settling velocities of particles: Larger particles settling through a suspension of smaller particles collide with them at a rate depending on their relative velocities. Commonly, Brownian motion contributes to the initial stages of flocculation, while the internal shearing dominates the formation of larger aggregates. It is also known that limiting floc sizes are obtained for certain shearing rates. The collision rates in all mechanisms are directly proportional to the concentration of suspended matter.

Despite the good understanding of these mechanisms, there is very little information concerning the settling rates of flocs. The change of the floc size along with its density during settling and the breaking of flocs in layers of higher shear makes the problem too complicated. Furthermore, the non-uniform composition of natural clay suspensions adds to the complexity. It seems that the problem is more tractable from a "macroscopic" point of view, that is, without trying to fully understand the process, but by simply studying the effective settling velocity of the flocs. Some field and laboratory experiments have been carried out for this purpose. Krone (20) from studies in the Savannah Harbor concludes that the settling velocities of the aggregates are of the order of 1 cm/sec, varying considerably between ebb and flood. These aggregates were found to have a specific weight of about 1.1 gr/cm^3 . Because of the high settling velocity, most of the suspended matter was deposited during high or low water slack and resuspended when the tidal velocities, and therefore the shear stress, increased during flood or ebb.

4.5 Settling Tube Experiments on Clay Suspensions

4.5.1 Experimental program and procedures

In order to get an overall quantitative idea of the settling rates of clay suspensions a laboratory experiment was carried out. Specifically, the experiment was intended to provide a set of equivalent settling velocities, without dealing with the details of the flocculation process.

A plexiglass tube, 90 cm high and of 21 cm inner diameter as shown in Figure 1, was initially filled with a uniform suspension of clay in seawater and the decrease of concentration over time was monitored through the extraction of samples by means of valves placed at 15 cm intervals along the tube. The samples were analyzed with respect to their "turbidity" values, by means of a HACH 2100A turbidimeter.

Turbidity measurements were made as an expedient for determining suspended sediment concentrations as opposed to laborious filtering procedures. Field samples from the Massachusetts Bay analyzed by both turbidity and gravimetric techniques provided the opportunity to correlate turbidity with concentration of total suspended matter (both organic and inorganic). This correlation appears to be linear, as can be seen in Figure 2, at least in the range of concentrations encountered, which are generally below 10 mg/l. Since the turbidimeter operates by measuring the scattering of light due to the particles in suspension it is apparent that not only the concentration but also the composition and size distribution of these particles affect the turbidity readings. Also, the presence of plankton increases the turbidity of the water, but does not contribute much to the weight of the matter collected on the filter. Thus, the scattering of the field data is reasonable in view of the variety of locations and conditions under which the samples were taken.

In the settling tube experiment kaolinite suspensions were first used. The material used was "Peerless No. 2 kaolinite" the same as

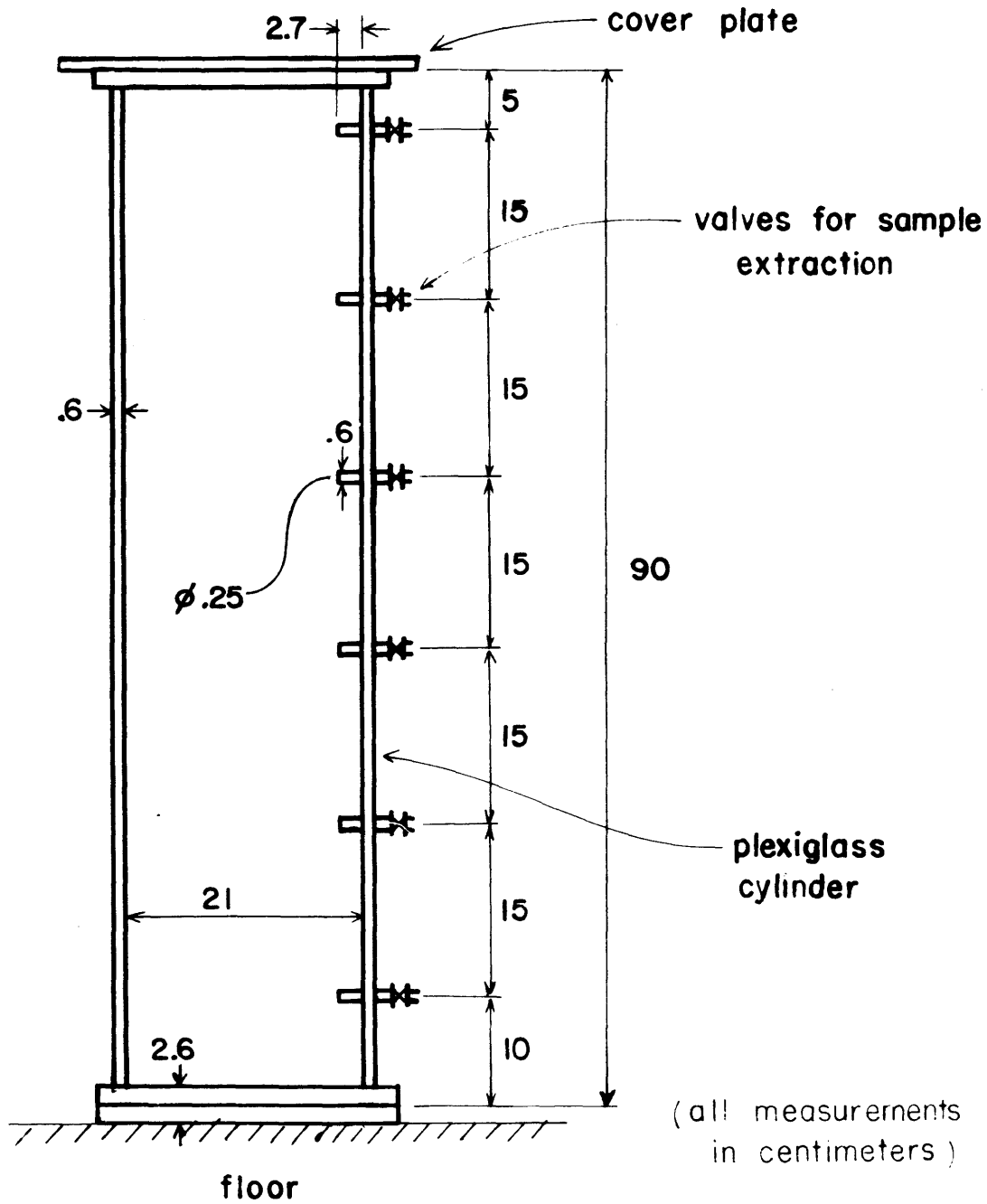


Figure 1
Sediment Settling Tube

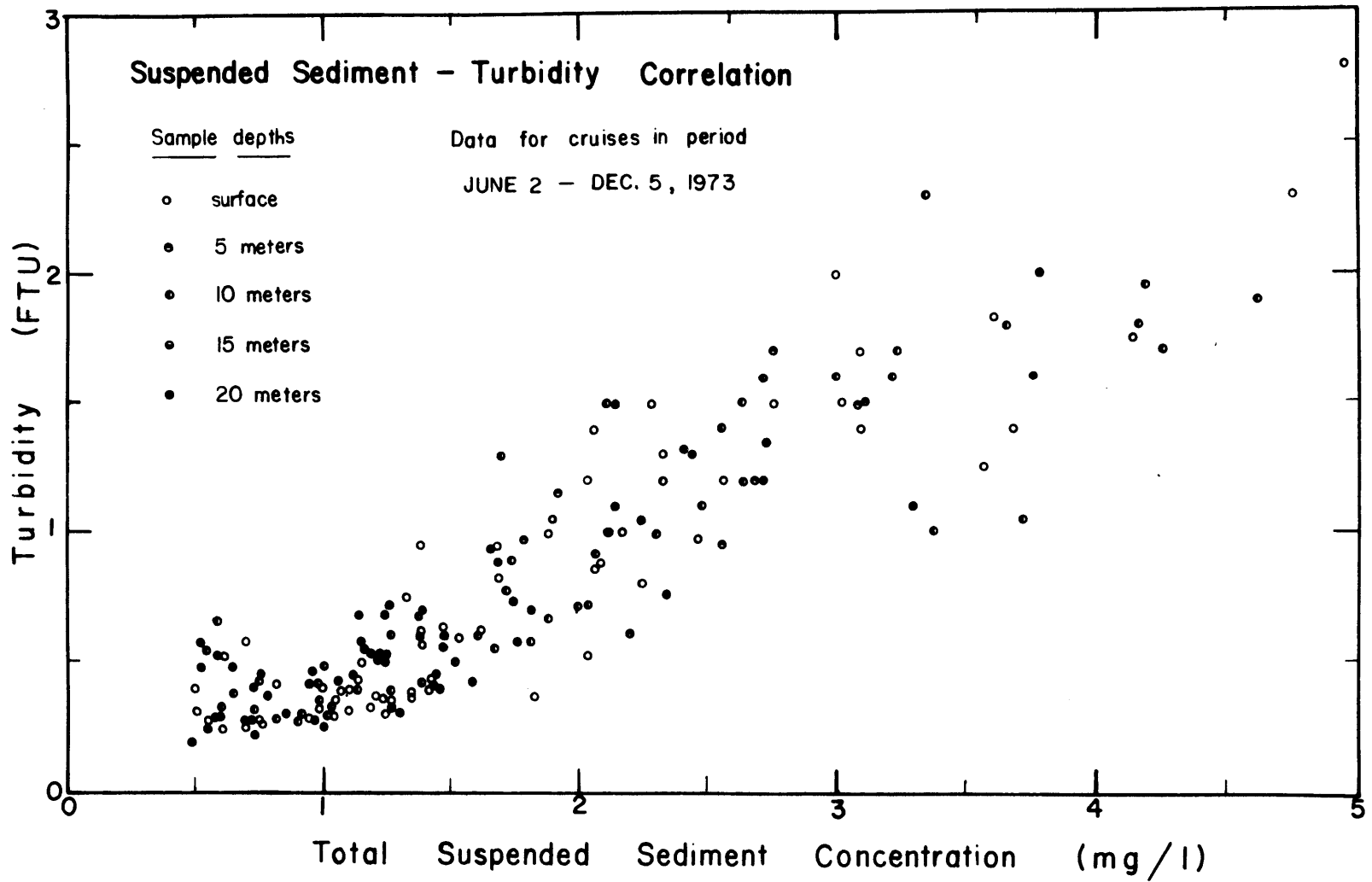


Figure 2

Correlation of Turbidity and Total Suspended Sediment Concentration from Field Data

that used by Partheniades in his experiments in a rotating channel several years ago. The experiment was repeated with illite and Boston Harbor mud. The illite was part of a sample of "Boston blue clay" being used for soil testing in the MIT Soil Mechanics Laboratory. The Boston Harbor mud was taken from the bottom of the harbor near Spectical Island. Both samples were oven-dried at 140^oF and powdered before being used in the experiment.

In each run a known weight of sediment was added to a known volume of seawater and the two vigorously mixed so as to achieve a uniform initial concentration. The initial uniformity was checked by taking samples at various depths immediately after the suspension was made. As long as their turbidity readings were approximately the same, the initial concentration was assumed uniform. These initial samples were poured back into the settling tube in order to maintain the original water elevation. A new sample was taken from the mid-depth and its turbidity was checked to see if it agreed with the average of the previous samples. It was then used for calibrating the turbidimeter for the particular suspension under consideration. The background turbidity was subtracted from all readings. The calibration, made with dilutions of this initial sample, indicated a good linear relation between turbidity and concentration in all cases. These calibration curves are presented in Figure 3. The background turbidity of the seawater used was recorded before adding the sediments; it was generally very low, about 0.2 FTU.

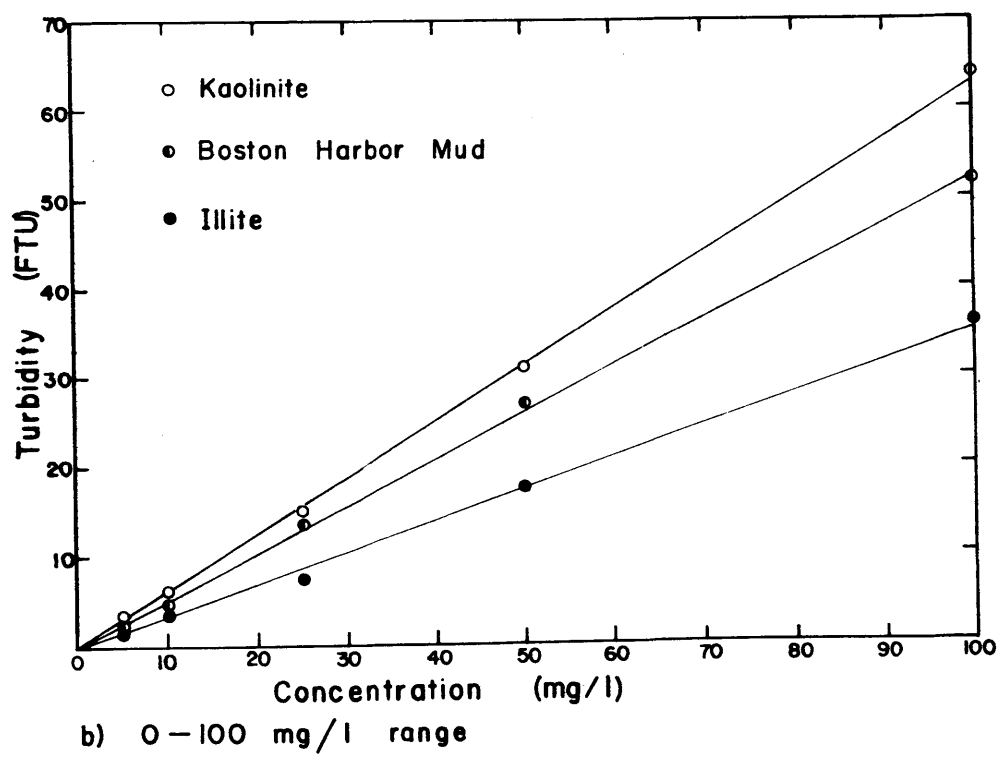
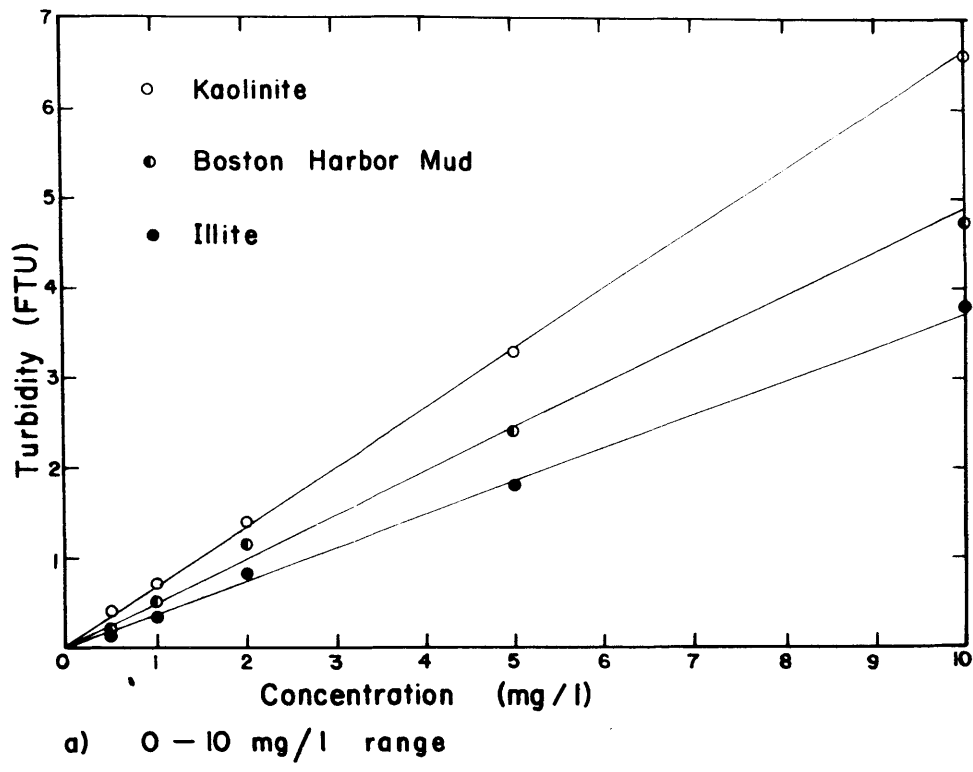
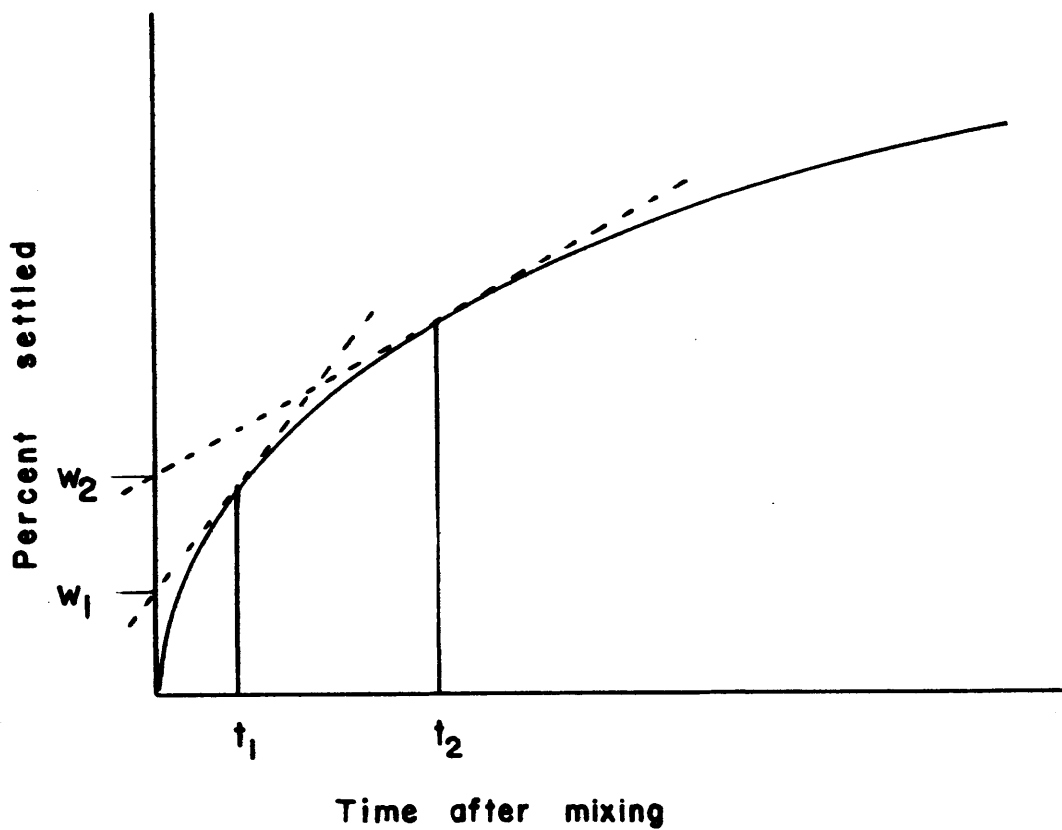


Figure 3
Turbidimeter Calibration Curves for Clay Suspensions

During each run samples were taken at certain times at various depths and their turbidity measured. The number of samples was limited to minimize the disturbance of the water column and to avoid drastic changes in the surface elevation. At first, the measurements indicated a rather rapid decrease in turbidity in all depths, with higher values always at the lower sample depths. For each set of measurements, after subtracting the background value, the average turbidity over the depth was computed. Due to the linearity of the turbidity-concentration relationship, the percent decrease in average turbidity represents the percent of the initial sediments that had settled below the bottom valve. The turbidity measurements are presented in Appendix A. Plots of percentage settled vs. time are shown in Figures 5 and 6.

The percentage of the sediment having an average settling time between t_1 and t_2 can be estimated graphically by drawing tangents to the sedimentation curve (drawn in linear scales) at t_1 and t_2 and finding the difference of the percentages w_1 and w_2 where these tangents intersect the ordinate axis (30). This technique is demonstrated in Figure 4. The corresponding settling velocity will be between H/t_1 and H/t_2 , where H is the depth of the water above the lowest valve. If the times are chosen so that they correspond to the settling velocities that separate the groups in Table 1, the respective percentages simply indicate the clay fractions (by weight) that macroscopically behave as if they belonged to one of these groups.



$w_2 - w_1 =$ percentage of sediments with settling velocities between H/t_1 and H/t_2 , where H is the total height of the settling tube.

Figure 4
Technique for Sediment Separation into Groups of Settling Velocities (30)

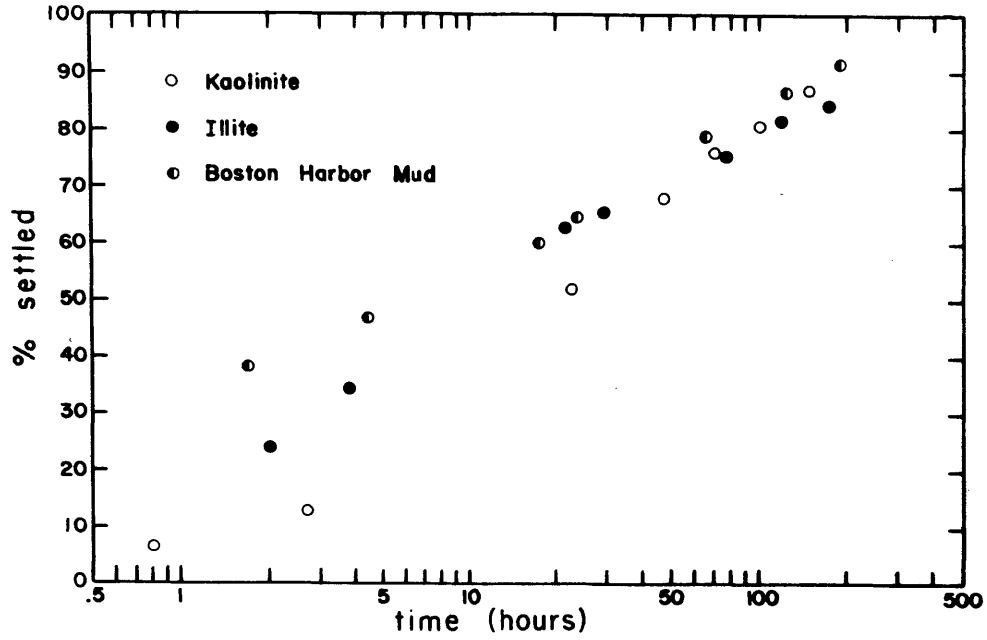


Figure 5 Settling Tube Results for the 10 mg/l Initial Concentration Runs

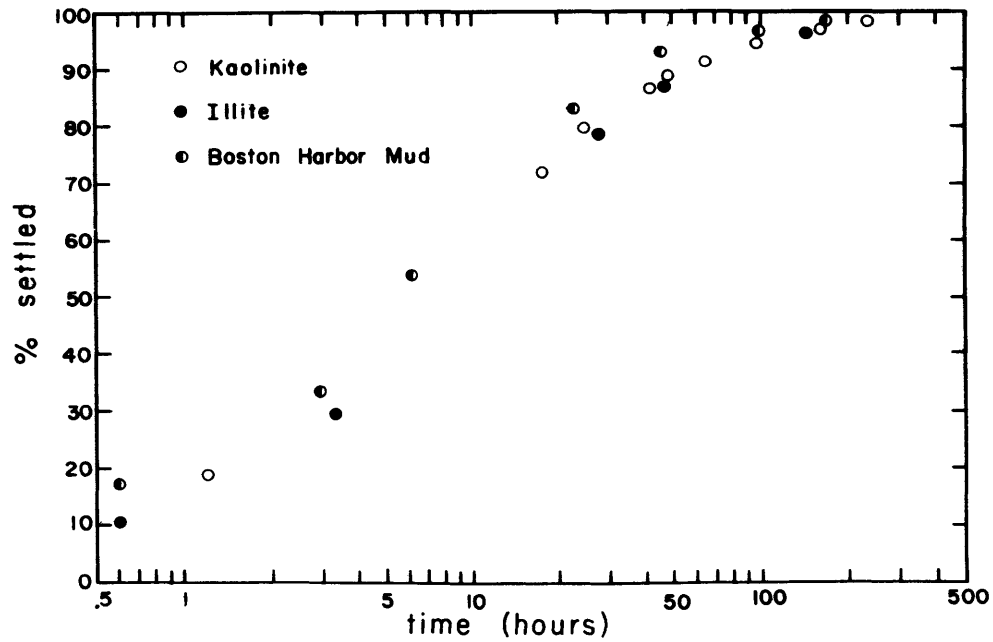


Figure 6 Settling Tube Results for the 100 mg/l Initial Concentration Runs

4.5.2 Discussion of results

The data plotted in Figures 5 and 6 illustrate a rather consistent settling behavior with respect to both the type of clay suspension used and the initial concentration of the suspension. Comparing first the three types of clay, it can be seen that the percentage of Boston Harbor mud settled out with time is higher than that of the kaolinite and of the illite in all cases. This is the result of a high initial deposition rate of the harbor mud, possibly due to the presence of non-clay particles with higher settling rates. The illite and kaolinite agree essentially for the two initial concentrations tested, except during the shorter settling times in the 10 mg/ℓ initial concentration runs.

The dependence of the settling on the initial concentration is more apparent than the dependence on clay type. Plotted on semi-logarithmic scales, the points for the runs with 10 mg/ℓ initial concentration form reasonably straight lines suggesting a relationship of the following form:

$$\% \text{ settled} = a \log(\text{time}) + b$$

where a and b are constants; a is the slope, while b is the value of percent settled at a time of one hour. Thus, for example, the following relationship follows for Boston Harbor mud:

$$\% \text{ settled} = 27 \log(\text{time}) + 30$$

As can be seen in the plot of Figure 5, this relationship does not hold

at values of time less than about 1 hour and obviously at times when the percent settled comes close to 100.

The runs with 100 mg/l initial concentration clearly show higher deposition rates. If there were no flocculation, it would be expected that the curves formed by the data points of a particular type of clay would coincide, because the settling rates and therefore the percent deposition with time would be the same regardless of concentration. However, since flocculation occurs, the percent deposition should be faster for a higher initial concentration due to the higher number of collisions.

The results of these experiments seem to be quite consistent in light of the low degree of scatter in the calibration curves (Figure 3a and Figure 3b). The fact that the lines for 10 mg/l and 100 mg/l initial concentration have almost identical slopes for each particular clay implies that turbidity measurements are appropriate in principle for determining sediment concentrations. However, the different slopes for the different clays mean that some other factors, such as particle size, affect turbidity also. This fact is important to consider in making conclusions about settling rates from the experimental data, for the grain size distribution of the material in suspension continuously changes during the run. This is because the larger particles settle first and also because flocculation forms new particles with different characteristics. This problem may control the reliability in an experiment such as the present one, for it is felt that the experimental techniques and equipment introduce relatively small error ($\pm 5\%$).

From the technique described in the previous section and illustrated in Figure 4, the results in Table 2 were obtained. These results depend, of course, upon the reliability of this technique and also upon that of the experiment.

Table 2. Distribution of Clays Tested into Groups

Material in Suspension	Initial Concentration (mg/l)	Percentage of Sample with Settling Velocity (cm/sec)		
		$w_s > 2.45 \times 10^{-3}$ (group 3)	$2.72 \times 10^{-4} < w_s < 2.45 \times 10^{-3}$ (group 4)	$w_s < 2.72 \times 10^{-4}$ (group 5)
Kaolinite	100	29%	56%	15%
Illite	100	29%	57%	14%
Boston Harbor Mud	100	41%	51%	8%
Kaolinite	10	14%	48%	38%
Illite	10	29%	40%	31%
Boston Harbor Mud	10	43%	24%	33%

In this tabular form it can again be seen that Kaolinite and Illite behave rather similarly, while Boston Harbor Mud has higher settling rates, that is, a higher percentage is settling at the rate of group 3.

CHAPTER 5

THE HORIZONTAL DISTRIBUTION OF AVERAGE CONCENTRATION

5.1 Solution of the Differential Equation

The distribution of the depth-averaged concentration $\bar{c}(x,y,t)$ is described by Equation (3-9):

$$\frac{\partial \bar{c}}{\partial t} + (U_{fs} + U_{Ts} \sin \omega t) \frac{\partial \bar{c}}{\partial x} + V_{Ts} \sin \omega t \frac{\partial \bar{c}}{\partial y} = E_x \frac{\partial^2 \bar{c}}{\partial x^2} + E_y \frac{\partial^2 \bar{c}}{\partial y^2} - \alpha \bar{c} \quad (5-1)$$

where U_{fs} , U_{Ts} , V_{Ts} represent mean-weighted values over the depth, taking into account the nonuniform sediment distribution. Following Harleman's method (12), by the change of variables:

$$\begin{aligned} \xi &= x - \int_{\tau}^t (U_{fs} + U_{Ts} \sin \omega t) dt = x - U_{fs} (t - \tau) + \frac{U_{Ts}}{\omega} (\cos \omega t - \cos \omega \tau) \\ &= x - U_{fs} (t - \tau) + \frac{U_{Ts} T}{2\pi} (\cos 2\pi \frac{t}{T} - \cos 2\pi \frac{\tau}{T}) \end{aligned} \quad (5-2a)$$

$$\eta = y - \int_{\tau}^t V_{Ts} \sin \omega t dt = y + \frac{V_{Ts} T}{2\pi} (\cos 2\pi \frac{t}{T} - \cos 2\pi \frac{\tau}{T}) \quad (5-2b)$$

$$s = \frac{\bar{c}}{c} e^{-\alpha(t-\tau)} \quad (5-2c)$$

Equation (5-1) is transformed to:

$$\frac{\partial s}{\partial t} = E_x \frac{\partial^2 s}{\partial \xi^2} + E_y \frac{\partial^2 s}{\partial \eta^2} \quad (5-3)$$

For an instantaneous injection of mass of dM at time τ , the resulting distribution of ds is

$$ds = dM \frac{\exp[-\frac{\xi^2}{4E_x(t-\tau)}]}{\sqrt{4\pi E_x(t-\tau)}} \frac{\exp[-\frac{\eta^2}{4E_y(t-\tau)}]}{\sqrt{4\pi E_y(t-\tau)}} \quad (5-4)$$

$$\text{hence, } \bar{dc} = ds e^{-\alpha(t-\tau)} \quad (5-4a)$$

or, using the original variables:

$$\bar{dc} = dM \frac{\exp[-\frac{[x - U_{fs}(t-\tau) + \frac{U_{Ts}T}{2\pi}(\cos 2\pi \frac{t}{T} - \cos 2\pi \frac{\tau}{T})]^2}{4E_x(t-\tau)}]}{4\pi(t-\tau)\sqrt{E_x E_y}} \exp[-\frac{[y + \frac{V_{Ts}T}{2\pi}(\cos 2\pi \frac{t}{T} - \cos 2\pi \frac{\tau}{T})]^2}{4E_y(t-\tau)} - \alpha(t-\tau)] \quad (5-5)$$

for a continuous injection $dM = m_1 d\tau$, and integrating over all values of τ :

$$\bar{c} = \int_0^t m_i \frac{\exp\left[-\frac{[x-U_{fs}(t-\tau) + \frac{U_{Ts}T}{2\pi}(\cos 2\pi \frac{t}{T} - \cos 2\pi \frac{\tau}{T})]^2}{4E_x(t-\tau)}\right]}{4\pi(t-\tau)\sqrt{E_x E_y}} \exp\left[-\frac{[y + \frac{V_{Ts}T}{2\pi}(\cos 2\pi \frac{t}{T} - \cos 2\pi \frac{\tau}{T})]^2}{4E_y(t-\tau)} - \alpha(t-\tau)\right] dt \quad (5-6)$$

where m_i = the mass rate of injection of suspended sediments of the particular group of interest; m_i can be written as

$$m_i = \Psi c_{oi} = \Psi \lambda_i c_o \quad (5-6a)$$

where Ψ = the volume rate of injection of the seawater-sediment mixture (volume/time)

c_{oi} = the initial concentration (by mass) of sediments of the group of interest in the mixture injected

c_o = the total initial sediment concentration (by mass) in the mixture injected

$\lambda_i = c_{oi}/c_o$, the fraction of the total sediment that belongs to the group of interest.

Equation (5-6) may be brought to non-dimensional form for purposes of generality. Choosing the tidal period T as the characteristic time and the depth h as the characteristic length scale, the non-dimensional (primed) variables are defined as follows:

$$t' = \frac{t}{T}, \quad \tau' = \frac{\tau}{T}, \quad x' = \frac{x}{h}, \quad y' = \frac{y}{h},$$

$$U'_{fs} = \frac{U_{fs}}{h/T}, \quad U'_{Ts} = \frac{U_{Ts}}{h/T}, \quad V'_{Ts} = \frac{V_{Ts}}{h/T},$$

$$E'_x = \frac{E_x}{h^2/T}, \quad E'_y = \frac{E_y}{h^2/T}, \quad \alpha' = \alpha T, \quad c' = \frac{\bar{c}}{\lambda_i c_o}$$

The non-dimensional concentration c' represents the ratio of the depth-averaged concentration \bar{c} at (x,y,t) to the initial concentration of the mixture for a particular group. The new form of Equation (5-6) is:

$$c' = \frac{WT}{h^3} \int_0^{t'} \frac{\exp\left[-\frac{[x' - U'_{fs}(t' - \tau') + \frac{U'_{Ts}}{2\pi}(\cos 2\pi t' - \cos 2\pi \tau')]^2}{4E'_x(t' - \tau')}\right]}{4\pi(t' - \tau')\sqrt{E'_x E'_y}} \exp\left[-\frac{[y' + \frac{V'_{Ts}}{2\pi}(\cos 2\pi t' - \cos 2\pi \tau')]^2}{4E'_y(t' - \tau')} - \alpha'(t' - \tau')\right] d\tau' \quad (5-7)$$

The integration cannot be carried out except by numerical techniques. A computer program to evaluate c' from Equation (5-7) was written and is presented in Appendix C.

The time until convergence to a quasi-steady state, as defined in Chapter 3, generally depends upon the values of the various parameters on the one hand, and the point (x,y) of interest on the other.

The two most important parameters are the decay rate, α , and the net drift. Higher values of α will cause the solution to converge more rapidly at all positions. The effect of the net drift, however, is highly related to the point (x,y) of interest. For points near the source its magnitude is not very important, but a point far from the source may not reach steady state for a long time if the net drift is small. This problem is discussed in Section 7.6, in relation to the runs made for the conditions found in Massachusetts Bay.

It must be noted that in the above solution the tacit assumption was made that the shore is not reached by the sediment "cloud", since no boundaries were considered. If the solution of Equation (5-7) shows that, in fact, no significant concentrations are found near the shore, then it is perfectly valid. Otherwise a correction can be made by means of a graphical application of the "method of images". In essence, the method assumes an imaginary source symmetric to the actual one with respect to the shoreline. The shoreline in this case has to be approximated by a straight line, since the correction would otherwise become too complicated. The concentrations due to the two sources are added together. This is graphically equivalent to "folding back" that part of the profile of $\bar{c}(x,y,t)$ which lies beyond the boundary. It may be recalled, however, that the model does not satisfactorily represent the conditions of the near-shore area for various other reasons (Chapter 3).

5.2 Net Drift and Tidal Velocities

With respect to circulation of coastal waters, of interest to this study are the directions and magnitudes of the tidal velocities

and any net drift. The latter is probably the most important hydrodynamic factor entering into the model, since it determines in the long run the direction and rate at which most of the sediments will move. Each area has its own characteristics in terms of geometrical configuration and prevailing meteorological conditions, both of which affect the general circulation; thus, estimates of the above parameters are usually difficult. The tidal velocity direction in an area does not vary much during the year, being approximately normal to the shoreline, while its amplitude depends primarily on tidal amplitude. By contrast, the short-term net drift is highly variable with the different seasons. The prevailing direction is usually parallel to the shoreline if wind is insignificant and the area of interest is not too far from the shore. The magnitude of the net drift, however, cannot be predicted by any simple means.

Physical as well as mathematical models are being used for studying circulation in coastal areas. It is beyond the scope of the present work to determine the velocity field in detail by using such methods.

Field measurements in the area of interest can provide valuable information about currents. There are basically two measuring techniques, current meters and drogues. Current meters give the magnitude and direction of the currents at certain points. The method is directly related to an Eulerian description of the flow field. This technique is desirable if one is interested in obtaining the flow history at specific points, for example, at the entrance to a harbor.

A current meter can be placed at any depth and is generally used for long-term measurements.

Drogues give the pathlines of water particles. This technique yields basically a Lagrangian representation of the flow field. A drogue is a fin or vane of high fluid resistance, suspended at a certain depth in the water from a flotation device. It has the measuring flexibility of the current meter in that it operates at different depths, but obviously the bottom must not be reached at any point along the drogue path. For this reason, drogues cannot be used to measure flows very close to the bottom. Because of the nature of the drogue method, long-term records are not feasible; the drogue must be followed by a vessel which monitors its position over time. Also, there is no way of keeping the drogue in a particular area of interest.

In spite of these difficulties, drogue measurements give a very valuable picture of net flows and circulations in large bodies of water. In particular with respect to the present study, the drogue movement simulates the path of a sediment particle in its lateral directions as long as there are no significant vertical currents. The spreading of a set of drogues can also provide estimates for the dispersion characteristics of the area. In fact, the results of drogue studies carried out over the last year in relation to the NOMES project were used to provide information on currents in the Massachusetts Bay, necessary for the application of the model in this area (Chapter 7).

Specifically, since the number of drogues in each study is small, (three or four), the movement of a vertical water column was examined

under the following simplifying assumptions:

1) Between drogues at different depths, the velocity changes approximately linearly.

2) Between the deepest drogue and the bottom the velocity follows a portion of a logarithmic curve.

3) Above the shallowest drogue the velocity is constant.

It can be argued that these assumptions do not agree with the logarithmic velocity profile used in Section 4.1 for the determination of the vertical diffusion coefficient ε_z and consequently with the normalized vertical distribution $\phi(\zeta)$. In fact, if the velocity profile were really logarithmic, its approximation by linear profiles over the various portions above the deepest drogue would be quite acceptable. However, the very limited field data on the vertical profile do not lead to any conclusion about its true shape. Under these circumstances, it is felt that the interpolation technique described above yields a reasonable description of the velocity profile.

The objective of the assumptions stated above is to convert the velocity profile to an equivalent step-function profile, with the values of the steps corresponding to the drogue velocities; thus, it is possible to associate with each drogue a fraction of the water column that moves on the average with the drogue velocity. Consequently, it is easy to define the mean movement of the water column at any time interval as the weighted average of the movements of the drogues at this interval, where the weights are the fractions of the column associated with every drogue (Figure 7).

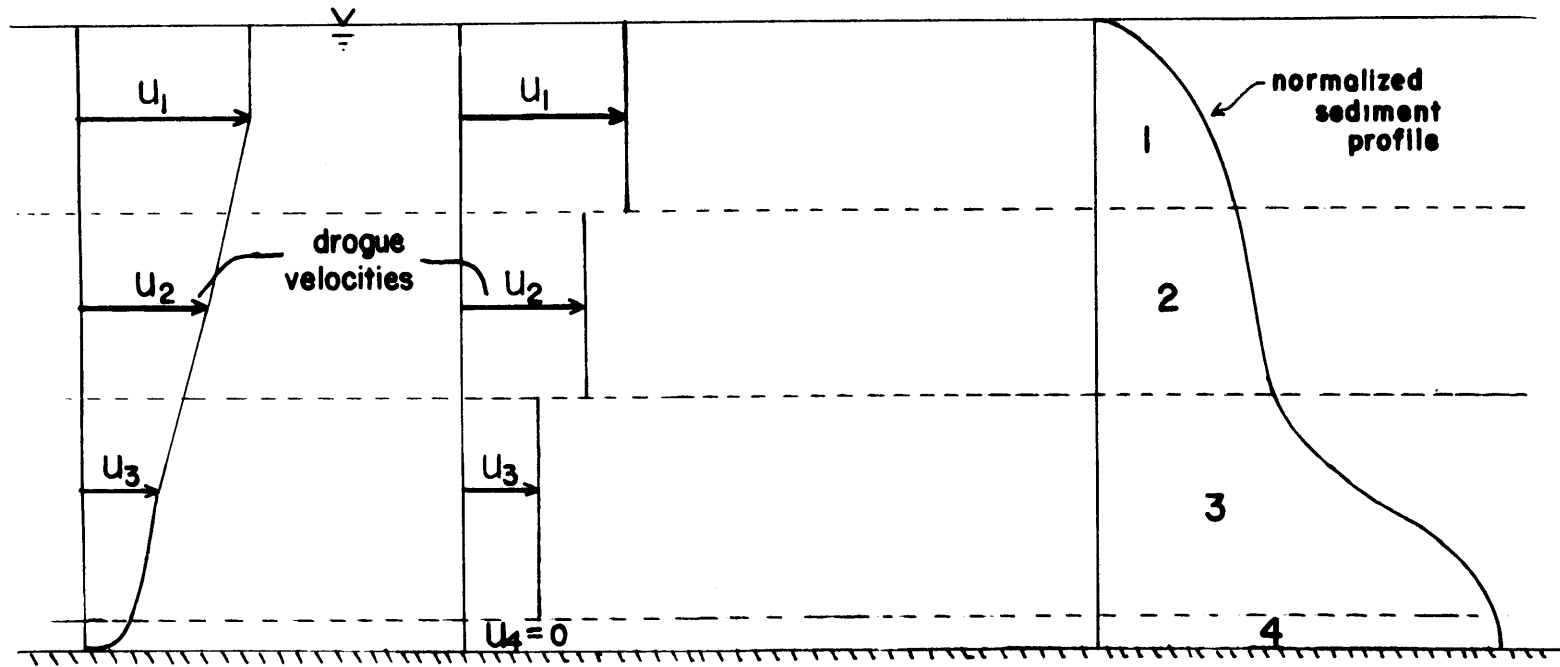


Figure 7

Schematic Representation of the Vertical Velocity Profile and the Weights Associated with the Drogues

The mean net drift over the depth can then be computed by the mean net movement of the water column over a complete tidal cycle. Any deviations from this net movement during the tidal cycle are then attributed to a sinusoidal tidal velocity. The assumption of a sinusoidal tide might be questioned. In many coastal areas the tide is not even symmetrical. Due to river discharge the ebb velocities are often higher than the flood velocities. However, most of the asymmetry of the tide can be incorporated into the net drift term. Thus, an "equivalent" sinusoidal velocity that, combined with the net drift, would move the drogues in approximately the same way as the natural currents can be evaluated. Since the interest of this study lies in the net effects of the current system in a relatively long time scale and not much in its detailed structure, the above approximation is acceptable.

Ultimately, the major interest of the study does not lie in the water velocities but, as indicated in Chapter 3, in the weighted velocities, taking into account the distribution of suspended sediments over the vertical. These velocities enter into the model as the advective terms of the dispersion Equation (5-1) for any particular group of sediments. Their estimate is quite straightforward based on the previous considerations. The drogue records can be used in the same way, the only difference being in the relative weights that each drogue is associated with. They will not depend only on the fractions of the water column as before, but rather on the areas of the normalized vertical concentration profile lying in these fractions (Figure 7).

Clearly, the weight on a drogue will be different for different sediment groups.

All these computations can be organized and performed through a computer program, which will be discussed in more detail in Chapter 7. This program is extended to provide estimates of the dispersion coefficient as will be seen in Section 5.3.

5.3 Dispersion Coefficients

Dispersion is the most difficult parameter to estimate. Values reported in the literature, mainly from one-dimensional studies, differ by as much as two orders of magnitude. Fortunately enough, the solution of dispersion equations for continuous input is not too sensitive to changes in the magnitude of this coefficient, as already indicated in Chapter 2.

It may be recalled that the dispersion coefficient is in fact a sum of two terms:

a) A horizontal turbulent diffusivity ϵ , due to large scale eddy motions.

b) A purely dispersive term E_d , due to velocity variations over the depth.

The value of the first at the sea surface can be predicted quite reliably by Okubo's empirical formula (22).

$$\epsilon = 0.01 \ell^{1.15} \quad (\text{in cm, sec units}) \quad (5-8)$$

where ℓ a characteristic length scale, initially defined as three times

the standard deviation of the concentration distribution along the axis of interest. The length scale is actually a characteristic of the region. It is not known what its relation is (if any) to the geometrical characteristics of the area considered, such as the depth h or the distance from the shore. It is conceivable, however, that the length scale should have a relation to the maximum size of eddies that can be developed around the source. For Lake Erie, Fochtman and Wnek (33) report a value of $\ell = 800$ ft. for a depth of $h = 27$ ft., indicating a relation $\ell = 30 h$. With specific information about the area of interest lacking a value of 30 to $50 h$ may be used for the determination of ϵ . Fochtman and Wnek further claim a slight linear decrease of ϵ with depth; the average value over the depth should be used in the model. However, the accuracy of the estimate of ϵ is not critical because its magnitude is normally much smaller than the dispersive term E_d .

This term can be derived from one-dimensional considerations, since the velocity field is assumed the same in all (x,y) positions. Thus, lateral variations do not exist and a value of E_d due to velocity variations over the vertical is appropriate. Its general form is:

$$E_d = \lambda h u_* \quad (5-9)$$

where h = the depth

u_* = the shear velocity

λ = a constant of proportionality

Values for λ that have been reported range from as low as 6 (Elder) to

as high as 500 (Glover). Taylor's formula (2-5), modified for open channels, yields $\lambda = 20$. These lower values, derived from theoretical assumptions and tested for ideal flow conditions, represent a lower limit of the actual value of the dispersion coefficient, which is usually higher by an order of magnitude. Harleman's suggestion for doubling Taylor's coefficient to account for natural nonuniformities gives $\lambda = 40$. With respect to u_* , an average value over the tidal cycle seems appropriate. The shear velocity is related to the mean velocity and the friction factor by the expression:

$$u_* = \sqrt{\frac{f}{8}} U \quad (5-10)$$

It is therefore evident that E_d is not the same in all horizontal directions but depends on the mean velocity along each axis. In fact, Equation (5-9) and Equation (5-10) indicate that E_d is proportional to the mean velocity (averaged over the tidal cycle) in a certain direction, provided that f can be considered constant throughout. For flat bed conditions it may be assumed that $f \approx 0.02$; hence $u_* = \frac{1}{20} U$.

Okubo (23) found that for an oscillating linear velocity profile the dispersion term is

$$E_{d,o} = \frac{1}{240} \frac{V_{\max}^2 h^2}{\bar{\epsilon}_z} \quad (5-11)$$

where V_{\max} = the velocity amplitude at the surface

$\bar{\epsilon}_z$ = the vertical diffusivity, assumed constant

He also found that for a steady current having a linear profile with a value at the surface equal to V_{\max}

$$E_{d,s} = \frac{1}{120} \frac{V_{\max}^2 h^2}{\bar{\epsilon}_z} \quad (5-12)$$

Since the mean velocity over the depth is half the value at the surface due to the linearity of the profile

$$(u_*)_{\max} = \frac{1}{2} \sqrt{\frac{f}{8}} V_{\max} = \frac{1}{40} V_{\max} \quad (\text{for } f = 0.02)$$

and for a sinusoidal oscillation

$$(u_*)_{\max} = \frac{2}{\pi} \frac{1}{40} V_{\max} = \frac{1}{63} V_{\max}$$

Also, $\bar{\epsilon}_z$ can be taken equal to the mean value of ϵ_z over the depth:

$\bar{\epsilon}_z = 0.067 hu_*$. Substituting in Equation (5-11)

$$E_{d,o} = \frac{1}{240} \frac{V_{\max}^2 h^2}{0.067 hu_*} = \frac{1}{240} \frac{(63)^2}{0.067} hu_* \approx 250 hu_* \quad (5-11a)$$

Similarly, for a steady current

$$E_{d,s} = 200 hu_* \quad (5-12a)$$

The estimates of the dispersion coefficients by these formulas are an order of magnitude higher than Taylor's predictions. They are probably overestimating the true values since a linear profile presents

more severe velocity variations over the depth than a logarithmic profile, which was previously considered (Section 5-2) close to reality. It is proposed herein that, in case of lack of information concerning the area of interest, a value for v a little higher than Harleman's, in the range 40 to 80, may be used.

It is generally desirable to obtain some field information on the dispersion characteristics of a specific coastal area in order to model it more realistically. Measurements of the horizontal dispersion coefficient can be made by monitoring the distribution over time of some tracer injected at a point. The basic idea of the experimental measurement lies in the fact that the variance of the distribution and the dispersion coefficient along an axis are related by the following equation, assuming that the distribution of the tracer is approximately Gaussian:

$$E = \sigma^2/2t \quad (5-13)$$

If the variance increases linearly with time, then E is constant. In reality, however, this is rarely the case. One of the reasons is that most experiments have dealt with instantaneous injections. Thus, the dispersion is expected to increase with the size of the dye patch, at least due to the diffusion term ϵ (Equation 5-8). The dispersion term E_d is supposedly constant (Equation 5-9). In fact, though, there is no way to have both constant velocity and constant dispersion. If the velocity is constant, the variance is increasing in proportion to t^2 and not to t . Fluctuations of the dispersion due to tidal variations

make the problem of estimating a reasonable "average" coefficient even more complicated. In the case of a continuous injection, however, the effective dispersion coefficient applicable to the whole area of interest is expected to be much more stable in terms of both tidal and real time.

It is worth noting that almost all previous experiments in the sea were carried out on the surface layer. Dye was the most common tracer used (Rhodamine B or WT). Thus, the values of the dispersion reported for various areas refer only to the diffusion term ϵ and more specifically to its value at the surface layer. Dispersion due to velocity variations over the depth could not be measured by this technique. Such measurements would require a uniform injection of dye over the depth and an exactly neutrally buoyant dye solution. The second requirement makes the application of dye techniques extremely difficult, if not impossible, in view of the slightly variable seawater density over the depth. The difficulties increase even more when it is desired to estimate dispersion of matter distributed nonuniformly over the depth.

In fact, most of the past work on dispersion coefficients was initiated in relation to the dispersion of pollutants, which are more or less neutrally buoyant and hence have a uniform concentration over the depth if injected from a vertical line source. Not much information exists on dispersion of particles having variable concentration over the depth, such as suspended sediments. For very fine sediments some approximation can be made by using the values given for uniform concentrations.

The drogues, which give values of the velocities encountered in the area, can also provide valuable, although not very accurate, information concerning dispersion characteristics. The basic requirement is that all drogues must be deployed at the same point and at the same time (at least approximately), but at different depths. The variance of their positions over time must subsequently be monitored. Since they always stay at the same depths, the variance of their positions depends on the velocity variations over the depth. The larger the number of drogues, the more accurate the estimate of the variance and therefore of the dispersion coefficient according to Equation (5-13).

In order to properly calculate the variance, the drogue positions must be appropriately weighted. The weight placed on a drogue will depend on the sediment group considered and can be found as indicated in Figure 7. The same program that computes the advective velocities can be extended to calculate the (weighted) variance of the drogues around the (weighted) mean position at various times and consequently, from Equation (5-13), the values of the dispersion coefficient at every time interval. An average value of the dispersion coefficient over a tidal cycle can therefore be calculated and used in Equation (5-1). It is evident from the above discussion that the value obtained through the drogues variance refers to the total dispersion coefficient $E = \epsilon + E_d$. Details of the computational procedures are presented in Chapter 7, in relation to the application of the model to the Massachusetts Bay.

CHAPTER 6

SYNTHESIS OF THE MODEL COMPONENTS

6.1 Concentration Distribution of a Group of Sediments

A group of sediments is characterized by its average settling velocity, as indicated in Table 1 (Section 4.3). For such a group the normalized vertical distribution is first computed according to Equation (4.7). This distribution provides the necessary information for calculating the parameters of the differential equation (5.1) of the horizontal distribution, specifically the value of the decay factor α , through Equation (4.12). Combined with drogoue measurements it also specifies appropriate values for the advective velocities and dispersion coefficients as indicated in Sections 5.2 and 5.3. The solution of the expression (5.7) for the horizontal distribution of concentrations can then be evaluated numerically. The concentration of suspended sediments for this particular group as a function of space and time is finally obtained by the relation:

$$c(x,y,z,t) = \bar{c}(x,y,t) \phi(\zeta) \quad (6-1)$$

according to the basic model assumption.

It should be obvious that, since $\bar{c}(x,y,t)$ refers to a quasi-steady state solution, Equation (6.1) for the determination of c is strictly applicable for times after the convergence of the solution for \bar{c} . The solution is also not applicable for spatial coordinates very close to the shore, as indicated in Chapter 3.

If the numerical integration of the expression for \bar{c} is carried out for times shorter than required for convergence to steady state, an approximation of the transient behavior of \bar{c} , and subsequently of $c(x,y,z,t)$, can be obtained. However, the results will be unreliable for times shorter than that necessary for vertical equilibrium, which has an upper bound of the order of $T' = h^2/\epsilon_z$; for example, typical values in the area of interest in Mass Bay are

$$h = 30 \text{ m}$$

$$u_* = 0.5 \text{ cm/sec}$$

$$\bar{\epsilon}_z = 0.067 hu_* = 0.067 \times 30 \times 0.005 = 0.01 \text{ m}^2/\text{sec}$$

$$\text{hence, } T' = \frac{30^2}{0.01} = 90,000 \text{ sec.}$$

This time is approximately two tidal cycles. Hence, this is the maximum time span after which reasonable transient results can be obtained.

With respect to the prediction of the concentration distribution after the end of the injection, the model can give approximate answers as long as vertical equilibrium continues to hold. Equation (6.1) is still applicable, but now the depth-averaged concentration is calculated with the integral of Equation (5.7) subject to the upper limit of the time of the end of the injection.

6.2 Total Sediment Concentration

In general, the suspended sediments introduced into the seawater have various sizes and settling velocities. For the purpose of this analysis, however, they can be classified into several discrete groups, for example into those indicated in Table 1 (Sec. 4.3). The percentage of each group forming the total sediment introduced is supposedly known, or can be found by measurements of settling velocities. These group percentages are determined in terms of settling velocities rather than of individual grain sizes. Thus, the increased settling rate of the clay fraction due to flocculation can be accounted for by including percentages of the clay material in the higher settling velocity groups. The settling tube experiments (Section 4.5) make it possible to obtain values for the assignment of the clay function to the other groups. These values will vary with such factors as the type of clay and the initial concentration of sediment.

For each group, the concentration $c(x,y,z,t)$ can be found by the model, as summarized in Section 6.1. Under the assumption that the distribution of particles of a group is independent of the presence of particles of another group, the total concentration of suspended sediments can be found as a weighted sum of the individual group concentrations at any point (x,y,z,t) . The weights for this calculation are defined by the composition of the mixture introduced.

It may be noted that, even if the ideal conditions assumed in the model actually exist, an instantaneous measurement of suspended sediment concentration at some point cannot be expected to agree with the above calculated $c(x,y,z,t)$. Due to random turbulent fluctuations in velocity and concentration, the solution is considered to represent an average value of $c(x,y,z,t)$ over some period of time Δt .

6.3 Rate of Deposition

The amount of sediments deposited at the bottom is quite important from the point of view of ecological balance.

The concentration near the bottom is at any time equal to

$$c(x,y,o,t) = \phi(o) \bar{c}(x,y,t)$$

and the rate at which the particles reach the bottom is $w_s \phi(o) \bar{c}(x,y,t)$.

Recalling that A is the overall probability that a particle settling to the bottom stays there, the rate at which particles of a certain group are deposited at the bottom follows as:

$$D = A w_s \phi(o) \bar{c}(x,y,t) \quad (6-2)$$

in units of mass/time x area, provided the sediment concentration c is expressed in mass per unit volume as a function of location and time. The spatial integration of D for any group over all x, y values should equal the rate of injection of sediment of this group, i.e.,

$$\int \int_{\text{all } x,y} D_i \, dx dy = m_i = \lambda_i \Psi c_o \quad (6-3)$$

It is conceptually simple to find the amount of sediment deposited between times t_1 and t_2 at a particular point (x,y) , more specifically in a unit area about a point. It can be computed as:

$$\int_{t_1}^{t_2} D dt = \int_{t_1}^{t_2} A w_s \phi(o) \bar{c}(x,y,t) dt = A w_s \phi(o) \int_{t_1}^{t_2} \bar{c}(x,y,t) dt \quad (6-4)$$

provided that steady state has been reached before t_1 .

The thickness of the layer of sediment deposited is

$$\delta = \frac{\int_{t_1}^{t_2} D dt}{\rho_e} \quad (6-5)$$

where ρ_e is the effective density of the material, considering it to be loosely deposited, that is,

$$\rho_w < \rho_e < \rho_s - \rho_w$$

where ρ_s is the sediment density

ρ_w is the density of seawater

It is evident that the amount deposited should be calculated for each group separately and then added together to obtain the total deposition.

The computation of the amount deposited requires a further numerical integration. It can be approximated by multiplying the average steady state deposition rate, $\bar{D}(x,y)$, by the duration of dredging. This \bar{D} can be obtained to the desired accuracy by averaging

the values of D for various tidal stages at a particular point. This technique is only applicable in the case of dredging of long duration, implying that the steady-state phase lasts much longer than the transient phase.

CHAPTER 7

APPLICATION OF DREDGING IN MASSACHUSETTS BAY

7.1 General Comments on the Project NOMES

In 1972, the National Oceanographic and Atmospheric Administration (NOAA) launched a three-year project to study the environmental effects of offshore mining for sand and gravel in the Massachusetts Bay as Project NOMES (New England Offshore Mining Environmental Study). Various physical, chemical and biological parameters were to be monitored before, during and after the dredging operation which was scheduled for the summer of 1974. An extensive data base was to be provided to develop mathematical models for the prediction of the environmental impact of future dredging operations and for the development of legal regulations of such activities.

The inability to find an economical use for the large amount of dredged material led to the termination of the project in the summer of 1973, after some baseline studies had been conducted.

This model was developed at M.I.T. under the belief that the experimental dredging would provide an excellent opportunity to study the dispersion of fine suspended sediments which are inevitable by-products of such operations. The model efforts were continued after the termination of the project in view of the data already obtained and of the importance of such predictive capacities for the coastal zone.

As one of the activities of the NOMES project, an extensive dispersion experiment was carried out by NOAA's Environmental Research Laboratory in collaboration with several other institutions in June 1973, just prior to the termination of the project. A large quantity of small glass beads and sphalerite particles was dumped at the proposed dredging site and the concentrations of both were monitored for 11 days at various locations in the Mass Bay (21, 13). The injection of the particles was almost instantaneous and near the sea surface. However, the results of the experiment should be useful at least for a qualitative comparison with the model predictions. Current observations by drogues were conducted by M.I.T. during this experiment as well as earlier in the past year and provided the hydrodynamic parameters for the application of the dispersion model.

In this chapter the procedures for the collection and analysis of these data are given and the validity of the model as applied to the Massachusetts Bay is discussed.

7.2 The Sediment Source

The NOMES operation was scheduled to run for a period of six weeks with a hopper dredge having a capacity of 10-15 thousand cubic yards of sediment, to be collected in 1 1/2 to 3 hours (3). An estimated 5% of the sediments would consist of fines less than 100 μ in diameter. While the sediment is pumped into the dredge, the fines are discharged back into the sea as overflow with the seawater.

It was estimated that between successive dredging periods, 6-8 non-working hours would be required by the dredge for the roundtrip to the dumping site at a desired location. With 15,000 yd³ of sand and gravel dredged in 1 1/2 hours, the amount of fines introduced is:

$$\frac{0.05 \times 15,000}{1.5} = 500 \text{ yd}^3/\text{hr} \quad (7-1a)$$

or

$$\frac{500 \times (0.91)^3}{3600} \text{ m}^3/\text{sec} \approx 0.1 \text{ m}^3/\text{sec} \quad (7.1b)$$

Despite the fact that the operation is intermittent, the long duration of the dredging (6 weeks) relative to non-working intervals permits to approximate the steady state actually reached as one of an "equivalent" continuous injection. With the working times of 1 1/2 hours and the intervals in between of 6-8 hours, the equivalent continuous injection of fines would result in a rate of discharge of about 20% of that calculated in (7.1) or

$$v = 0.02 \text{ m}^3 \text{ fines}/\text{sec} \quad (7-2)$$

This is not necessarily valid if the working hours coincide always with the same parts of the tidal cycle. However, it is reasonable to assume here that the working hours occur more or less during different parts of the tidal period.

The volume rate defined above refers to actual volume of fines. If the material were in a compact state its density would approach 2.65 gr/cm³. Since in this case the material is loose, it is assumed herein that the concentration of the volume injected is

approximately 1 gr/cm^3 or 10^6 mg/l .

The dredge site was to be located at latitude $42^\circ 21'$ North and longitude $70^\circ 49'$ West, as shown in the chart, Figure 8, and has an area of about 0.8 by 0.5 nautical miles. For the application of the model, the source is assumed to be located at the center of this area. It is also assumed that there is enough mixing caused by the nature of the injection to consider it as a uniform line source.

The bottom depth is assumed constant and equal to its value at the dredging site, i.e., 30 meters. The complex shoreline can be approximated by a set of straight lines, as also shown in Figure 8. This configuration makes it possible to deal with cases in which the sediment "cloud" reaches the shore, as discussed in Section 5.1.

7.3 Composition of the Initial Mixture

As indicated in Chapter 3, the application of the model calls for a separation of the fine sediment discharged into several groups, each characterized by its average settling velocity. The separation displayed in Table 1 will be followed.

Grain size distribution data for the fines of the dredging area are essential. In the case of Mass Bay, about 70 core samples have been obtained from various locations and depths. Grain size distributions of the fines have been obtained through hydrometer analyses at the University of New Hampshire (32). The samples indicated a very consistent composition in the range below 60μ , primarily containing inorganic clay of low plasticity and inorganic silt.

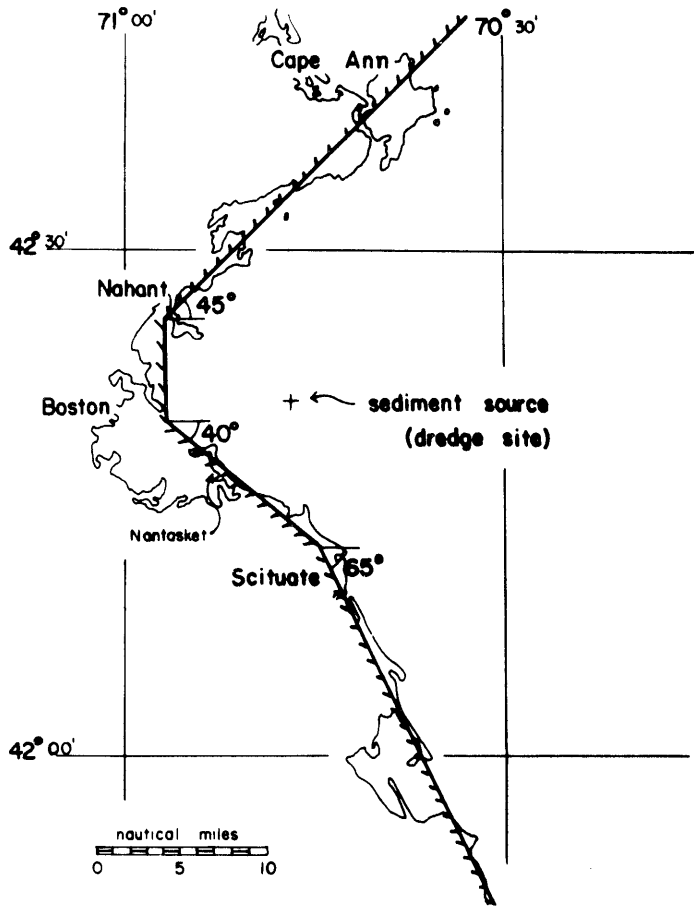


Figure 8 Approximate Geometry of Massachusetts Bay

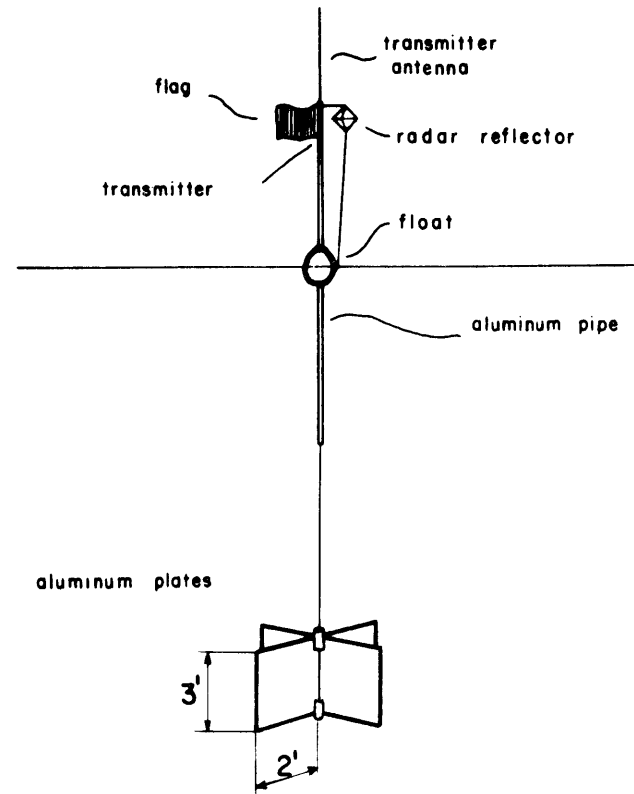


Figure 9 Drogue Used in Massachusetts Bay Current Studies

The specific gravity of the samples ranged from 2.30 to 2.90, averaging 2.60 - 2.65. This value for specific gravity indicates that Equation (4.13a), from which the settling velocities in Table 1 were derived, is valid.

The results of the UNH studies were presented in the form of classical grain size distribution curves. In terms of the 5 groups presented in Table 1, these curves yielded the following average sample composition:

fine sand	$60\mu < d < 100\mu$	10%
coarse silt	$20\mu < d < 60\mu$	13%
medium silt	$6\mu < d < 20\mu$	14%
fine silt	$2\mu < d < 6\mu$	13%
clay	$d < 2\mu$	50%

However, the grain size of the particle is not the most important quantity for the model. The critical factor is the settling velocity, w_s , which is indeed a function of grain size, but which is also influenced by other factors, such as shape, surface; and state of flocculation. Because the clay fraction of the fines is most affected by flocculation, a number of settling tube experiments on various clays were performed (Section 4.5). According to the results, the clay fraction can be distributed into different settling groups. A settling tube experiment with material from the bottom of the dredging site had been planned, but the termination of the project did not allow the necessary sampling. Based on the results

of the runs with other fine materials with 10 mg/l initial concentration, as was shown in Table 2 (Section 4.5.2), it may be assumed that the clay fraction contributes to the following groups, in terms of settling rates:

$$w_s = 0.68 \times 10^{-4} \quad 35\%$$

$$w_s = 1.36 \times 10^{-3} \quad 40\%$$

$$w_s = 1.43 \times 10^{-2} \quad 25\%$$

The results of the 10 mg/l initial concentrations were used instead of the 100 mg/l, because the former is more representative of the concentrations possibly predominating about the source due to the injection rate calculated in Section 7.2.

Incorporating these results with the data obtained by UNH, the resulting distribution into groups was computed and is shown in Table 3.

Table 3: Composition of Dredging Fines in Terms of Settling Velocity

Group No.	Mean Settling Velocity (cm/sec)	Percentage of Fines
1	0.462	10%
2	0.136	13%
3	$0.143 \cdot 10^{-1}$	27%
4	$0.136 \cdot 10^{-2}$	33%
5	$0.68 \cdot 10^{-4}$	17%

7.4 Background Concentrations of Suspended Sediment

Because of the nature of the mathematical model, a non-zero value of concentration, c , will be obtained at all spatial positions. Of course, very small values will be overshadowed by the "ambient" sediment concentrations existing under natural conditions. Thus, background data are needed to determine the extent of the dredging impact. Any position with a concentration increase of at least the same order of magnitude as the ambient can be considered "affected" by the dredging.

Beginning in January 1973 suspended sediment measurements were taken in Massachusetts Bay under the NOMES project. Samples were analyzed through filtering techniques and through light scattering by means of the turbidimeter described in Section 4.5. The correlation of turbidity with sediment concentrations appears rather encouraging, at least for the low concentrations encountered in the Bay, as was seen in Figure 2. Details of the procedures of monitoring turbidity and suspended sediments are given by Frankel and Pearce (10).

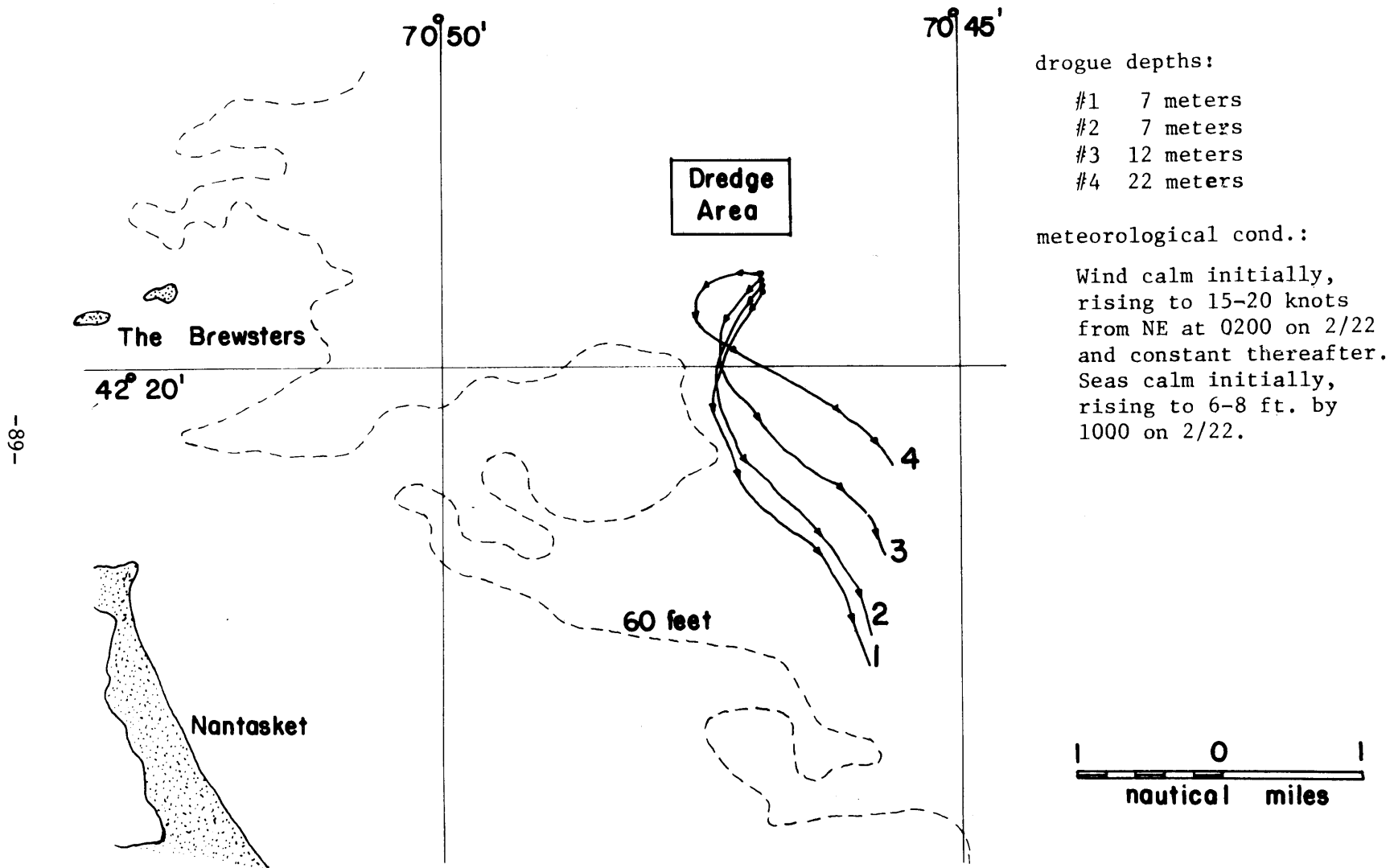
The measurements indicate an average suspended load in the Bay of about 1 mg/l. This includes both organic and inorganic matter. Consequently, the areas of actual dredging impact are those for which the concentration increase is of the order of this value. The dredging effect can be considered minor in areas with a much smaller amount of concentration increase. In addition, the effects

of the shoreline, as discussed in Section 5.1, need not be considered if the concentrations obtained by the model are very small near the shore.

7.5 Determination of Parameters from Drogue Data

As was explained in Chapter 5, current measurements are extremely important to the model. With respect to the application of the model in the Massachusetts Bay the only suitable field data were obtained through three drogue studies carried out in the first part of 1973. The type of drogue used is shown in Figure 9. During each of these studies three or four drogues were deployed at various depths at approximately the same point. They were then tracked for at least a full tidal cycle, their positions being recorded approximately every hour. These data made it possible to obtain values of the net drift, of the tidal velocities, of the dispersion coefficients along with some information on the velocity variations over the depth. The pathlines of the drogues in these studies are given in Figures 10, 11 and 12. A full account of the methods and instrumentation used can be found in a report by the authors (4).

A computer program has been developed to carry out the evaluation of the model parameters from the drogue data and the actual computations of the model. The procedure is divided essentially into two parts. First, the drogue and sediment data are used to solve the vertical concentration distribution, to obtain average net drift and tidal velocities, and to compute the decay rate and dispersion



-68-

Figure 10
Drogue Paths in the Study of February 21-22, 1973

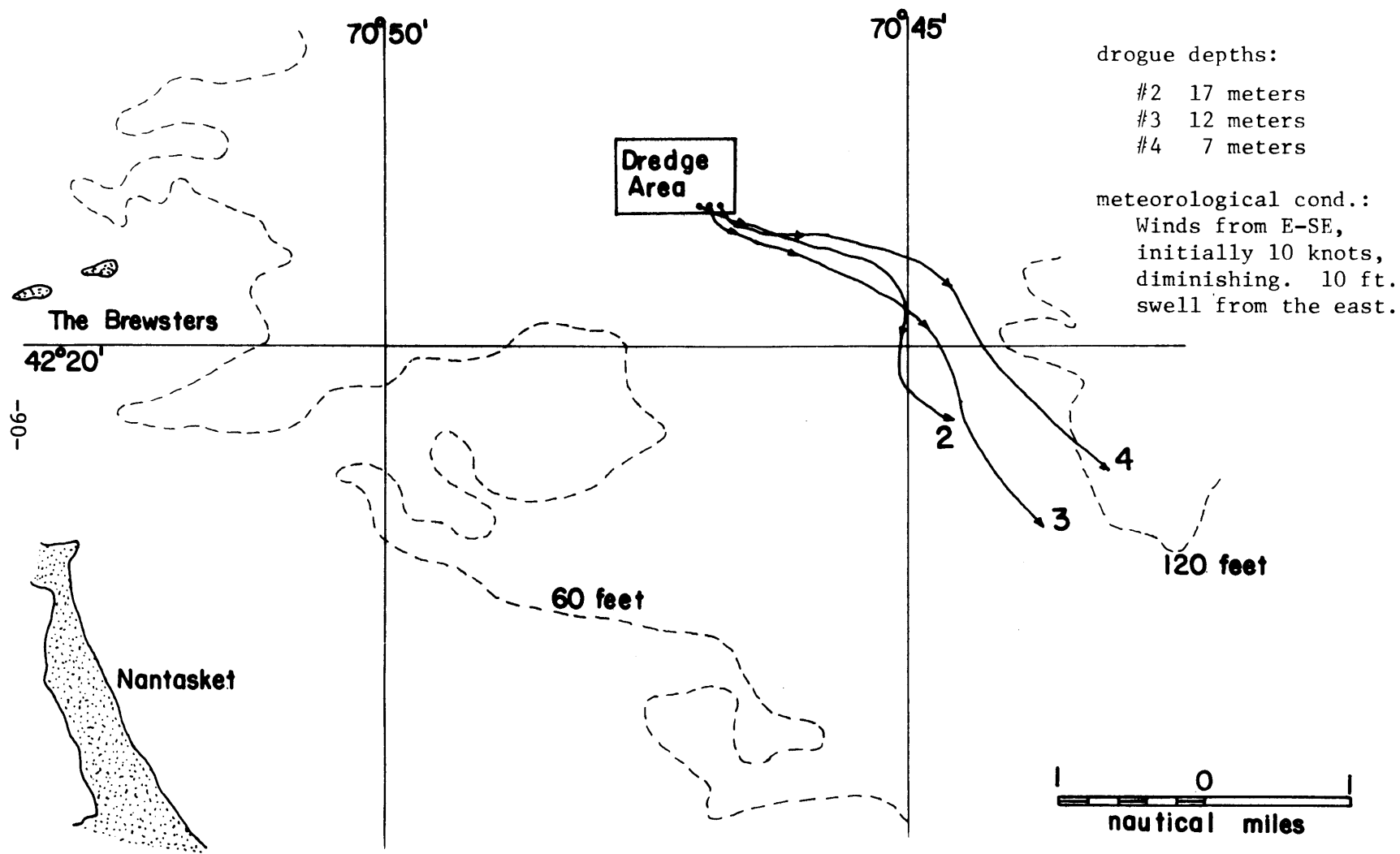


Figure 11

Drogue Paths in the Study of March 28-29, 1973

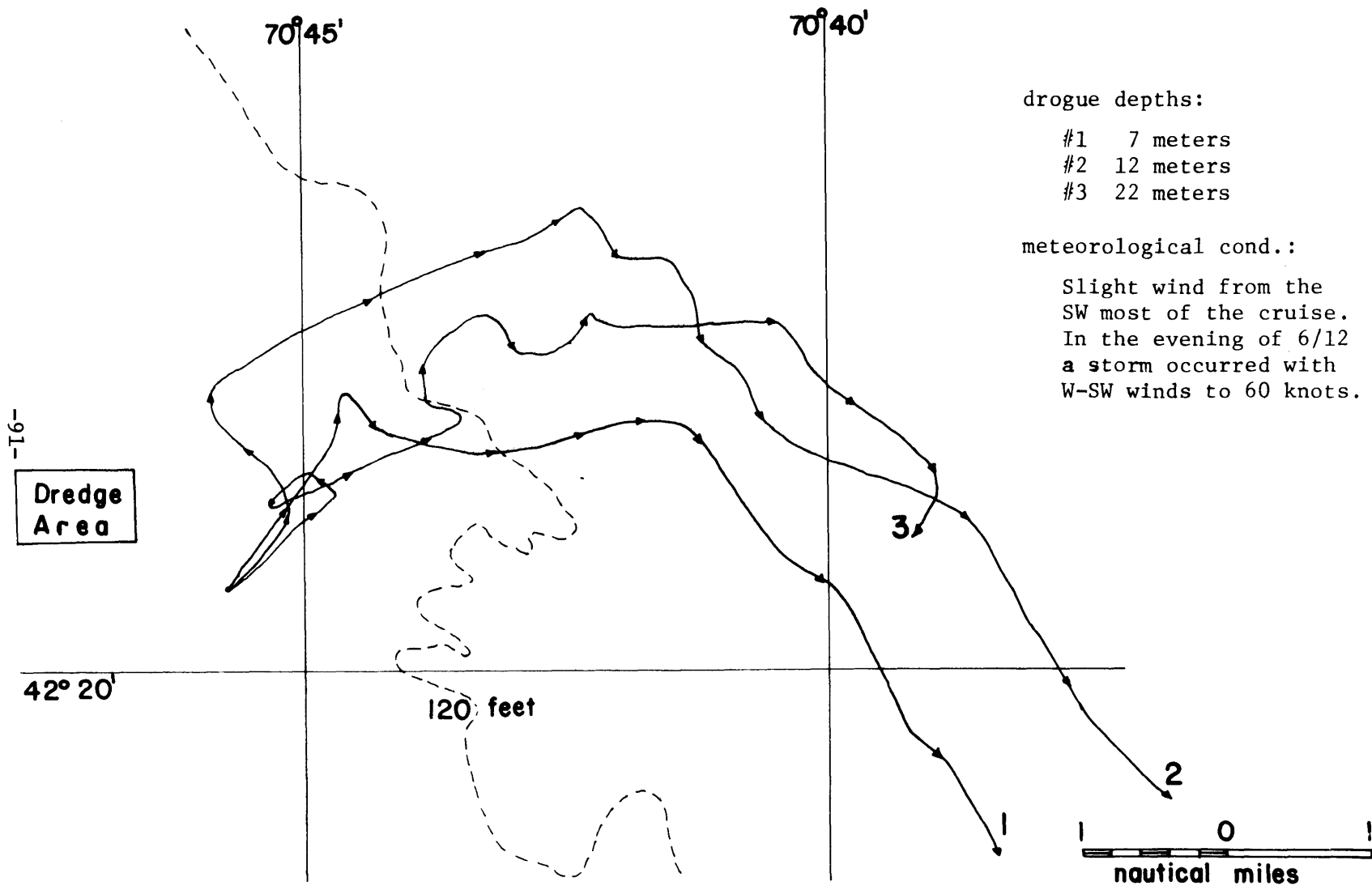


Figure 12
 Drogue Paths in the Study of June 11-12-13, 1973

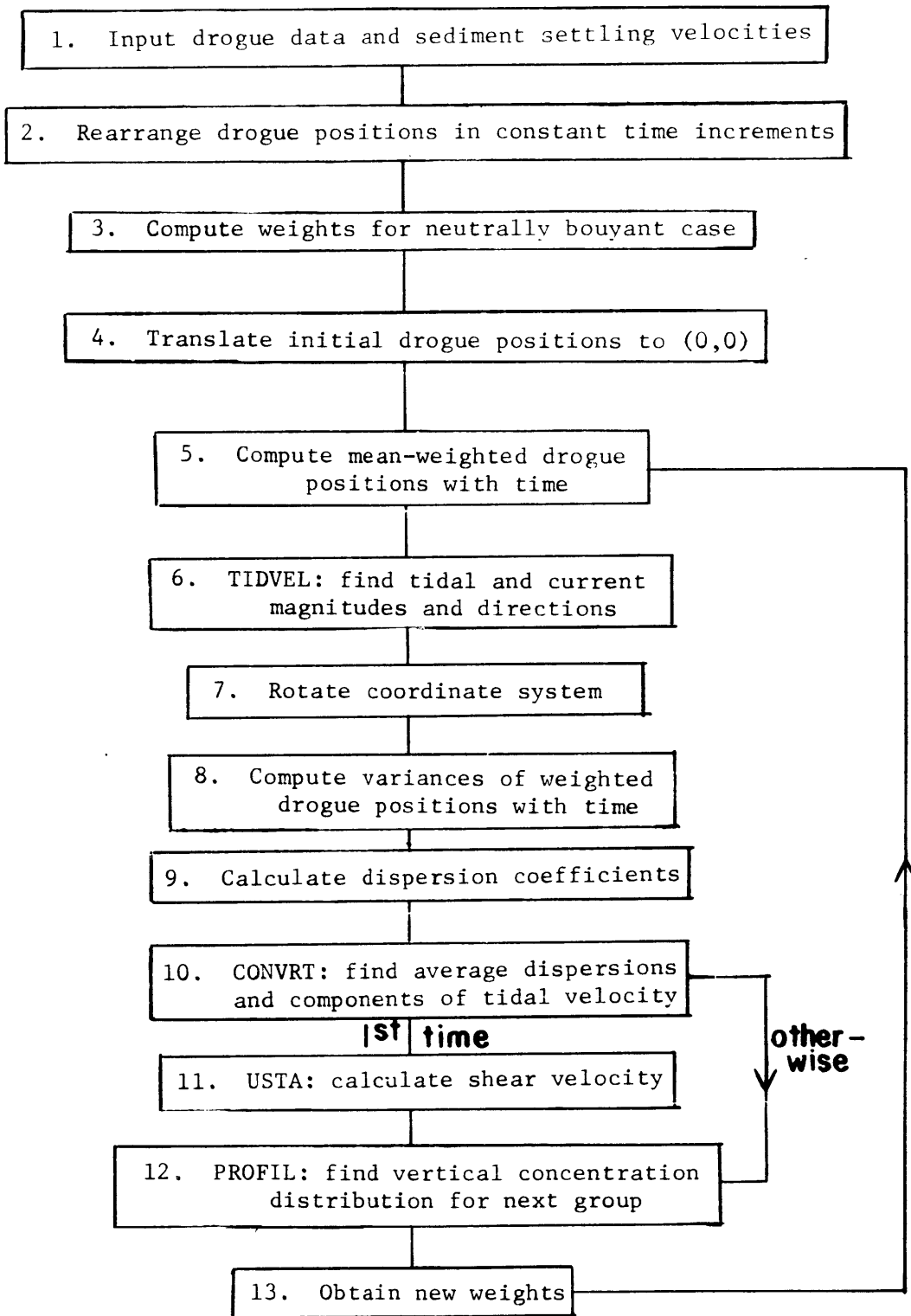


Figure 13
Flow Chart of Model Procedures

coefficients. In the second part, this information is used to solve the horizontal dispersion equation (5.7). The first part procedure is outlined in Figure 13 and described step by step below. The FORTRAN source program is listed in Appendix B.

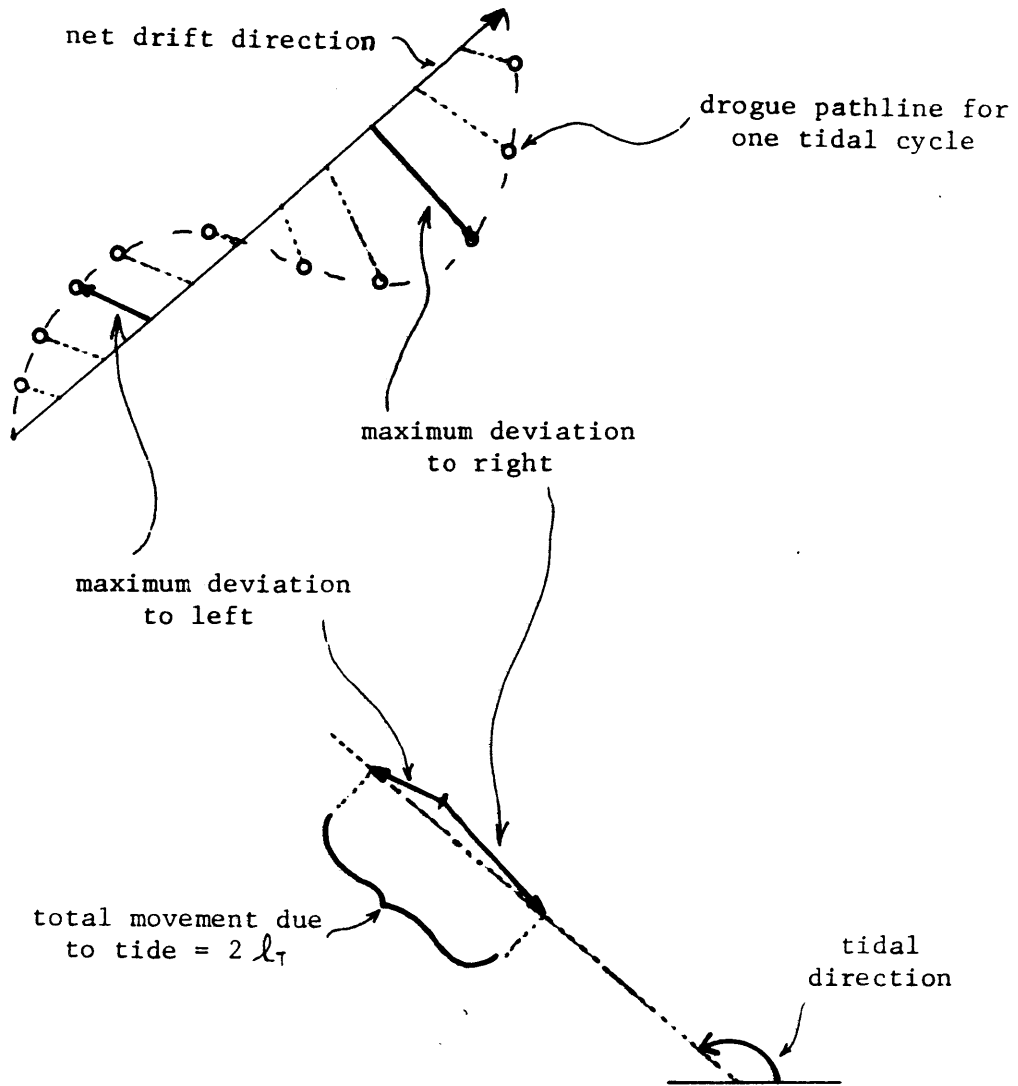
1. The first step is the input of the drogue and sediment data along with other necessary information. For each drogue, a series of positions and times is given denoting the drogue path. The drogue depth and the mean depth of the bottom over the drogue path is also required.

The only sediment data needed are the settling velocities for each of the 5 different groups of particles shown in Table 3, with the initial concentration of each group.

Other additional information includes values for the analysis starting time and the time increment to be used in Step 2, a depth increment for the integration of the vertical sediment distribution (Step 12), and a value for Von Karman's universal constant, k .

2. The drogue data are adjusted next so that a specified time interval exists between drogue positions. This requires interpolation between the actual drogue positions, which should not introduce any significant error since there are enough actual data points in the 3 drogue studies being analyzed. The results of this operation yield a table of simultaneous drogue positions, North and East, with the corresponding times evenly spaced.

3. The weights attributed to the drogues are computed by the technique described in Section 5.2.
4. The drogue paths are all translated in space so that each drogue starts at position (0,0). This step simplifies the velocity and the dispersion calculations. It does not introduce significant error, since the initial positions of the drogues are close together in all cases.
5. The mean drogue positions at different times are calculated. (The need for the simultaneous drogue positions as computed in step 2 is now clear). The drogue positions for each time are not simply averaged, they are averaged with respect to the weighting factors computed in Step 3 or Step 13. From these, the mean-weighted velocities are calculated.
6. The Subroutine TIDVEL computes the tidal and net drift velocities. The procedure begins by selecting the drogue record covering one full tidal cycle (see Figure 14). The distance the drogue travels in this period divided by the tidal time, 12.4 hours, is denoted the net drift velocity; the direction of travel is the net drift direction. The remaining deviation about this net drift is considered to be due to the tidal current. The maximum deviation to the left and to the right of the net drift is calculated. Both distance and direction for these maxima are recorded. The difference between these two vectors is the total movement due to the tide, $2\ell_T$. (see Figure 14).



$$\text{max. tidal velocity} = 2\pi l_T / T$$

Figure 14

Technique for Determining Magnitude and Direction of Tidal Velocities

An equivalent sinusoidal tide, that is, one which causes the same total movement, should have a maximum velocity given by the formula:

$$\sqrt{U_T^2 + V_T^2} = \frac{\pi}{2} \frac{2\ell_T}{T/2} = \frac{2\pi\ell_T}{T} \quad (7-3)$$

The direction of the equivalent tide is also given by the direction of the vector $2\ell_T$.

7. The coordinate system is now rotated so the new x-axis is in the direction of the net drift.
8. The variances of the weighted drogue positions at times found in Step 2 are now calculated for both the x and y axes. (Due to the previous rotation, these variances are in the direction of the net drift and normal to the net drift).
9. From these two series of variances, the dispersions in the x and y directions are found. The formula for the determination of dispersion from the variance is

$$E = \frac{\Delta(\sigma^2)}{2(\Delta t)} \quad (7-4)$$

where σ^2 is the variance

t is the time

From this it can be seen that the dispersion may be a function of time. It has been generally found that the dispersion increases slightly with time. This is probably due to the fact that as the drogues spread, they may enter zones of different eddy motions,

characterized by different length scales. Thus, their motion is more subject to random influences as they spread further apart. However, as mentioned, constant dispersion coefficients from averages over a tidal cycle will be used in this study.

10. In subroutine CONVRT, the average dispersion coefficients over the selected tidal cycle are calculated. Also, the components of the tidal velocity along the net drift and normal to the net drift are found.

11. In subroutine USTA the shear velocity, u_* , is found from:

$$u_* = \sqrt{\frac{f}{8}} U_m \quad (7-5)$$

where f is the roughness coefficient

U_m is the magnitude of the mean water velocity

A value of the roughness coefficient, f , equal to 0.02 was used. This value is appropriate as a mean value for flat bed conditions. It should be noted that the water velocity used includes both the tidal and the net drift components of the current. In other words, the total length of the path line of the mean drogue positions over one tidal cycle divided by the tidal time constitutes the magnitude of U_m .

Up to this point, the procedure deals with purely hydrodynamic characteristics, the main purpose being to define an appropriate value of u_* for the determination of the normalized vertical sediment distribution.

12. The integration of Equation (4.8) is performed in subroutine PROFIL, to yield the solution of the normalized suspended sediment distribution in the vertical direction, $\phi(\zeta)$, for a particular settling velocity w_s .

13. In subroutine WEIGHT the normalized sediment distribution, $\phi(\zeta)$, found in Step 12, is used to compute the weights for the drogues, based on the vertical spacing of the drogues, in addition to the values of $\phi(\zeta)$ at the drogue depths. The complete computation technique was discussed in Section 5.2. For this new set of weights the procedure is repeated beginning with Step 5 but with the exception of Step 11. Instead of the mean water drift and tidal velocities, the respective mean transport rates for a certain group of sediments (identified by its settling velocity) are now calculated. Similarly, instead of the dispersion coefficients of the water body, the effective dispersions, appropriate for the various sediment groups, are found.

It may be noted that the coordinate system for each sediment group will be slightly different due to the different values of the drift direction obtained for each case. This is reasonable in view of the directional differences for the drogues at various depths and of the "heavier" particles being dominated by the velocities at lower depths. However, the "lighter" particles, being distributed more evenly over the depth, will be affected by the velocities at all depths. The values of the parameters obtained from the data of the three field trips are presented in Tables 4, 5, and 6.

Table 4

Parameters for Conditions of February 21-22, 1973

Mean depth h = 25m		Shear Velocity $u_* = 0.533$ cm/sec				
Dimensional parameters	Units	Grp 1	Grp 2	Grp 3	Grp 4	Grp 5
Net drift magnitude, U_{fs}	cm/sec	5.28	6.82	8.10	8.24	8.24
Max tidal velocity, $\sqrt{U_{Ts}^2 + V_{Ts}^2}$	cm/sec	9.62	10.52	10.16	10.10	10.10
Max tide along drift axis, U_{Ts}	cm/sec	7.26	7.34	6.48	6.36	6.36
Max tide normal to drift axis, V_{Ts}	cm/sec	6.30	7.52	7.84	7.84	7.84
Dispersion along drift axis, E_x	$cm^2 \cdot 10^5 / sec$	1.85	1.18	0.83	0.78	0.78
Dispersion normal to drift axis, E_y	$cm^2 \cdot 10^5 / sec$	0.008	0.20	0.25	0.24	0.24
Average horizontal dispersion, $\sqrt{E_x E_y}$	$cm^2 \cdot 10^5 / sec$	0.12	0.48	0.46	0.43	0.43
Drift direction	° from E	-55	-60	-65	-66	-66
Tidal direction	° from E	-14	-14	-15	-15	-15
Angle between drift and tide	degrees	41	46	50	51	51
Dimensionless parameters						
Net drift magnitude, $U_{fs} T/h$		96	125	148	151	151
Max tidal velocity, $(\sqrt{U_{Ts}^2 + V_{Ts}^2}) T/h$		166	192	184	184	184
Max tide along drift axis, $U_{Ts} T/h$		132	134	118	116	116
Max tide normal to drift axis, $V_{Ts} T/h$		116	138	144	144	144
Dispersion along drift axis, $E_x T/h^2$		870	860	610	575	570
Dispersion normal to drift axis, $E_y T/h^2$		6	150	182	175	175
Decay factor, αT		101	10.1	0.32	0.025	0.001
Values for the parameters of the water itself are identical to those of group 5						

Table 5

Parameters for Conditions of March 28-29, 1973

Mean depth $h = 30\text{m}$		Shear Velocity $u_* = 0.479 \text{ cm/sec}$				
Dimensional parameters	Units	Grp 1	Grp 2	Grp 3	Grp 4	Grp 5
Net drift magnitude, U_{fs}	cm/sec	2.83	6.53	8.83	9.05	9.07
Max tidal velocity, $\sqrt{U_{Ts}^2 + V_{Ts}^2}$	cm/sec	2.74	5.66	6.36	6.38	6.38
Max tide along drift axis, U_{Ts}	cm/sec	1.44	2.76	2.56	2.46	2.44
Max tide normal to drift axis, V_{Ts}	cm/sec	2.32	4.94	5.84	5.88	5.88
Dispersion along drift axis, E_x	cm^2/sec	3.32	3.24	1.74	1.57	1.55
Dispersion normal to drift axis, E_y	cm^2/sec	0.001	0.036	0.14	0.15	0.15
Average horizontal dispersion, $\sqrt{E_x E_y}$	cm^2/sec	0.058	0.34	0.49	0.48	0.48
Drift direction	° from E	-40	-39	-37	-37	-37
Tidal direction	° from E	18	21	29	30	30
Angle between drift and tide	degrees	58	60	66	67	67
Dimensionless parameters						
Net drift magnitude, $U_{fs} T/h$		43	99	134	137	138
Max tidal velocity, $(\sqrt{U_{Ts}^2 + V_{Ts}^2}) T/h$		42	86	96	96	96
Max tide along drift axis, $U_{Ts} T/h$		22	42	40	38	38
Max tide normal to drift axis, $V_{Ts} T/h$		36	54	88	90	90
Dispersion along drift axis, $E_x T/h^2$		1680	1640	880	790	785
Dispersion normal to drift axis, $E_y T/h^2$		1	18	70	76	77
Decay factor, αT		87	9.3	0.27	0.021	0.001
Values for the parameters of the water itself are identical to those of group 5						

Table 6
Parameters for Conditions of June 11-12, 1973

Mean depth h = 35m	Shear Velocity $u_* = 0.433$ cm/sec					
Dimensional parameters	Units	Grp 1	Grp 2	Grp 3	Grp 4	Grp 5
Net drift magnitude, U_{fs}	cm/sec	2.14	4.58	6.80	7.06	7.09
Max tidal velocity, $\sqrt{U_{Ts}^2 + V_{Ts}^2}$	cm/sec	3.10	5.68	6.38	6.48	6.50
Max tide along drift axis, U_{Ts}	cm/sec	3.10	5.69	6.16	6.16	6.18
Max tide normal to drift axis, V_{Ts}	cm/sec	0.14	0.22	1.70	2.02	2.06
Dispersion along drift axis, E_x	10^5 cm ² /sec	1.27	1.50	1.41	1.34	0.94
Dispersion normal to drift axis, E_y	10^5 cm ² /sec	0.002	0.22	0.84	0.93	0.94
Average horizontal dispersion, $\sqrt{E_x E_y}$	10^5 cm ² /sec	0.050	0.57	1.09	1.12	1.12
Drift direction	° from E	40	42	41	40	40
Tidal direction	° from E	43	45	57	58	58
Angle between drift and tide	degrees	3	3	16	18	18
Dimensionless parameters						
Net drift magnitude, $U_{fs} T/h$		28	60	89	92	92
Max tidal velocity, $(\sqrt{U_{Ts}^2 + V_{Ts}^2}) T/h$		40	74	83	84	84
Max tide along drift axis, $U_{Ts} T/h$		40	74	80	80	80
Max tide normal to drift axis, $V_{Ts} T/h$		2	4	22	26	26
Dispersion along drift axis, $E_x T/h^2$		470	560	525	500	495
Dispersion normal to drift axis, $E_y T/h^2$		1	85	315	345	350
Decay factor, αT		80.5	8.85	0.237	0.018	0.001
Values for the parameters of the water itself are identical to those of group 5						

Once the hydrodynamic parameters (mean transport rates and dispersion coefficients) and the normalized vertical concentration profiles of the sediment groups in each drogue study are determined, they are used to solve the horizontal depth-averaged dispersion equation. The decay factor, α , is computed as

$$\alpha = Aw_s \phi(0)/h$$

wherein A is assumed as unity. All parameters are expressed in non-dimensional form, using the depth h as the reference length and the tidal period $T = 45600$ sec as the reference time. Then the integration (5.7) is performed numerically, using a non-dimensional time increment of $\frac{\Delta t}{T} = 0.05$.

The lines of equal concentration for each case are plotted in Figures 15, 16, 17. This is done only for groups 3, 4, 5. Groups 1 and 2 do not yield any significant average concentrations at distances more than a mile from the source. For purposes of comparison, each figure was drawn as if the input consisted 100% from sediments of the respective group. To get the actual concentrations, the values presented must be multiplied by the percentages shown in Table 3.

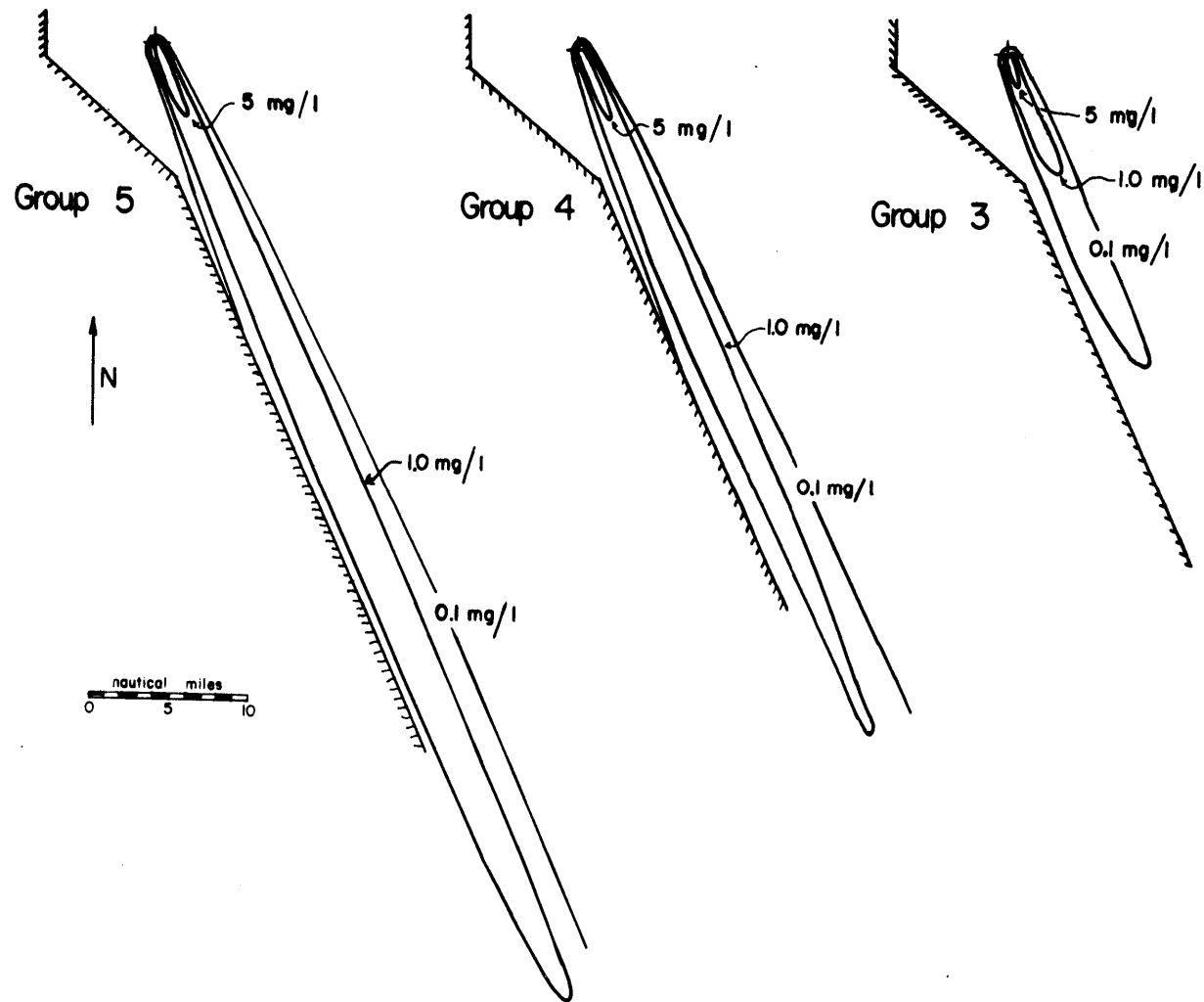


Figure 15

Distribution of Average Concentration for Conditions of February 21-22, 1973

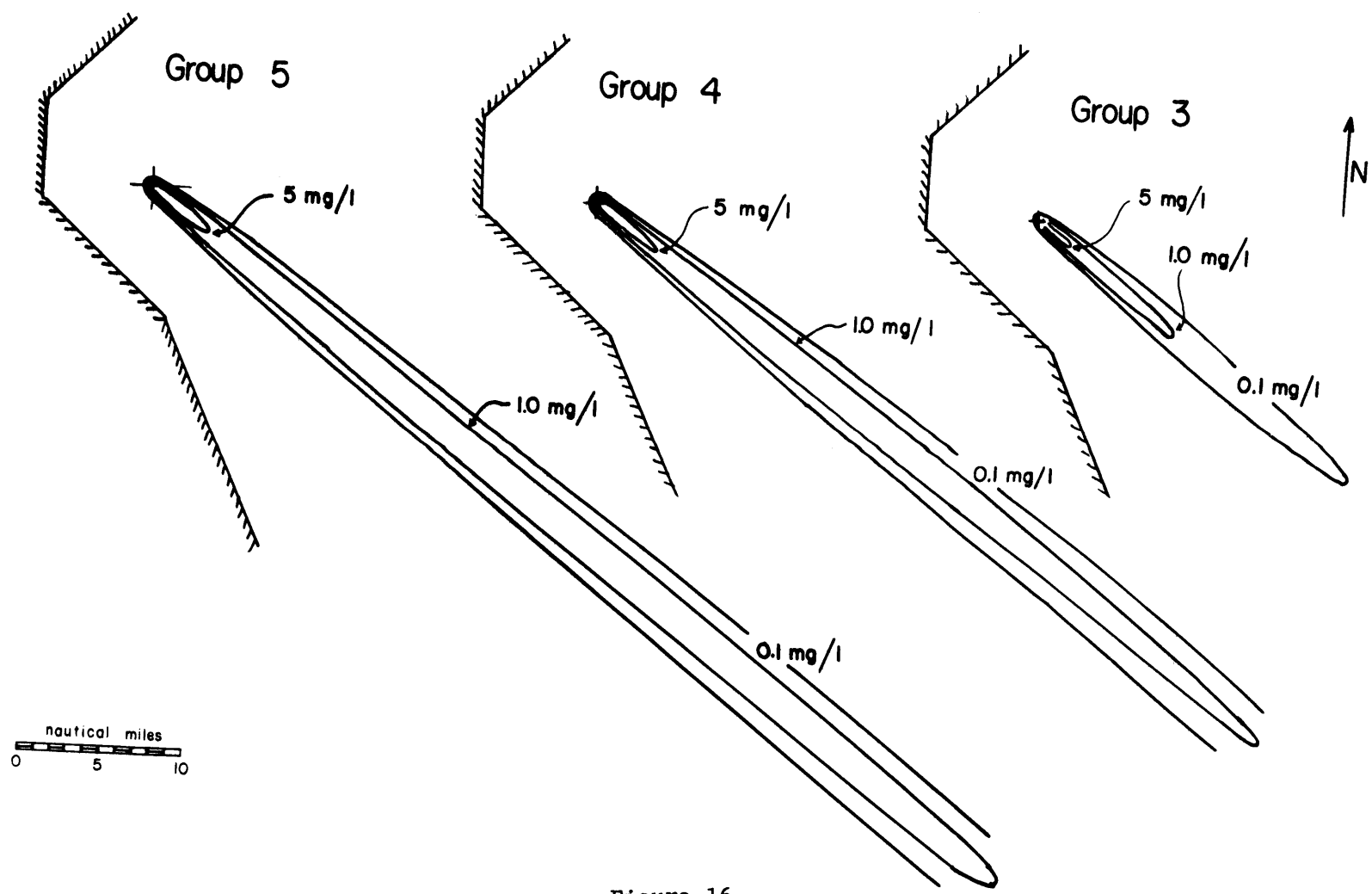


Figure 16

Distribution of Average Concentration for Conditions of March 28-29, 1973

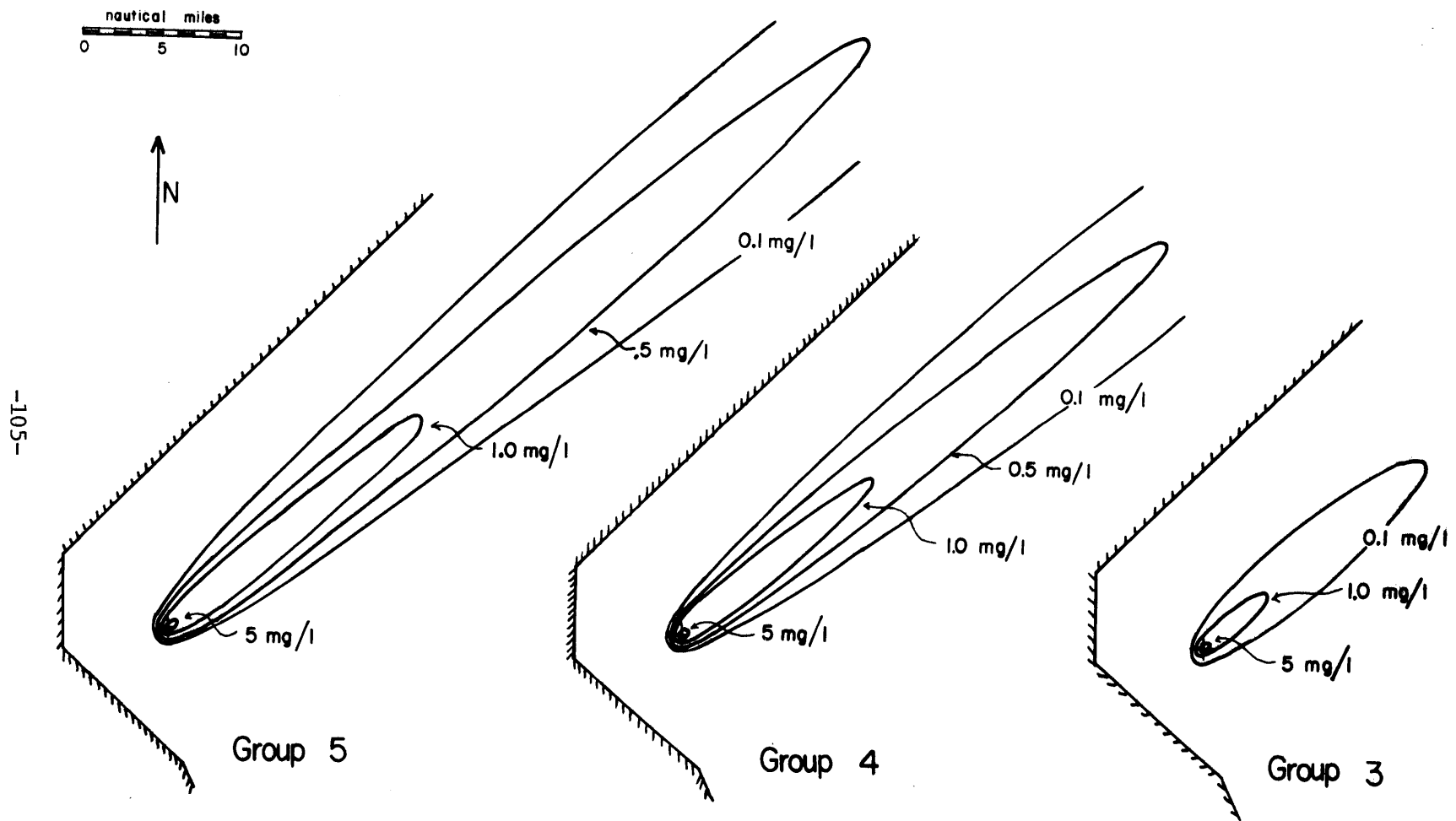


Figure 17

Distribution of Average Concentration for Conditions of June 11-12, 1973

7.6 Results and Discussion

Several things can be noted about the values of the parameters listed in Tables 4, 5, and 6.

First, there is a consistent increase of the mean transport rates both tidal and non-tidal, from group 1 to group 5. This was expected, since the lower velocities near the bottom are more heavily weighted in the first sediment groups. The differences are very slight between groups 3, 4, and 5 because of their nearly uniform vertical profiles. The tidal velocities are higher in February, when the tidal amplitude was larger. The drift velocities are generally of the same order of magnitude as those of the tides. The ratio of tidal to drift magnitudes is larger for the first groups, possibly indicating a more uniform tidal profile, with relatively high velocities near the bottom. The drift velocities of about 7-10 cm/sec for the water itself are in good agreement with values reported from other studies and discussed in more detail in another report by the authors (4).

The prevailing drift direction is SE. In June, the drogues, after moving for several hours to NE, changed direction and continued SE, which was the direction of the March and February drogues, also (Figures 10, 11, 12). The direction of transport is very much the same for all the groups, on each cruise, the difference among them being much smaller than the differences between the three cruises. This indicates that the water moves at approximately the same

direction at all depths. It should be mentioned here that the shallowest drogue is at a 7m depth, thus directional changes near the surface, due to short-duration winds, could not be measured; also, drogues were not placed close to the bottom to avoid interference with the sea bed.

The shear velocity did not change much in the three cases, having an approximate magnitude of 0.5 cm/sec.

With respect to the dispersion coefficients, it is seen that the effective value of the longitudinal dispersion (i.e., along the drift direction) decreases from group 1 to 5. This is because of the presence of high concentrations of group 1 near the bottom, where the velocity gradients are higher. By contrast, the lateral dispersion (i.e., normal to the drift direction) increases markedly from group 1 to 5. Due to the absence of any constant shear flow normal to the net drift, the nonuniform suspensions are not easily dispersed.

The average horizontal dispersion for the water body defined as the geometrical mean of the two values is remarkably similar in February and March, but twice as high in June. This increase is mostly due to the lateral dispersion. It may be due to the stratified conditions prevailing in June, in contrast to February and March. In Table 7, theoretical predictions for the eddy diffusion terms by Okubo's formula (Section 5.3) are presented for $\ell = 30h$. Also shown are the dispersion terms, following the formula $E_{\alpha} = \lambda h u_{*}$, where E_d u_{*} in any direction is assumed to be 1/20 of the mean velocity

Table 7

Dispersion Coefficients ($10^5 \text{ cm}^2/\text{sec}$)

	February	March	June
Eddy Diffusivity ϵ	0.040	0.050	0.060
E_d along drift axis			
Elder ($\lambda = 6$)	0.092	0.106	0.132
Taylor ($\lambda = 20$)	0.305	0.350	0.430
Harleman ($\lambda = 40$)	0.61	0.70	0.85
$\lambda = 80$	1.22	1.40	1.70
Okubo ($\lambda = 200$)	3.05	3.50	4.30
Measured values	0.78	1.56	1.33
E_d normal to drift axis			
Elder ($\lambda = 6$)	0.038	0.036	0.014
Taylor ($\lambda = 20$)	0.126	0.120	0.050
Harleman ($\lambda = 40$)	0.26	0.24	0.10
$\lambda = 80$	0.52	0.48	0.20
Okubo ($\lambda = 200$)	1.30	1.20	0.50
Measured values	0.24	0.15	0.94

magnitude in that direction.

It is seen that estimates, with values of λ 40 to 80, are in most cases close to the true values; only the dispersion normal to the drift axis in June is severely underestimated.

The dispersion patterns resulting from the model for the three sets of conditions (Figures 15, 16, 17) clearly indicate that the drift direction is the most important hydrodynamic feature affecting the movement of suspended matter for the conditions investigated. Unfortunately, it is highly variable. The assumption of a constant drift is too restrictive and does not in general represent natural conditions. The drift direction changes both in time and space, as the result of wind shifts, inlets, general circulation, etc. The prevailing direction, however, for Western Massachusetts Bay, seems to be SE. Occasional changes of the drift from this direction may conceivably spread the sediments more in the lateral direction and less in the longitudinal. Thus, the model results overestimate the length but underestimate the width of a natural dispersion plume. If the drift were truly constant, the narrow isoconcentration lines would be quite reasonable. The material could not spread much due to the assumed lateral uniformity in the velocity field. The value of the dispersion coefficient normal to the drift axis becomes then the primary factor influencing the width of the isoconcentration lines. This is evident by comparison of the March and June plots (Figures 16, 17). The tide,

as will be seen later, does not materially affect the width but just moves the plume back and forth, about the drift direction. The value of the dispersion coefficient along the drift axis is, by contrast, quite insignificant in light of the very important role of the drift velocity in determining the total length of dispersion. This can be seen by comparing the lengths of the plots of February and June (Figures 15, 17).

However, the decay factor, α , a function of the sediment settling velocity, is even more important in determining the extent of the plume of the suspended matter. This is readily seen by comparing the plots for groups 3, 4 and 5 for any set of conditions, although the advective and dispersion terms are approximately the same for the three groups. The importance of A becomes now clear. If it were taken as 0.5 instead of unity, the result would be the same as if the settling velocity were divided by 2.

The time needed for the solution to reach steady state at a particular point was found to depend primarily upon the decay constant and the magnitude of the net drift. This time, expressed in number of tidal cycles, can be approximately given as

$$n = \frac{L}{T \cdot U_f} + 4 \quad (7-6)$$

wherein L = distance from the source

U_f = net drift velocity.

This holds, provided the decay factor is such that significant concentrations are eventually found at the point under consideration. Thus, the time to convergence for the model runs was less than 5 tidal periods for groups 1 and 2, about 12 for group 3, 20 to 25 for group 4 and more than 30 for group 5. In fact, the plots presented in Figures 15 and 16 for group 5 are for a time of 30 tidal cycles, due to restrictions in computer time. The equilibrium profiles are slightly longer. Of course, for points near the source steady state was reached much sooner for all groups.

In order to provide more specific information on the effects of a possible dredging operation, representative values for the parameters of the model, estimated from those appearing in Tables 4, 5 and 6, were used for another run of the model. The values used are listed in Table 8. The normalized vertical profiles for the 5 groups are shown in Figure 18. The decay factors were computed as $\alpha = \frac{w_s \phi(0)}{h}$, considering $A = 1$.

The results of the depth averaged concentration \bar{c} are presented in Figure 19, in distorted scales, the x-axis being parallel to the net drift direction. The coordinates are presented in non-dimensional units, i.e., multiples of the depth. The distances to which several concentrations extend are tabulated in Table 9.

The effect of the tide, as seen in Figure 19c, is basically a shift of the isoconcentration lines along the tidal direction.

Table 8

Average Conditions

Depth h = 30m		Shear Velocity $u_* = 0.5$ cm/sec				
Non-dimensional Parameters	Group 1	Group 2	Group 3	Group 4	Group 5	
Net drift magnitude, U_{fs} T/h	50	90	125	130	130	
Max tidal velocity, $(\sqrt{U_{Ts}^2 + V_{Ts}^2})T/h$	80	110	120	120	120	
Angle between drift and tide, degrees	50°	55°	60°	60°	60°	
Dispersion along drift axis, E_x T/h ²	1000	1000	650	600	600	
Dispersion normal to drift axis, E_y T/h ²	3	80	150	160	160	
Decay constant, αT	87.3	8.95	0.27	0.021	0.001	

Table 9

Length, in Multiples of the Depth, of Area
with Concentration \bar{c} Larger than Indicated

(for average conditions)

\bar{c} (mg/l)	Group 1	Group 2	Group 3	Group 4	Group 5
0.5	20	60	750	-	-
1.0	18	50	510	2000	3600
2.0	16	40	280	850	1080

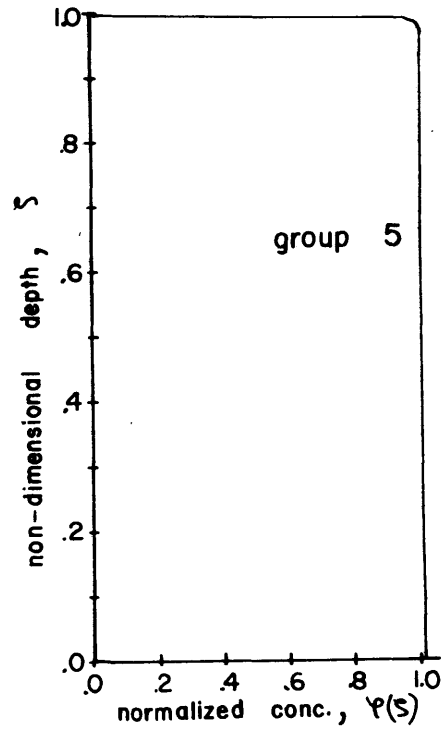
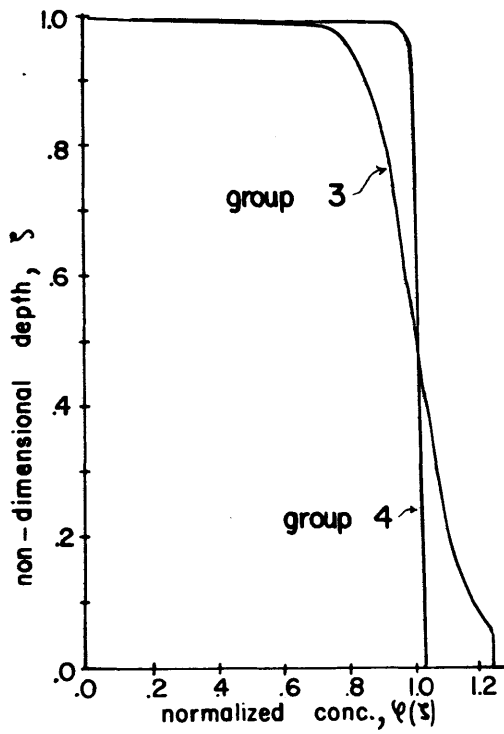
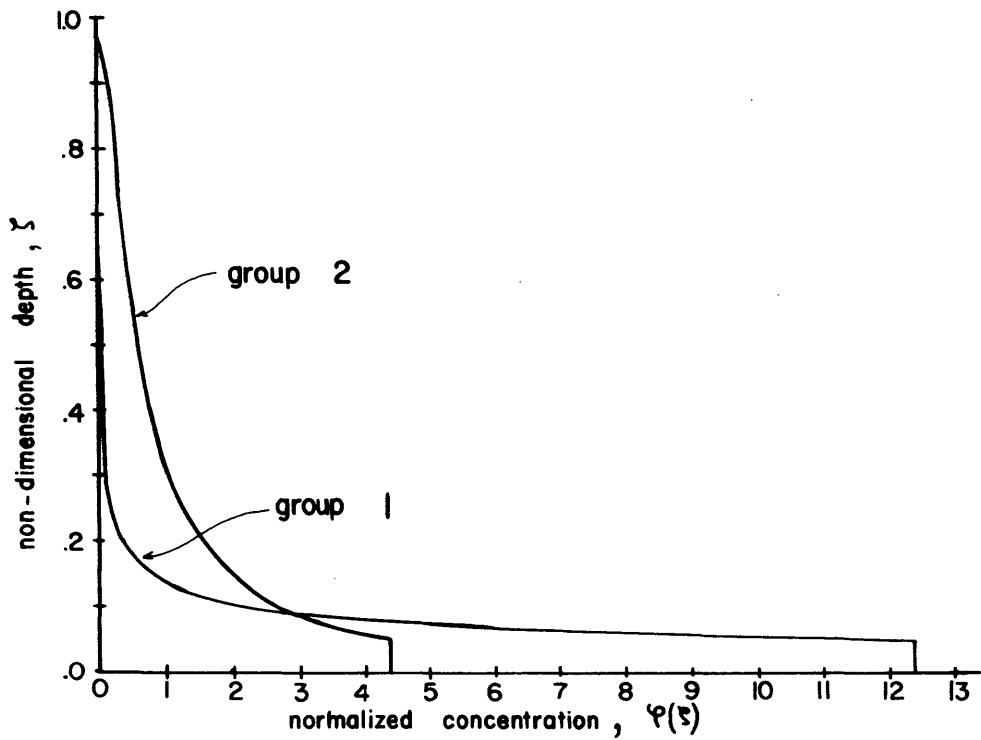
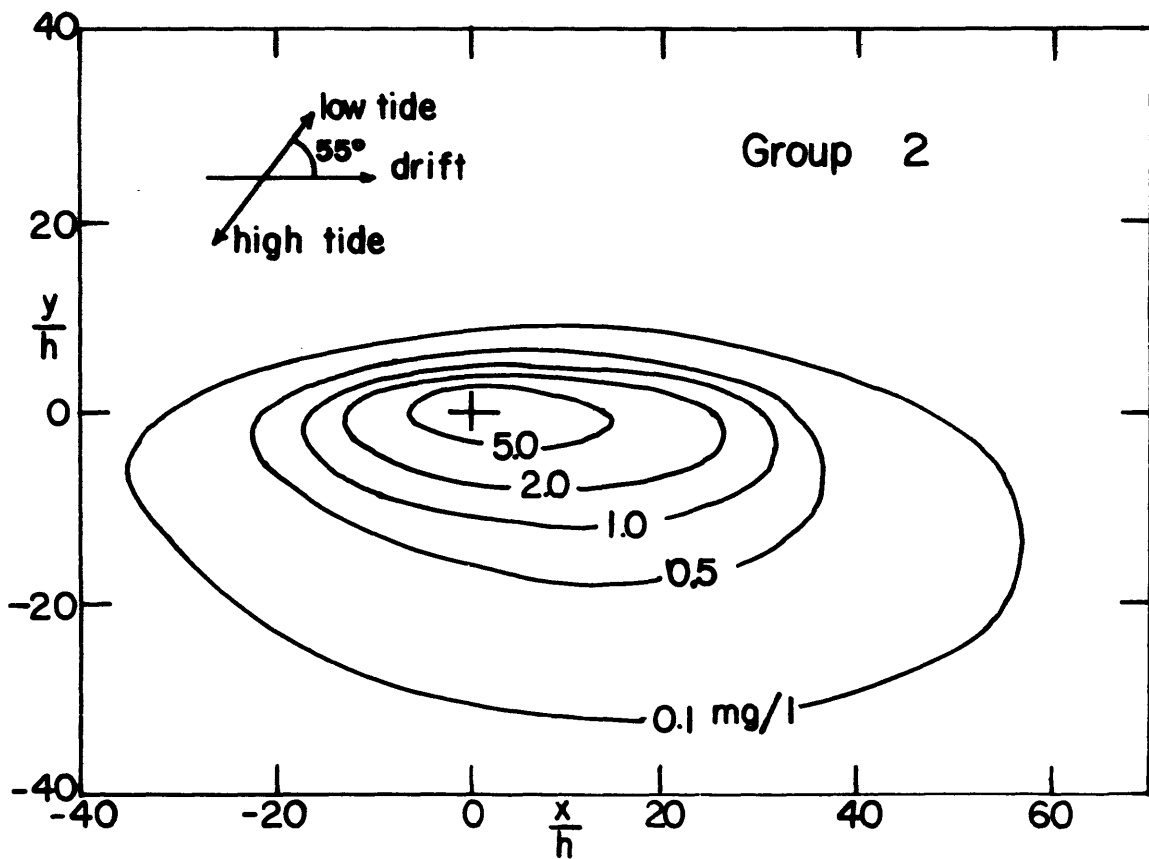
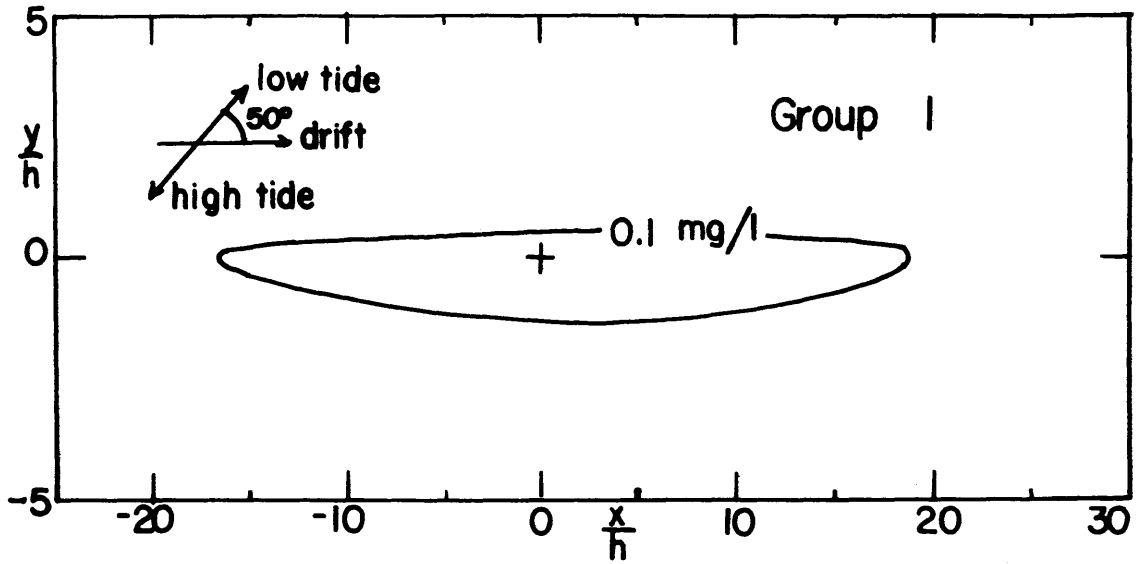


Figure 18

Normalized Vertical Profiles Under Average Conditions



Figures 19a,b
 Distribution of Average Concentration, \bar{c} , of Groups 1 and 2
 under Average Conditions, at High Water Slack

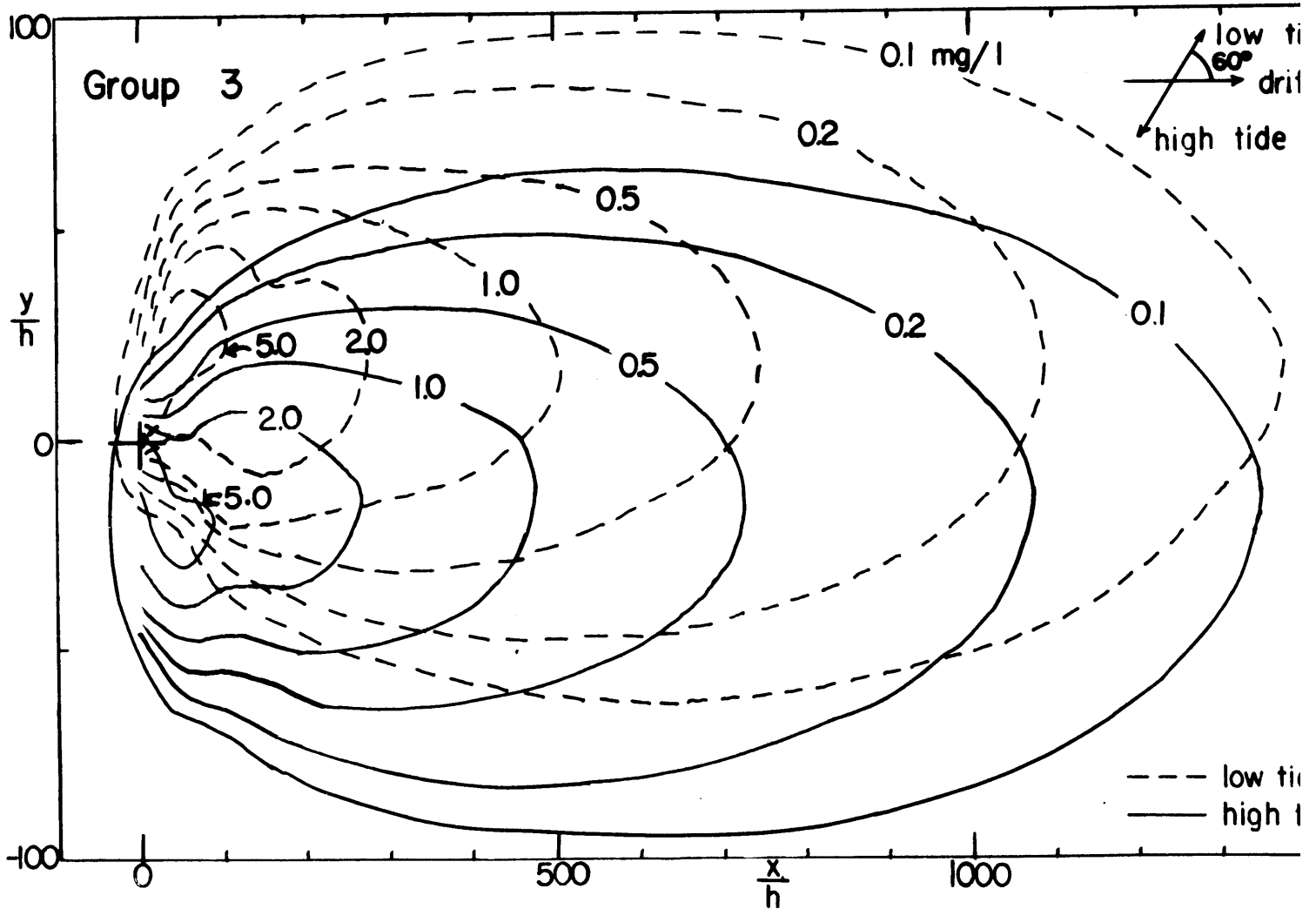
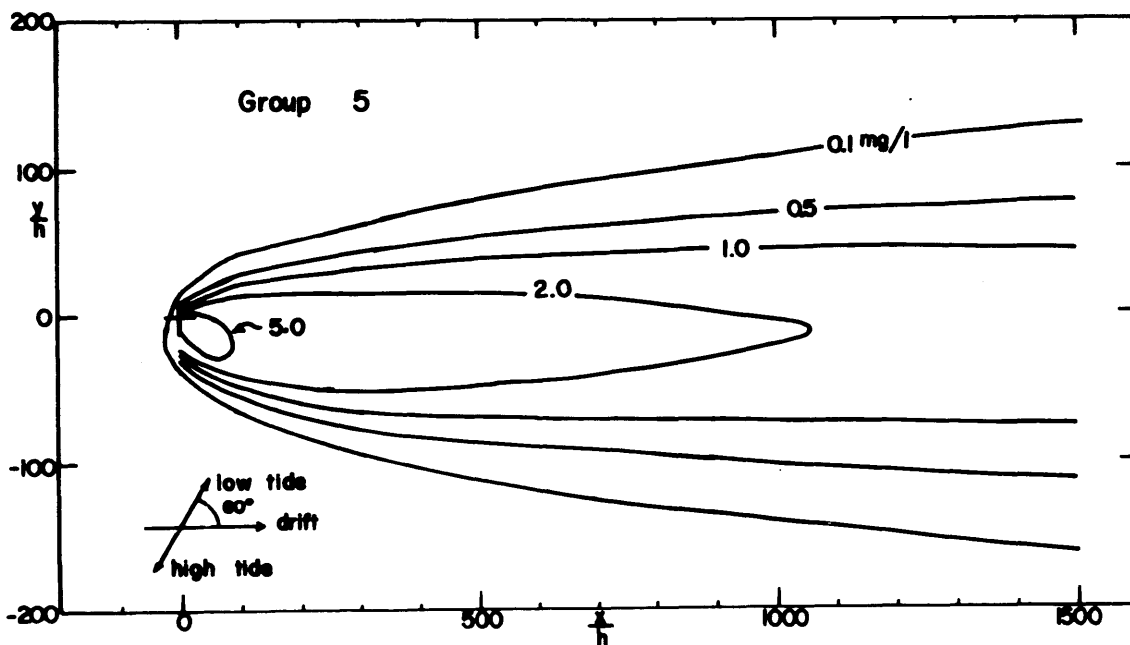
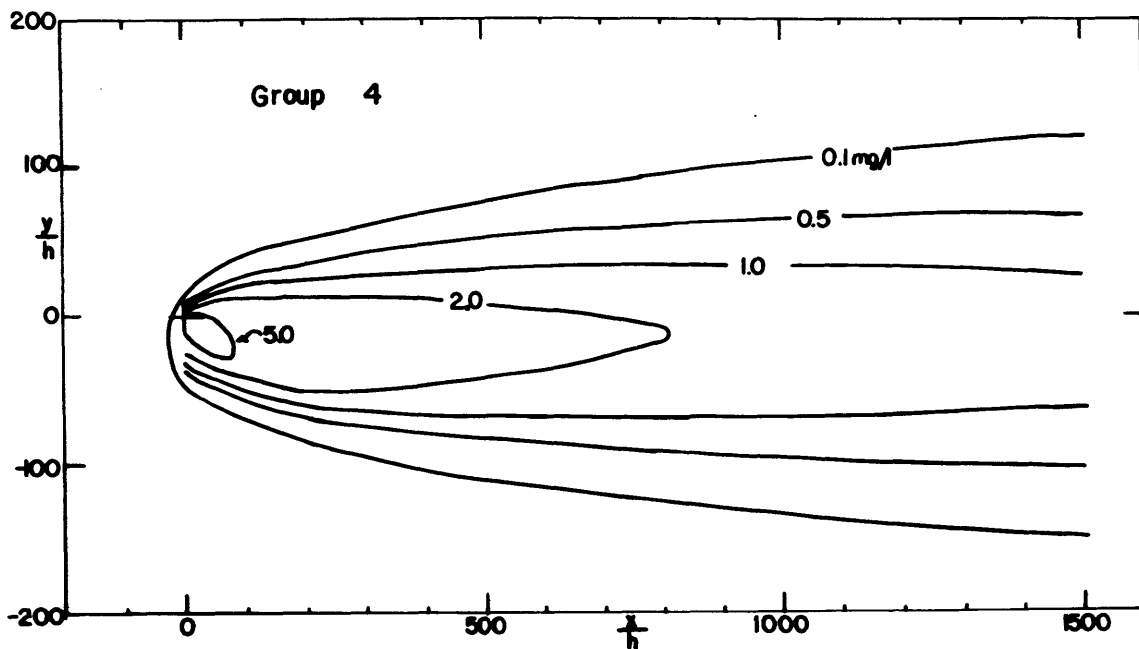


Figure 19c

Distribution of Average Concentration, \bar{c} , of Group 3 under Average Conditions



Figures 19d,e
 Distribution of Average Concentration, \bar{c} , of Groups 4 and 5
 under Average Conditions, at High Water Slack

The dependence on tidal time is more pronounced in the vicinity of the source, where the width of the plume is small. However, the model is not reliable in such small distances, as discussed in Section 3.2.

As was indicated in Section 6.3, the deposition of sediments on the bottom over a period of time can also be evaluated by the present model. Naturally, the limitations concerning the reliability of results for the suspended matter also apply to the results for the deposition. As an example, the average deposition rates (mass per unit time per unit area) are shown in Figure 20 for the sediment group 3, under the average conditions stated in Table 8. The average of the values of \bar{c} at high and low water at a point was taken as a representative value over the tidal cycle. Hence, the average deposition rate was computed by multiplying this value by $w_s \phi(0)$. The resulting iso-deposition curves are almost symmetrical about the drift axis. They are valid after steady-state has been reached. By multiplying the values given on the figure by the duration of dredging, the amount of sediments deposited at various locations can be found. This amount, as well as the rate of deposition, are quite important from an ecological point of view. Nevertheless, even more important for an overall assesment of the dredging impact are the percentages of the total sediment discharge settled within a certain distance from the source.

An approximate calculation was carried out in the following way. The areas of the iso-deposition lines of Figure 20 were measured by a planimeter and, by assuming linear interpolation between the curves, the total deposition in gr/tidal cycle within each curve was computed. These quantities were related to the total amount injected which is $0.02 \times 10^6 \times 45600 = 912 \times 10^6$ gr/tidal cycle. The results are presented in Figure 21. It must be pointed out that the linear interpolation used overestimates the true percentages that are deposited within a certain area. For an accurate calculation many more iso-deposition lines between those of Figure 20 are needed.

With respect to the verification of the model, adequate information is lacking for the time being. The actual dredging operation in the summer of 1974 would have been an excellent opportunity for a quantitative evaluation of the model's weaknesses and for its improvement. The previously mentioned "glass bead study" (Section 7.1) can provide only qualitative information, mainly because it involved an instantaneous injection. At this time only preliminary data on the number of sphalerite particles found in suspension in various places in the Bay during the experiment are available (13). A total amount of 2.9×10^{15} sphalerite particles was introduced into the sea. The predominant particle size was between 1 and 8μ but their density was larger than that of the natural silt or clay, being about 4.0 gr/cm^3 . Therefore their settling velocities are close to those of the sediment groups 3 and 4 considered

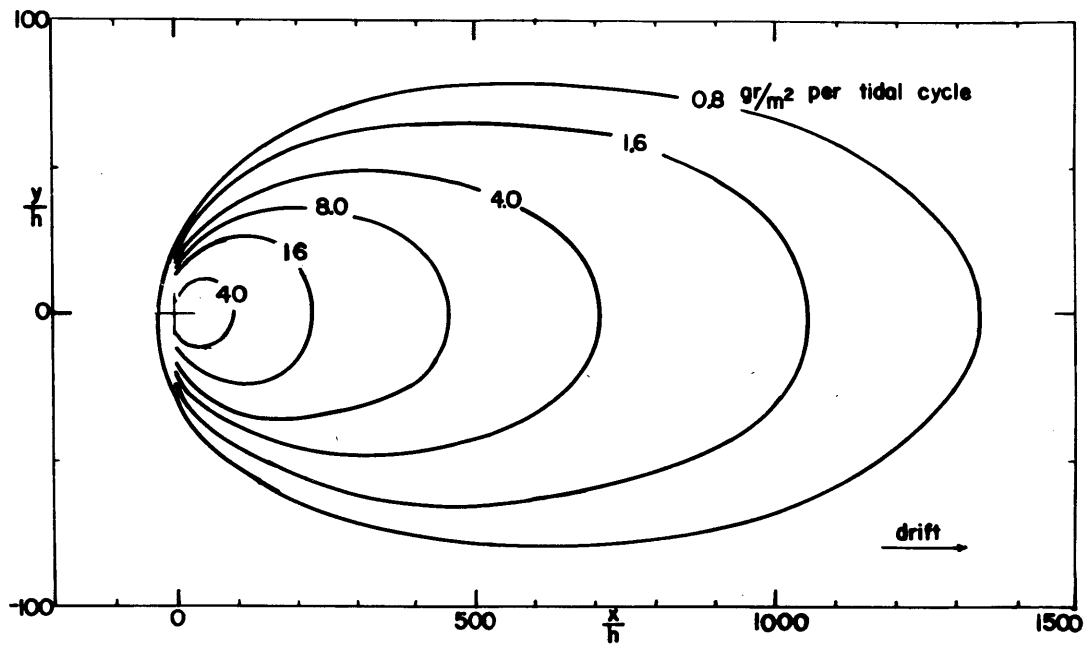


Figure 20 Deposition Rates of Sediment Group 3 Under Average Conditions

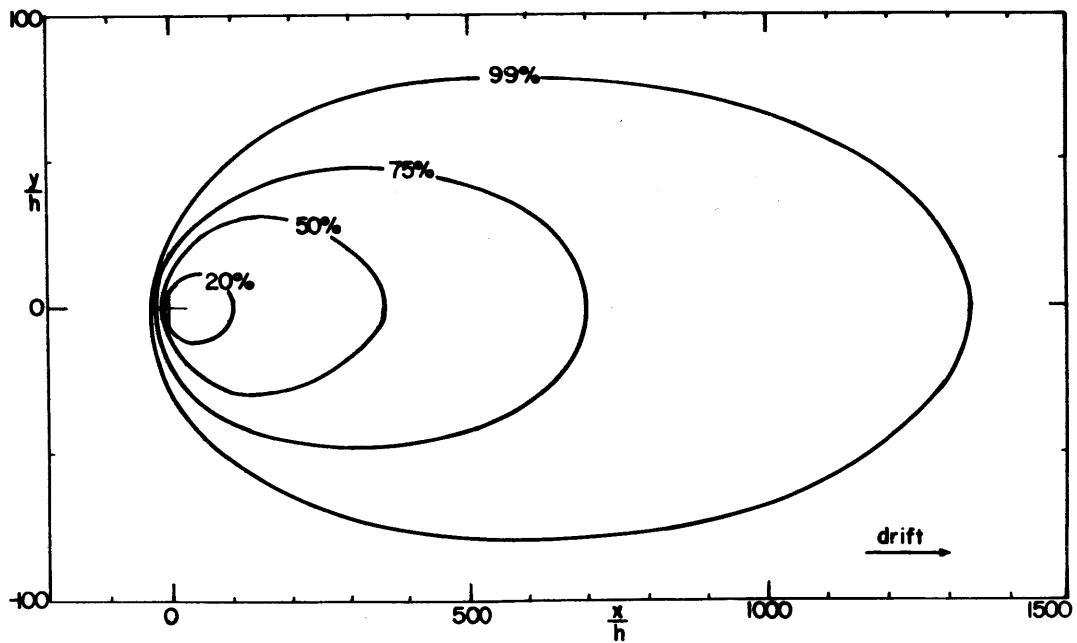


Figure 21 Percentage of Total Discharge of Group 3 Deposited Within Area Shown, Under Average Conditions

in this study. The plume closely followed the mean drogue path (Figure 12), thus confirming the primary importance of the drift direction. The particles moved initially E-NE and ultimately SE. Their spread about the mean direction was large, and apparently due to the changes in the drift with time and space. The presence of concentrations of 300 particles/liter in Cape Cod Bay 5 days or 10 tidal cycles after the injection indicates a net SE drift of about $\frac{25\text{n. miles}}{5 \text{ days}} = 5\text{n. miles/day} \approx 10 \text{ cm/sec}$, which confirms the average values obtained from the drogue studies. The drogue data cover a relatively small area around the proposed dredging site and the conclusions based on these should not be extended to the entire Bay without reservation. The drift velocity is possibly higher in the Southern part of the Bay, and a circulation pattern is probably present around Cape Cod Bay. The fact that the beads travelled all the way to Cape Cod, a distance of about 1500 times the depth, further indicates that the model predictions with respect to length of the dispersing plume are close to reality. It may be mentioned that at the time of the glass bead study such a distance of travel was quite unexpected.

ERRATA - T. R. #179

Page 10: 4th line should read
m = Mass rate of injection of the sediment mixture

Page 12: 10th line should read
v = Kinematic viscosity

Page 33: Equation (3.10a) should read

$$\alpha = \frac{w_s}{h} [\phi(0) - \phi(1)] + \frac{1}{h^2} \left[\left(\epsilon_\zeta \frac{\partial \phi}{\partial \zeta} \right)_{\zeta=0} - \left(\epsilon_\zeta \frac{\partial \phi}{\partial \zeta} \right)_{\zeta=1} \right]$$

Page 71: 4th line

v should be λ

Page 80: 2nd line from the bottom should read
predictive capabilities

Page 124: Reference 1 should read
Environmental Equip. Div., EG&G, Waltham, Massachusetts,
December 1972

CHAPTER 8

CONCLUSIONS AND RECOMMENDATIONS

The model presented herein was necessarily based on simplifying assumptions, so that an analytical solution could be found. It is basically intended to give the equilibrium distribution of suspended sediments, injected from a continuous vertical line source. The transient behavior of the dispersing sediment plume can also be estimated under certain conditions (as indicated in Section 6.1). In addition, information is provided on the deposition patterns to be expected from such a continuous source of sediments.

The relative importance of the various parameters entering into the model, investigated in Section 7.6, is established and it is shown that the net drift and the sediment settling velocity are the primary factors determining the distribution of the suspended matter around the source. Also of importance is the dispersion coefficient in a direction normal to the net drift.

A technique was developed for the analysis of drogue data to yield values for the advective and dispersion terms, taking into account the nonuniformity of the sediment distribution over the vertical. Actual data were used for determining these values for the Massachusetts Bay. However, only 3 or 4 drogues were used in each case, and the tracks covered in the field studies were relatively short. More extensive data, for longer periods of time, are needed in order to estimate the hydrodynamic parameters over the long distances that the fines are

expected to travel according to the models results. In the analysis of such long-term drogue data the change of net drift between tidal cycles can be incorporated to yield an approximate net water movement composed of a sequence of linear segments in the appropriate directions. In that case, the model could be modified and the plume adjusted so as to follow the changing net drift direction. In this way the model could be extended to any form of water movement prevailing in a certain area. The tidal component could also be similarly adjusted. The assumption of constant net drift in the present model does not reflect natural conditions in view of the resulting long dispersion patterns. If it is to be maintained, a much larger value for the lateral dispersion coefficient should probably be used in order to increase the spread of the suspended matter. With the present model the width of the sediment cloud is underestimated, while the prediction of the length is, at least, conservative.

Nevertheless, probably the most important restriction of the model is the assumption of one-layer shear flow. This assumption allowed use of the same vertical equilibrium distribution as in open channels and, furthermore, a significant simplification in the structure of the model, through independent treatment of the horizontal and vertical distributions. Secondary currents due to density variations, however, are often very important to the transport and dispersion of suspended sediments. If the suspended matter is assumed to be carried by density currents near the sea bed, the model could possibly be applied for the reduced height of that current. The non-dimensional

plots given in Figures 19, 20 and 21 would be applicable approximately although the advective and dispersion terms would have to be redefined. The main difficulty for such an extension of the model lies in the violation of the surface boundary condition.

Despite the limitations discussed so far, it is believed that the present model is a relatively simple tool that can predict to some approximation the impact of dredging or other similar activities in the coastal zone. The preliminary results of the "glass bead study" of NOMES seem, at this point, quite encouraging.

Further research is necessary to relax some of the restrictive assumptions employed in this model. A better understanding of the effects of flocculation on the settling rates of fines is very desirable. Also, the hydrodynamic characteristics must be modeled in relation to the meteorological conditions. Until such additional research produces more realistic inputs, the model developed in this study can be useful provided it is applied with full understanding of the inherent assumptions and limitations involved.

REFERENCES

1. C.S. Ahn and P.E. Smith: "The first report on a study to forecast nuclear power plants effects on coastal zones", Environmental Equipment Division, Waltham, Massachusetts, December 1972
2. ASCE Task Committee on Sedimentation: "Sediment Transportation Mechanics: D. Suspension of Sediment", J. Hydraulics Div., ASCE, No. HY 5, September 1963
3. W.R. Boehmer: "A Preliminary Exercise in Modeling the 'Rain of Fines'", Div. of Mineral Resources, Dept. of Natural Resources, Commonwealth of Massachusetts, Spring 1973
4. G. Christodoulou, W.F. Leimkuhler and B.R. Pearce: Unpublished report on current measurements by drogues in Massachusetts Bay, M.I.T., Department of Civil Engineering, September 1973
5. A.N. Diachishin: "Dye Dispersion Studies", Journal of the Sanitary Eng. Div., ASCE, Vol. 89, No. SA1, January 1963
6. W.F. Dobbins: "Effects of Turbulence on Sedimentation", Trans. ASCE, Vol. 109, Paper No. 2218, 1944
7. H.A. Einstein and R.B. Krone: "Experiments to Determine Modes of Cohesive Sediment Transportation in Salt Water", Journal of Geophysical Research, Vol. 67, April 1962
8. J.W. Elder: "The Dispersion of Marked Fluid in Turbulent Shear Flow", Journal of Fluid Mechanics, Vol. 5, May 1959
9. H.B. Fischer: "The Mechanics of Dispersion in Natural Streams", Journal of the Hydraulics Div., ASCE, Vol. 93, No. HY 6, November 1967
10. S.L. Frankel and B.R. Pearce: "Determination of Water Quality Parameters in the Massachusetts Bay (1970-1973)", Ralph M. Parsons Laboratory for Water Resources and Hydrodynamics, M.I.T., Department of Civil Engineering, Technical Report No. 174, November 1973
11. W.H. Graf: "Hydraulics of Sediment Transport", McGraw-Hill Book Company, 1971
12. D.R.F. Harleman: "One-Dimensional Models", Chapter 3 in "Estuarine Modelling: An Assessment" by TRACOR, Inc., for the Water Quality Office, EPA, February 1971

13. W.N. Hess: "Preliminary report on the NOMES glass bead experiment", NOAA Environmental Research Lab., Boulder, Colorado, July 5, 1973
14. E.R. Holley, D.R.F. Harleman and H.B. Fischer: "Dispersion in Homogeneous Estuary Flow", Journal of the Hydraulics Div., ASCE, Vol. 96, No. HY 8, August 1970
15. E.R. Holley and D.R.F. Harleman: "Dispersion of Pollutants in Estuary Type Flow", Hydrodynamics Lab., M.I.T., Department of Civil Engineering, Technical Report No. 74, January 1965
16. A.T. Ippen: "The Distribution of Suspended Material over Cross-sections of Open Channels", unpublished manuscript, 1934
17. A.T. Ippen: "A New Look at Sedimentation in Turbulent Streams", Journal of the Boston Society of Civil Engineers, July 1971
18. H.E. Jobson and W.W. Sayre: "Vertical Transfer in Open Channel Flow", Journal of the Hydraulics Div., ASCE, Vol. 96, No. HY 3, March 1970
19. H.E. Jobson and W.W. Sayre: "Predicting Concentration Profiles in Open Channels", Journal of the Hydraulics Div., ASCE, Vol. 96, No. HY 10, October 1970
20. R.B. Krone: "A Field Study of Flocculation as a Factor in Estuarial Shoaling Processes", Technical Bulletin No. 19, Committee on Tidal Hydraulics, Corps of Engineers, June 1972
21. Marine Geology and Geophysics Lab., AOML: "Preliminary Plan for the NOMES Tracer Experiment", May 15, 1973
22. A. Okubo: "Oceanic Diffusion Diagrams", Deep Sea Research, Vol. 18, 1971
23. A. Okubo: "The Effect of Shear in an Oscillatory Current on Horizontal Diffusion from an Instantaneous Source", Oceanology and Limnology, Vol. 1, No. 3, 1967
24. E. Partheniades: "A Summary of the Present Knowledge of the Behavior of Fine Sediments in Estuaries", Hydrodynamics Lab., M.I.T., Department of Civil Engineering, Technical Note No. 8, June 1964
25. E. Partheniades: "Erosion and Deposition of Cohesive Sediments", Chapter 20 in "Sedimentation - Symposium to Honor Professor H.A. Einstein", edited by H.W. Shen, Berkeley, 1971

26. H. Rouse: "Fluid Mechanics for Hydraulic Engineers", 2nd Ed., Dover, New York, 1961
27. W.W. Sayre: "Dispersion of Silt Particles in Open-Channel Flow", Journal of the Hydraulics Div., ASCE, Vol. 95, No. HY 3, May 1969
28. S.P. Sullivan and F. Gerritsen: "Dredging Operation Monitoring and Environmental Study, Kawaihae Harbor, Hawaii", J. Look Lab. of Oceanographic Engineering, Technical Report No. 25, Department of Ocean Eng., University of Hawaii, September 1972
29. W.C. Taggart, C.A. Yermoli, S. Montes and A.T. Ippen: "Effects of Sediment Size and Gradation on Concentration Profiles in Turbulent Flow", Ralph M. Parsons Laboratory for Water Resources and Hydrodynamics, M.I.T., Department of Civil Engineering, Technical Report No. 152, August 1972
30. Tennessee Valley Authority, Corps of Engineers, Dept. of Agriculture, Geological Survey, Bureau of Reclamation, Indian Service and the Iowa Institute of Hydraulic Research: "Methods of Analyzing Sediment Samples", Report No. 4 in "A Study of Methods Used in Measurement and Analysis of Sediment Loads in Streams", University of Iowa, November 1941
31. Tetra Tech, Inc.: "Further Studies on the Prediction of the Radioactive Debris Distribution Subsequent to a Deep Underwater Nuclear Explosion", Final Report, October 1969
32. P.M. Vogel: "Intermediate Grain Size Distribution Data", Campus Correspondence, University of New Hampshire, March 28, 1973
33. W.T. Wnek and E.G. Fochtman: "Mathematical Model for Fate of Pollutants in Near-Shore Waters", Illinois Inst. of Tech. Research Institute, April 1972

APPENDIX A

SETTLING TUBE MEASUREMENTS

Run No. 1
Kaolinite

Initial Concentration 100 mg/l
Initial Turbidity Reading 64 FTU
Background Turbidity 0.15 FTU

Time (hrs.)	Turbidity Readings (FTU)						Percent Settled
	1	2	3	4	5	6	
1.2	47	-	53	-	55	57	18.6
17.8	18	-	-	17.5	-	18	71.8
24.8	13	-	13.0	-	-	13	79.7
41.8	9.0	-	8.7	-	-	8.4	86.5
48.5	7.2	-	7.1	-	-	7.2	89.0
64.3	5.4	-	5.6	-	-	5.5	91.5
96.8	3.6	-	3.7	-	-	3.7	94.3
160.6	2.0	-	2.0	-	-	2.1	97.0
233.0	1.3	1.3	1.3	1.6	1.3	1.3	98.2

Run No. 2
Kaolinite

Initial Concentration 10 mg/l
Initial Turbidity Reading 7.0 FTU
Background Turbidity 0.40 FTU

Time (hrs.)	Turbidity Readings (FTU)						Percent Settled
	1	2	3	4	5	6	
0.8	6.1	-	6.6	-	-	6.9	6.5
2.7	6.0	-	6.1	-	-	6.4	12.7
22.9	3.3	-	3.9	-	-	3.2	52
47.3	2.2	-	2.5	-	-	2.8	68
70.5	2.0	-	1.95	-	-	2.05	76
100.6	1.5	-	1.7	-	-	1.75	80.5
149.3	-	1.3	-	1.25	-	1.6	87.1
265.8	-	0.68	-	0.67	-	0.67	95.9

Run No. 3
Illite

Initial Concentration 10 mg/l
Initial Turbidity Reading 4.0 FTU
Background Turbidity 0.20 FTU

Time (hrs.)	Turbidity Readings (FTU)						Percent Settled
	1	2	3	4	5	6	
2.0	2.6	-	3.2	-	-	3.1	25.1
3.8	2.2	-	2.8	-	-	2.8	35.0
21.7	1.75	-	1.6	-	-	1.5	63.2
29.3	1.35	-	1.5	-	-	1.5	66.7
77.4	1.1	-	1.1	-	-	1.15	76.0
119.2	0.96	-	0.87	-	-	0.83	83.2
173.1	0.70	-	0.77	-	-	0.83	84.8

Run No. 4
Illite

Initial Concentration 100 mg/l
Initial Turbidity Reading 36 FTU
Background Turbidity 0.20 FTU

Time (hrs.)	Turbidity Readings (FTU)						Percent Settled
	1	2	3	4	5	6	
0.6	24	29.5	33.5	-	35	36	10.2
3.3	17	-	23	-	-	32	29.5
27.7	7.6	-	8.0	-	-	8.1	78.5
47.0	4.75	-	5.0	-	-	5.0	86.7
142.0	1.6	-	1.5	-	-	1.5	96.2

Run No. 5
Boston Harbor Mud

Initial Concentration 10mg/l
Initial Turbidity Reading 5.0 FTU
Background Turbidity 0.25 FTU

Time (hrs.)	Turbidity Readings (FTU)						Percent Settled
	1	2	3	4	5	6	
1.7	2.4	-	3.4	-	-	3.5	37.2
4.6	2.1	-	2.9	-	-	3.1	46.3
17.4	2.0	-	2.0	-	-	2.5	60.0
23.8	1.75	-	1.9	-	-	2.15	64.5
65.8	1.1	-	1.3	-	-	1.6	78.7
124.1	0.88	-	0.92	-	-	0.88	86.3
189.9	0.62	-	0.62	-	-	0.65	91.7

Run No. 6
Boston Harbor Mud

Initial Concentration 100 mg/l
Initial Turbidity Reading 52 FTU
Background Turbidity 0.15 FTU

Time (hrs.)	Turbidity Readings (FTU)						Percent Settled
	1	2	3	4	5	6	
0.6	35.5	-	43.5	-	-	47	17.2
2.9	23	-	33	-	-	39	33.3
6.1	16	-	25	-	-	28	53.8
22.7	5.8	-	7.2	-	-	9.7	82.7
45.3	1.9	-	3.3	-	-	5.5	93.2
99.0	1.95	-	2.15	-	-	1.9	96.4
169.1	0.98	-	1.01	-	-	1.02	98.5
244.3	0.50	-	0.54	-	-	0.51	99.3

APPENDIX B

COMPUTER PROGRAM FOR ANALYSIS OF DROGUE DATA.

```

0001      DIMENSION T(5,50), X(5,50), Y(5,50),DEPTH(6),W(6),DST(50)
0002      DIMENSION XX(5,50), YY(5,50),XXMEAN(50),YYMEAN(50),XXVAR(50)
0003      DIMENSION YYVAR(50),EX(50),EY(50),PHI(61),CUM(61),Z(61),VXX(50)
0004      DIMENSION VYY(50),SEP(6)
0005      DIMENSION WS(5)
0006      READ (5,300) NO
0007      300  FORMAT(I3)
0008      DO 299 IJK=1,NO
0009      NUMWT=0
0010      READ(5,40)STT,TINT,BOTDEP
0011      40  FORMAT(F8.0,F7.0,F5.0)
0012      READ(5,301) CAPP,NSTEP,NCYC
0013      301  FORMAT(F4.2,I4,I3)
0014      REAC(5,308) NWS
0015      308  FORMAT(I2)
0016      READ(5,309)(WS(I),I=1,NWS)
0017      309  FORMAT(5F12.7)
0018      I=1
0019      M=1
0020      3  READ(5,10) N,IDEP,IH,IM,IS,IY,IX
0021      10  FORMAT(I3,11X,I3,I3,I2,I2,I8,I8)
0022      IF(N+1) 12,4,5
      C
      C  SIGNAL ALL UNUSED ELEMENTS OF ARRAY WITH
      C  NEGATIVE NUMBER
      C
0023      4  DO 1 III=I,50
0024      T(M,III)=-10000000.
0025      1  CONTINUE
0026      I=1
0027      M=M+1
0028      GO TO 3
      C
      C  PUT INTEGER INFORMATION INTO REAL ARRAYS
      C
0029      5  T(M,I)=FLOAT(3600*IH+60*IM+IS)
0030      X(M,I)=FLOAT(IX)
0031      Y(M,I)=FLOAT(IY)
0032      DEPTH(M)=FLOAT(IDEP)
0033      I=I+1
0034      GO TO 3
      C
      C  SIGNAL UNUSED ELEMENTS OF LAST ARRAY AS WITH OTHERS
      C
0035      12 DO 13 III=I,50
0036      T(M,III)=-10000000.
0037      13 CONTINUE
      C
      C  MAKE TIME CORRECTIONS SO THAT TIME IS ALWAYS INCREASING
      C
0038      DO 30 K=1,M
0039      DO 25 KK=1,49
0040      Q=T(K,KK+1)-T(K,KK)

```

```

0041          IF(Q) 17,25,25
0042          17  DO 23 KKK=KK,49
0043          T(K,KKK+1)=T(K,KKK+1)+86400.
0044          23  CONTINUE
0045          25  CONTINUE
0046          30  CONTINUE
              C
              C   SET UP DESIRED TIME ARRAY
              C
0047          DST(1)=STT
0048          DO 32 J=1,49
0049          DST(J+1)=DST(J)+TINT
0050          32  CONTINUE
0051          JJ=50
              C
              C   ASSOCIATE X AND Y VALUES WITH DESIRED TIME ARRAY
              C
0052          DO 60 L=1,M
0053          I=1
0054          J=1
0055          33  IF(DST(J)-T(L,I)) 50,35,35
0056          35  IF(DST(J)-T(L,I+1)) 42,42,55
0057          42  DT=(DST(J)-T(L,I))/(T(L,I+1)-T(L,I))
0058          XX(L,J)=X(L,I)+(X(L,I+1)-X(L,I))*DT
0059          YY(L,J)=Y(L,I)+(Y(L,I+1)-Y(L,I))*DT
0060          50  J=J+1
0061          GO TO 33
0062          55  I=I+1
0063          IF (T(L,I)+1) 57,57,35
              C
              C   LENGTH USED IS THAT OF THE SMALLEST ARRAY
              C
0064          57  IF(JJ-J) 60,58,58
0065          58  JJ=J-1
0066          60  CONTINUE
0067          MP=M+1
0068          MZ=M-1
0069          DO 80 L=1,MZ
0070          IF(L-1) 65,65,68
0071          65  F2=0
0072          GO TO 73
0073          68  F2=(DEPTH(L-1)+DEPTH(L))*0.5
0074          73  F1=(DEPTH(L)+DEPTH(L+1))*0.5
0075          W(L)=(F1-F2)/BOTDFP
0076          80  CONTINUE
0077          DFAC=1.-DEPTH(M)/BOTDFP
0078          W(M+1)=DFAC/(9.+ALOG(DFAC))
0079          W(M)=1.-W(M+1)-(DEPTH(M-1)+DEPTH(M))/(2.*BOTDFP)
0080          WRITE(6,310)
0081          310  FORMAT(1H1)
0082          WRITE(6,119)
0083          119  FORMAT(3X,'FOR NEUTRALLY BOYANT PARTICLES')
0084          WRITE(6,120) (W(L),L=1,MP)

```

```

0085      120  FORMAT(2X,' WEIGHTS',1X,10F6.3)
0086      XX(M+1,1)=XX(M,1)
0087      YY(M+1,1)=YY(M,1)
0088      DO 82 J=1,JJ
0089      XX(M+1,J)=XX(M+1,1)
0090      YY(M+1,J)=YY(M+1,1)
0091      82  CONTINUE
0092      DO 86 L=1,MP
0093      DO 88 J =2,JJ
0094      XX(L,J)=(XX(L,J)-XX(L,1))*30.5
0095      YY(L,J)=(YY(L,J)-YY(L,1))*30.5
0096      88  CONTINUE
0097      XX(L,1)=0.
0098      YY(L,1)=0.
0099      86  CONTINUE
0100      DO 96 J=1,JJ
0101      96  DST(J)=DST(J)-STT
0102      87  DO 84 J=1,JJ
0103      XXMEAN(J)=0.
0104      YYMEAN(J)=0.
0105      XXVAR(J)=0.
0106      YYVAR(J)=0.
0107      84  CONTINUE
0108      DO 90 J=1,JJ
0109      DO 89 L=1,MP
0110      XXMEAN(J)=XXMEAN(J)+XX(L,J)*W(L)
0111      YYMEAN(J)=YYMEAN(J)+YY(L,J)*W(L)
0112      89  CONTINUE
0113      90  CONTINUE
0114      DO 92 J=2,JJ
0115      VXX(J)=(XXMEAN(J)-XXMEAN(J-1))/TINT
0116      VYY(J)=(YYMEAN(J)-YYMEAN(J-1))/TINT
0117      92  CONTINUE
0118      CALL TIDVEL(NCYC,JJ,DST,XXMEAN,YYMEAN,TINT,DRIFMG,DRIFDR,UT,
1TIDEOR,LAST)
0119      WRITE (6,130)
0120      130  FORMAT('      TIME',5X,'MEAN X',5X,'MEAN Y',8X,'C VAR',8X,'N VAR',
19X,'DISP C',8X,'DISP N',7X,'VEL X',5X,'VEL Y')
0121      WRITE (6,131)
0122      131  FORMAT(3X,'(SEC)',6X,'(CM)',6X,'(CM)',7X,'(CM2/SEC)',5X,'(CM2/SEC)
1',5X,'(CM2/SEC)',5X,'(CM2/SEC)',4X,'(CM/SEC)',2X,'(CM/SEC)',/)
0123      ST=SIN(DRIFDR)
0124      CT=CCS(DRIFDR)
0125      DO 95 J=1,JJ
0126      XM=XXMEAN(J)*CT+YYMEAN(J)*ST
0127      YM=-XXMEAN(J)*ST+YYMEAN(J)*CT
0128      DO 94 L=1,MP
0129      XXX=XX(L,J)*CT+YY(L,J)*ST
0130      YYY=-XX(L,J)*ST+YY(L,J)*CT
0131      XXVAR(J)=XXVAR(J)+W(L)*(XXX-XM)**2
0132      YYVAR(J)=YYVAR(J)+W(L)*(YYY-YM)**2
0133      94  CONTINUE
0134      95  CONTINUE

```



```

0135          DO 195 J=2,JJ
0136          EX(J)=(XXVAR(J)-XXVAR(J-1))/(2.*TINT)
0137          EY(J)=(YYVAR(J)-YYVAR(J-1))/(2.*TINT)
0138          195  CONTINUE
0139          DO 141 J=2,JJ
0140          WRITE (6,140) DST(J),XXMEAN(J),YYMEAN(J),XXVAR(J),YYVAR(J)
0141          1,EX(J),EY(J),VXX(J),VYY(J)
0142          140  FORMAT (3F10.0,4E14.5,2F10.3)
0143          141  CONTINUE
0144          CALL CONVRT(NCYC, LAST, DRIFMG, DRIFDR, UT, TIDEDR, EX, EY)
0145          293  IF(NUMWT)294,294,295
0146          294  CALL USTA (NCYC, JJ, VXX, VYY, DST, USTAR, TINT)
0147          295  NUMWT=NUMWT+1
0148          IF(NWS-NUMWT)299,83,83
0149          83   WS1=WS(NUMWT)
0150          WRITE (6,315)WS1
0151          315  FORMAT('1',3X,'NORMALIZED VERTICAL PROFILE FOR SETTLING VELOCITY',
0152          1F12.7,2X,'CM/SEC',/)
0153          CALL PROFIL(PHI,CUM,Z,WS1,USTAR,CAPPA,NSTEP,BOTDEP)
0154          CALL WEIGHT(W,SFP,DEPTH,CUM,M,BOTDEP,Z,NSTEP)
0155          GO TO 87
0156          299  CONTINUE
          CALL EXIT
          END

```

```

0001      SUBROUTINE TIDVEL(NCYC,JJ,DST,XXMEAN,YYMEAN,TINT,DRIFMG,DRIFDR,
          IUT,TIDEDR,LAST)
          C
          C      THIS ROUTINE COMPUTES THE MEAN WEIGHTED TIDAL AND NET DRIFT
          C      VELCCITIES GIVEN THE MEAN WEIGHTED DROGUE MOTION (XXMEAN,YYMEAN)
          C
0002      DIMENSION DST(50),XXMEAN(50),YYMEAN(50)
0003      WRITE(6,311)
0004      311  FORMAT(1H1)
0005      PI=3.14159
0006      NDST=45600./TINT
0007      REM=45600.-NDST*TINT
0008      LAST=NCYC+NDST
0009      IF(LAST-JJ)15,15,14
0010      14  WRITE(6,301)
0011      301  FORMAT(/,,' TIDAL CYCLE OVERRUNS RECORD IN TIDVEL
          1 COMPUTATIONS MADE ON REDUCED AVAILABLE CYCLE')
          LAST=JJ
          REM=0.
          XXMEAN(LAST+1)=XXMEAN(LAST)
          YYMEAN(LAST+1)=YYMEAN(LAST)
0015      15  XLAST=XXMEAN(LAST)+(XXMEAN(LAST+1)-XXMEAN(LAST))*REM/TINT
          YLAST=YYMEAN(LAST)+(YYMEAN(LAST+1)-YYMEAN(LAST))*REM/TINT
0017      XDRIF=XLAST-XXMEAN(NCYC)
0018      YDRIF=YLAST-YYMEAN(NCYC)
0019      CYCDUR=DST(LAST)-DST(NCYC)+REM
0020      DVELX=XDRIF/CYCDUR
0021      DVELY=YDRIF/CYCDUR
          C
          C      DIRECTION OF NET DRIFT
          C
0023      DIRECT=ATAN(YDRIF/XDRIF)
0024      IF(XDRIF)20,25,25
0025      20  IF(YDRIF)21,22,22
0026      21  DIRECT=DIRECT-PI
0027      GO TO 25
0028      22  DIRECT=DIRECT+PI
0029      25  DRIFDR=DIRECT
          DEGDIR=DRIFDR*(180./PI)
0031      DRIFMG=SQRT((XDRIF)**2+(YDRIF)**2)/45600.
0032      WRITE(6,303) DRIFMG,DEGDIR
0033      303  FORMAT(/,3X,'NET DRIFT=',F10.3,2X,'CM/SEC',10X,'DIRECTION FROM
          1 EAST',F10.3)
          DEVM1=0.
          DEVM2=0.
          XDEV1=0.
          YDEV1=0.
          XDEV2=0.
          YDEV2=0.
          NP=NCYC+1
          DO 38 LL=NP, LAST
0041      XD=DVELX*TINT*(LL-NCYC)+XXMEAN(NCYC)
0042      YD=DVELY*TINT*(LL-NCYC)+YYMEAN(NCYC)
0043

```

```

0044          DEVM=SQRT((XXMEAN(LL)-XD)**2+(YYMEAN(LL)-YD)**2)
0045          CALL TEST(NTEST,XXMEAN(NCYC),YYMEAN(NCYC),XXMFAN(LL),YYMFAN(LL),
1          DIRECT)
0046          IF(NTEST)31,31,34
0047          31  IF(DEVM1-DEVM)32,38,38
0048          32  XDEV1=XXMEAN(LL)-XD
0049          YDEV1=YYMEAN(LL)-YD
0050          DEVM1=DEVM
0051          GO TO 38
0052          34  IF(DEVM2-DEVM)35,38,38
0053          35  XDEV2=XXMEAN(LL)-XD
0054          YDEV2=YYMEAN(LL)-YD
0055          DEVM2=DEVM
0056          38  CONTINUE
0057          XDEV=(XDEV1-XDEV2)
0058          YDEV=(YDEV1-YDEV2)
0059          TIDDIR=ATAN(YDEV/XDEV)
0060          TIDEDR=TIDDIR
0061          TIDDEG=TIDEDR*(180./PI)
          C
          C   MAX. TIDAL VEL. = DISP. OVER 1/2 CYCLE * PI/TIME OF CYCLE
          C
0062          DEVT=SQRT(XDEV**2+YDEV**2)
0063          UT=DEVT*3.14159/CYCDUR
0064          WRITE (6,304) UT,TIDDEG
0065          304  FORMAT(/,3X,'MAX TIDAL VELOCITY=',F10.3,2X,'CM/SEC',10X,
1'DIRECTION FROM EAST',F10.3,/)
0066          999  RETURN
0067          END

```

```

0001          SUBROUTINE TEST(NTEST,X0,Y0,X1,Y1,DIRECT)
0002          PI=3.14159
0003          X=X1-X0
0004          Y=Y1-Y0
0005          DIREC1=ATAN(Y/X)
0006          IF(X)20,25,25
0007          20  IF(Y)21,22,22
0008          21  DIREC1=DIREC1-PI
0009          GO TO 25
0010          22  DIREC1=DIREC1+PI
0011          25  CONTINUE
0012          IF(DIRECT-DIREC1)38,38,30
0013          30  IF(DIRECT-DIREC1-PI) 36,36,38
0014          36  NTEST=1
0015          GO TO 99
0016          38  NTEST=-1
0017          99  RETURN
0018          END

```

```

0001      SUBROUTINE CONVRT(NCYC, LAST, DRIFMG, DRIFDR, UT, TIDEDR, EX, EY)
0002      DIMENSION EX(50), EY(50)
0003      EXS=0.
0004      EYS=0.
0005      NNCYC=NCYC+1
0006      DO 190 J=NNCYC, LAST
0007      EXS=EXS+EX(J)
0008      EYS=EYS+EY(J)
0009      190  C JNTINUE
0010      AVEY=EXS/(LAST-NCYC)
0011      AVEY=EYS/(LAST-NCYC)
0012      THETA=ABS(DRIFDR-TIDEDR)
0013      TIDEC=UT*COS(THETA)
0014      TIDEN=UT*SIN(THETA)
0015      WRITE(6,191) TIDEC, TIDEN
0016      191  FORMAT(/,3X,' TIDE ALONG DRIFT AXIS',F10.3,2X,'CM/SEC',10X,
1' TIDE NORMAL TO IT',F10.3,2X,'CM/SEC')
0017      WRITE(6,192) AVEY, AVEY
0018      192  FORMAT(/,3X,' AVERAGE DISPERSION COEFF. ALONG DRIFT AXIS',F12.5,2X,
1'CM2/SEC',10X,'NORMAL TO IT',F12.5,2X,'CM2/SEC')
0019      RETURN
0020      END

```

```

0001      SUBROUTINE USTA (NCYC, JJ, VXX, VYY, DST, USTAR, TINT)
C
C      THIS ROUTINE COMPUTES THE SHEAR VELOCITY FROM A TWO
C      DIMENSIONAL TRACK OF DROGUE POSITIONS, USING THE VELOCITY
C      MAGNITUDES
C
0002      DIMENSION DST(50), VXX(50), VYY(50)
0003      CVEL=C.
0004      NDST=45600./TINT
0005      LAST=NCYC+NDST
0006      LLAST=LAST-1
0007      IF(JJ-LAST)41,42,42
0008      41  WRITE(6,341)
0009      341  FORMAT(/,2X,'RECORD TOO SHORT FOR TIDAL CYCLE DESIRED IN USTA')
0010      LLAST=JJ-1
0011      42  DO 115 LLL=NCYC, LLAST
0012      CVEL=CVEL+SQRT(VXX(LLL+1)**2+VYY(LLL+1)**2)
0013      115  CONTINUE
0014      117  VELAV=CVEL/(LLL-NCYC+1)
C
C      ASSUMING THAT FRICTION COEFFICIENT, F, =.02
C
0015      USTAR=VELAV/20.
0016      WRITE(6,331) USTAR
0017      331  FORMAT(/,3X,'USTAR=',F10.3,2X,'CM/SEC',/)
0018      RETURN
0019      END

```

```

0001          SUBROUTINE PROFIL(PHI,CUM,Z,WS,USTAR,CAPPA,NSTEP,ROTDEP)
              C
              C THE PROGRAM COMPUTES THE NORMALIZED VERTICAL CONCENTRATION
              C PROFILE FO A GIVEN DEPTH, SHEAR VELOCITY, AND SETTLING RATE.
              C
0002          DIMENSION PHI(61),S2(61),CUM(61),Z(61)
0003          Q=WS/(USTAR*CAPPA)
0004          Z(1)=0.
0005          RSTEP=NSTEP
0006          DZ=1./RSTEP
0007          CUM(1)=0.
0008          N=NSTEP+1
0009          DO 50 I=1,N
0010             IF(Z(I)-.05) 25,25,30
0011             ZZ=.05
0012             GO TO 40
0013             30 ZZ=Z(I)
0014             40 S2(I)={{(1./ZZ-1.)/19.}**Q
0015             IF (I-N) 42,43,43
0016             42 Z(I+1)=Z(I)+DZ
0017             43 IF(I-1)50,50,45
0018             45 S3=.5*(S2(I)+S2(I-1))*DZ
0019             CUM(I)=CUM(I-1)+S3
0020             50 CONTINUE
0021             S5=1./CUM(N)
0022             WRITE(6,448)
0023             448 FORMAT(5X,'Z',10X,'PHI')
0024             DO 60 I=1,N
0025             PHI(I)=S5*S2(I)
0026             WRITE(6,450) Z(I),PHI(I)
0027             450 FORMAT(2X,F8.3,5X,E12.5)
0028             60 CONTINUE
0029             RETURN
0030             END

```

```

0001      SUBROUTINE WEIGHT(W,SEP,DEPTH,CUM,M,BOTDEP,Z,NSTEP)
0002      DIMENSION SEP(6),W(6),CUM(61),DEPTH(6),Z(61),ZZ(61),WT(6),DCUM(61)
0003      MP=M+1
0004      MZ=M-1
0005      DO 65 L=1,MZ
0006      SEP(L)=.5*(DEPTH(L+1)+DEPTH(L))/BOTDEP
0007      65 CONTINUE
0008      DFAC=1.-DEPTH(M)/BOTDEP
0009      SEP(M)=1.-DFAC/(9.+ALOG(DFAC))
0010      L=1
0011      NN=NSTEP+1
0012      DO 66 I=1,NN
0013      ZZ(I)=1.-Z(I)
0014      DCUM(I)=CUM(NN)-CUM(I)
0015      66 CONTINUE
0016      DO 70 I=1,NN
0017      IF(ZZ(NN-I+1)-SEP(L))70,68,68
0018      68 SFAC=(SEP(L)-ZZ(NN-I+2))/(ZZ(NN-I+1)-ZZ(NN-I+2))
0019      WT(L)=(DCUM(NN-I+2)+SFAC*(DCUM(NN-I+1)-DCUM(NN-I+2)))/CUM(NN)
0020      L=L+1
0021      IF(L-M)70,70,72
0022      70 CONTINUE
0023      72 DO 80 L=1,M
0024      IF(L-1)75,75,77
0025      75 W(L)=WT(L)
0026      GO TO 80
0027      77 W(L)=WT(L)-WT(L-1)
0028      80 CONTINUE
0029      W(M+1)=1.-WT(M)
0030      WRITE(6,120) (W(L),L=1,MP)
0031      120 FORMAT(/,2X,'WEIGHTS',1X,10F6.3)
0032      RETURN
0033      END

```

APPENDIX C

COMPUTER PROGRAM FOR THE HORIZONTAL
DISTRIBUTION OF AVERAGE CONCENTRATION

```

0001      3      READ(5,8) IH,ITT,VCLR
0002      8      FORMAT(I2,I6,F6.3)
0003      H=IH
0004      TT=ITT
0005      IF(H)1,2,2
0006      2      DO 70 K=1,5
0007      READ (5,10) IXS,IYS,IXL,IYL,IO,T,T1,DT
0008      10     FORMAT(I3,I4,I4,I4,I4,F6.2,F6.2,F6.3)
0009      XS=IXS
0010      YS=IYS
0011      XL=IXL
0012      YL=IYL
0013      O=IO
0014      READ(5,11) IEO,IEN,IUD,IVT,IVN,A,ANG
0015      11     FORMAT(2I7,3I5,F7.3,F7.2)
0016      ED=IEO
0017      EN=IEN
0018      VT=IVT
0019      UD=IUD
0020      VN=IVN
0021      P=3.14159
0022      WRITE(6,9) K
0023      9      FORMAT('1',2X,'FOR SEDIMENT GROUP NO.',I3)
0024      WRITE(6,19) ANG
0025      19     FORMAT(' DRIFT DIRECTION IS',F8.2,' DEGREES FROM EAST')
0026      WRITE(6,12)
0027      12     FORMAT('//,' DIMENSIONLESS PARAMETERS:')
0028      WRITE(6,13) IUD,IVT,IVN
0029      13     FORMAT(' NET DRIFT VELOCITY',I5,5X,'MAX TIDAL VELOCITY ALONG DRI
0030      IFT AXIS',I5,5X,'NORMAL TO IT',I5)
0031      14     WRITE(6,14) IEO,IEN
0032      14     FORMAT(' DISPERSION COEFFICIENTS-',5X,' ALONG DRIFT AXIS',I7,5X,
0033      1'NORMAL TO IT',I5)
0034      WRITE(6,16) T,T1,DT
0035      16     FORMAT(2X,'TIME= ',F6.2,5X,'END OF INJECTION AT', F6.2,5X,'STEP OF
0036      1 INTEGRATION',F6.3)
0037      WRITE(6,17) A
0038      17     FORMAT(' DECAY FACTOR',F10.4)
0039      WRITE(6,18)
0040      18     FORMAT('/',' X Y C(PAR)/CO',/)
0041      M=XL/D
0042      N=YL/D
0043      M1=(M+1)/2
0044      N1=(N+1)/2
0045      M2=2*M1+1
0046      N2=2*N1+1
0047      X=XS-M1*D
0048      Y=YS-N1*D
0049      ANG=P*ANG/180.
0050      DO 60 I=1,M2
0051      DO 65 J=1,N2
0052      XPRIME=X*COS(ANG)+Y*SIN(ANG)
0053      YPRIME=-X*SIN(ANG)+Y*COS(ANG)

```



```

0051      T2=0.
0052      Q1=0.
0053      Q3=0.
0054      49  IF(T1-T2) 100,51,51
0055      51  S1=(XPRIME-UD*(T-T2)+(.5*VT/P)*(COS(2*P*T)-COS(2*P*T2)))**2
0056      R1=4*FD*(T-T2)
0057      F1=S1/R1
0058      S2=(YPRIME+ (.5*VN/P)*(COS(2*P*T)-COS(2*P*T2)))**2
0059      R2=4*EN*(T-T2)
0060      F2=S2/R2
0061      F3=A*(T-T2)
0062      F=F1+F2+F3
0063      R=4*P*(T-T2)*SQRT(FD*EN)
0064      Q=Q1
0065      IF(F-100.) 55,55,56
0066      55  Q1=(EXP(-F))/R
0067      GO TO 57
0068      56  Q1=0.
0069      57  T2=T2+DT
0070      IF(T2-NT) 49,49,52
0071      52  Q2=.5*(Q+Q1)*DT
0072      Q3=Q3+Q2
0073      GO TO 49
0074      100 CB=VDLR*TT*Q3/(H**3)
0075      WRITE(6,20) X,Y,CB
0076      20  FORMAT(F9.1,F9.1,4X,E10.3)
0077      Y=Y+D
0078      65  CONTINUE
0079      X=X+D
0080      Y=YS-N1*D
0081      60  CONTINUE
0082      70  CONTINUE
0083      GO TO 3
0084      1  CALL EXIT
0085      END

```